

# Flood Defence Nagoya

## Multidisciplinary Project

V. van Delft  
G. Dorgelo  
I.M.H. van der Reijden  
T.M. Spannenburg

MP256



# Flood Defence Nagoya

Multidisciplinary Project

by  
V. van Delft  
G. Dorgelo  
I.M.H. van der Reijden  
T.M. Spanenburg

Team MP256

Project duration: July 9, 2018 – August 31, 2018  
Supervisors: Dr. Eng. R. Tsubaki, Nagoya University  
Dr. ir. P.C.J. Hoogenboom, TU Delft  
Dr. ir. D.J. Peters, TU Delft



# Preface

Before you lies the report "Flood Defence Nagoya", written by four students from Delft University of Technology, the Netherlands. It has been written as part of the participation of the course 'CIE4061: Multidisciplinary Project' at the TU Delft, a course focusing on conducting research, at home or abroad. In this study, both master programs 'Hydraulic Engineering' and 'Structural Engineering' play a role in the assessment of the problem in Nagoya, Japan's fourth largest city. We were involved in researching, designing, and writing this report from July to August 2018.

The project has been carried out in collaboration with Nagoya University and Chubu Regional Development Bureau. Dr. Eng. R. Tsubaki of Nagoya University supervised us in the research and design stages of this research. Mr. Tsubaki also guided our communication with Chubu Regional Development Bureau, which provided us with information and data to use in investigation. Two supervisors from the TU Delft guided us in the process: Dr. ir. P.C.J. Hoogenboom and Dr. ir. D.J. Peters. This report forms an alternative master plan for Chubu Regional Development Bureau in order to mitigate the probability of flooding in Nagoya City.

We would like to thank Mr. Tsubaki for his excellent guidance, support and provision of work-space during this project. We also wish to thank our supervisors from TU Delft; Mr. Hoogenboom and Mr. Peters. Both advised us multiple times on how to approach and solve certain challenges. Lastly, we would like to thank the staff members of Chubu Regional Development Bureau for providing us all the necessary information we needed for this report.

We hope you enjoy your reading.

Group MP256:

- V. van Delft;
- G. Dorgelo;
- I.M.H. van der Reijden;
- T.M. Spannenburg.

Nagoya, August 30<sup>th</sup>, 2018

# Abstract

At the Shonai River around Nagoya, Japan, several flood related problems occur. These problems occur at different locations, each with its own problems or limitations. The desired safety level as requested by the government is that the river should be able to have a discharge which has a probability of failure of once in 200 years. At many locations, the current probability of failure is lower than once in 50 years. This has led to the following research question:

## ***How can the discharge capacity of the Shonai River be improved to modern standards?***

The report has been divided in four phases. The first phase is used to formulate the final research question. This phase focuses on which part of the Nagoya urban area is most prone to flooding. Three kinds of flooding were examined: by peak river discharge, impact by tsunamis and impact by storm surge. The area is already well protected against tsunamis due to the natural shape of the bay Nagoya is situated to. The coastline is well protected against storm surges in the second half of the 20<sup>th</sup> century. At the river banks however, flood safety is still below the desired level. In the area, risks are relatively high along the Shonai River. Therefore, it has been decided to focus on the threats around the Shonai River.

As already described above, there are several locations along the river with safety risks. In phase 2, several locations and solutions are described to increase the capacity of the river. One major problem is the bottleneck around the Biwajima bridges, where four bridges are narrowing the river. At this location, the desired safety level of a flood discharge occurring once in 200 years is still far away. After discussion with officials of the Shonai River office, it was found that this problem was most urgent. Therefore, it had been chosen to elaborate further on this option in phase 3 and 4.

In phase 3, several options are described to remove the bottleneck. The first option is to replace the bridges with more clearance and larger spans. The second option is to remove the bridges and replace them for tunnels. The third and last option is to construct a bypass along the river, with flow through a tunnel. The Shonai River office is already working on a plan to raise the bridges, thus the first option has been dropped. The second option required large amounts of space for the tunnels. Therefore, it had been decided to work out the third option of creating a bypass. To minimise the impact of such a bypass and its construction on the surrounding area, the decision is made to construct a bored tunnel.

In the fourth and final phase the solution is verified. This is done concerning structural, hydraulic and construction method aspects. All the aspects are found to be possible. In hydraulic aspect, it is found that the required discharge capacity to reach a once in 200 year safety level equals 4250 m<sup>3</sup>/s. The current discharge capacity is found to be 2850 m<sup>3</sup>/s. Therefore, the bypass should have a minimal discharge capacity of 1400 m<sup>3</sup>/s. When using a bored tunnel, it is found that two tunnels with the maximal internal diameter of 16 m should be applied. On top of that, because the concrete surface is to rough in the best circumstances, it was decided to apply an epoxy layer on the surface. Using such a layer, it is found that the total discharge capacity becomes 1490 m<sup>3</sup>/s.

The construction of the tunnel would take 137 weeks to complete. The total costs are estimated to be in the order of ¥60,000,000,000, or 60 billion yen, equivalent to 463 million euro. In comparison, the plan of the river office to replace the bridges would cost ¥68,400,000,000. It can be concluded that this option is a reasonable alternative for the current plan.

# Contents

Preface	ii
Abstract	iii
Contents	iv
List of Figures	x
List of Tables	xv
List of Symbols	xvii
Introduction	1
<b>I Phase I: Preparation and investigation</b>	<b>2</b>
<b>1 Investigation of Nagoya area</b>	<b>3</b>
1.1 Project location . . . . .	3
1.2 Current protection . . . . .	4
<b>II Phase II: Assessment of possible solutions</b>	<b>5</b>
<b>1 Options to improve the Shonai River</b>	<b>6</b>
<b>III Phase III: Drafts of solutions</b>	<b>8</b>
<b>1 Proposal of different solutions</b>	<b>9</b>
1.1 Tunnel underneath the Shonai River . . . . .	9
1.2 Replace Tokaido Railway bridges with new ones . . . . .	10
1.3 Replace Tokaido Railway bridges with a tunnel . . . . .	11
<b>2 Discharge</b>	<b>12</b>
<b>3 Bypass tunnel</b>	<b>13</b>
3.1 Reference projects . . . . .	13
3.2 Location . . . . .	13
3.3 Inlet and outlet structure . . . . .	14
3.4 Bored tunnel . . . . .	15
3.4.1 Required dimensions of the tunnel . . . . .	15
3.5 Pneumatic caisson . . . . .	16
3.5.1 Dimensions based on capacity . . . . .	16
3.5.2 Structural calculations . . . . .	16
3.5.3 Transportation of caissons . . . . .	17
3.6 In-situ tunnel . . . . .	17
3.6.1 Dimensions based on capacity . . . . .	17
3.7 Immersed tunnel . . . . .	17
<b>4 New Tokaido Railway bridges</b>	<b>18</b>
4.1 Type of bridge . . . . .	18
4.2 Conceptual calculations . . . . .	19
<b>5 Railway tunnel</b>	<b>20</b>
5.1 Lay-out of railway tunnel . . . . .	20
5.1.1 Building area . . . . .	22
<b>6 Determination of solution</b>	<b>23</b>



<b>IV Phase IV: Verification of single solution</b>	<b>24</b>
<b>1 Proposed location</b>	<b>25</b>
<b>2 Tunnel flow</b>	<b>26</b>
2.1 Tunnel characteristics . . . . .	26
2.2 Flow profile . . . . .	26
2.3 Effect on river . . . . .	26
2.4 Debris . . . . .	28
2.5 Sediment . . . . .	28
2.6 Scour protection . . . . .	28
<b>3 Inlet and outlet structure</b>	<b>30</b>
3.1 Structural design tube . . . . .	30
<b>4 Structural design tunnel</b>	<b>32</b>
4.1 Design of tunnel lining . . . . .	32
4.1.1 Loads . . . . .	33
4.1.2 Calculation by Plaxis 2D . . . . .	33
4.1.3 Evaluation of the results . . . . .	33
<b>5 Structural design of building pit</b>	<b>35</b>
<b>6 Construction planning</b>	<b>38</b>
<b>7 Cost estimate</b>	<b>42</b>
<b>Conclusions</b>	<b>44</b>
<b>Recommendations</b>	<b>45</b>
<b>Bibliography</b>	<b>46</b>
<b>V Appendices of Phase I</b>	<b>51</b>
<b>A River characteristics</b>	<b>52</b>
A.1 Flood history . . . . .	53
A.2 Current protection . . . . .	54
<b>B Storm surge characteristics</b>	<b>55</b>
<b>C Tsunami characteristics</b>	<b>57</b>
<b>D Value of region</b>	<b>59</b>
D.1 Population density . . . . .	59
D.2 Land usage . . . . .	59
D.3 Cultural value . . . . .	60
<b>E Determining project location</b>	<b>61</b>
<b>F Current bathymetry and protection</b>	<b>62</b>
E1 Coast . . . . .	62
E1.1 Coast of Mie prefecture . . . . .	62
E1.2 Coast of Aichi prefecture . . . . .	63
E2 Ise Bay . . . . .	64
E2.1 Bathymetry Ise Bay . . . . .	64
<b>G Seismic identification</b>	<b>65</b>
<b>H Japanese hydraulic engineering and future vision</b>	<b>66</b>

<b>VI Appendices of Phase II</b>	<b>67</b>
<b>I Shin River + adaptations</b>	<b>68</b>
I.1 Description solution . . . . .	68
I.2 Advantages . . . . .	69
I.3 Disadvantages . . . . .	69
<b>J Covered version of Shin River</b>	<b>70</b>
J.1 Description solution . . . . .	70
J.2 Advantages . . . . .	70
J.3 Disadvantages . . . . .	71
<b>K Bottleneck near Biwajima</b>	<b>72</b>
K.1 Description solution . . . . .	72
K.2 Advantages . . . . .	73
K.3 Disadvantages . . . . .	73
<b>L Use of existing dams upstream</b>	<b>74</b>
L.1 Description solution . . . . .	74
L.2 Advantages . . . . .	75
L.3 Disadvantages . . . . .	75
<b>M Creating new dam/weir upstream</b>	<b>76</b>
M.1 Description solution . . . . .	76
M.2 Advantages . . . . .	77
M.3 Disadvantages . . . . .	77
<b>N Construction of new artificial river</b>	<b>78</b>
N.1 Description solution . . . . .	78
N.1.1 Extension of the Yamasaki River . . . . .	78
N.1.2 Connection Shonai River to Yahagi River . . . . .	78
N.2 Advantages . . . . .	78
N.3 Disadvantages . . . . .	78
<b>O Discharge (metro) tunnel system</b>	<b>80</b>
O.1 Description solution . . . . .	80
O.1.1 Permanent conversion . . . . .	80
O.1.2 Hybrid tunnels . . . . .	81
O.2 Advantages . . . . .	81
O.3 Disadvantages . . . . .	81
<b>P Multiple-Criteria Decision Analysis</b>	<b>82</b>
<b>VII Appendices of Phase III</b>	<b>84</b>
<b>Q Yearly Extreme Discharge Data Shonai River (1960-2016)</b>	<b>85</b>
<b>R Calculation of discharge values</b>	<b>86</b>
R.1 Design discharge. . . . .	86
R.1.1 Extreme value analysis . . . . .	86
R.1.2 Effect of climate change . . . . .	90
R.2 Discharge capacity. . . . .	91
R.2.1 Cross-sectional profile . . . . .	91
R.2.2 Bed characteristics . . . . .	92
R.2.3 Single flood characteristics . . . . .	92
R.2.4 Design capacity . . . . .	92
R.3 Discharge capacity new structure . . . . .	94

<b>S</b>	<b>Soil characteristics</b>	<b>95</b>
<b>T</b>	<b>Design calculation of bypass tunnel</b>	<b>98</b>
	T.1 Bored Tunnel . . . . .	98
	T.1.1 Calculation of required dimensions using Chézy . . . . .	98
	T.1.2 Calculation of required dimensions . . . . .	98
	T.1.3 Depth of tunnel . . . . .	100
	T.1.4 Calculation of forces and strength of concrete lining . . . . .	101
	T.2 Pneumatic caisson tunnel . . . . .	102
	T.2.1 Calculation of required dimensions using energy loss . . . . .	102
	T.2.2 Depth of caisson . . . . .	103
	T.2.3 Structural analysis . . . . .	104
	T.3 In-situ tunnel . . . . .	107
	T.3.1 Calculation of required dimensions . . . . .	107
<b>U</b>	<b>Design calculations of Shinkansen bridge</b>	<b>108</b>
	U.1 Effect of reducing piers . . . . .	108
	U.2 Common Shinkansen bridges . . . . .	108
	U.3 Conceptual design structure . . . . .	109
	U.4 Concrete slab verification . . . . .	109
	U.4.1 Resistance . . . . .	111
	U.5 Steel truss verification . . . . .	112
	U.5.1 Loads . . . . .	113
	U.6 Pier verification . . . . .	116
	U.6.1 Truss-Pier connection . . . . .	118
	U.6.2 Pier . . . . .	119
	U.7 Foundation verification . . . . .	121
	U.8 Discharge capacity with proposed plan . . . . .	124
	U.9 Construction . . . . .	124
<b>V</b>	<b>Concrete slab FEM results</b>	<b>125</b>
<b>W</b>	<b>Calculations of the Shinkansen tunnel</b>	<b>130</b>
	W.1 Buoyancy . . . . .	130
	W.1.1 Bored tunnel . . . . .	130
	W.1.2 Rectangular tunnel . . . . .	130
<b>VIII</b>	<b>Appendices of Phase IV</b>	<b>133</b>
<b>X</b>	<b>Calculation of flow velocity in bypass</b>	<b>134</b>
	X.1 Parameters . . . . .	134
	X.2 Small Losses . . . . .	135
	X.2.1 Inlet . . . . .	135
	X.2.2 Friction in pipe . . . . .	135
	X.2.3 Outlet . . . . .	136
	X.2.4 Discharge in bypass . . . . .	136
	X.3 Flow profile in tunnel . . . . .	136
<b>Y</b>	<b>Effect on river</b>	<b>140</b>
	Y.1 Deriving backwater curve expression . . . . .	140
	Y.2 Deriving cross-sectional parameters . . . . .	141
	Y.3 Backwater magnitude estimation . . . . .	142
<b>Z</b>	<b>Sediment settlement</b>	<b>143</b>
	Z.1 Sediment discharge of Shonai River . . . . .	143
	Z.2 Sediment discharge distribution . . . . .	143
	Z.3 Settling after flood . . . . .	143



<b>AA Morphology and scour protection</b>	<b>145</b>
AA.1 Initial morphological response in river . . . . .	145
AA.2 Scour protection . . . . .	146
AA.2.1 Erosion river . . . . .	146
AA.2.2 Inlet and outlet structure . . . . .	147
<b>AB Creating a bored tunnel</b>	<b>148</b>
AB.1 Type of TBM . . . . .	148
AB.2 Boring steps . . . . .	148
AB.2.1 Step 1: Stability bore shield . . . . .	148
AB.2.2 Step 2: Movement of the TBM . . . . .	150
AB.2.3 Step 3: Placement of the concrete lining . . . . .	150
AB.2.4 Step 4: Grouting the tail void . . . . .	151
AB.3 TBM at the first and last metres . . . . .	151
<b>AC Structural design of tunnel</b>	<b>153</b>
AC.1 Structural design of the tunnel . . . . .	153
<b>AD Use of Plaxis FEM program</b>	<b>155</b>
<b>AE Structural design building pit</b>	<b>169</b>
AE.1 Type of building pit . . . . .	169
AE.2 Dimensions of building pit . . . . .	169
AE.3 Pressure on diaphragm walls . . . . .	171
AE.4 Structural calculations . . . . .	173
AE.4.1 Conventional reinforcement . . . . .	173
AE.4.2 Glass fibre reinforcement . . . . .	174
<b>AF Structural design in- and outlet tube</b>	<b>177</b>
AF.1 Construction process . . . . .	179
AF.2 Structural design . . . . .	179
AF.2.1 Bottom segment . . . . .	180
AF.2.2 One ring - start tube . . . . .	187
AF.2.3 Bottom segment - centre tube . . . . .	192
AF.2.4 One ring - centre tube . . . . .	193
AF.3 Uplift . . . . .	194
<b>AG Design inlet and outlet structure</b>	<b>196</b>
AG.1 Shape . . . . .	196
AG.2 Separation sill . . . . .	197
AG.3 Flow over sill . . . . .	197
AG.4 Construction method . . . . .	198
<b>AH Construction Process</b>	<b>199</b>
AH.1 Construction site . . . . .	199
AH.1.1 Construction process of the construction site, inlet . . . . .	199
AH.1.2 Planning of the construction site, inlet . . . . .	199
AH.1.3 Costs of the construction site, inlet . . . . .	199
AH.1.4 Construction process of the construction site, outlet . . . . .	199
AH.1.5 Planning of the construction site, outlet . . . . .	200
AH.1.6 Costs of the construction site, outlet . . . . .	200
AH.2 Excavation starting and reception shaft . . . . .	201
AH.2.1 Construction process . . . . .	201
AH.2.2 Planning . . . . .	206
AH.2.3 Costs . . . . .	207
AH.3 Bored tunnel . . . . .	208
AH.3.1 Construction process . . . . .	208
AH.3.2 Planning . . . . .	208
AH.3.3 Costs . . . . .	209
AH.3.4 Additional safety measurements . . . . .	209

---

AH.4 In- and outlet tubes . . . . .	.210
AH.4.1 Construction process. . . . .	.210
AH.4.2 Planning . . . . .	.214
AH.4.3 Costs . . . . .	.215
AH.4.4 Additional safety measurements . . . . .	.215
AH.5 Sill and funnel . . . . .	.216
AH.5.1 Construction process. . . . .	.216
AH.5.2 Planning . . . . .	.216
AH.5.3 Costs . . . . .	.216
AH.5.4 Additional safety measurements . . . . .	.216
<b>AI Unit costs</b>	<b>218</b>
<b>AJ Slides of given presentation</b>	<b>220</b>

# List of Figures

1.1	Map of regions and prefectures of Japan . . . . .	3
1.2	Nagoya area maps . . . . .	4
1.1	Tunnel system under Shonai River . . . . .	9
1.2	Options for tunnel inlet . . . . .	10
1.3	Bridges near Biwajima . . . . .	10
1.4	2000 Tokai extreme water levels at Tokaido bridges . . . . .	11
2.1	Probability curve of discharge load and capacity . . . . .	12
3.1	Location of the tunnel underneath Shonai solution . . . . .	14
3.2	Suggestion for the cross-section of the tunnel . . . . .	14
3.3	Concrete lining [15]. A close look give visual to the gaps in the lining where bolts can be installed. These bolts are placed to connect the individual segments to each other . . . . .	15
3.4	cross-section of the two bored tunnels . . . . .	16
3.5	Location of the caisson tunnel underneath populated area . . . . .	17
4.1	Shonai River Shinkansen Bridge . . . . .	18
4.2	Shinkansen bridges with larger spans . . . . .	19
4.3	Conceptual truss layout 3x70m . . . . .	19
5.1	Slope from current rail track level down to tunnel level . . . . .	21
5.2	cross-section of the rectangular tunnel below the river . . . . .	21
5.3	Area map of a new tunnel for the railway. Yellow: Tunnel entrance, Red: Tunnel, Black: Crossing railway, Orange: Main road . . . . .	22
1.1	Location of the bypass . . . . .	25
2.1	Tunnel characteristics . . . . .	27
2.2	Flow velocity inside the tunnel . . . . .	27
2.3	Backwater curve at location of bypass . . . . .	27
2.4	Debris barriers . . . . .	28
2.5	Short term morphological response of the river to the bypass . . . . .	29
3.1	Inlet structure and sill . . . . .	30
3.2	Transition tube inlet and outlet . . . . .	31
3.3	Construction process transition tube. Red parts indicate the step, black dots indicate bolts. . . . .	31
4.1	Overview of modelled soil layer and tunnel (Soil A: Sand, Slightly silty clayey; Soil B: Sand, Greatly silty clayey; Soil C: Sand, Clean moderate; Soil D: Gravel silty solid) . . . . .	32
4.2	Settlement of the area due to construction of the tunnel . . . . .	34
4.3	Rankin scale for settlement damage . . . . .	34
5.1	Left: Structural scheme without underwater concrete floor; Right: Structural scheme with underwater concrete floor . . . . .	37
7.1	Integration with super levee . . . . .	45
A.1	General map of rivers in the Greater Nagoya Area . . . . .	52
A.2	Elevation over distance comparison European and Japanese rivers . . . . .	53
A.3	Monthly average discharge . . . . .	53
A.4	Current state Shonai River protections . . . . .	54



B.1	Map of storm surge tide level and significant wave height in Ise Bay . . . . .	55
B.2	Graph of storm surge tide level . . . . .	56
B.3	Possible place for storm surge barrier . . . . .	56
C.1	Maximum water level offshore at the bay entrance . . . . .	57
C.2	Time lapse of tsunami height for a wave height of 3 m and period of 3000 s . . . . .	58
D.1	Population density . . . . .	59
D.2	Land use of the Nagoya area . . . . .	60
E.1	Sections of the Shonai River . . . . .	61
F.1	Locations of the coastlines belonging to Mie and Aichi prefecture [4] . . . . .	62
F.2	Bathymetry of the Mie coast . . . . .	63
F.3	Bathymetry of the Aichi coast . . . . .	63
F.4	Ise bay bathymetry . . . . .	64
G.1	Earthquake of 2011 . . . . .	65
I.1	Current Inlet structure at Shonai River . . . . .	68
J.1	Rough sketch of new situation with covered Shin river (dimension are not to scale) . . . . .	71
K.1	Bridges across the Shonai River at Biwajima . . . . .	72
K.2	Option to build a canal within the dikes . . . . .	73
K.3	Possible trajectories of bypass canals . . . . .	73
L.1	Locations of the dams and of the Shonai River . . . . .	74
M.1	Possible dam locations . . . . .	76
N.1	Use of Yamasaki River to diverge discharge . . . . .	79
O.1	Flood discharge diversion by converting metro tunnels to drainage pipes . . . . .	80
O.2	Flood discharge diversion by converting tunnels to drainage pipes . . . . .	81
R.1	Yearly maximum discharge . . . . .	86
R.2	Discharge probability of exceedance curve for several distributions . . . . .	87
R.3	Discharge probability of exceedance curve with upper and lower boundaries . . . . .	89
R.4	Average discharge per month at present and at the end of the 21 <sup>st</sup> century . . . . .	90
R.5	Increasing fluctuation of the annual precipitation in Japan [71] . . . . .	91
R.6	cross-section at bridges . . . . .	91
R.7	Distance between Biwajima and Tokaido bridges . . . . .	92
R.8	Discharge over time of single flood . . . . .	93
R.9	Probability curve of discharge capacity . . . . .	94
R.10	Probability curve of discharge load and capacity . . . . .	94
R.11	Limit state probability curve . . . . .	94
T.1	Principle of buoyancy of the tunnel . . . . .	100
U.1	Shinkansen bridges with larger spans . . . . .	109
U.2	Conceptual truss layout 3x70 m . . . . .	109
U.3	Loads on bridge. Red: wheel loads. Brown: rail track load. Entire concrete slab is loaded by self-weight. . . . .	111
U.4	Moment-distribution graphs . . . . .	111
U.5	Shear-distribution graphs . . . . .	112
U.6	Maximum allowed deflection of high speed train bridges . . . . .	113
U.7	Truss profile . . . . .	114
U.8	Support reactions of truss design . . . . .	116

U.9	Design bridge pier - structure . . . . .	117
U.10	Connection truss to pier . . . . .	118
U.11	Load schematisation bridge pier . . . . .	119
U.12	Design bridge pier, foundation . . . . .	121
U.13	Total load on foundation . . . . .	122
V.1	$m_{xx}$ distribution graph . . . . .	125
V.2	$m_{yy}$ distribution graph . . . . .	126
V.3	$m_{xy}$ distribution graph . . . . .	127
V.4	$\nu_{xx}$ distribution graph . . . . .	128
V.5	$\nu_{yy}$ distribution graph . . . . .	129
W.1	Principle of buoyancy of the tunnel . . . . .	131
W.2	cross-section of the rectangular tunnel below the river . . . . .	131
X.1	Longitudinal profile of velocity in the tunnel. Left: 1D velocity profile at a certain location in the tunnel, right: velocity profile along the tunnel axis . . . . .	137
X.2	Velocity in stream wise direction at the turbulent boundary layer . . . . .	138
X.3	Velocity distribution in the cross-section of the tunnel . . . . .	139
Y.1	Momentum balance of a river . . . . .	140
Y.2	Backwater curve at location of bypass . . . . .	142
Y.3	Derivative of cross-sectional area . . . . .	142
AA.1	Initial morphological response during a flood when using the bypass . . . . .	146
AA.2	Development of scour depth over time . . . . .	146
AA.3	Recreational use of inlet and outlet structure . . . . .	147
AB.1	Front of TBM, with principle of face stability [13] . . . . .	149
AB.2	Slide of lecture by dr. ir. W. Broere . . . . .	149
AB.3	Pressure distributions in soil . . . . .	150
AB.4	Full ring of tunnel segments . . . . .	151
AB.5	Grouting the void behind the tail . . . . .	152
AD.1	Project properties . . . . .	155
AD.2	Soil data: Sand, Slightly silty clayey . . . . .	156
AD.3	Soil data: Sand, Slightly silty clayey . . . . .	157
AD.4	Soil data: Sand, Greatly silty clayey . . . . .	157
AD.5	Soil data: Sand, Greatly silty clayey . . . . .	158
AD.6	Soil data: Sand, Clean moderate . . . . .	158
AD.7	Soil data: Sand, Clean moderate . . . . .	159
AD.8	Soil data: Gravel, slightly silty solid . . . . .	159
AD.9	Soil data: Gravel, slightly silty solid . . . . .	160
AD.10	Left: coordinates of Line load; Right: Value of line load . . . . .	160
AD.11	Loads given by trains . . . . .	161
AD.12	Left tunnel coordinates input . . . . .	161
AD.13	Left tunnel segment input . . . . .	162
AD.14	Tunnel lining input . . . . .	162
AD.15	Left tunnel properties input . . . . .	163
AD.16	Right tunnel coordinates . . . . .	163
AD.17	Right tunnel segment input . . . . .	164
AD.18	Right tunnel properties input . . . . .	164
AD.19	Mesh settings . . . . .	165
AD.20	Cross view of excavated tunnel . . . . .	165
AD.21	Left: General soil conditions phase 1; Right: Conditions of excavated soil phase 1 . . . . .	166
AD.22	Left: Tunnel lining conditions phase 1; Right: General soil conditions phase 2; . . . . .	166
AD.23	Left: Conditions of excavated soil phase 2 ; Right: Tunnel lining conditions phase 2; . . . . .	167

AD.24	Left: General soil conditions phase 3; Right: Conditions of excavated soil phase 3 . . . . .	167
AD.25	Left: Tunnel lining conditions phase 3; Right: General soil conditions phase 4; . . . . .	168
AD.26	Left: Conditions of excavated soil phase 4 ; Right: Tunnel lining conditions phase 4; . . . . .	168
AE.1	Starting structure of TBM in the starting shaft . . . . .	170
AE.2	Width dimensions of building pit . . . . .	170
AE1	Transition tube surface to tunnel . . . . .	177
AE2	Sketches tube ring and curvature . . . . .	177
AE3	Sketches individual segments . . . . .	178
AE4	Construction process transition tube. Red parts indicate the step, black dots indicate bolts. . . . .	179
AE5	Situations checked on strength . . . . .	179
AE6	Bottom segment bending moment model . . . . .	180
AE7	Bottom segment - start tube, Mxx . . . . .	181
AE8	Bottom segment - start tube, Myy . . . . .	181
AE9	Bottom segment - start tube, Mxy . . . . .	181
AE10	Bottom segment - start tube, X displacements . . . . .	182
AE11	Bottom segment - start tube, Y displacements . . . . .	182
AE12	Bottom segment - start tube, Z displacements . . . . .	182
AE13	Bottom segment connection model . . . . .	184
AE14	Bottom segment - start tube, reaction forces X direction . . . . .	184
AE15	Bottom segment - start tube, reaction forces Y direction . . . . .	185
AE16	Bottom segment - start tube, reaction forces Z direction . . . . .	185
AE17	Bottom segment - start tube, principle stresses . . . . .	185
AE18	Bottom segment bending moment model . . . . .	187
AE19	One ring - start tube, Mxx . . . . .	188
AE20	One ring - start tube, Myy . . . . .	188
AE21	One ring - start tube, Mxy . . . . .	188
AE22	One ring - start tube, X displacements . . . . .	189
AE23	One ring - start tube, Y displacements . . . . .	189
AE24	One ring - start tube, Z displacements . . . . .	189
AE25	One ring connection model . . . . .	190
AE26	Bottom segment - start tube, reaction forces X direction . . . . .	191
AE27	Bottom segment - start tube, reaction forces Y direction . . . . .	191
AE28	Bottom segment - start tube, reaction forces Z direction . . . . .	191
AE29	Bottom segment - start tube, principle stresses . . . . .	192
AE30	Rotation reaction forces . . . . .	193
AE31	Load scheme uplift . . . . .	194
AG.1	Outline of inlet/outlet structure . . . . .	196
AG.2	Sill of inlet/outlet structure . . . . .	197
AG.3	Dimensions of inlet/outlet structure . . . . .	197
AG.4	Flow profile over the sill . . . . .	198
AH.1	Area of building site Inlet . . . . .	200
AH.2	Area of building site outlet . . . . .	201
AH.3	Phase 0, clear construction site, installations installed . . . . .	202
AH.4	Phase 1, placing conducting structures . . . . .	202
AH.5	Phase 2, constructing diaphragm walls . . . . .	203
AH.6	Steps to create a diaphragm wall . . . . .	203
AH.7	Phase 3, excavating the pit . . . . .	203
AH.8	Phase 4, installing first wall anchor row . . . . .	204
AH.9	Phase 5, excavating the pit . . . . .	204
AH.10	Phase 6, installing second wall anchor row . . . . .	205
AH.11	Phase 7, excavating the pit . . . . .	205
AH.12	Phase 8, installing third wall anchor row . . . . .	205
AH.13	Phase 9, installing tension piles . . . . .	205



---

AH.14 Phase 10, installing UWC . . . . .	206
AH.15 Phase 11, anchoring the walls . . . . .	206
AH.16 Transition tube surface to tunnel . . . . .	210
AH.17 Construction process transition tube. Red parts indicate construction steps. . . . .	210
AH.18 Top view construction site . . . . .	211
AH.19 Lowering of concrete segments tube . . . . .	211
AH.20 Connection segment to crane . . . . .	212
AH.21 Backfilling process . . . . .	212
AH.22 Backfilling process . . . . .	213
AH.23 Part tube to be removed indicated in red . . . . .	213
AH.24 Epoxy spray equipment . . . . .	214

# List of Tables

1.1	MCDA of different masterplans . . . . .	7
2.1	Distributions of the used parameters . . . . .	12
3.1	Maximal forces at the end of the caisson elements . . . . .	16
3.2	Forces at the maximal bending moment in between the ends of the caisson elements . . . . .	17
4.1	Internal forces within concrete lining . . . . .	33
5.1	Building pit dimensions . . . . .	35
5.2	Different types of building pits . . . . .	35
5.3	Building pit dimensions . . . . .	36
5.4	Left: Height of the anchors; Right: Internal forces . . . . .	36
5.5	Dimensions of reinforcement in cross-sections . . . . .	37
6.1	Construction phases inlet structure, pre-boring . . . . .	38
6.2	Construction phases outlet structure, pre-boring . . . . .	38
6.3	Construction phases tunnel boring . . . . .	39
6.4	Construction phases outlet structure, post-boring . . . . .	39
6.5	Construction phases inlet structure, post-boring . . . . .	39
7.1	Summary of project costs. Conversion of 1 EUR = 130 YEN. . . . .	43
A.1	Years of flooding with affected houses per river . . . . .	54
G.1	JMA Seismic Intensity Scale . . . . .	65
P1	MCDA of different masterplans . . . . .	82
P2	MCDA of different masterplans . . . . .	83
Q.1	Yearly Extreme Discharge Data Shonai River . . . . .	85
R.1	Manning values for individual materials . . . . .	92
R.2	Discharge, water depth, area and wetted perimeter . . . . .	93
R.3	Distributions of the used parameters . . . . .	94
S.1	Characteristics of subsoil . . . . .	95
T.1	Dimensions of the bored tunnel . . . . .	99
T.2	Dimensions of a pneumatic caisson tunnel . . . . .	103
T.3	Reinforcement calculations at the element ends . . . . .	106
T.4	Reinforcement calculations at the location of the maximum bending moment between the element ends . . . . .	106
U.1	Cross-sectional characteristics of proposed 3x70 span bridge . . . . .	108
U.2	Loads taken into account . . . . .	110
U.3	Resulting bending moments concrete slab using beam theory . . . . .	112
U.4	Parameters bending moment capacity concrete slab . . . . .	113
U.5	Parameters bending moment capacity concrete slab . . . . .	113
U.6	Extreme truss elements . . . . .	114
U.7	Parameters truss-pier connection calculations . . . . .	118
U.8	Parameters bridge pier calculations, strength criterion . . . . .	119
U.9	Parameters bridge pier calculations, slenderness criterion . . . . .	120

U.10	Parameters bridge foundation . . . . .	122
U.11	Cross-sectional characteristics of proposed 3x70 m span bridge . . . . .	124
X.1	Description of the used parameters . . . . .	134
AC.1	Internal forces within concrete lining . . . . .	153
AD.1	Characteristics of subsoil . . . . .	156
AE.1	Different types of building pits . . . . .	169
AE.2	Active soil along the diaphragm wall . . . . .	172
AE.3	Table for bending moment for glass fibre reinforcement . . . . .	176
AE1	Parameters Diana FEA tube models . . . . .	180
AE2	Bending moments - start tube, bottom segment . . . . .	183
AE3	Parameters bottom segment bending capacity . . . . .	183
AE4	Bending moments and capacities bottom segment - start tube . . . . .	183
AE5	Bottom segment - start tube, centre coordinates bolt groups, with origin in the centre of the tube. . . . .	184
AE6	Reaction force components per connection. X and Z are perpendicular to shaft, Y is parallel to the shaft. . . . .	186
AE7	Parameters bolted connection . . . . .	186
AE8	Bending moments - start tube, one ring . . . . .	190
AE9	Bottom segment - start tube, centre coordinates bolt groups, with origin in the centre of the tube. . . . .	190
AE10	Reaction force components per connection . . . . .	192
AE11	Reaction force components per connection . . . . .	193
AE12	Reaction force components per connection . . . . .	193
AE13	Parameters transition tube uplift . . . . .	194
AE14	Volumes bodies for uplift . . . . .	194
AE15	Selfweight and uplift forces . . . . .	195
AG.1	Grid characteristics of the sill model . . . . .	198
AH.1	Dimensions of temporary dike . . . . .	200
AH.2	Construction phases excavation pit inlet . . . . .	207
AH.3	Construction phases excavation pit outlet . . . . .	207
AH.4	Total equipment costs . . . . .	207
AH.5	Total material costs . . . . .	207
AH.6	Construction phases tunnel boring . . . . .	208
AH.7	Tunneling costs of several TBM diameters. Costs in €, x1000 . . . . .	209
AH.8	Construction planning outlet tube . . . . .	214
AH.9	Construction planning inlet tube . . . . .	214
AH.10	Costs of tube construction and finishing tunnel. For sources of cost rates, see appendix AI. . . . .	215
AH.11	Construction phases sill and funnel, outlet side . . . . .	217
AH.12	Construction phases sill and funnel, inlet side . . . . .	217
AH.13	Costs of sill and funnel. For sources of cost rates, see appendix AI. . . . .	217
AI.1	Cost per unit . . . . .	219

# List of Symbols

## Latin characters

$A$	=	Cross-sectional area	[m <sup>2</sup> ]
	=	Creep factor	[-]
$A_{4400}$	=	Cross-sectional area; discharge of 4400 m <sup>3</sup> /s	[m <sup>2</sup> ]
$A_{gl}$	=	Area of glass fibre reinforcement	[m <sup>2</sup> ]
$A_i$	=	Cross-sectional area of location i	[m <sup>2</sup> ]
$A_{i+1}$	=	Cross-sectional area after location i	[m <sup>2</sup> ]
$A_{i-1}$	=	Cross-sectional area before location i	[m <sup>2</sup> ]
$A_s$	=	Area of reinforcement	[m <sup>2</sup> ]
	=	Shaft cross-sectional area	[m <sup>2</sup> ]
$A_{shearrein.}$	=	Area of shear reinforcement	[m <sup>2</sup> ]
$A_{sw}$	=	Cross-sectional area of reinforcement per meter	[m <sup>2</sup> /m]
$b$	=	Width	[m]
$B$	=	Cross-sectional width	[m]
	=	Reinforcement factor	[-]
	=	Ballast	[N]
$B_1$	=	Cross-sectional width at location 1	[m]
$B_2$	=	Cross-sectional width at location 2	[m]
$B_{4400}$	=	Cross-sectional width; discharge of 4400 m <sup>3</sup> /s	[m]
$B_{bypass}$	=	Cross-sectional width of bypass	[m]
$B_{river}$	=	Cross-sectional width of river	[m]
$c$	=	Concrete cover thickness	[m]
$c_b$	=	Sediment concentration at the bed	[-]
$c_f$	=	Skin friction coefficient	[-]
$C$	=	Chézy coefficient	[m <sup>1/2</sup> /s]
	=	End bending moments factor	[-]
$CDF$	=	Cumulative distribution function	[-]
$CDF_{exp}$	=	Cumulative exponential distribution function	[-]
$CDF_{gum}$	=	Cumulative Gumbel distribution function	[-]
$CDF_{wei}$	=	Cumulative Weibull distribution function	[-]
$C_{n0}$	=	Dudeck's factor normal force lining bored tunnel	[-]
$C_{n2}$	=	Dudeck's factor normal force lining bored tunnel	[-]
$C_m$	=	Dudeck's factor bending moment lining bored tunnel	[-]
$d$	=	Water depth	[m]
	=	Effective concrete height	[m]
	=	Embedded depth foundation	[m]
$d_e$	=	Equilibrium water depth	[m]
$d_{50}$	=	Median particle diameter	[m]
$D$	=	Diameter	[m]
$D_h$	=	Hydraulic diameter	[m]
$E_{concrete}$	=	Elasticity modulus concrete	[N/m <sup>2</sup> ]
$E_s$	=	Elasticity modulus	[N/m <sup>2</sup> ]
$E_{soil}$	=	Elasticity modulus soil	[N/m <sup>2</sup> ]
$E_{gl}$	=	Elasticity modulus glass fibre	[N/m <sup>2</sup> ]
$f$	=	Friction factor	[-]
	=	Yield stress	[N/m <sup>2</sup> ]
$f_{cd}$	=	Concrete yield stress design value	[N/m <sup>2</sup> ]
$f_{ck}$	=	Concrete yield stress characteristic value	[N/m <sup>2</sup> ]
$f_{ct,0.05}$	=	Characteristic axial tensile strength of concrete	[N/m <sup>2</sup> ]
$f_{ctd}$	=	Design value axial tensile strength of concrete	[N/m <sup>2</sup> ]

$f_{ctk,0.05}$	=	5 % Fractile axial tensile strength of concrete	[N/m <sup>2</sup> ]
$f_{ub}$	=	Ultimate tensile strength	[N/m <sup>2</sup> ]
$f_{yd}$	=	Steel yield stress design value	[N/m <sup>2</sup> ]
$f_{yk}$	=	Steel yield stress characteristic value	[N/m <sup>2</sup> ]
$F$	=	Force	[N]
$F_f$	=	Force by friction	[N]
$F_g$	=	Force by gravity	[N]
$F_{p,1}$	=	Momentum pressure force on side 1	[N]
$F_{p,2}$	=	Momentum pressure force on side 2	[N]
$F_{support}$	=	Support reaction force	[N]
$F_{soil}$	=	Force by soil	[N]
$F_E$	=	Reaction force on connection	[N]
$F_{Ed}$	=	Design value of reaction force on connection	[N]
$F_{t,Ed}$	=	Design value of tensile force per joint	[N]
$F_{t,Rd}$	=	Design value of tensile resistance per joint	[N]
$F_v$	=	Vertical force	[N]
$F_{v,Ed}$	=	Design value of shear force per joint	[N]
$F_{v,Rd}$	=	Design value of shear resistance per joint	[N]
$F_{x,E}$	=	Force in x-direction	[N]
$F_{x,Ed}$	=	Design value of the force in x-direction	[N]
$F_{y,E}$	=	Force in y-direction	[N]
$F_{y,Ed}$	=	Design value of the force in y-direction	[N]
$F_{z,E}$	=	Force in z-direction	[N]
$F_{z,Ed}$	=	Design value of the force in z-direction	[N]
$F_{wheel}$	=	Point force by Bullet train wheel	[N]
$F_{up}$	=	Upward water force	[N]
$g$	=	Gravitational constant	[m/s <sup>2</sup> ]
$G$	=	Own weight	[N]
$h$	=	Height	[m]
$h_0$	=	Original water depth	[m]
$h_s$	=	Scour depth	[m]
$H_b$	=	Bend energy loss	[m]
$H_{cont}$	=	Contraction energy loss	[m]
$H_f$	=	Friction energy loss	[m]
$H_{inlet}$	=	Inlet energy loss	[m]
$H_{mix}$	=	Mixing energy loss	[m]
$H_{outlet}$	=	Outlet energy loss	[m]
$H_{sep}$	=	Seperation energy loss	[m]
$H_t$	=	Transition energy loss	[m]
$H_{total}$	=	Total energy loss	[m]
$i$	=	Buckling radius of gyration	[-]
	=	MCDA masterplan number	[-]
	=	Water surface gradient in uniform flow	[-]
$i_b$	=	Bed slope	[-]
$I_{cr}$	=	Critical direction second moment of inertia	[m <sup>4</sup> ]
$j$	=	MCDA criteria number	[-]
$k$	=	Sediment - discharge distribution factor	[-]
	=	Strickler coefficient	[m <sup>1/3</sup> /s]
	=	Dimension parameter for shear capacity	[-]
$k_2$	=	Shear resistance factor	[-]
$k_h$	=	Parameter for shear stress	[-]
$k_s$	=	Roughness height	[m]
$k_x$	=	Multiplication factor	[-]
$k_z$	=	Multiplication factor	[-]
$k_\lambda$	=	Parameter for shear stress	[-]
$K_0$	=	Neutral soil stress factor	[-]



$K_a$	=	Active soil stress factor	[-]
$K_e$	=	Head loss coefficient in entrance	[-]
$K_b$	=	Head loss coefficient in bend	[-]
$K_{cont}$	=	Head loss coefficient for contraction	[-]
$K_s$	=	Horizontal soil pressure coefficient	[-]
$K_E$	=	Head loss coefficient in expansion	[-]
$l$	=	Step-length	[m]
$L$	=	Length	[m]
$L_{buc}$	=	Buckling length	[m]
$m$	=	Embankment slope ratio	[-]
	=	Engelund-Hansen coefficient	[/]
$M$	=	Bending moment	[Nm]
$M_{Ed}$	=	Bending moment load design value	[Nm]
$M_{Rd}$	=	Bending moment resistance design value	[Nm]
$M_u$	=	Bending moment resistance	[Nm]
$M_{xx}$	=	Bending moment in xx direction	[Nm]
$M_{yy}$	=	Bending moment in yy direction	[Nm]
$n$	=	Engelund-Hansen coefficient	[-]
	=	Number of options	[-]
	=	Number of tunnels	[-]
	=	Number of bolts	[-]
	=	Manning's roughness coefficient	[s/m <sup>1/3</sup> ]
	=	Ratio load and resistance force	[-]
$n_{bars}$	=	Number of steel bars	[-]
$n_{wheels}$	=	Number of train wheels	[-]
$N$	=	Normal force	[N]
$N_c$	=	Normal force in concrete	[N]
$N_{cr}$	=	Critical buckling force	[N]
$N_q$	=	Bearing capacity factor for soil coverage	[-]
$N_s$	=	Normal force in steel	[N]
$N_{Ed}$	=	Normal force load design value	[N]
$N_{Rd}$	=	Normal force resistance design value	[N]
$N_\gamma$	=	Bearing capacity factor for self-weight	[-]
$p'_{max}$	=	Bearing capacity	[kPa]
$P$	=	Wetted cross-sectional perimeter	[m]
$P_{4400}$	=	Wetted cross-sectional perimeter; discharge of 4400 m <sup>3</sup> /s	[m]
$P_{water}$	=	Water pressure	[kPa]
$q$	=	Specific discharge	[m <sup>2</sup> /s]
$q_{track}$	=	Rail track load	[N/m]
$q_s$	=	Specific sediment discharge	[m <sup>2</sup> /s]
$Q$	=	Discharge	[m <sup>3</sup> /s]
$Q_1$	=	Discharge at location 1	[m <sup>3</sup> /s]
$Q_2$	=	Discharge at location 2	[m <sup>3</sup> /s]
$Q_{1/200}$	=	Discharge probability of exceedance of 1/200	[m <sup>3</sup> /s]
$Q_{1/200,exp}$	=	Discharge exponential probability of exceedance of 1/200	[m <sup>3</sup> /s]
$Q_{1/200,gum}$	=	Discharge Gumbel probability of exceedance of 1/200	[m <sup>3</sup> /s]
$Q_{1/200,wei}$	=	Discharge Weibull probability of exceedance of 1/200	[m <sup>3</sup> /s]
$Q_{bypass}$	=	Discharge of the bypass	[m <sup>3</sup> /s]
$Q_{plate}$	=	Distributed load by weight of concrete plate	[N/m <sup>2</sup> ]
$Q_{O,1}$	=	Momentum of discharge on side 1	[m <sup>3</sup> /s]
$Q_{O,2}$	=	Momentum of discharge on side 2	[m <sup>3</sup> /s]
$Q_{rail}$	=	Distributed load by weight of rails	[N/m <sup>2</sup> ]
$Q_{river}$	=	Discharge of the river	[m <sup>3</sup> /s]
$Q_s$	=	Sediment discharge	[m <sup>3</sup> /s]
$Q_{s,bypass}$	=	Sediment discharge through bypass	[m <sup>3</sup> /s]
$Q_{s,river}$	=	Sediment discharge through river	[m <sup>3</sup> /s]

$Q_{s,total}$	=	Sediment discharge total	[m <sup>3</sup> /s]
$Q_u$	=	Uniform discharge	[m <sup>3</sup> /s]
$r$	=	Radius	[m]
	=	Distance from circle centre	[m]
	=	Turbulent fluctuation	[-]
$r_0$	=	Maximum distance from circle centre / radius	[m]
$R$	=	Hydraulic radius	[m]
$Re$	=	Reynolds number	[-]
$s$	=	Distance	[m]
$s_q$	=	Shape factor for soil coverage	[-]
$s_\gamma$	=	Shape factor for self-weight	[-]
$S_f$	=	Friction slope	[-]
$S_i$	=	MCDA total score for masterplan i	[-]
$S_{i,j}$	=	MCDA masterplan i criteria score for criteria j	[-]
$t$	=	Thickness	[m]
	=	Time	[s]
$u$	=	Flow velocity	[m/s]
$\bar{u}$	=	Time averaged flow velocity	[m/s]
$u_0$	=	Mean flow velocity	[m/s]
$\bar{u}_c$	=	Average critical flow velocity	[m/s]
$u_{max}$	=	Maximum flow velocity	[m/s]
$u_{river}$	=	Flow velocity river	[m/s]
$u_*$	=	Shear velocity	[m/s]
$u.c.$	=	Unity check	[-]
$V$	=	Shear force	[N]
	=	Volume	[m <sup>3</sup> ]
$V_{ballast}$	=	Volume of ballast	[m <sup>3</sup> ]
$V_{Ed}$	=	Shear force	[N]
$V_{Rd}$	=	Shear capacity	[N]
$V_{Rd,c}$	=	Shear capacity concrete	[N]
$V_{Rd,c,min}$	=	Minimum shear capacity concrete	[N]
$V_{Rd,s}$	=	Shear capacity reinforcement	[N]
$V_{soil}$	=	Soil volume above tunnel	[m <sup>3</sup> ]
$w$	=	Concrete section width	[m]
	=	Width of the tunnel	[m]
$w_j$	=	MCDA weight factor for criteria j	[-]
$W_{yy}$	=	Section modulus in yy-direction	[m <sup>3</sup> /m]
$x$	=	Distance	[m]
$x_u$	=	Concrete compressive zone height	[m]
$y$	=	Surface elevation from average river bed	[m]
$z_b$	=	Elevation of bed level	[m]
$z$	=	Distance reinforcement and centre of compressive zone	[m]

## Greek characters

$\alpha$	=	Shape factor area compressive zone	[-]
	=	Buckling imperfection factor	[-]
	=	Amplification factor for velocity	[-]
	=	Relative flexural rigidity lining bored tunnel	[-]
$\alpha_{cw}$	=	Shear capacity with reinforcement coefficient	[-]
$\alpha_{exp}$	=	Exponential distribution parameter	[-]
$\alpha_v$	=	Tensile resistance factor	[-]
$\alpha_{wei}$	=	Weibull distribution parameter	[-]
$\beta$	=	Number of standard deviation in mean	[-]
	=	Shape factor compressive zone	[-]
	=	Velocity profile factor	[-]
	=	Gumbel distribution parameter	[-]
	=	Relative ring rigidity lining bored tunnel	[-]
$\gamma$	=	Material factor	[-]
$\gamma_{ballast}$	=	Specific weight ballast	[kN/m <sup>3</sup> ]
$\gamma_c$	=	Material factor of concrete	[-]
$\gamma_{concrete}$	=	Specific weight concrete	[kN/m <sup>3</sup> ]
$\gamma_s$	=	Material factor of steel	[-]
$\gamma_{sat}$	=	Saturated specific weight	[kN/m <sup>3</sup> ]
$\gamma'_{soil}$	=	Effective weight of soil	[kN/m <sup>3</sup> ]
$\gamma_{unsat}$	=	Unsaturated specific weight	[kN/m <sup>3</sup> ]
$\gamma_{water}$	=	Specific weight water	[kN/m <sup>3</sup> ]
$\gamma_{M2}$	=	Material factor steel connections	[-]
$\delta$	=	Angle of internal friction	[°]
$\Delta$	=	Relative density	[-]
$\theta$	=	Angle of reinforcement	[°]
$\kappa$	=	Von Karman constant	[-]
$\lambda$	=	Buckling non-dimensional slenderness	[-]
$\lambda_{exp}$	=	Exponential distribution parameter	[-]
$\lambda_{wei}$	=	Weibull distribution parameter	[-]
$\mu$	=	Mean value of normal distribution	[/]
	=	Gumbel distribution parameter	[-]
$\nu$	=	Kinematic viscosity	[m <sup>2</sup> /s]
$\rho$	=	Density	[kg/m <sup>3</sup> ]
	=	Reinforcement ratio	[%]
$\sigma$	=	Stress	[N/m <sup>2</sup> ]
	=	Standard deviation of normal distribution	[/]
$\sigma_{cp}$	=	Compressive stress	[N/m <sup>2</sup> ]
$\sigma_h$	=	Horizontal stress	[N/m <sup>2</sup> ]
$\sigma'_h$	=	Horizontal effective stress	[N/m <sup>2</sup> ]
$\sigma_v$	=	Vertical stress	[N/m <sup>2</sup> ]
$\sigma'_v$	=	Vertical effective stress	[N/m <sup>2</sup> ]
$\tau_0$	=	Wall shear stress	[N/m <sup>2</sup> ]
$\tau_1$	=	Allowable stress in concrete	[N/m <sup>2</sup> ]
$\tau_d$	=	Concrete shear stress	[N/m <sup>2</sup> ]
$\tau_{gl}$	=	Allowable stress in glass fibre shear reinforcement	[N/m <sup>2</sup> ]
$\Phi$	=	Buckling parameter	[-]
$\Phi'$	=	Internal friction angle	[°]
$\chi$	=	Buckling reduction factor	[-]
$\omega_{gl}$	=	Ratio of glass fibre reinforcement	[%]

## Special characters

$\emptyset$	=	Diameter	[m]
-------------	---	----------	-----

# Introduction

Japan is a country well known for its natural disasters. With an average of 26 typhoons per year and normal heavy rain, rainfall can cause frequent and severe flooding of rivers. The Shonai River in Nagoya is one of these rivers that often reaches flood levels. Although the average discharge on this river is only  $25 \text{ m}^3/\text{s}$ , peak discharge can be more than 100 times as large. The  $3489 \text{ m}^3/\text{s}$  flood in the year 2000 (Heisei 12) resulted in massive damage in Nagoya and neighbouring areas. Because of this, river management has decided to upgrade their river defence system to meet a probability of flooding of once every 200 years. In the past 18 years, embankments have been improved on many locations. However, one essential location has had no improvements at the time of writing, creating a bottleneck during peak discharge. This bottleneck is trapped by four bridges, one of them supporting the railway of the famous Tokaido Shinkansen bullet train, the busiest railway of Japan. Widening of this cross-section or enlarging of the embankments is prohibited by the supports of the bridges. This results in a problem, since improvement of the discharge capacity is necessary. Therefore, this report will answer the following problem statement:

***How can the discharge capacity of the Shonai River be improved to modern standards?***

The answer to this question will be found using an investigation with multiple phases. Phase I focuses on Nagoya metropolitan area and identifies whether the water defence system is most vulnerable on sea-side, bay-side, or river-side. Phase II analyses seven possible solutions to improve the discharge in the Shonai River. Most try to mitigate the problem by reducing the discharge at the vital location. An Multiple-Criteria Decision Analysis showed which option shall be analysed further to improve the local discharge capacity. Phase III presents different drafts of realising the solution chosen in the previous phase and compares the results. One of the mentioned drafts will be investigated excessively in phase IV. This part will form an alternative master plan for Chubu Regional Development Office to handle the current problems of the Shonai River.

# I

## Phase I: Preparation and investigation

# Investigation of Nagoya area

*This chapter uses appendices A, B, C, D, E, F, G and H.*

This phase covers the preparation done prior to the main subject of this report. Several aspects of the region had been studied, not only to learn about the geography of the area, but also to discover some of the critical points in the local flood safety. Furthermore, this phase has been used to find out about the function of Japanese cultural and social system, concerning flood safety.

## 1.1. Project location

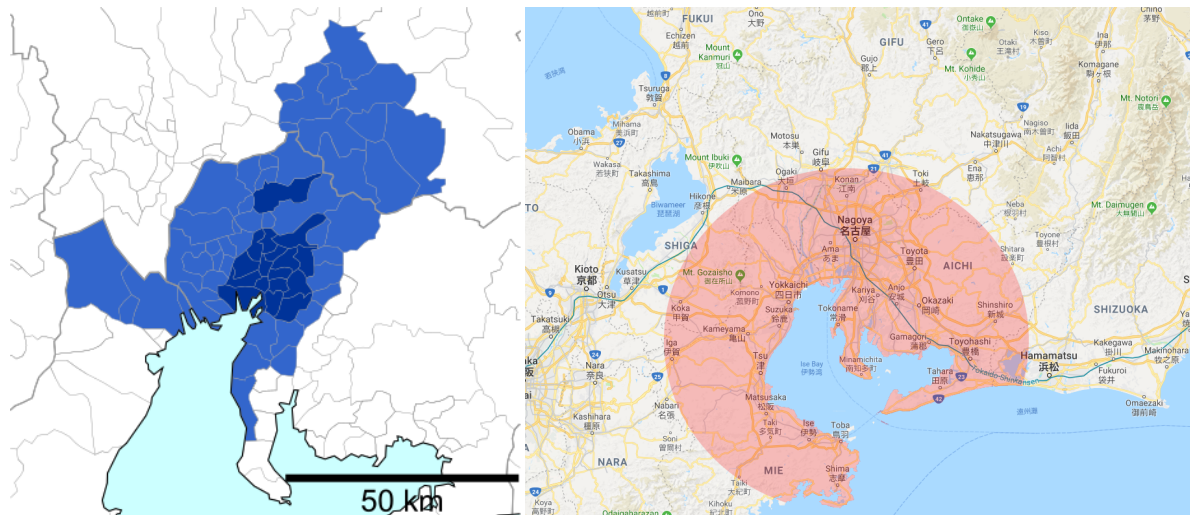
Japan is a country which is split into eight different regions, roughly dividing the country based on culture. Although regions do not have an official administrative unit, they are used for grouping areas. The eight regions are indicated with colours in figure 1.1. This report will primarily focus on the Chubu region, which is indicated in cyan. The large rivers in Japan, called 'Class A rivers', are regulated by regional development bureaus. The catchment area of all Class A rivers combined covers 63 percent [1] of the total area of Japan.



Figure 1.1: Map of regions and prefectures of Japan [2]

The first governmental level below the national level, will be found in the prefectures. Japan has 47 prefectures in total, nine of which are found in Chubu. These prefectures are: Aichi, Fukui, Gifu, Ishikawa, Nagano, Niigata, Shizuoka, Toyama, and Yamanashi. The former, Aichi, is the prefecture which this report will mainly discuss. Neighbouring prefectures like Gifu, Shizuoka and Mie (Kansai region) also play a role in the flood defence system considered in this report. Figure 1.1 indicates all the prefecture in Japan. Governments on a prefecture level take care of the 'Class B rivers', which catchment areas cover 29% of Japan [1].

Nagoya, the city of focus of this report, is the capital of the Aichi prefecture. Although the city-boundaries are defined as indicated in dark blue in figure 1.2a, the metropolitan area, called Chukyo metropolitan area, of the city is significantly larger than that. This metropolitan area has a population of more than 9.3 million, with the city itself having 2.3 million citizens. In this report, 'Nagoya metropolitan area' or 'Nagoya area' will refer to the area surrounding Nagoya and two bays; Ise Bay and Mikawa Bay. The general area has been indicated in figure 1.2b.



(a) Map of Nagoya area [3]

(b) Map of Nagoya metropolitan area [4]

Figure 1.2: Nagoya area maps

## 1.2. Current protection

Appendix A shows an analysis of the many rivers that pass through Nagoya Area. It shows that four of these rivers have flooded often in the past decades. Flood protection standards have been improved and made more strict. However, not all cross-sections have been improved yet. This forms a risk for the flood safety of the city.

Storm surges (see appendix B) and tsunamis (see appendix C) do not form a significant risk for the city of Nagoya. The shape of the bay dampens and mitigates all incoming waves. Additionally, most of the city and its population is located further away from the bay, several meters above sea-level (see appendix D). Only the harbour and the rural area in the west is susceptible for sea-side waves. However, this part of the city has already been protected well. Current bathymetry and protection around the bay and ocean shows to be quite adequate (see appendix F).

Because of what is mentioned above, it has been determined to investigate the flood protection surrounding the rivers in Nagoya. More specifically, the Shonai River will be investigated since this river has had the most severe floods in the past decades.

Appendix G analyses the presence of earthquakes in the region. This data can be used for the simulation of seismic activity. Traditional Japanese building methods have also been investigated and have been elaborated on in appendix H.



# II

## Phase II: Assessment of possible solutions

## Options to improve the Shonai River

*This chapter uses appendices I, J, K, L, M, N, O and P.*

This phase analyses the vulnerable sections of the Shonai River during high discharge. Several solutions are presented to meet the Japanese safety standards and reduce the occurrence of flooding. Specifically, the downstream and middle area of the Shonai River have been considered since this area is most populated and discharge is maximal at this location. The local government is looking at measures to increase the capacity, mainly by reinforcing the dikes and dredging. The local officials have requested to look at alternative solutions to reduce the occurrence of flooding [5]. The following solutions are proposed:

- **Usage of the Shin River plus adaptations:** This solution focuses on using the Shin River as emergency canal. The Shin is a canal that runs parallel to the downstream end of the Shonai and debouches into Ise Bay. With an overflow construction, the water from the Shonai River can be guided to the Shin reducing the discharge in the Shonai downstream of the overflow. In the past this overflow was used, however after a major flood in the Shin this was no longer accepted by the local population. In this solution the flow to the Shin could be controlled by a structure, to regulate the discharge in the canal. Furthermore, additional measurements could be taken to increase flood safety at the Shin itself. The disadvantage of this solution is that it requires space, of which there is little in urban areas. Elaboration of this solution can be found in appendix I.
- **Transforming the Shin into an underground river:** Another option is to cover the Shin with a concrete slab. Just as for the previous option the water from the Shonai will be diverted to the Shin. However, flooding in the Shin cannot occur due to the fact that it is covered. This ensures the safety of the surrounding citizens. The top of the concrete slab will be at street level, leading to only a small reduction in discharge capacity of the Shin. Advantages of this solution are increased safety and the fact that the area above the concrete slab could be used for other purposes. The disadvantage of covering such a long stretch with concrete slabs is that it is likely to be expensive. See appendix J for further elaboration.
- **Improving the bottleneck near Biwajima:** Along the downstream end of the Shonai River, near a place called Biwajima, four bridges span across the river. Three of them are railway bridges of which one for the Shinkansen train, the fourth bridge is used by car traffic. The Shonai River is narrower at this section and widening is limited due to the bridges. Additionally, the bridge piers and decks decrease the local discharge capacity. Thus, the bridges form a bottleneck in the Shonai River. This could be solved by increasing the discharge capacity of the section. A possible solution is to increase the bridge height by replacing the bridges. Another option is to divert the water around the bridges. This could be done by constructing a canal or a tunnel. Appendix K gives a further elaboration on possible solutions to increase the discharge capacity.
- **Use of existing dams upstream:** In the upstream part of the Shonai River some dams are present. Making these dams controllable leads to more control of the Shonai River. This could increase the flood safety. However, the impact of this solution is not large as the capacity of the dams are limited. Appendix L gives further explanation on the solution.

- **Construction of a new dam or weir upstream:** This solution looks at the possibilities of placing a new dam or weir in the upstream reach of the Shonai River. Some possible locations are presented in appendix M. However, the elevations in this region are often not high enough, making it difficult to implement a dam. Additionally, weirs have the disadvantage of increasing the flood probability upstream of the weir. Thus, this is not a proper solution on itself.
- **Construction of new artificial river:** This option looks at creating a new river to divert the water into Ise Bay. A river similar to the Shin will be constructed. The disadvantage of this solution is that current property should be removed. Elaboration of this solution can be found in appendix N.
- **Use of underground metro tunnels:** This option focuses at using existing infrastructure to divert water from the Shonai River. The diversion could be done by using the metro tunnels present in the city. Permanent conversion of the tunnels would lead to closing of the present metro line. Another option is to convert existing tunnels into hybrid tunnels. Here, tunnels are adjusted to be transformed temporarily into drainage pipes. During floods the metro operations would shut down. If there is low discharge, the tunnel could still be used for metros. A disadvantage of using metro tunnels is that the capacity is only limited. Furthermore, it could still be necessary to widen the tunnels, which increase the costs. See appendix O for further elaboration.

After elaboration of the ideas, a Multiple-Criteria Decision Analysis (MCDA) has been used to determine which option will be investigated further. An elaboration on the MCDA is shown in appendix P. The scores of the solutions are shown in table 1.1. It shows that improving the bottleneck near Biwajima has the best potential to improve the flood safety of the river. Phase III will take a deeper look into this concept.

Category	Weight	Shin		Shin covered		Bridge cutoff		Existing dams		New dam		New weir		New river 1		New river 2		Metro perm		Metro temp	
		Rating	Score	Rating	Score	Rating	Score	Rating	Score	Rating	Score	Rating	Score	Rating	Score	Rating	Score	Rating	Score	Rating	Score
Impact on Shonai River	10	9	90	8	80	10	100	1	10	2	20	2	20	3	30	5	50	4	40	4	40
Destruction of area	7	-4	-28	-1	-7	-1	-7	-1	-7	-7	-49	-5	-35	-8	-56	-10	-70	-3	-21	-3	-21
Effect on environment	5	-1	-5	-5	-25	-2	-10	-1	-5	-8	-40	-6	-30	3	15	2	10	0	0	0	0
Additional risks	8	-8	-64	-2	-16	-1	-8	-2	-16	-5	-40	-4	-32	-8	-64	-5	-40	-5	-40	-7	-56
Social obstruction	5	-10	-50	-5	-25	-2	-10	-1	-5	-7	-35	-4	-20	-10	-50	-8	-40	-10	-50	-5	-25
Near important locations	8	0	0	0	0	-2	-16	0	0	-3	-24	-2	-16	-8	-64	0	0	0	0	0	0
Construction hindrance	4	-3	-12	-8	-32	-5	-20	0	0	-6	-24	-5	-20	-8	-32	-8	-32	-6	-24	-8	-32
Aesthetics	3	0	0	7	21	4	12	0	0	0	0	0	0	3	9	2	6	0	0	0	0
Technical feasibility	3	7	21	5	15	6	18	10	30	4	12	5	15	2	6	1	3	6	18	4	12
Required maintenance	5	-4	-20	-4	-20	-4	-20	-2	-10	-4	-20	-3	-15	-4	-20	-4	-20	-3	-15	-6	-30
Costs	8	-5	-40	-8	-64	-3	-24	-2	-16	-8	-64	-5	-40	-9	-72	-10	-80	-8	-64	-9	-72
Future revenue	6	0	0	10	60	0	0	0	0	3	18	0	0	0	0	0	0	-5	-30	0	0
<b>Total</b>			<b>-108</b>		<b>-13</b>		<b>15</b>		<b>-19</b>		<b>-246</b>		<b>-173</b>		<b>-298</b>		<b>-213</b>		<b>-186</b>		<b>-184</b>

Table 1.1: MCDA of different masterplans

# III

## Phase III: Drafts of solutions

## Proposal of different solutions

*This chapter uses appendices J, O and Q.*

Based on the MCDA of the previous phase, it has been decided to look for solutions to solve the bottleneck now posed near Biwajima. Several options have already been provided in the previous phase. In this phase, the following options will be further investigated:

- Bypass tunnel underneath the Shonai
- Replace Tokaido Railway bridges with new ones
- Replace Tokaido Railway bridges with a tunnel

Each solution has been described briefly in this chapter. The next chapter will describe an estimation of the design discharge that fits the set probability of occurrence. In the chapters following afterwards, preliminary designs of the options are presented. These designs were made to estimate the feasibility of the solutions, both structural as hydraulical.

### 1.1. Tunnel underneath the Shonai River

One solution is to dredge the river, but this would decrease the bearing capacity of foundations of the bridges and other nearby structures. Therefore, it has been decided to explore an option where a tunnel is built underneath the Shonai River, starting upstream of the bridges and surfacing just downstream. By doing so, the cross-section of the river is increased locally, increasing the capacity. This solution is similar to the ones provided in appendices J and O.

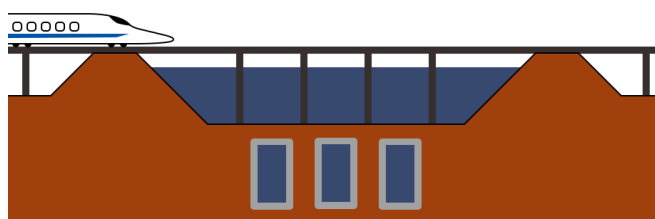


Figure 1.1: Tunnel system under Shonai River

The system consists of the tunnels themselves, an inlet structure upstream of the bridges and an outlet downstream of the bridges. The tunnels run parallel underneath the Shonai until they have passed the bridges. From here, the water goes back into the river again, either gravity driven or by means of pumping. The tunnels can be constructed by means of an in-situ tunnel, a Tunnel Boring Machine, Pneumatic caissons or submerging caissons. The inlet can be made passive or active, referring to whether action is required when high water occurs and allow it to flow into the tunnels. An example of a passive inlet would be a raised hole in the ground, where water would flow into when a certain level is reached. The outlet may consist of a simple opening or a set of pumps.

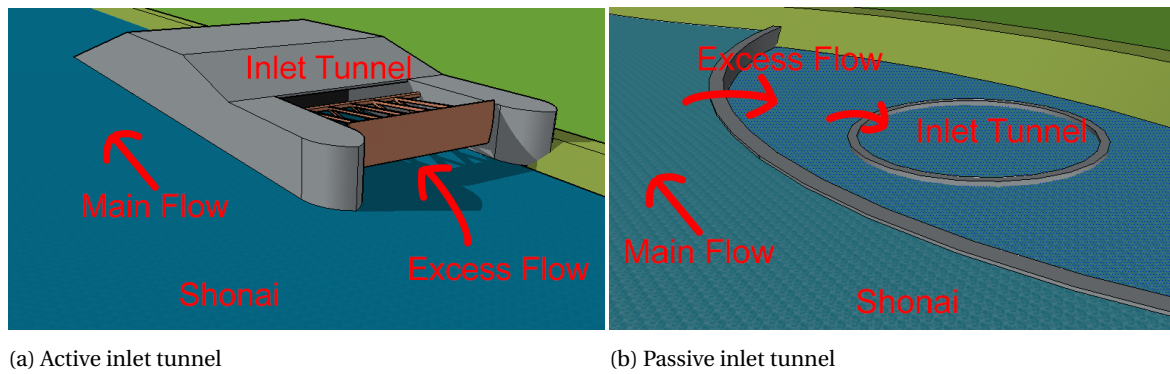


Figure 1.2: Options for tunnel inlet

**Advantages**

- When completed, takes little space up on the surface
- Can yield large increase in discharge capacity
- Lower risk of flooding, compared to diverging the flood to other waterways
- Far less foundations in the way on the trajectory, compared to tunnelling a diversion
- Requires no modification to Tokaido railway lines

**Disdvantages**

- Likely to be more expensive than a new bridge
- Could cause settlements of bridges and buildings

**1.2. Replace Tokaido Railway bridges with new ones**

For this solution, it has been decided to only focus on the Tokaido Railway bridges. This is because plans for the Biwajima car bridge are already in progress: a part of the land around the bridge has already been purchased and construction is expected to start in 2021 [6]. The Biwajima car bridge formed the largest part of the bottleneck, followed by the Tokaido ones [7]. No concrete plans have been formed yet for the Tokaido bridges, as discussions with the railway company continue. Both lines running across, the Tokaido Shinkansen and Tokaido Main Line, belong to some of the busiest railway lines worldwide, concerning cumulative passenger number [8]. Both lines are operated by the Japanese Railway Group, which is a private company. This is contrary to their Dutch counterpart Nederlandse Spoorwegen, or NS, which has the government as main shareholder. Thus, because the railways are both busy and owned by a private company, it makes negotiations more difficult.



Figure 1.3: Bridges near Biwajima [4]

However, the bridge still poses a problem for the flood safety. The columns do not only reduce the wet cross-section, but also introduces turbulence. This added turbulence increases the friction, reducing the flow capacity even more. Lastly, the bridge has been constructed too low concerning the required safety level. During

the 2000 Tokai rainfall, flood levels reached the bottom of the bridge girder. During this flood, a maximum discharge of approximately  $3500 \text{ m}^3/\text{s}$  occurred (see Appendix Q), whereas the required discharge capacity is slightly higher, namely  $3765 \text{ m}^3/\text{s}$  (see calculations in section 2). Therefore, it has been decided to investigate the option of modifying the Tokaido railway bridges.



Figure 1.4: 2000 Tokai extreme water levels at Tokaido bridges [9]

Modifying or replacing the bridge would include increasing the height and span and reducing total column width. This will increase the wet cross-section and reduce the perimeter, increasing the hydraulic radius. Using the Chézy relation as used in section 2, this means the discharge capacity increases, removing the bottleneck.

#### Advantages

- Physically removes the bottleneck
- Likely to have low impact on direct environment

#### Disadvantages

- Bridge have to be raised sufficiently in order to foresee future needs
- Disruption train services

### 1.3. Replace Tokaido Railway bridges with a tunnel

Instead of replacing the Tokaido Railway bridges with new ones, an alternative is to construct a tunnel underneath the Shonai. This has a similar effect as making a new bridge. By removing the bridge, the wet cross-section is increased, allowing for a larger discharge capacity. Furthermore, by removing the piers, all turbulence previously induced by the bridge, is removed, in turn increasing discharge capacity. An advantage of a tunnel over a bridge is that one no longer needs to take into account the dike height. Where a bridge could limit dike levels, a tunnel will not.

#### Advantages

- Physically removes the bottleneck
- Likely to have low impact on direct environment
- No issue with possible future dike raises, compared to a new bridge

#### Disadvantages

- Disruption train services
- Generally more expensive than railway bridges
- Requires large approach to gain depth



# 2

## Discharge

*This chapter uses appendix R.*

An extreme value analyses using data of 57 years has been executed in appendix section R.1. The data found in Biwajima showed that the extreme values can be best approximated with an exponential distribution. A Weibull- and Gumbel distribution have been curve-fitted as well, but showed less accuracy. The exponential distribution has been used to find a 1:200 year design discharge of 4120 m<sup>3</sup>/s. Climate change effects have been taken into account for a 100-year period, resulting in a final design discharge of 4250 m<sup>3</sup>/s.

To estimate the area and wetted perimeter (see appendix section R.2), the cross-section at Biwajima Bridge has been used. Taking into account the columns of the bridge, concludes that the area of the cross-section equals 1235 m<sup>2</sup> with a wetted perimeter of 310 m. The roughness coefficient of the Shonai has been calculated based on data and is equal to 0.0184 s/m<sup>1/3</sup>. Applying the relation between Chézy and Manning gives the corresponding Chézy coefficient needed to calculate the design capacity. This design capacity has been calculated using the Chézy equation valid for steady uniform flow, where the design gradient equals 7.6E-04. Since a flood wave is non-uniform, the adapted formula will be used in which the water depth gradient is taken into account. This gives a design capacity of 3765 m<sup>3</sup>/s at the Tokaido bridge. As can be concluded from table 2.1, the design capacity is significantly more than the present capacity. A safety value of  $\beta = 4.3$  has been used to calculate the needed extra discharge capacity. Calculations in section R.3 show that room for 1400 m<sup>3</sup>/s should be realised. The increase has been shown in figure 2.1.

Direction	Symbol	Distribution	Mean	Std	Unit
Design capacity	$Q_{1/200}$	Deterministic	4250	–	m <sup>3</sup> /s
Manning coefficient	$n$	Normal	1.84E-02	9.2E-04	s/m <sup>1/3</sup>
Area	$A$	Normal	1235	12.35	m <sup>2</sup>
Wetted perimeter	$P$	Normal	310	3.1	m
Bed slope	$i_b$	Normal	7.6E-04	2.3E-05	–
Discharge	$Q$	Normal	3765	209.6	m <sup>3</sup> /s

Table 2.1: Distributions of the used parameters

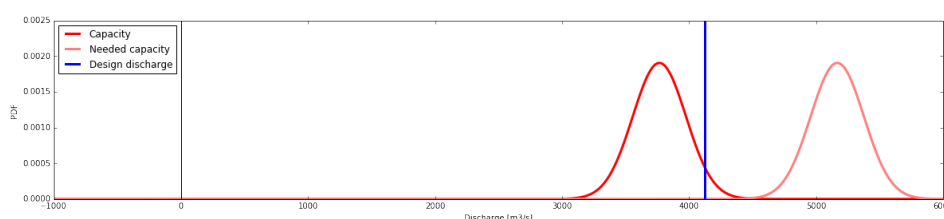


Figure 2.1: Probability curve of discharge load and capacity

# 3

## Bypass tunnel

*This chapter uses appendices S and T.*

This chapter elaborates on the proposed solution of the tunnel underneath or along the river. More details on the location and some initial dimensions will be presented, see appendix T for calculations. Using these dimensions an estimate of the costs has been made. Four options will be discussed:

- Bored tunnel
- Immersed tunnel
- Pneumatic caissons
- In-situ tunnel

### 3.1. Reference projects

The idea of creating a bypass tunnel for flood mitigation has also been executed in Austin and San Antonio, Texas, USA. In Austin the water is taken from the river (Waller Creek) and diverted through a tunnel underneath the Waller Creek into a lake. Here the inlet is located in a pond in a park from which the tunnel goes straight down to the desired depth. The Waller Creeks flow regime is similar to that of the Shonai; low discharges with extreme flood events. Since the tunnel is connected to a lake, the water is pumped from the lake back into the Waller Creek in case of low discharge. This will prevent stagnant water inside the tunnel. The tunnel has a length of 1.7 km with a maximum width of 8 m. The costs for the Waller Creek flood tunnel were around \$144 million. [10]

In San Antonio a flood tunnel has been constructed to protect the major part of the city. The tunnel has a length of 5 km and a width of 7 m. Water is diverted from the San Antonio River and transported back to the river after 5 km. The inlet is located 10 m above the outlet, this ensures gravity to drive the flow. A pumping facility is made to ensure water circulation in case of low discharge. The total costs for this tunnel were about \$111 million. [11]

Flood tunnels however can pose risks. Water quality inside the tunnel should be maintained, meaning stagnant water should be avoided. This could be fulfilled by using pumps for circulation (as in San Antonio project). In case the water in the tunnel flows faster than in the river itself, this could cause problems downstream of the tunnel. This has to be taken into account when designing the outflow structure. Furthermore, side channels and tunnels can influence the sediment discharge inside the river changing the morphology and ecology of the system.

### 3.2. Location

For the flood tunnel of the Shonai River, the tunnel should at least cover the stretch containing the bridges. Use can be made of the parks upstream and downstream to make the construction of the inlet and outlet of the tunnel more convenient. In this way the length of the tunnel will be approximately 2.5 km. Another option is to make the inlet of the tunnel just upstream of the bridges. For this option buildings have to be

removed to place the inlet. This course will have a length of around 1.2 km. Figure 3.1 gives the suggested courses of the tunnel.



Figure 3.1: Location of the tunnel underneath Shonai solution [4]

### 3.3. Inlet and outlet structure

For the design of the inlet and outlet it is important to prevent debris from entering the tunnel and provide an unhindered flow of the water. This could be realised by a correct configuration and location of the inlet and outlet. They should be located behind a sill or gate, only to be used during larger discharges. Placing the inlet and outlet outside of the river leads to less to none impact on the flow profile inside the river while low discharge.

It is desired to come to the right depth of the tunnel as fast as possible without too much energy losses. A suggestion for the inlet and outlet is to create an opening in the ground (see figure 3.2). The required depth of the tunnel could be reached with two bends. The amount of energy lost depends on the chosen radius of the bend. To prevent losses due to sharp bends, it could also be possible to place the tunnel near the inlet/outlet at a gradient. However, this option requires more space to obtain the required depth and could induce problems due to soil bursting and uplift. To optimise the inlet structure a funnel shaped inlet and outlet will be made. This decreases the turbulence at the inlet and outlet and thus the energy loss.

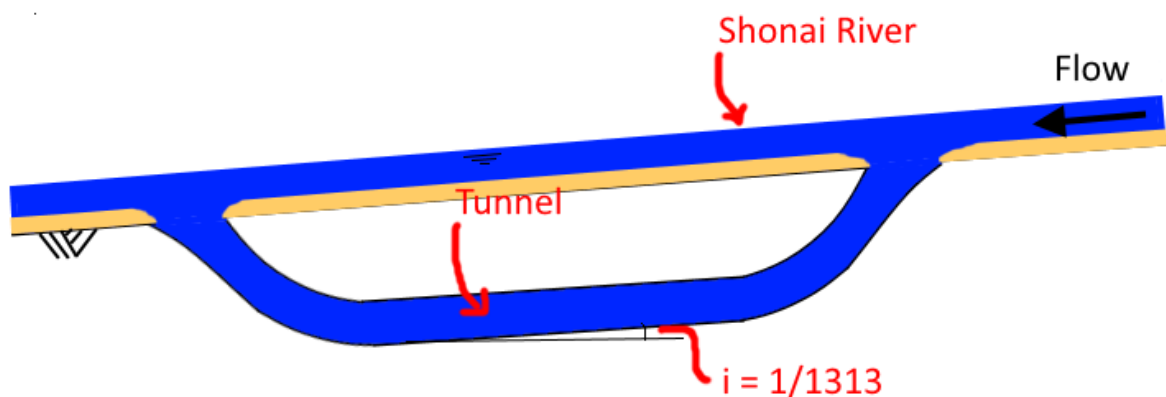


Figure 3.2: Suggestion for the cross-section of the tunnel [10]

### 3.4. Bored tunnel

This section elaborates on the option to create a bored tunnel. This construction method disturbs the environment less. However, the costs will be higher compared to other construction methods. The focus will be on the main, bored part of the tunnel. The inlet and outlet structure will be discussed and designed globally. The radius of the tunnel will be limited, since Tunnel Bore Machines (TBMs) have a certain maximum diameter. The current largest TBM has a diameter of 19 m [12]. Thus, 18.8 m has been set as a limit for the outer diameter, leaving 0.2 m for the shield of the bore front [13]. As a design rule, the thickness of the concrete lining is 5% of the inner diameter. This gives that the maximal inner diameter has a value of 17 m.

#### 3.4.1. Required dimensions of the tunnel

Since the tunnel will be bored, the cross-section will be circular. The unknown to determine will be the radius of the inner profile of the tunnel. The required discharge of the bypass equals  $1400 \text{ m}^3/\text{s}$ , see appendix R.3. Since the tunnel is lined with concrete, cast in steel forms, the roughness height is between 0.3-3 mm [14]. However, since the concrete segments have to be bolted to the next one once installed, little holes in the lining are present (see figure 3.3). This will decrease the smoothness of the lining and thus slightly increase the roughness height. Because this number for this specific case is not known, still a value of 0.3 mm will be chosen since smooth concrete will be used.



Figure 3.3: Concrete lining [15]. A close look give visual to the gaps in the lining where bolts can be installed. These bolts are placed to connect the individual segments to each other

Using Chézy, some energy losses due to curves in the tunnel and the in- and outlet have been neglected. Using energy head differences instead of the Chézy relation gives a different solution. Losses at the entrance, outflow and bends are not taken into account by Chézy, only friction losses. Hence, using the tunnel diameter and flow velocity calculated by Chézy gives too much energy losses inside the tunnel, reducing the used capacity. Therefore, the following results are retrieved using energy losses. The head difference between the inlet and outlet of the tunnel is approximately equal to the head difference in the Shonai River over the same stretch, which equals 1.90 m. Following from the calculations, two tunnels with an inner diameter of 16.8 m are needed. These correspond to a velocity of 4.3 m/s inside the tunnel. In a deterministic sense this is over designed by 36 %, however uncertainties are present, and in a probabilistic design the required area will increase.

For a first estimation of the dimensions of the structure of the tunnel, some rough estimations based on existent bored tunnel design have been made. Firstly, to determine the loads, it has to be known on which depth the tunnel will be placed. The depth depends on buoyancy of the tunnel and face stability of the tunnel bore (see appendix AB). In this phase, only buoyancy will be considered. In phase IV, the face stability of the TBM will be considered as well. The tunnel will be located below the river bed, resulting in a water pressure which is always present. The tunnel will be designed on the case that it is not filled with water, making the outside water pressure the only load beside self-weight. To resist the upward water force, the top of the tunnel should be at a depth of 8 m below the river bed, at T.P. -8.5 m (see appendix section T.1). A cross-section of the tunnels is shown in figure 3.4. In here the distance between the two tunnels has been assumed to be the diameter of the tunnel, 18.5 m [13]. As stated earlier, the governing load case is when the tunnel is empty and pressure from outside is maximum. This maximal pressure is reached when the water level in the river

is maximal. This maximum water level equals T.P. +9 m. Using the model of Duddeck for bored tunnels, the forces within the concrete tunnel lining have been calculated. The calculations can be found in appendix T.1. For this model, the vertical soil and water pressure at the bottom of the tunnel (T.P. -17.25 m) must be known. This was found to be 172.5 kPa and 267.5 kPa respectively. This resulted in a maximum compressive normal force of 3950 kN/m and bending moment of 576 kNm/m. The bending moment resulted in a maximum tensile stress of 4.8 N/mm<sup>2</sup>, which required reinforcement. Using a reinforcement ratio of 0.24%, a bending moment capacity of 671 kNm has been found.

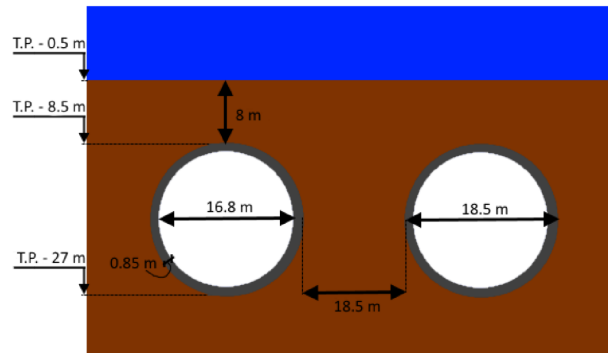


Figure 3.4: cross-section of the two bored tunnels

### 3.5. Pneumatic caisson

To construct a bypass, it is possible to use pneumatic caissons. Pneumatic caissons are a widely used method in Japan, with much applications in built environment. In Tokyo, a highway tunnel has been built with the use of pneumatic caissons, where the highway goes underneath an existing Shinkansen viaduct. Settlement toleration of the viaduct were set to a few mm [16]. Within the bottleneck in the Shonai river, a Shinkansen bridge is present as well, making or similar conditions.

#### 3.5.1. Dimensions based on capacity

The dimensions of the caisson have again been determined based on the energy losses in bends, in- and outflow. When applying caissons with an inner width of 10 m and height of 15 m, the flow velocity becomes 3.7 m/s for the long tunnel variant. Thus, the required area to transport the design discharge should equal 378 m<sup>2</sup>, see appendix section T.2 for calculations. The area of one caisson equals 150 m<sup>2</sup>, therefore three tunnels are necessary for the required capacity. To account for uncertainties, the deterministic design cross-sectional area has been increased by 19% using these dimensions.

#### 3.5.2. Structural calculations

The thickness of the concrete slabs has first been estimated to be equal to 1.5 m for the vertical slabs, 1 m for the bottom and top slabs. It has been assumed that, when the caisson is in position at depth and empty, the loads are maximal, and such, that will be the governing load case. The depth of the caisson in its final position is based on buoyancy. To maintain flow in the river during low discharges, the tunnel will not be used and can be empty for maintenance. When empty, but groundwater is still present, buoyancy becomes a failure mechanism. To prevent that, the top of the tunnel should be at least at T.P. -6 m, 5.5 m below the river bed. Using the software MatrixFrame, we find the internal forces presented in tables 3.1 and 3.2. It was found that these forces can be resisted by introducing reinforcement, with a reinforcement ratio of maximal 1.1%. Shear reinforcement was found to be unnecessary. All the calculations can be found in appendix section T.2.

Element	Maximal bending moment (kNm)	Maximal shear force (kN)	Maximal normal force (kN)
Bottom slab	3560	1940	1900
Vertical slab	3560	1900	1940
Top slab	2760	1350	1160

Table 3.1: Maximal forces at the end of the caisson elements





# 4

## New Tokaido Railway bridges

*This chapter uses appendices U and V.*

Instead of creating a bypass for the water to flow, one can also consider removing the obstacle. Currently, four bridges create a bottleneck together for the flow, with one soon to be replaced. This chapter will take a look at the effects of removing the bridge piers of the Shinkansen bridge and the railway bridge beside it. Of course, this would require a complete new structures. As can be seen in figure 4.1, the Shinkansen bridge has 8 piers in its current state.



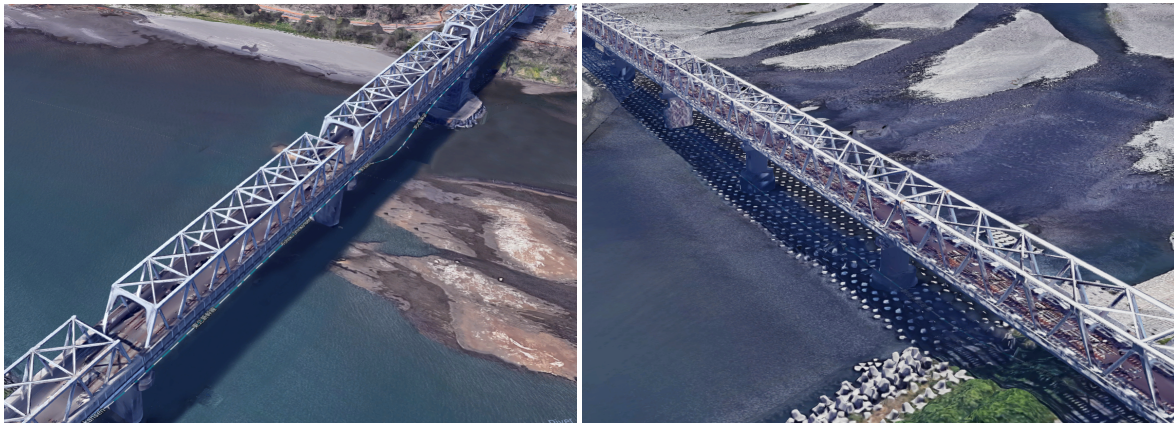
Figure 4.1: Shonai River Shinkansen Bridge [4]

### 4.1. Type of bridge

With modern standards and knowledge, it is very well possible to construct a bridge that only requires two or three piers between embankments. This chapter presents a conceptual design for the Shinkansen bridge, since this bridge provides most flow restrictions. Furthermore, the requirements for a Shinkansen railway bridge are more governing compared to the other bridges running across. Bridges with larger spans are for example the Tohoku Shinkansen Tonekawa Bridge or the Tokaido Shinkansen Fujikawa Bridge. Illustrations of these two bridges have been added to figure 4.2. Please note that both bridges are truss bridges. Investigation of all Shinkansen bridges showed that for short span, box-girder bridges are favoured for the high speed rail. Longer span bridges have all been constructed with the use of a truss design.

The increase of cross-sectional area and reduction of perimeter will increase the capacity of the Shonai. Present capacity has been found to be  $3765 \text{ m}^3/\text{s}$ , as of chapter 2. Removing the bridge piers of the bridges will bring up the capacity and has the potential to fulfil safety requirements. To check whether this is indeed valid, a conceptual design has been made for the bridge. See Appendix U for detailed calculations. A continuous warren truss design with 4 supports has been chosen. The bridge consists of 3 spans of 70 m, see figure 4.3. It has a height of 10 meters, a width of 12 meters and a repetitive length of 10 meters. Concrete slabs are to be attached to the bottom of the truss to support the track.





(a) Tohoku Shinkansen Tonekawa Bridge [4]

(b) Tokaido Shinkansen Fujikawa Bridge [4]

Figure 4.2: Shinkansen bridges with larger spans

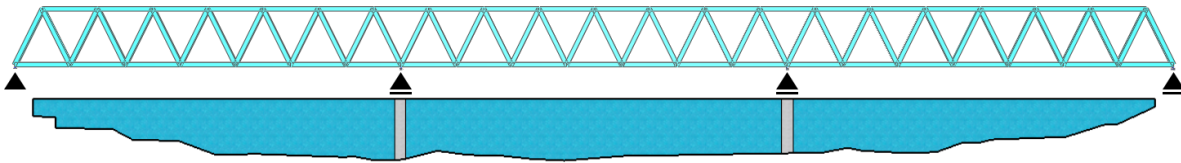


Figure 4.3: Conceptual truss layout 3x70m

## 4.2. Conceptual calculations

Using finite element software MatrixFrame, a plated structure (10 x 12 m) has been simulated to calculate the bending moments on the element. The forces used for this calculation are:

- Self weight truss
- Self weight slab
- Self weight rails
- Moving load Shinkansen train

Resistance calculations show that a slab thickness of 700 mm is required, and the truss must be constructed using RHS1000x500x50 profiles.

Support reactions on the piers have been used to estimate the sizes of these supports. The supports consist of a pier with a thickness of 1.3 m, founded on a shallow foundation with width of 4 m. Given this value, a flow simulation has been executed. This calculation showed that the flow capacity of the cross-section is 5257 m<sup>3</sup>/s, more than the required 4250 m<sup>3</sup>/s. Erection of the bridge is advised by constructing three sections further down-stream, or making use of a cranes to directly manufacture the elements on location is advised.

# 5

## Railway tunnel

*This chapter uses appendices S and W.*

A Third option to remove the bottleneck is replacing the railway bridge with a tunnel. In this case, the river flow does not experience resistance from a bridge, resulting in a larger discharge capacity. Two options for tunnels will be discussed: A bored tunnel and a tunnel with a rectangular cross-section.

### 5.1. Lay-out of railway tunnel

The current railway bridges consist of 6 rail way tracks, of which 2 are separated and part of the Shinkansen Tokaido line. When situated next to each other, the tracks have a centre-to-centre distance of 4.62 m (see figure U.3). Using the same distances in the tunnel design, the total width becomes 30 m wide, excluding structure elements.

To reach the tunnel from the current railway system, a new track should be constructed under a slope running down to the tunnel. The current railways running towards the current bridge are at a level of T.P. +7.5 m at the city side, and T.P. +10 m at the north side [17]. Based on the regulations which are applicable for the Japanese railways, the maximum slope is 2.5% for railway tracks and the curvature radius of slopes has a minimum of 10 km [18].

Curved shaped tunnels with a diameter of 9.5 m have been used for Shinkansen railways with two tracks [19]. This has been used as a reference for a bored tunnel. For a first estimation, 10 m has been used as diameter. This gives that in total 3 tunnels have to be bored. To prevent uplift of the tunnel, it has been found that the top of tunnel has to be at a depth of 4.8 m below the river bed, at T.P. -5.3 m. For calculations, see appendix W. The rail track is 8 m below the top of the tunnel, at T.P. -13.3 m. Using the requirements described above, we find that the entrance to the tunnel gets a transition length of 1085 m for the city side (see figure 5.1), 1185 m for the north side.

For the option to use a rectangular structure, three building methods are applicable: in-situ, immersed caissons or pneumatic caissons. Which method will be used will be determined in the next phase when this solution is chosen to be elaborated on.

Based on the regulations for Japanese railways, a height within the tunnel of 7 m above the rail track is sufficient [18]. Below, 1 m will be reserved for ballast for the rail track. This gives that the inner height of the tunnel structure equals 8 m. The tunnel will be divided into three section with each two tracks, leading to a width of 10 m per section [18]. Structural elements assumed to be 1 m thick. See figure 5.2 for the profile.

For a rectangular hollow tunnel under the groundwater table, upward forces due to buoyancy can pose a problem. In total, the buoyancy force equals 3400 kN. The height of the soil above the structure should be 2.5 m to provide sufficient downward force, taking into account self weight of the tunnel and ballast. This gives that the top of the rail track is at T.P. -11 m. Using the same method as done earlier with the bored tunnel, we find that the entrance to the tunnel needs a length of 990 m for the city side, and 1090 m for the north side.

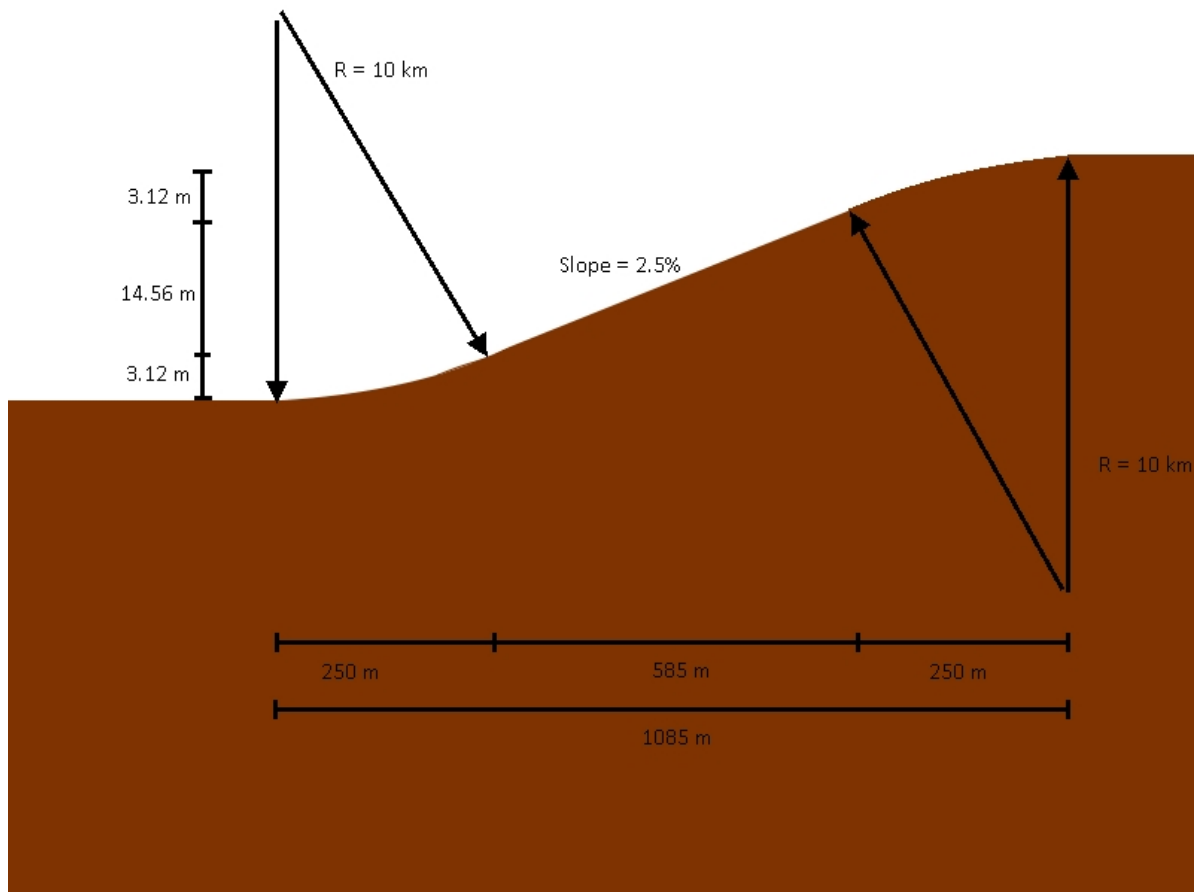


Figure 5.1: Slope from current rail track level down to tunnel level

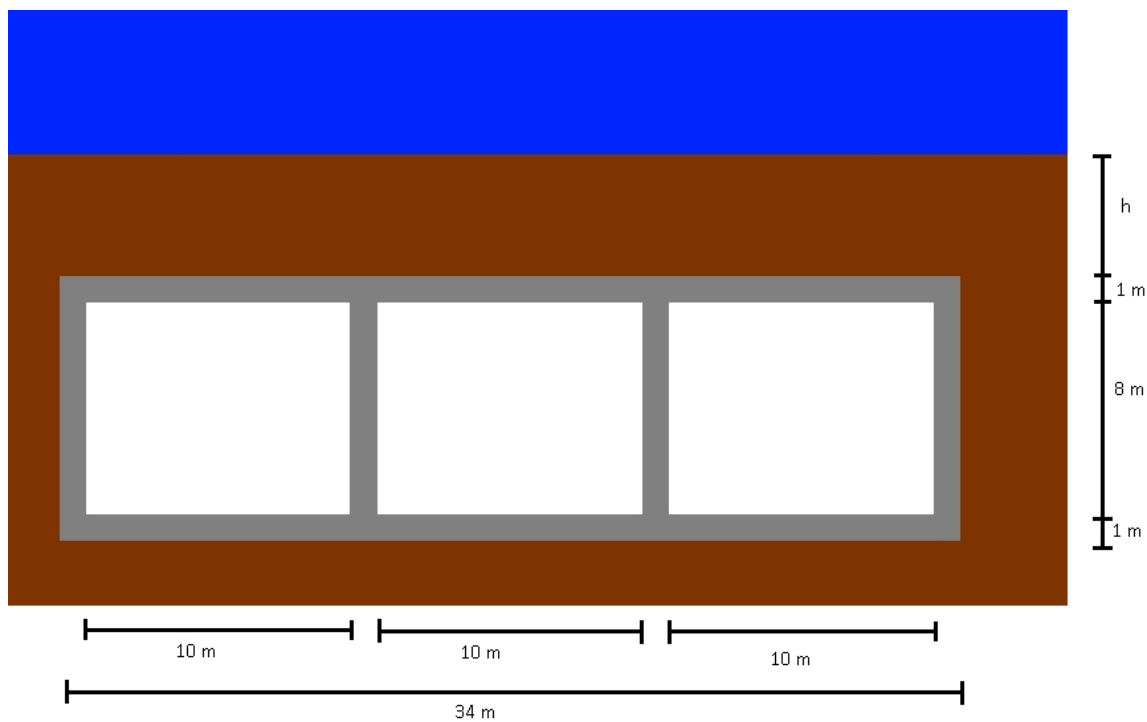


Figure 5.2: cross-section of the rectangular tunnel below the river

### 5.1.1. Building area

Based on the required dimensions of the tunnel and entrances found above, the structure has been schematised in figure 5.3. To keep the trains running while constructing, the new railway track should be build next to the current on. As visible, this will cost an enormous amount of current developed area which should be demolished. The track itself requires a width of 30 m, excluding the structure. Taking extra space for the construction site into account, the width of the site is at least 50 m, over a length of 2.5 km. Due to the sheer amount of space required, it has been decided not to elaborate on this option.

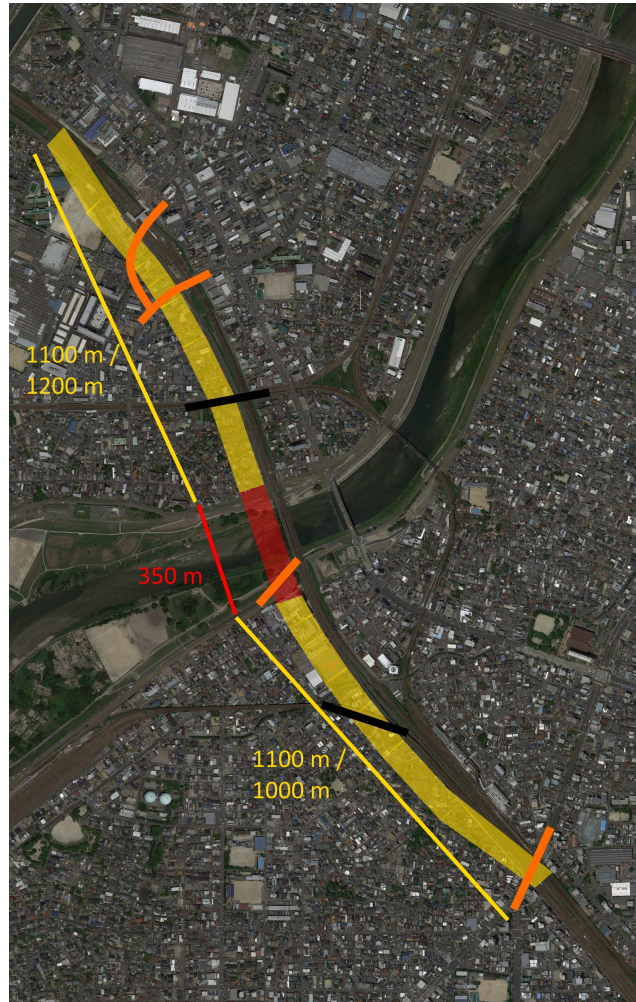


Figure 5.3: Area map of a new tunnel for the railway. Yellow: Tunnel entrance, Red: Tunnel, Black: Crossing railway, Orange: Main road

# 6

## Determination of solution

Three options have been considered to increase the capacity of the Shonai River near the Shinkansen bridge:

- Bypass tunnel underneath the Shonai
- Replace Tokaido Railway bridges with new ones
- Replace Tokaido Railway bridges with a tunnel

The railway tunnel has been disregarded because it would require too much space. A decision between replacing multiple bridges or constructing a tunnel had to be made. Replacing the railway bridges would disrupt train services of the Tokaido Shinkansen, one of the busiest lines in Japan. Furthermore, the railways are owned by the private company Japan Railway Group, making negotiations more difficult. Lastly, at the time of writing, the Chubu Regional Development Bureau of the Shonai River had developed a plan to replace the bridges. Hence, it has been decided to not further investigate the option of replacing the railway bridges with new ones.

It has thus been decided to focus on the possible construction of a tunnel below the river, to create room for discharge during floods. Multiple solutions for the construction type, inlet location, inlet type, outlet location, outlet type, tunnel diameter, number of tunnels and tunnel coating will be investigated further in this report.

The short tunnel variant with a length of around 1.2 km will be chosen since this requires less materials and construction costs. The river inlet will be constructed just upstream of the bridges, the outlet in the flood plain downstream. The short tunnel variant will go underneath residential area since this is shorter and easier to construct.

A bored tunnel will be made instead of using caissons, as calculations showed that for the latter three parallel tunnels would be required, instead of two. That would require very long construction times and very large areas needed. Therefore, the use of caissons have been disregarded. This solution of a short, bored tunnel will be further investigated in phase IV.

# IV

## Phase IV: Verification of single solution



## Proposed location

Figure 1.1 shows the trajectory of the bypass of the bored tunnel. The outlet is located near 13.6 K, which is at the floodplain downstream of the bridges. The inlet will be located near 15.0 K, just upstream of the bridges. The bypass will have a length of 1.2 km corresponding to a river length of 1.4 km.

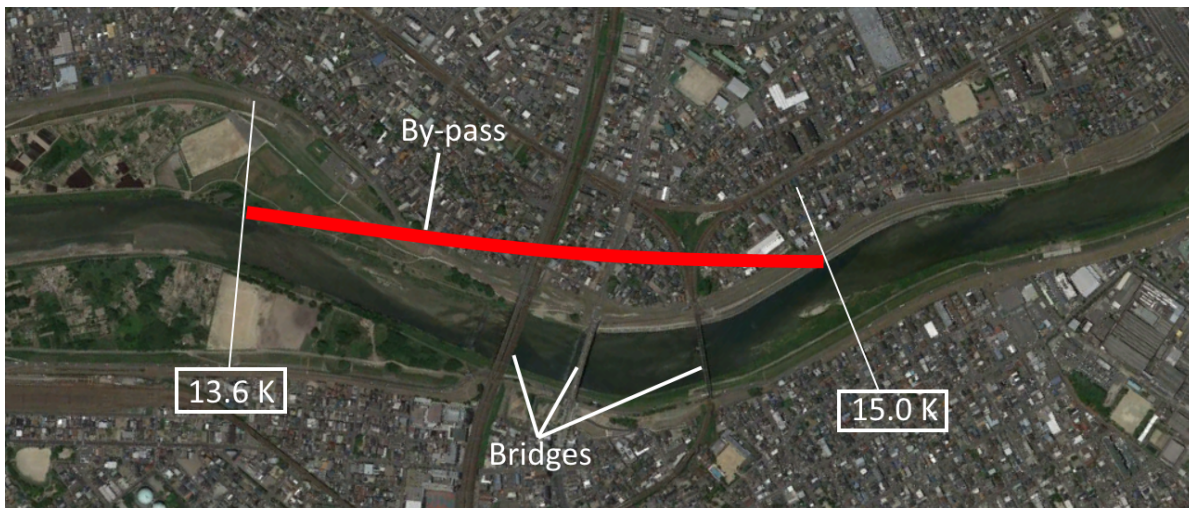


Figure 1.1: Location of the bypass

The following chapter describes the flow characteristics in the bypass and its effect on the river. After this, the inlet and outlet structure of the bypass are described. Structural integrity of the tunnel and building pit verifications are shown next. Lastly, a construction planning and cost estimate is presented.

# 2

## Tunnel flow

*This chapter uses appendices X, Y, Z and AA.*

### 2.1. Tunnel characteristics

To calculate the tunnel characteristics, use has been made of the energy loss in the Shonai River compared to the energy loss inside the tunnel. The loss in the Shonai has been determined by dividing the length of the section by the water surface slope of the river. This gives the water level difference and thus the head loss, equal to 0.75 m. Thus, the head difference inside the tunnel should be equal to 0.75 m. From calculations it was found that this is the case for:

- Two tunnels;
- Inner diameter = 16.0 m;
- Flow velocity = 3.70 m/s;
- Epoxy applied;

The required capacity is 1400 m<sup>3</sup>/s. After calculations, it was found that the diameter of 16 m, without additional measurement, was not sufficient to reach this capacity with two tunnels. Increasing the diameter is technical impossible and a third tunnel would become expensive. It has been decided to apply an epoxy layer to decrease the resistance within the tunnel. When applying such a layer, the discharge capacity becomes approximately 1490 m<sup>3</sup>/s, slightly higher than the required capacity of 1400 m<sup>3</sup>/s. Probabilistic calculations have been used to come to the capacity. Therefore, parameters have a distribution to account for uncertainties. The diameter has been chosen that it suffices 95% of the time of flooding. See appendix X for calculations.

### 2.2. Flow profile

The flow inside the tunnel is turbulent due to the large velocity and dimensions. This leads to a velocity distribution over the vertical of the tunnel as shown in figure 2.2a, with a maximum velocity of 4.27 m/s and a mean of 3.70 m/s. Figure 2.2b shows a cross-sectional view of the velocity distribution inside the tunnel. Calculations for these flow profiles can be found in appendix section X.3. Due to the turbulent flow the velocity gradient near the wall is large, leading to a wall shear stress of 10.9 N/m<sup>2</sup>.

### 2.3. Effect on river

Backwater effects will be found in the river both at the location of the bypass and upstream of the bypass. Figure 2.3 shows the backwater curve for the measurement. A decrease of about 0.50 m is expected around the bypass. The 200 m interval combined with the extreme fluctuating cross-sectional areas result in the unusual behaviour found upstream of section 16.4 km and around section 15.4 km. Deeper analysis of the results are discussed in appendix Y.



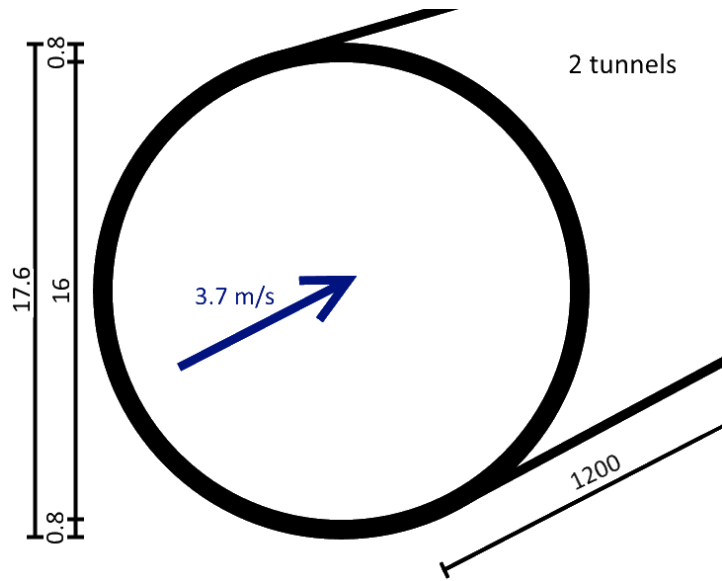


Figure 2.1: Tunnel characteristics

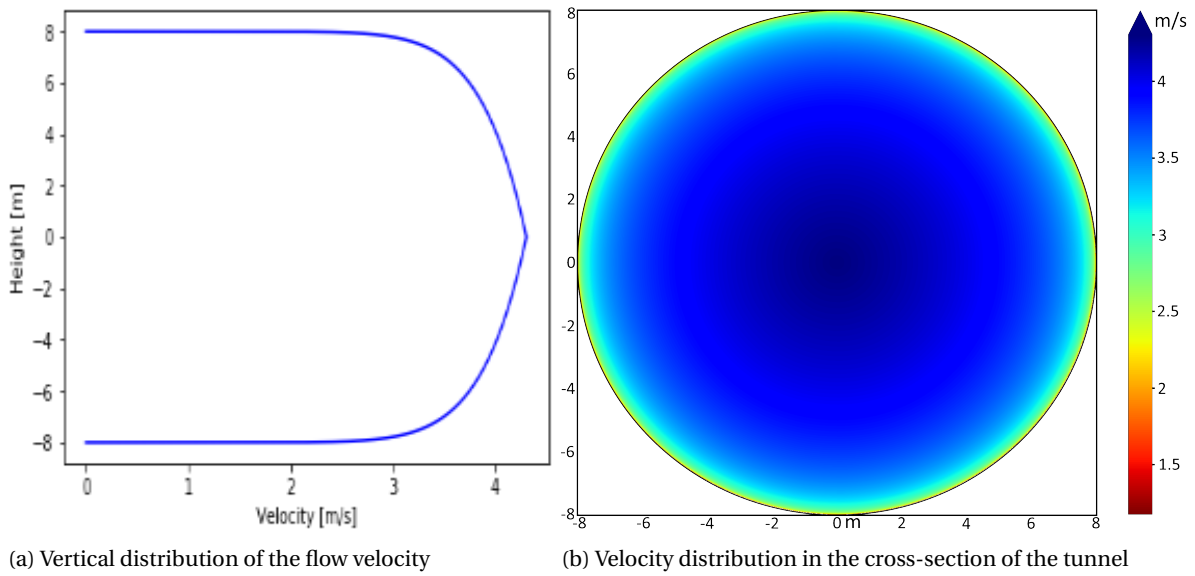


Figure 2.2: Flow velocity inside the tunnel

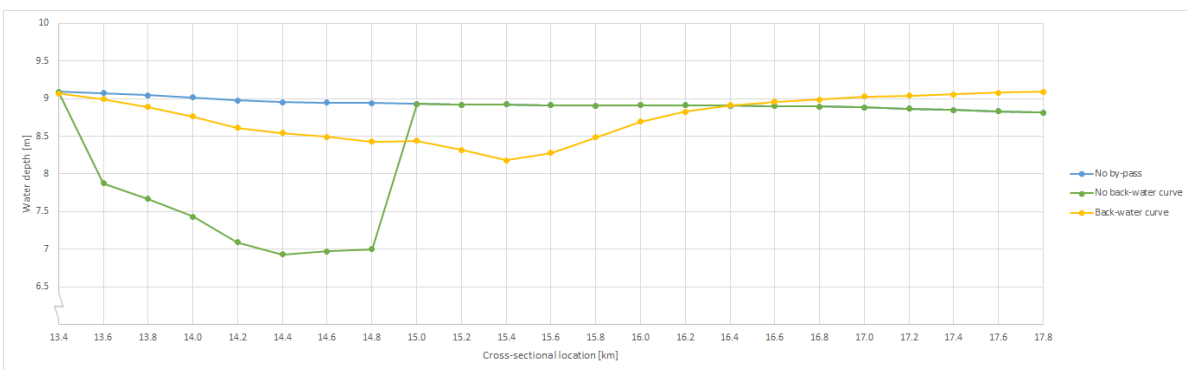


Figure 2.3: Backwater curve at location of bypass

## 2.4. Debris

During floods, large amounts of debris from the upstream area can be transported by the river, for example trees. It should be avoided that this debris blocks or damages the tunnel. This problem can for example be solved by making use of floating barriers just in front of the gate entrance. Figure 2.4a shows an example of such a barrier. Since the debris floats on the river, it is caught behind the barrier. Figure 2.4b shows the location of the barrier in front of the tunnel entrance. In this way the debris will not move into the side channel and keeps following the Shonai River.



(a) Example of a debris barrier [20]

(b) Location of debris barrier. Red: Debris Barrier [4]

Figure 2.4: Debris barriers

## 2.5. Sediment

Settlement of sediment can cause several problems in the proposed tunnel. It may increase the roughness of the tunnel and decrease the effective flow area of the section. Both will influence the efficiency of the tunnel. Because of this, the maximum magnitude of sedimentation has been examined.

It has been assumed that the bed and bank protection just upstream of the tunnel is sufficient such that no extra sediment will be suspended. Also, because of the high velocity in the pipe, no sediment will settle while the tunnel is used with maximum capacity. However, at the end of a flood, settlement will occur since water in the tunnel will come to a hold.

The magnitude of suspended sediment has been measured for certain discharges. A value of 11 g/L was found to correspond to the design discharge of 4250 m<sup>3</sup>/s. This value was found by extrapolating known sediment curvatures of the Shonai River. The relation between flow rate and sediment distribution over the bypass and river gives that 13% of the sediment moves into the bypass, see appendix Z for calculations. Because of this, the concentration in the bypass becomes 1.44 g/L. Using the fact that the volume of the tunnel equals 2.41E+05 m<sup>3</sup> leads to a maximum sediment amount of 347E+03 kg inside the tunnel. This is equal to 289 kg of sediment for every meter length.

Cleaning the tunnels must be done after every use, therefore a system should be installed to move the sediment out of the tunnels. It is advised to make use of pumps and running water to transport the water. This mechanism is often implemented in sand mines to flush sand out of the mine.

## 2.6. Scour protection

Due to the bypass the morphological response of the river changes. Figure 2.5 gives the initial response of the river, with  $x = 0$  downstream of the bypass. Appendix AA shows the details about how this response is derived.

From the figure it can be seen that a scour pit is likely to form at the outlet. This scour hole will have a depth of approximately 1.2 m. Thus a bed protection has to be made to prevent instability of the sill at the outlet. The length is dependent on the stability slope of the bed. It is known that a slope of 1:15 ensures stability for

loosely packed sand [21]. Therefore, the bed protection should have a length of  $15 * 1.2 = 18$  m. The protection consists of loose rocks of stone class  $LM_A$  5-40 with a range of 5-40 kg, as stated by Dutch NEN norms. The rocks will be placed on fascine mattresses to ensure permeability. Appendix AA gives more details on determining the scour depth and stone class.

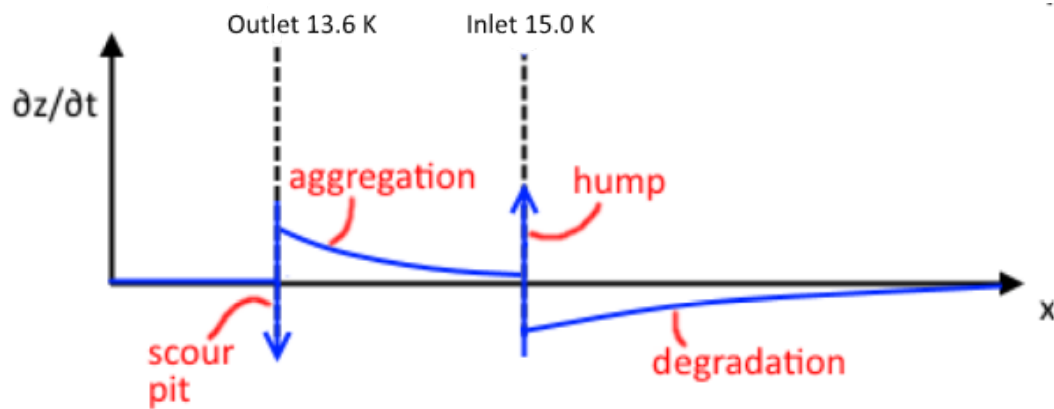


Figure 2.5: Short term morphological response of the river to the bypass

Figure 2.5 only gives a short term response. Long term effects have been deemed negligible since most of the time the bypass will not be operational. Therefore, the bypass has no significant impact on the equilibrium morphology of the Shonai River.

The area of the inlet and outlet structure will be made in such a way that it creates recreational space for citizens. At the inlet and outlet respectively the flow contraction and expansion areas are made of concrete to withstand the high flow velocities. The remaining area will be used to create baseball fields and tennis courts with grass and concrete paths around it. For an impression of the site and further details reference is made to appendix AA.

## Inlet and outlet structure

*This chapter uses appendices AF and AG.*

Design of the inlet has been elaborated in appendix AG. This appendix describes all dimensions. Figure 3.1 gives an impression of the structure in the Shonai River. The inlet will be protected by a sill, to make sure the tunnels will not flood on regular basis. The crest of the sill is at T.P. +4.7 m. By doing so, the existing river ecology is disturbed as little as possible. Furthermore, it allows for maintenance between floods. The outlet structure is to be made in a similar fashion. The angle of the connection with the river will differ slightly because of the geometric properties of the river. Appendix AG gives an indication of the flow over the sill.

A gate had been considered as well. This has the advantage that one is able to control the flow better. However, the costs of a gate are expected to be significantly higher. This is not only due to the construction costs, but also the maintenance. For this reason, it was decided to apply a sill.

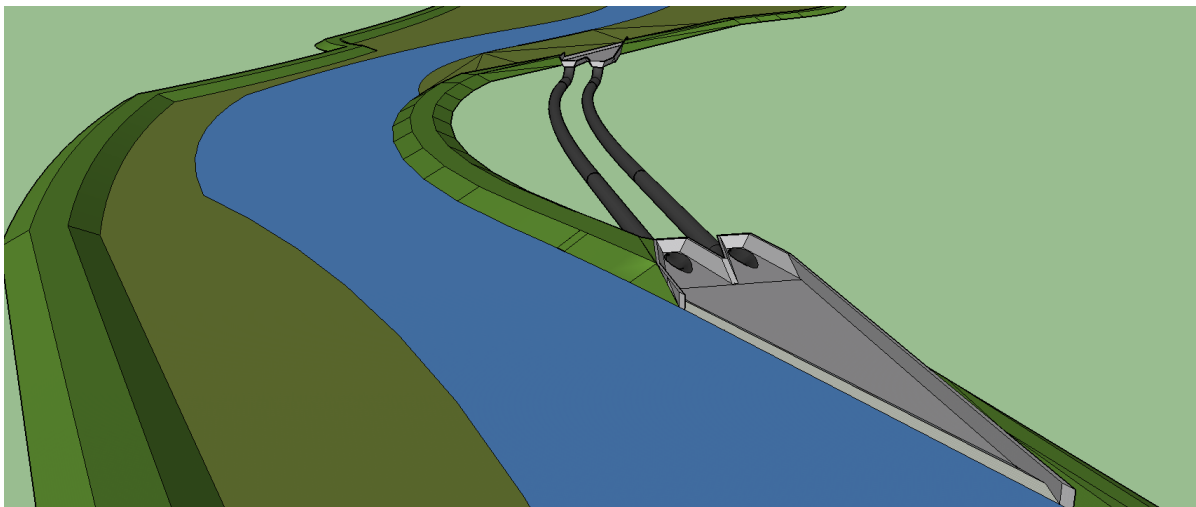


Figure 3.1: Inlet structure and sill

### 3.1. Structural design tube

The inlet and outlet tube will be constructed using tunnel segments, as presented in figures 3.2 and 3.3. The tunnel segments will have the same thickness and reinforcement as used for the bored tunnel. The segments are to be bolted to each other. The structure during the construction phase has been checked using finite element analysis software Diana. For detailed strength calculations, see appendix AF.

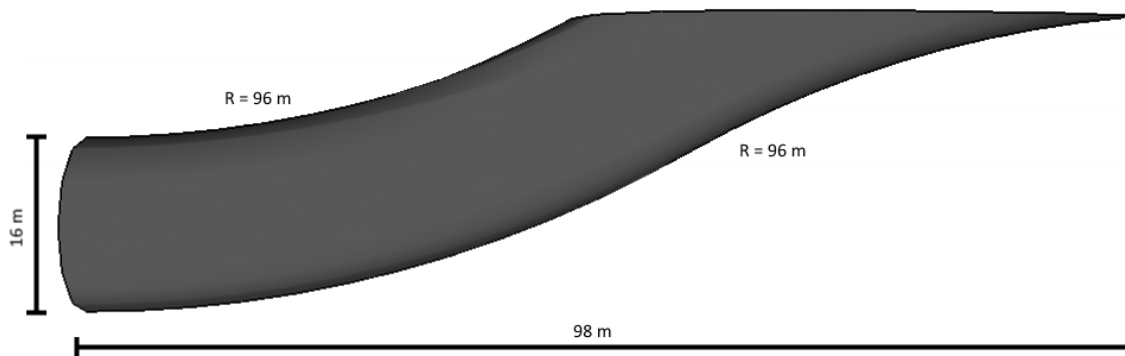


Figure 3.2: Transition tube inlet and outlet

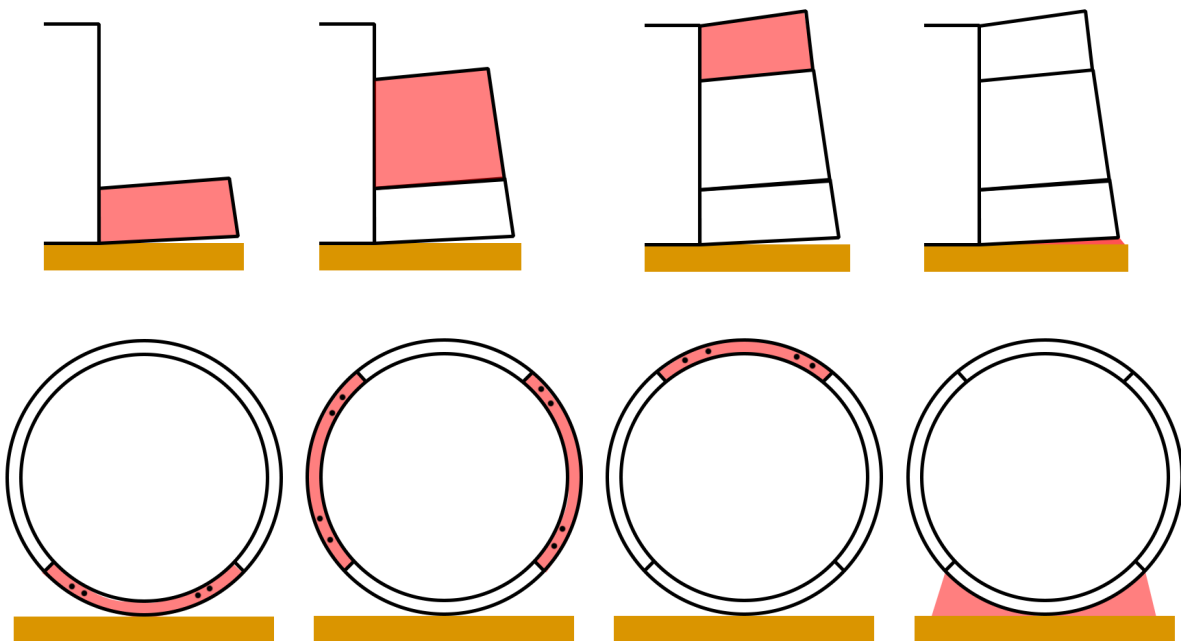


Figure 3.3: Construction process transition tube. Red parts indicate the step, black dots indicate bolts.

# 4

## Structural design tunnel

*This chapter uses appendices S, AB AC and AD.*

### 4.1. Design of tunnel lining

For the design of the tunnel, finite element program Plaxis 2D has been used. The soil-structure schematisation in the program is presented in figure 4.1. The input used for the program is given in appendix AD.

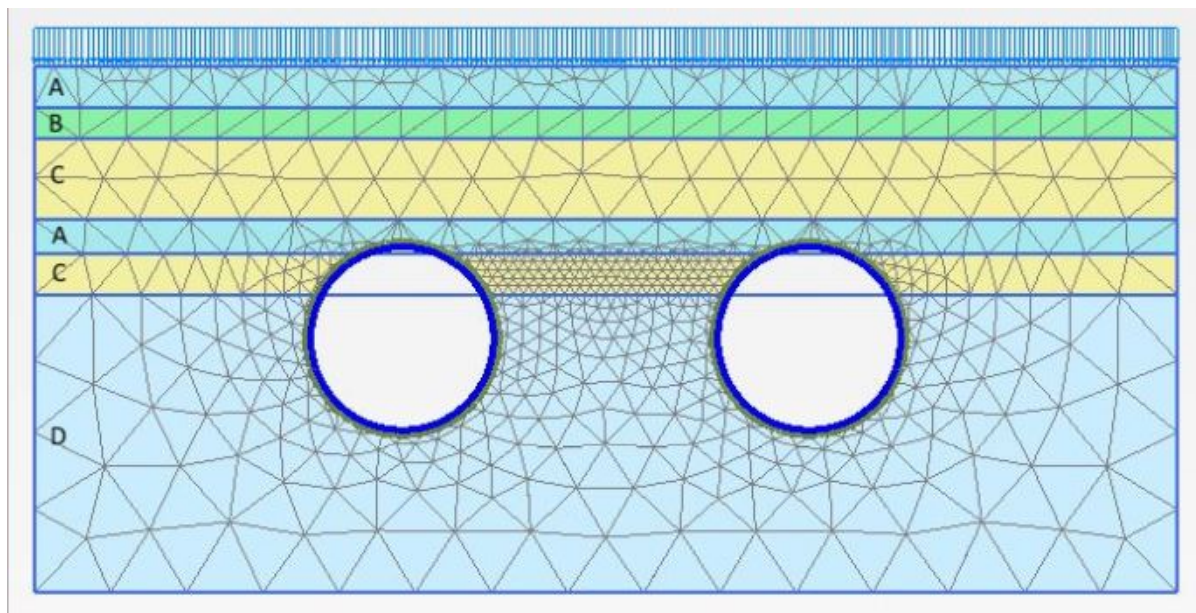


Figure 4.1: Overview of modelled soil layer and tunnel (Soil A: Sand, Slightly silty clayey; Soil B: Sand, Greatly silty clayey; Soil C: Sand, Clean moderate; Soil D: Gravel silty solid)

During tunnel boring, excavation and placing of tunnel lining takes place in different phases. This results in the development pressures, both in the soil as in the concrete lining of the structure. The phases have been elaborated on in appendix AB. Taking this into account while simulating with Plaxis, the forces within the occurring concrete lining have been determined.

### 4.1.1. Loads

The main loads on the structure are the soil and water pressures. Along the trajectory of the tunnel, the surface level is most of the time at T.P. +5 m [17]. In appendix AB, it was found that the top of the tunnel should be at T.P. -9 m or below at some locations, there where the ground surface is lower. This level has been assumed for the whole trajectory. Therefore, the depth of the top of the tunnel becomes 14 m. The groundwater level is at T.P. -1 m.

The tunnel has to cross the embankment of the Shinkansen railway tracks. The embankment has a height of 5 m, resulting in an additional vertical soil stress of  $5 \text{ m} * 20 \text{ kN/m}^3 = 100 \text{ kPa}$ . For the train load, the same value of 62 kN per wheel has been taken into account, as calculated in appendix U.

### 4.1.2. Calculation by Plaxis 2D

The load on the structure depends of the depth, curvature and displacement of the structure. The displacement in turn is dependent on the stiffness of the soil and the structure. Hence, Plaxis has been used for the design, as seen in figure 4.1.

Plaxis is capable of taking afore mentioned factors into account. However, the program cannot incorporate cracked cross-sections into the calculations. In the case of a concrete tunnel, cracks are likely to occur, reducing the stiffness. This introduces a complexity, as the load and displacement are dependent on each other. An iterative process is required. After the first Plaxis simulation, the curvature of the tunnel can be requested from the software. Using a  $M - \kappa$  diagram, a new bending stiffness can be determined and inserted into the software, after which another Plaxis simulation can be run again. This gives new settlements and new curvatures, leading to a new stiffness from the  $M - \kappa$  diagram, until an equilibrium has been reached.

This iterative process has been carried out. After several runs, it was found that for lower stiffnesses, internal forces got more distributed. Settlements on the other hand remained approximately the same. Furthermore, the longer the iterations went on, the lower the internal forces became. This was due to the fact that Plaxis calculates the thickness of the tunnel lining based on the bending stiffness. Therefore, it was not possible to reach an equilibrium. It has been decided to use the internal forces obtained when the tunnel was at its stiffest, as these proved to be the maximums. This is on the conservative side.

### 4.1.3. Evaluation of the results

The results for the settlement are presented in figure 4.2. The internal forces are summarised in table 4.1. Those forces are based on deterministic calculations done by Plaxis. A safety factor of 1.5 has been applied on the forces, instead of applying factors on the input variables. This is because many of these parameters, when taken probabilistic, can have both positive and negative effects on the internal forces. For example, a larger soil stiffness would reduce displacements, but also increase the horizontal stresses on the tunnel. It was found that, using concrete class C55/67, reinforcement of  $\varnothing 40\text{-}100\text{mm}$  is required at each side of the element to resist both positive as negative bending moment as shear forces. See appendix AC for detailed calculations.

Force	Deterministic value	Design value
Minimum Normal Force (kN)	-2171	-3257
Maximum Normal Force (kN)	-479	-719
Minimum Shear Force (kN)	+471	+707
Maximum Shear Force (kN)	-401	-602
Minimum Bending Moment (kNm)	-1686	-2529
Maximum Bending Moment (kNm)	+1496	+2244

Table 4.1: Internal forces within concrete lining

As seen in figure 4.2 below, a maximum settlement of 34 mm on the surface and 38 mm at the top of the tunnel lining has been found. The slope of the settlement has a maximum value of 1/500. Where the total settlement is maximal, the settlement slope is approximately 1/1000.



Settlement can cause damage to surrounding buildings leading to structural failure. Based on figure 4.3, it has been concluded it is possible for damage to occur to buildings. However, none of this damage would be structural, meaning no safety risks occur due to the settlements. Besides, the factor which should causes the most structural damage, the settlement slope, falls in the class where the risk is negligible. Therefore, no to very small damage to surrounding is expected to occur

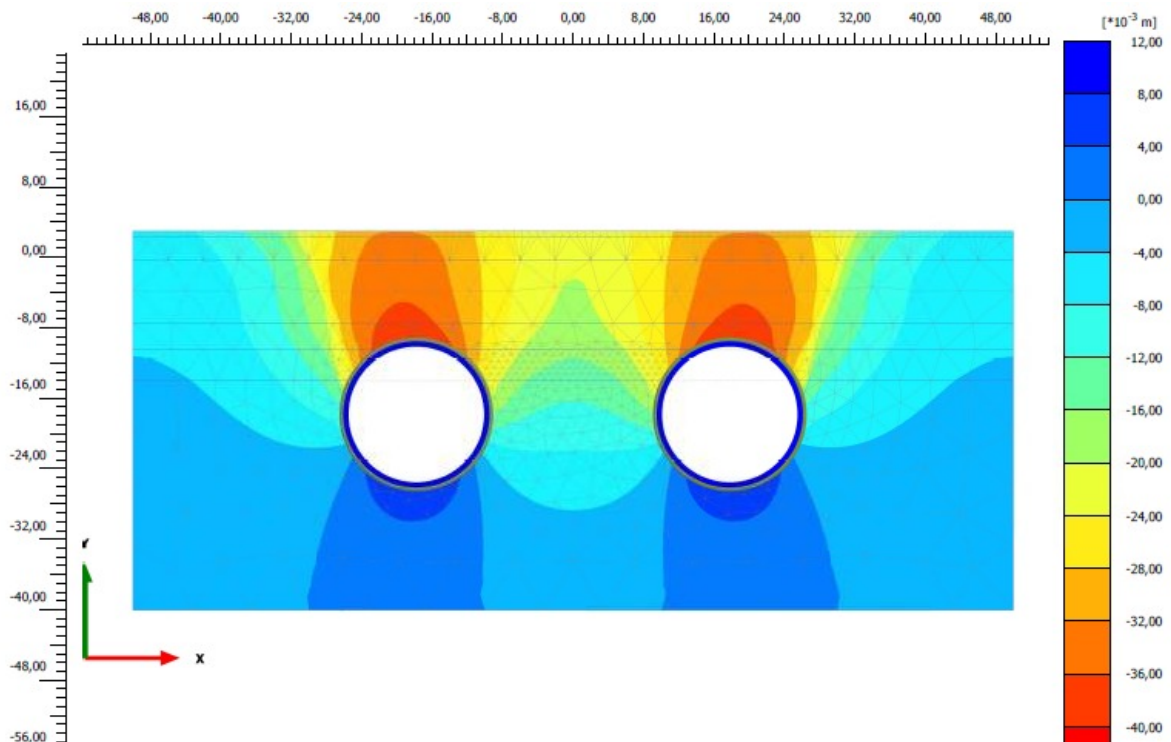


Figure 4.2: Settlement of the area due to construction of the tunnel

Figure 4.3: Typical values of maximum building slope and settlement for damage risk assessment (Rankin, 1988)

Risk Category	Maximum slope of building	Maximum settlement of building (mm)	Description of risk
1	Less than 1/500	Less than 10	Negligible; superficial damage unlikely
2	1/500 - 1/200	10-50	Slight; possible superficial damage which is unlikely to have structural significance
3	1/200 - 1/50	50-75	Moderate; expected superficial damage and possible structural damage to buildings, possible damage to relatively rigid pipelines
4	Greater than 1/50	Greater than 75	High; expected structural damage to buildings. Expected damage to rigid pipelines, possible damage to other pipelines

Figure 4.3: Rankin scale for settlement damage [22]



# 5

## Structural design of building pit

*This chapter uses appendices S and AE.*

For the TBM to start boring, it must be deep enough. In order to achieve this, a start and reception shaft have to be dug. These shafts will later be used as building pits for the inlet and outlet structures. The dimensions of the building pit are presented in table 5.1.

	<b>Dimension</b>
Ground surface	T.P. +3 m
Top of bottom floor	T.P. -28 m
Depth	31 m
Length	100 m
Width	60 m

Table 5.1: Building pit dimensions

For the structure type of the building pit, the options of a pneumatic caisson, diaphragm walls and sheet pile walls have been considered. The pros and cons are listed in table 5.2. Based on this table, it was decided to use diaphragm walls. Sheet piles have been ruled out, mainly because of the required excavation depth of 31 m. Furthermore, it has been opted to go for diaphragm walls, as the costs of a pneumatic caisson are expected to be significantly higher.

<b>Wall type</b>	<b>Advantages</b>	<b>Disadvantages</b>
Pneumatic caisson	Much applied method within Japan Can reach large depth TBM can bore through concrete walls	Expensive method Requires a lot of power Applying anchors not possible
Diaphragm wall	TBM can bore through concrete walls Can reach large depths	Semi-expensive
Sheet piles	Easy and cost effective method	Depth of excavation limited Prone to deflection in gravelly soil TBM can't bore through wall

Table 5.2: Different types of building pits

Because the pit has a large depth, anchors or struts are required to support the walls. Because a large open space is required for the TBM, struts are not possible. Therefore, anchors are to be used, with a total of three rows. In the table below, the levels of the anchors and other dimensions have been estimated. Because of the water head difference, an UnderWater Concrete (UWC) floor will be applied, combined with tension piles. The diaphragm walls will end 2 m below the UWC floor.

	<b>Dimension</b>
Wall thickness	1.5 m
UWC floor thickness	1 m
Center to center distance anchors (m)	2

Table 5.3: Building pit dimensions

In order for the TBM to get through the diaphragm wall, a so-called soft eye will be installed. With this method, a part of the steel reinforcement bars in the wall have been replaced by glass fibre reinforcement. The TBM is able to bore through the glass fibre reinforced concrete, while not through steel reinforced. The strength of the glass fibre bars are in the order of magnitude of 600 MPa [23], depending on the manufacturing. The glass fibres are linear elastic, contrary to the yielding behaviour of steel. The difference in material behaviour has to be taken into account for the rebar calculations. Using a glass fibre soft eye for tunnelling has been used in several projects already [24].

*During this project, finite soil element analysis software Plaxis has been used for the tunnel design. This software was also to be used for the building pit. When calculations for the building pit started, the TU Delft license expired and the software became unavailable. Other software for soil retaining structures were unavailable as well. Therefore, MatrixFrame has been used for an estimate.*

For the design of the building pit, MatrixFrame has been used, this however has some shortcomings. Because the soil has been added as load which does not depend on the deformation of the structure, the load is only an estimation. On top of that, the true behaviour of the anchors cannot be calculated, as the spring stiffness is unknown. Therefore, the anchors have been schematised as rigid supports. Additionally, the settlements of the soil cannot be calculated. Due to these factors, only an estimate can be given of the forces. These calculations should therefore be seen only as a feasibility design. The results have been summarised in this chapter, for full calculations see appendix AE.

The wall is schematised in MatrixFrame as presented in figure 5.1. Because the UWC floor will act as a strut, an extra support has been added. Two load combinations have been considered:

- Fully excavated, no water head difference, no UWC applied
- Fully excavated, maximum water head difference, UWC applied

In both load combinations, the load caused by the soil is the same. Assumed is that the horizontal soil pressure is fully active on the retaining side and fully passive on the excavation side. Because different soil layers are present (see appendix S), the pressure on the wall fluctuates not only due to the depth, but also due to the type of soil. The horizontal soil pressures are as presented in appendix AE. The passive horizontal soil pressure is only present in the gravel layer between T.P. -29 m and T.P. -31 m. At the bottom of this layer, it is equal to 92 kPa.

In table 5.4, three different configurations for the anchors height are given. All three options have been calculated and the results of the internal forces given in the same table. Based on this table, it has been decided to use option 3.

<b>Option</b>	<b>First row (m T.P.)</b>	<b>Second row (m T.P.)</b>	<b>Third row (m T.P.)</b>	<b>Maximum bending moment (kNm)</b>	<b>Maximum shear force (kN)</b>
1	-5	-13	-21	2650	1480
2	-5	-13	-25	2835	1715
3	-5	-17	-25	2280	1240

Table 5.4: Left: Height of the anchors; Right: Internal forces

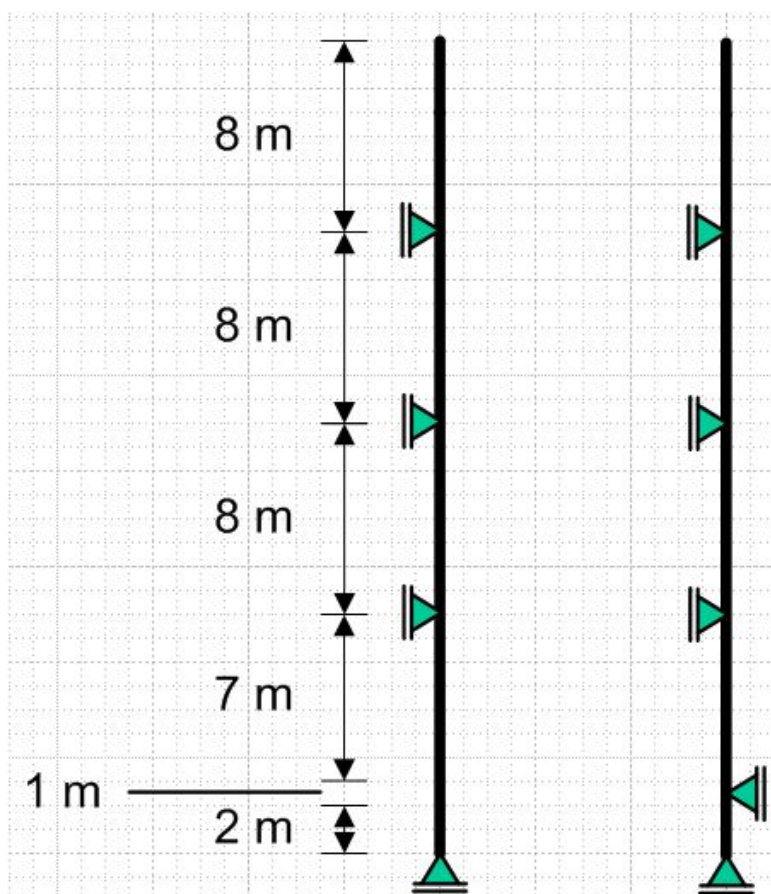


Figure 5.1: Left: Structural scheme without underwater concrete floor; Right: Structural scheme with underwater concrete floor

The internal forces as found in table 5.4 have been determined using a deterministic approach. A load factor of 1.5 has been applied to account for soil uncertainties, as well as the simplifications introduced by using MatrixFrame. This gives that the diaphragm wall should be able to resist a bending moment  $M_{Ed}$  of 3420 kNm and a shear force  $F_{Ed}$  of 1860 kN.

In appendix AE, the capacity of the cross-section has been determined. A thickness of 1.5 m proved to be sufficient. C55/67 has been used as concrete class. The dimensions and number of reinforcement bars is given in table 5.5. For this calculations, a technical document on glass fibre reinforcement of SchöckComBAR has been used [23].

#### Steel reinforcement

Longitudinal bars	Ø40 – 165 mm
Shear reinforcement	Ø24 – 100 mm
$M_{Rd}$	4579 kNm
$V_{Rd}$	7100 kN
U.C.	1.0

#### Glass fibre reinforcement

Longitudinal bars	Ø32 – 110 mm
Shear reinforcement (dowels)	Ø16 – 500 mm

Table 5.5: Dimensions of reinforcement in cross-sections

# 6

## Construction planning

*This chapter uses appendices AH.*

A planning has been made for the construction of the bypass. The construction phases have been described in the following tables. The planning itself can be found on pages 40 and 41 after the tables. Note that matching colours indicate activities in a similar category. The whole project is expected to last for 137 weeks.

Phase	Description	Start week	Weeks
1	Install utilities	1	1
2	Demolish houses & clear site	2	12
3	Site preparation & installing equipment	14	4
4	Construct diaphragm walls	18	14
5	Excavate pit & install anchors	32	24
6	Driving tension piles	56	5
7	Cast underwater concrete floor	61	1
8	Pumping dry pit & curing UWC floor	62	2

Table 6.1: Construction phases inlet structure, pre-boring

Phase	Description	Start week	Weeks
9	Install utilities	29	1
10	Clear site	30	2
11	Site preparation & installing equipment	32	4
12	Construct diaphragm walls	36	14
13	Excavate pit & install anchors	50	24
14	Driving tension piles	74	5
15	Cast underwater concrete floor	79	1
16	Pumping dry pit & curing UWC floor	80	2

Table 6.2: Construction phases outlet structure, pre-boring

Phase	Description	Start week	Weeks
17	Supplying TBM parts	58	1
18	TBM assembly	59	8
19	Boring tunnel #1	67	15
20	Transport TBM back to start	82	4
21	Boring tunnel #2	86	15
22	TBM disassembly	101	6

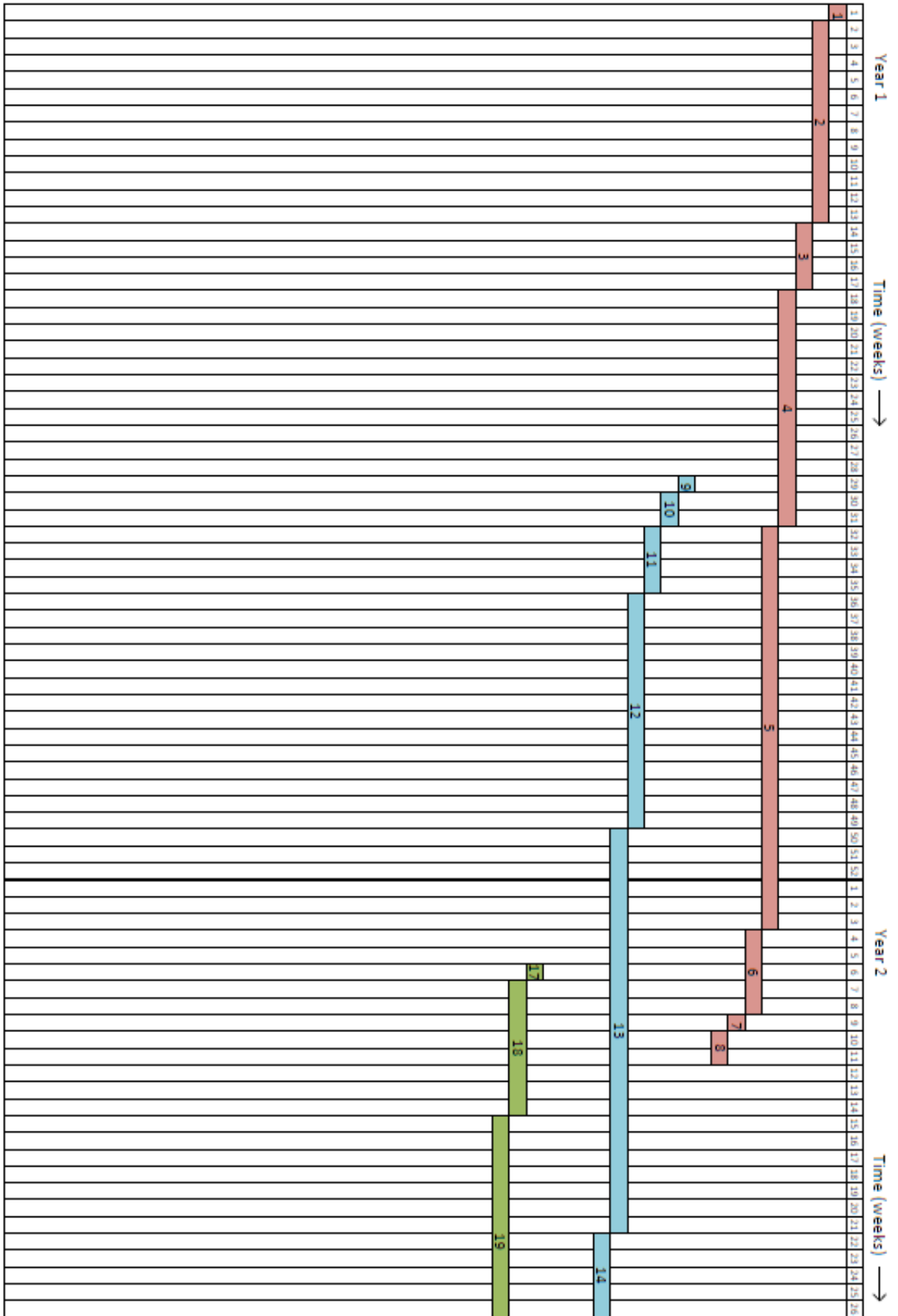
Table 6.3: Construction phases tunnel boring

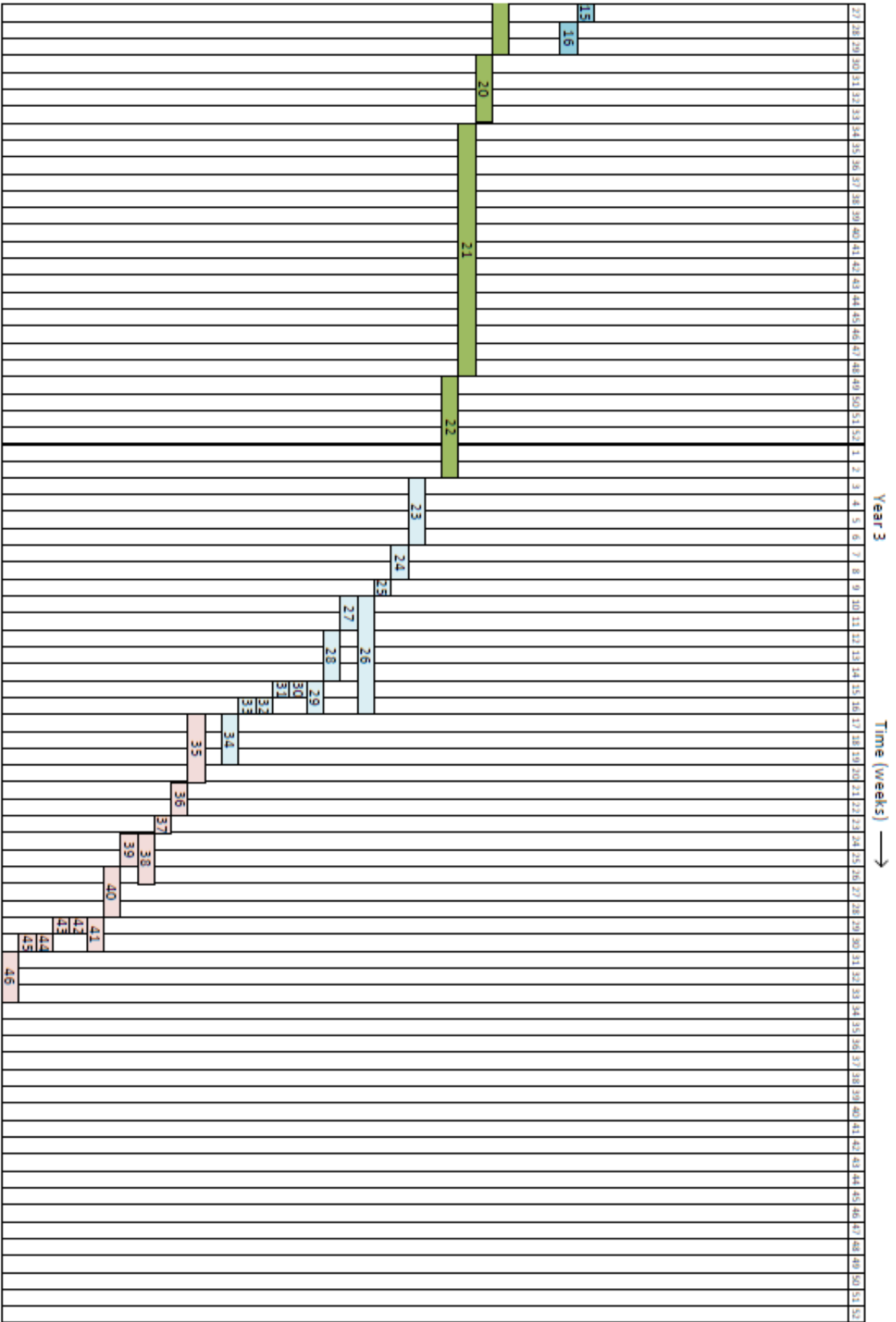
Phase	Description	Start week	Weeks
23	Construction transition tubes	107	4
24	Backfilling & compacting soil pit	111	2
25	Scabbling tubes	113	1
26	Applying epoxy, starting at outlet	114	7
27	Excavating & levelling funnel area	114	2
28	Applying formwork, casting & curing floor	116	3
29	Applying formwork, casting & curing funnel	119	2
30	Placing L-shaped walls side & backfilling	119	1
31	Excavate dike to sill level	119	1
32	Place concrete block protection sill	120	1
33	Place bed protection	120	1
34	Clean up site & install sports facilities	121	3

Table 6.4: Construction phases outlet structure, post-boring

Phase	Description	Start week	Weeks
35	Construction transition tubes	121	4
36	Backfilling & compacting soil pit	125	2
37	Scabbling tubes	127	1
38	Applying epoxy, starting at outlet	128	3
39	Excavating & levelling funnel area	124	2
40	Applying formwork, casting & curing floor	130	3
41	Applying formwork, casting & curing funnel	133	2
42	Placing L-shaped walls side & backfilling	133	1
43	Excavate dike to sill level	133	1
44	Place concrete block protection sill	134	1
45	Place bed protection	134	1
46	Clean up site & install sports facilities	135	3

Table 6.5: Construction phases inlet structure, post-boring





# 7

## Cost estimate

*This chapter uses appendices AH and AI.*

A cost estimate has been made for the current design and planning. The results have been summarised in table 7.1.

The total cost of the project has been estimated at € 462,718,693, or ¥60,153,430,116. The more detailed version of the cost estimate can be found in appendix AH. Calculations have been carried out in euros and converted afterwards with a conversion rate of 1 EUR = 130 YEN. An indexation increase of 20% has been applied. This covers for example risk, profit and other uncertainties.



	<b>Cost in EUR</b>	<b>Cost in YEN</b>
<i>Construction Site</i>		
Property purchase	€ 115,000,000	¥14,950,000,000
Property sale	-€ 15,000,000	-¥1,950,000,000
Temporary dike	€ 1,000,000	¥130,000,000
<b>Total</b>	<b>€ 101,000,000</b>	<b>¥13,130,000,000</b>
<i>Excavation start and reception shaft</i>		
Excavators	€ 1,100,000	¥143,000,000
Anchor drives	€ 480,000	¥62,400,000
Pontoons	€ 288,000	¥37,440,000
Tension piledrivers	€ 320,000	¥41,600,000
UWC installation equipment	€ 200,000	¥26,000,000
Diaphragm wall	€ 12,138,000	¥1,577,940,000
Anchors	€ 597,600	¥77,688,000
Excavation soil	€ 3,590,400	¥466,752,000
UWC material	€ 3,300,000	¥429,000,000
Tension piles	€ 871,200	¥113,256,000
Man-hours	€ 1,347,200	¥175,136,000
<b>Total</b>	<b>€ 24,232,400</b>	<b>¥3,150,212,000</b>
<i>Bored tunnel</i>		
<b>Total</b>	<b>€ 185,000,000</b>	<b>¥24,050,000,000</b>
<i>In- and outlet tubes</i>		
Tube lining	€ 24,720,000	¥3,213,600,000
Backfilling excavation pit	€ 1,088,027	¥141,443,510
Epoxy spray equipment	€ 1,400,000	¥182,000,000
Epoxy	€ 16,678,084	¥2,168,150,920
Man-hours	€ 5,376,000	¥698,880,000
<b>Total</b>	<b>€ 49,262,111</b>	<b>¥6,404,074,430</b>
<i>Sill and funnel</i>		
Soil excavation	€ 400,000	¥52,000,000
Concrete for funnel	€ 1,010,400	¥131,352,000
Plywood formwork	€ 20,000	¥2,600,000
Concrete L-shaped walls	€ 500,000	¥65,000,000
Concrete blocks sill	€ 1,125,000	¥146,250,000
Riprap	€ 1,125,000	¥146,250,000
Faggots	€ 900,000	¥117,000,000
Grass	€ 20,000	¥2,600,000
Sports facilities	€ 220,000	¥28,600,000
Man-hours	€ 124,000	¥16,120,000
<b>Total</b>	<b>€ 5,444,400</b>	<b>¥707,772,000</b>
<i>Miscellaneous</i>		
Site overhead - inlet	€ 4,110,000	¥534,300,000
Site overhead - outlet	€ 2,850,000	¥370,500,000
Cranes	€ 13,700,000	¥1,781,000,000
<b>Total</b>	<b>€ 20,660,000</b>	<b>¥2,685,800,000</b>
<b>Project Total</b>	<b>€ 385,598,911</b>	<b>¥50,127,858,430</b>
<b>Project Total + 20% indexation</b>	<b>€ 462,718,693</b>	<b>¥60,153,430,116</b>

Table 7.1: Summary of project costs. Conversion of 1 EUR = 130 YEN.

## Conclusions

The answer to the question *'How can the discharge capacity of the Shonai River be improved to modern standards?'* can be answered for multiple locations. Due to the limited time of the research group and the requirement to give well elaborated solutions, the question has only been answered for one location. However, this location is the most critical location along the Shonai River. The most critical location is a bottleneck which is located at the Biwajima bridges along the river. Several options are available to remove this bottleneck. The local government has introduced a plan to replace these bridges. This report proposes a different solution: the creation of a bypass. The urban location of the bottleneck meant options were limited concerning the creation of resolving the bottleneck. The chosen solution of removing the bottleneck consists of a bored tunnel. To raise the discharge capacity of the river to modern standards, a discharge occurring once every 200 years should be seen as a design target. It has been calculated that an additional capacity of  $1400 \text{ m}^3/\text{s}$  is required, this proposal offers  $1490 \text{ m}^3/\text{s}$ . To reach this value, the tunnel surface has to be covered in an epoxy layer, which prevents the necessity of boring larger or more tunnels.

The existing plan of the local officials costs ¥68.4 billion. As a comparison, the proposed alternative has an estimated cost of ¥60 billion. This was calculated based on general Dutch prices, but it is expected that the price in Japan will be in the same order. One can conclude that the proposed plan is a good alternative for the existing plan of the local government to improve the discharge capacity of the Shonai River to modern Japanese standards.

# Recommendations

Following from this report, the following recommendations are made:

- It is recommended to look into various specifications, such as: specific soil conditions, roughness of several cross-sections, exact flow profiles and various construction steps. This report presented a first estimation for the design of the bypass. Further investigation of details will result in a more specific assessment of the flow profile, which leads to a saver design.
- For the determination of the discharge capacity of the Shonai River, a certain amount of uncertainty has been taken into account in this design. This reduced the current capacity of the section significantly. It is recommended to obtain more exact values of the used parameters so the uncertainty could be reduced. This will potentially lead to less water that needs to be diverged into the bypass.
- Another recommendation is to elaborate more on solutions to reduce the soil settlement. The bypass tunnel goes underneath the Shinkansen line. The railway company does not allow large settlements. Therefore, one could think of options like soil improvement to decrease the settlements at this location. The effectiveness and feasibility of solutions should be checked.
- It is recommended to make a more elaborated investigation on the amount of sediment that will remain in the tunnel after a flood. An initial estimation is presented in this report. However, several assumptions have been made during calculations. Additionally, solutions for managing the sediment after a flood should be assessed.
- This report did not focus on the noise pollution and vibrations caused by the flowing water. It should be investigated if these effects are below acceptable limits to prevent opposition of the local population. The same yield for dynamic response of the structure and subsoil.
- A further study into the effects of climate change on the Shonai River should be conducted. The current conclusions about climate change are based on a single study about the precipitation change of Japan in general. More local data could give a better estimation of the climate effect.
- Lastly, the presented idea can also be combined with a super levee. Construction of super levees near rivers has been proposed on several locations in Japan. An example of such an integration is shown in figure 7.1. It is recommended to look into such an option as well.

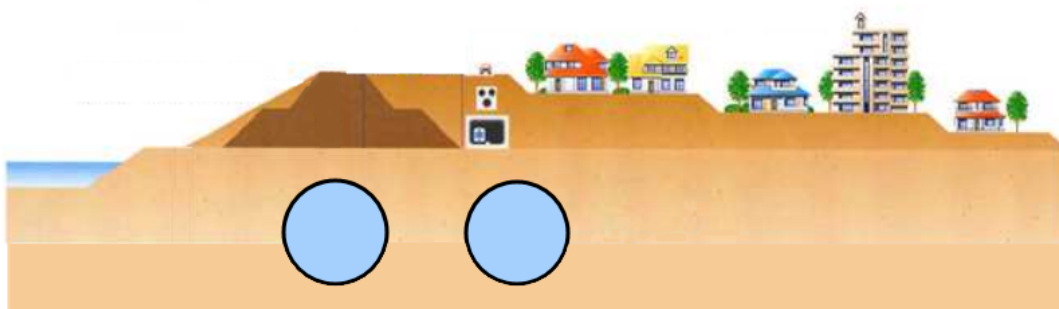


Figure 7.1: Integration with super levee

# Bibliography

- [1] Transport Ministry of Land, Infrastructure and Tourism. River administration in japan, 2007. URL [http://www.mlit.go.jp/river/basic\\_info/english/admin.html](http://www.mlit.go.jp/river/basic_info/english/admin.html). Accessed on July 19th, 2018.
- [2] Tokyoship. Regions and prefectures of japan 2, 2011. URL [https://commons.wikimedia.org/wiki/File:Regions\\_and\\_Prefectures\\_of\\_Japan\\_2.svg](https://commons.wikimedia.org/wiki/File:Regions_and_Prefectures_of_Japan_2.svg). Accessed on July 10th, 2018.
- [3] Rarelibra. Nagoya metropolitan employment area, 2016. URL [https://commons.wikimedia.org/wiki/File:Nagoya\\_Metropolitan\\_Employment\\_Area.svg](https://commons.wikimedia.org/wiki/File:Nagoya_Metropolitan_Employment_Area.svg). Accessed on July 10th, 2018.
- [4] Google. Maps, 2018. URL <https://maps.google.com>. Accessed on June 3rd, 2018.
- [5] N. Shu. Personal communication, 2018-07-18.
- [6] Transport Ministry of Land, Infrastructure and Shonai River Office Tourism, Chubu Regional Development Bureau. Shonai river specific structure remodeling project (jr shinkansen bridge). Technical report, 2017.
- [7] Transport Ministry of Land, Infrastructure and Shonai River Office Tourism, Chubu Regional Development Bureau. Meeting, 2018-07-18. Location: Shonai River Office.
- [8] Central Japan Railyway Company. Annual report 2012, 2012. URL [http://english.jr-central.co.jp/company/ir/annualreport/\\_pdf/annualreport2012-02.pdf](http://english.jr-central.co.jp/company/ir/annualreport/_pdf/annualreport2012-02.pdf). Accessed on July 24th, 2018.
- [9] Transport Ministry of Land, Infrastructure and Shonai River Office Tourism, Chubu Regional Development Bureau. Tokai torrential rain 15 years; memory of disaster to the future, 2016. URL [http://english.jr-central.co.jp/company/ir/annualreport/\\_pdf/annualreport2012-02.pdf](http://english.jr-central.co.jp/company/ir/annualreport/_pdf/annualreport2012-02.pdf).
- [10] Ed Hill. Waller creek flood tunnel, austin, texas, usa, 2014. URL <http://floodlist.com/protection/waller-creek-flood-tunnel-austin-texas-usa>. Accessed on August 2nd, 2018.
- [11] John W. Gonzalez. Solution to downtown flooding giant, invisible, 2015. URL <https://www.expressnews.com/150years/major-stories/article/History-River-Tunnel-0711-6378378.php>. Accessed on August 2nd, 2018.
- [12] Tracking the world's mega-tbms, Unknown. URL <https://www.tunneltalk.com/Discussion-Forum-Mega-TBMs.php>. Accessed on August 2nd, 2018.
- [13] *Reader CIE5305 Tunnels 2017*. 2017.
- [14] Donald F. Elger, Barbara C. Williams, Clayton T. Crowe, and John A. Roberson. *Engineering Fluid Mechanics*. Wiley, Singapore, 2014.
- [15] Tunnel boring machine (tbm) method, Unknown. URL <http://www.p3planningengineer.com/productivity/tunneling/tunneling.htm>. Accessed on August 2nd, 2018.
- [16] Applicability of pneumatic caisson method. 2017.
- [17] Geographical condition map. URL [https://maps.gsi.go.jp/#17/35.186072/136.870412/&ls=english%7C1cm25k\\_2012%7Crelief&blend=01&disp=001&lcd=relief&vs=c1j0h0k0l0u0t0z0r0s0f1](https://maps.gsi.go.jp/#17/35.186072/136.870412/&ls=english%7C1cm25k_2012%7Crelief&blend=01&disp=001&lcd=relief&vs=c1j0h0k0l0u0t0z0r0s0f1). Accessed on August 3th, 2018.
- [18] Railway bureau MLIT. Technical regulatory standards on japanese railways, 2012.
- [19] Naoki Fujii. An overview of japan's high-speed railway : Shinkansen.
- [20] floating barrier systems. URL <http://www.armorfloat.com/>. Accessed on August 8th, 2018.
- [21] Gerrit J. Schiereck and updated by Henk Jan Verhagen. *Introduction to Bed, bank and shore protection*. Delft Academic Press, Delft, the Netherlands, 2016.

- [22] W.J. Rankin et al. Ground movements resulting from urban tunnelling: Predictions and effects. Technical report, 1988.
- [23] SchökComBAR. Schökcombar, technische informatie. Technical report.
- [24] ATP. Soft eye tbm passage through. URL [http://www.atp-frp.com/Brochure\\_SOFT\\_EYE.pdf](http://www.atp-frp.com/Brochure_SOFT_EYE.pdf).
- [25] Hiroshi Kadomura Takashi Oguchi, Kyoji Saito and Michael Grossman d. Csis discussion paper nr. 27: Fluvial geomorphology and paleohydrology in japan. Technical report, 2005.
- [26] Aline te Linde. Hydrologische consequenties van klimaatverandering, 2013. URL <https://www.slideshare.net/alinetelinde/201205-pao-te-linde>. Accessed on July 11th, 2018.
- [27] Hydrology and Kyoto University Water Resources Research Laboratory. Shonai-gawa. Technical report, 2013.
- [28] Hydrology and Kyoto University Water Resources Research Laboratory. Nagara-gawa. Technical report, 2013.
- [29] Ibi basin comprehensive flood control measures Review Committee. Comprehensive flood control measures plan in ibi basin. Technical report, 2007.
- [30] Transport Ministry of Land, Infrastructure and Tourism. Main disaster of the kiso river - flood damage equipment, 2017. URL [http://www.cbr.mlit.go.jp/kisojyo/saigai/02\\_kiso.html](http://www.cbr.mlit.go.jp/kisojyo/saigai/02_kiso.html). Accessed on July 10th, 2018.
- [31] Transport Ministry of Land, Infrastructure and Tourism. Outline of basin and river of shonai river system. Technical report, 2005.
- [32] Toshiyuki Adachi. Flood damage mitigation efforts in japan, 2009. URL [http://www.mlit.go.jp/river/basic\\_info/english/pdf/conf\\_09-0.pdf](http://www.mlit.go.jp/river/basic_info/english/pdf/conf_09-0.pdf). Accessed on July 11th, 2018.
- [33] Dr. Eng. R. Tsubaki. Personal communication, 2018-07-10.
- [34] T. Murakami et al. Prediction of maximum possible storm surges in ise bay under a future climate. 2012.
- [35] Koji Teranishi. Construction of nagoya storm-tide-preventing breakwater. *ICCE*, No. 10:1157–1182, 1966.
- [36] Masaru Yamashiro Hiroyasu Kawai1, Noriaki Hashimoto and Tomohiro Yasuda. Uncertainty of extreme storm surge estimation by high wind sea surface drag coefficient and future typhoon change.
- [37] Nobuhito MORI Sooyoul KIM Yoko SHIBUTANI, Sota NAKAJO and Hajime MASE. Estimation of worst-class tropical cyclone and storm surge, and its return period -case study for ise bay. March 2015.
- [38] Kentaro Imai, Kenji Satake, and Takashi Furumura. Amplification of tsunami heights by delayed rupture of great earthquakes along the nankai trough. *Earth, Planets and Space*, 62:427–432, April 2010.
- [39] Shohei Fujita, Shigeru Kato, and Takumi Okabe. Spatial distribution of maximum tsunami water level and its arrival time in ise bay and mikawa bay. *Journal of Japan Society of Civil Engineers, Ser. B3 (Ocean Engineering)*, 72:169–174, 2016.
- [40] The Japan Times. Anticipating a major nankai trough quake, November 2017. URL <https://www.japantimes.co.jp/opinion/2017/11/05/editorials/anticipating-major-nankai-trough-quake/>. Accessed on June 4th, 2018.
- [41] City of Nagoya. Natural disasters, 2017. URL <http://www.city.nagoya.jp/en/page/0000013882.html>. Accessed on July 11th, 2018.
- [42] NASA. Global rural-urban mapping project (grump), v1, population density grid, v1, 2000. URL <http://sedac.ciesin.columbia.edu/data/set/grump-v1-population-density/data-download>. Accessed on June 4th, 2018.

- [43] Shisuzou. Aichi prefecture application area, 2018. URL <https://japonyol.net/land-use-aichi.html>. Accessed on July 10th, 2018.
- [44] MLIT. Shonai, 2018. URL [http://www.cbr.mlit.go.jp/shonai/cams/?map\\_M2.htm](http://www.cbr.mlit.go.jp/shonai/cams/?map_M2.htm). Accessed on July 10th, 2018.
- [45] Judith Bosboom and Marcel J.F. Stive. *Coastal Dynamics I*. Delft Academic Press, Delft, the Netherlands, January 2015.
- [46] Navionics. Chart viewer, 2017. URL <https://webapp.navionics.com/#boating@7&key=%7DulrEkto%60Y>. Accessed on June 3rd, 2018.
- [47] Topographic-map.com. Nagoya, 2018. URL <http://en-hk.topographic-map.com/places/Nagoya-8919203/>. Accessed on July 10th, 2018.
- [48] USGS. World - m6+ in 2017, 2018. URL <https://earthquake.usgs.gov/earthquakes/browse/m6-world.php?year=2017>. Accessed on June 3rd, 2018.
- [49] National Research Institute for Earth Science and Disaster Prevention. Basic knowledge of earthquakes, 2008. URL [https://web.archive.org/web/20080504170142/http://www.hinet.bosai.go.jp/about\\_earthquake/part1.htm](https://web.archive.org/web/20080504170142/http://www.hinet.bosai.go.jp/about_earthquake/part1.htm). Accessed on June 5th, 2018.
- [50] JMA. Jma seismic intensity scale (1949) and reference items (1978), 2018. URL <http://www.hp1039.jishin.go.jp/eqchreng/at2-3.htm>. Accessed on June 5th, 2018.
- [51] JMA. Summary of tables explaining the jma seismic intensity scale, 2018. URL <http://www.jma.go.jp/jma/en/Activities/intsummary.pdf>. Accessed on June 5th, 2018.
- [52] Japan Property Central. Earthquake building codes in japan, 2018. URL <http://japanpropertycentral.com/real-estate-faq/earthquake-building-codes-in-japan/>. Accessed on July 11th, 2018.
- [53] National Research Institute for Earth Science and Disaster Prevention. 2011 off the pacific coast of tohoku earthquake, strong ground motion. Technical report.
- [54] KLEMENT TOCKNER KEIGO NAKAMURA and KUNIHICO AMANO. River and wetland restoration: Lessons from japan. *BioScience*, 56, 2006.
- [55] River Office Shonai River. Shonai river. Technical report, 2016.
- [56] Shonai river office MLIT. River project of shonai river. Technical report, Unknown.
- [57] River Office Shonai River. Origawa dam. Technical report, 2013.
- [58] Japan Dam Foundation. Teirinji disaster prevention dam [gifu prefecture], 2009. URL <http://damnet.or.jp/cgi-bin/binranA/All.cgi?db4=1102>. Accessed on July 13th, 2018.
- [59] Japan Dam Foundation. Hiyoshi disaster prevention dam [gifu prefecture], 2005. URL <http://damnet.or.jp/cgi-bin/binranA/All.cgi?db4=1118>. Accessed on July 13th, 2018.
- [60] Japan Dam Foundation. Tazawa disaster prevention dam [gifu prefecture], 2009. URL <http://damnet.or.jp/cgi-bin/binranA/All.cgi?db4=1124>. Accessed on July 13th, 2018.
- [61] Road Traffic Technology. Smart (stormwater management and road tunnel), kuala lumpur, 2017. URL <https://www.roadtraffic-technology.com/projects/smart/>. Accessed on July 13th, 2018.
- [62] ITS International. Success of kuala lumpur's dual purpose tunnel, 2012. URL <http://www.itsinternational.com/categories/detection-monitoring-machine-vision/features/success-of-kuala-lumpurs-dual-purpose-tunnel/>. Accessed on July 13th, 2018.
- [63] Chubu Regional Development Bureau. Time flow rate monthly table search, 2017. URL <http://www1.river.go.jp/cgi-bin/SrchWaterData.exe?ID=305081285511090&KIND=6&PAGE=0>. Accessed on July 19th, 2018.

- [64] MLIT. Development of rivers in the chubu region. Technical report, 2013.
- [65] Kuciv Kyoto. Shonai-gawa. Technical report, 2004.
- [66] Transport Ministry of Land, Infrastructure and Tourism. Basic info shonai. Technical report, 2002.
- [67] Sunmin Kim, Eiichi Nakakita, Yasuto Tachikawa, and Kaoru Takara. Precipitation changes in japan under the a1b climate change scenario. *Annual Journal of Hydraulic Engineering, JSCE*, 54, 2010.
- [68] Yoshinobu Sato, Toshiharu Kojiri, Yuri Michihiro, Yasushi Suzuki, and Eiichi Nakakita. Estimates of climate change impact on river discharge in japan based on a super-high-resolution climate model. *Terr. Atmos. Ocean. Sci.*, 23:527–540, 2012.
- [69] IPCC. The projections of the earths future climate, 1996. URL <https://www.ipcc.ch/ipccreports/tar/wg1/029.htm>. Accessed on July 17th, 2018.
- [70] Tomohiro Yasuda, Hajime Mase, and Nobuhito Mori. Projection of future typhoons landing on japan based on a stochastic typhoon model utilizing agcm projections. *Hydrological Research Letters*, 4:65–69, 2010.
- [71] Transport Ministry of Land, Infrastructure and Tourism. River administration in japan. Technical report, 2007.
- [72] Transport Ministry of Land, Infrastructure and Shonai River Office Tourism, Chubu Regional Development Bureau. River project of shonai river: Resilient to disasters. Technical report, 2001.
- [73] Transport Ministry of Land, Infrastructure and Chubu Regional Development Bureau Tourism. 川の防災情報：水位観測所付近の川の断面図 (disaster prevention information of river: a cross section of a river near the water level observatory), 2018. URL <http://www.river.go.jp/kawabou/ipSuiiKobetu.do?init=init&obsrvId=2178200400012&gamenId=01-1002&timeType=60&requestType=1>. Accessed on July 19th, 2018.
- [74] Manning's n values, 2006. URL [http://www.fsl.orst.edu/geowater/FX3/help/8\\_Hydraulic\\_Reference/Mannings\\_n\\_Tables.htm](http://www.fsl.orst.edu/geowater/FX3/help/8_Hydraulic_Reference/Mannings_n_Tables.htm). Accessed on August 3th, 2018.
- [75] Japan River Association. Shonair, chubu r.b., outline of river system. URL [http://www.japanriver.or.jp/river\\_law/kasenzu/kasenzu\\_gaiyou/chubu\\_r/053syonai.htm](http://www.japanriver.or.jp/river_law/kasenzu/kasenzu_gaiyou/chubu_r/053syonai.htm). Accessed on July 23th, 2018.
- [76] MLIT. Geological survey of outsourced design of lojushima island. Technical report.
- [77] N700 series shinkansen, . URL [https://en.wikipedia.org/wiki/N700\\_Series\\_Shinkansen](https://en.wikipedia.org/wiki/N700_Series_Shinkansen). Accessed on August 3th, 2018.
- [78] Shinkansen, . URL <https://en.wikipedia.org/wiki/Shinkansen>. Accessed on August 3th, 2018.
- [79] The European Union. En1990: Eurocode - basis of structural design. Technical report, 2018.
- [80] Rhs, 2018. URL <http://www.ipisteel.eu/en/images/stories/ipisteel/rhs.jpg>. Accessed on August 3th, 2018.
- [81] J. Wardenier. Steel structures ii - rhs joints slides, 2017.
- [82] Chubu Regional Development Bureau. Shonai river water system river improvement plan. Technical report. Translated from Japanese.
- [83] Losses in pipeline systems, . URL <http://www.nzdl.org/gsd1mod?e=d-00000-00---off-0hd1--00-0---0-10-0---0---0direct-10---4-----0-11--11-en=-50---20-about---00-0-1-00-0--4---0-0-11-10-OutfZz-8-00&cl=CL1.11&d=HASH011f05bf8734d88d1a080257.13.1&gt=1>. Accessed on August 8th, 2018.
- [84] David Apsley. Friction laws. URL <https://personalpages.manchester.ac.uk/staff/david.d.apsley/lectures/turbbl/friction.pdf>. Accessed on August 10th, 2018.

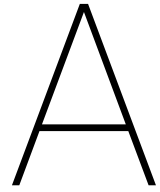


- [85] Dr.ir. G.H.W. Schoups. Water system analysis (water control): Channel flow - nonuniform flow.
- [86] E. Mosselman. River dynamics - river bifurcations part 2, slides, 2016.
- [87] Rubber Flooring Inc. Outdoor sports tiles, . URL <https://www.rubberflooringinc.com/interlocking-tile/outdoor-sports-tiles.html#>. Accessed on August 22nd, 2018.
- [88] Dr. Ir. W. Broere. Tunnel face stability.
- [89] Numbeo. Property prices in nagoya, japan. URL <https://www.numbeo.com/property-investment/in/Nagoya?displayCurrency=EUR>. Accessed on August 23th, 2018.
- [90] Bodemrichtlijn. Ontgraven met kerende constructie, kosten grond- en waterkerende constructies. URL <https://www.bodemrichtlijn.nl/Bibliotheek/bodemsaneringstechnieken/c-grondverzet/c3-ontgraven-met-eeen-grond-en-waterkerende-constructie/ontgraven-met-kerende-constructie-kosten-grond-en-waterkerende-c8816>. Accessed on August 24th, 2018.
- [91] Rotterdamse Baan. Volg de tunnelboor-machine. URL <https://www.waarisdeboor.nl/>. Accessed on August 23th, 2018.
- [92] Shani Wallis. Spray-on waterproofing - finding real application. URL <https://tunneltalk.com/Spray-on-waterproofing-Finding-real-application.php>. Accessed on August 23th, 2018.
- [93] Bluey Technologies. Bluseal tunnel liner systems - bluey technologies. URL <http://www.bluey.com.au/project/bluseal-tunnel-liner-systems>. Accessed on August 24th, 2018.
- [94] JBA Consulting; Angus Pettit JBA Consulting; Ray Pickering JBA Consulting Kevin Keating, JBA Consulting; Peter May. Cost estimation for fluvial defences – summary of evidence. Technical report, 2015.
- [95] Prof.ir. A.Q.C. van der Horst. Cie4170 - information for cost comparison and estimate. Accessed on November 29th, 2017.
- [96] Inc. CostHelper. Cost of epoxy flooring - estimates and prices paid. URL <https://home.costhelper.com/epoxy-floor.html>. Accessed on August 24th, 2018.
- [97] JBA Consulting; Angus Pettit JBA Consulting Paul Jones, JBA Consulting; Kevin Keating. Cost estimation for channel management – summary of evidence. Technical report, 2015.
- [98] Tuin en Gras. Kosten graszoden? scherpe grasmatten prijs bij tuin en gras. URL <https://www.tuinengras.nl/prijzen-graszoden#prijs-gras-leggen>. Accessed on August 24th, 2018.
- [99] Rubber Flooring Inc. Outdoor sports tiles - discount outdoor gym tiles, . URL <https://www.rubberflooringinc.com/interlocking-tile/outdoor-sports-tiles.html#>. Accessed on August 24th, 2018.
- [100] Matéflex. Tennis court resurfacing with matéflex ii » mateflex. URL <http://www.mateflex.com/products/mateflex-ii/>. Accessed on August 24th, 2018.



# V

## Appendices of Phase I



## River characteristics

An overview of the main rivers in the Greater Nagoya Area is presented in the following map:



Figure A.1: General map of rivers in the Greater Nagoya Area [4]

Nagoya has been built on the alluvial Nobi Plain, which was formed by several rivers. In the west lie the rivers Kiso, Ibi and Nagara, sometimes referred as 'Kiso Three Rivers'. From the north-east comes the Shonai River, or Shonogawa, from where it crosses Nagoya city to the harbour. The Shonai River system consists of multiple rivers going through the city as well, both natural and man-made. The two other main rivers in Nagoya City are the Shin and Tempaku, with the Shin having been dug to divert water from the Shonai among others. In the southern part of the area flows the Yahagi river, ending in the Mikawa Bay. Furthermore to the south is the Toyokawa river, also ending in the Mikawa Bay.

There are several differences between European and Japanese rivers. First, Japanese rivers are on average shorter and steeper, in a higher discharge speed. Figure A.2 compares distance-elevation profiles of several Japanese rivers and rivers world wide. Secondly, maximum discharges occur at different times of the year. Whereas European rivers peak at the start of the year, Japanese ones have maximum discharge during the summer, in the typhoon season. This has been illustrated by comparing the Shonai River with the (Dutch) Rhine and Meuse, shown in figure A.3.

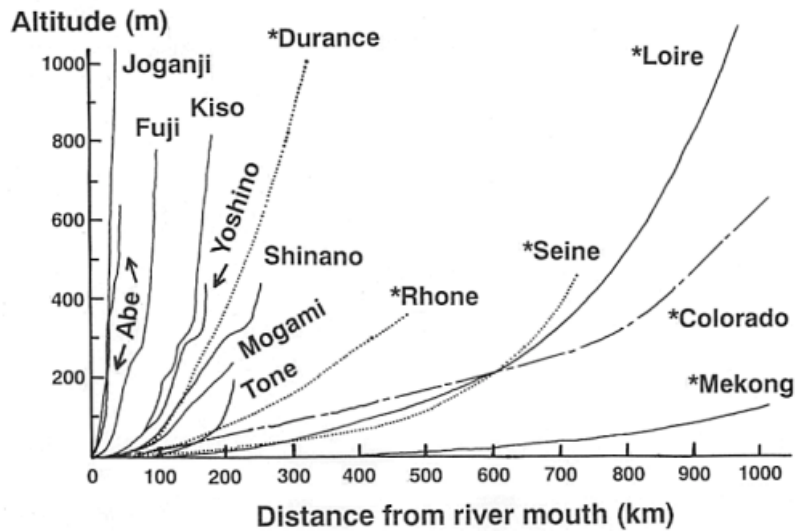


Figure A.2: Elevation over distance comparison European and Japanese rivers [25]

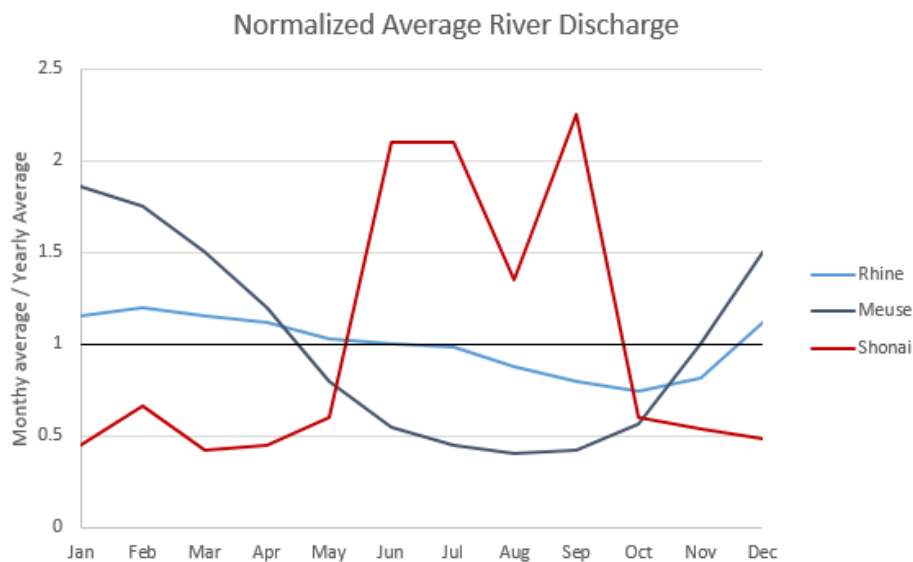


Figure A.3: Monthly average discharge [26] [27]

### A.1. Flood history

Nagoya has had several river floods occur, mainly caused by typhoons and heavy rainfall. Table A.1 shows the years river floods happened, as well as the number of affected houses.

**Affected houses due to floods per year per river**

Year	Nagara	Ibi	Shonai	Kiso
1957	0	0	22428	0
1959	27521	4576	140596	354427
1960	8342	0	0	0
1961	24126	11080	39775	889
1970	0	0	0	198
1972	0	0	2347	0
1974	0	9313	0	0
1975	0	0	10422	0
1976	41462	22351	8713	0
1983	0	0	8035	4588
1986	0	159	0	0
1988	0	0	1990	0
1989	0	0	655	0
1990	67418	1135	0	0
1991	0	0	6456	0
1999	0	0	121	0
2000	0	0	34049	0
2002	0	972	0	0
2004	0	1065	0	0

Table A.1: Years of flooding with affected houses per river. Nagara: [28], Ibi: [29], Kiso: [30], Shonai: [31]

**A.2. Current protection**

Safety standards in Nagoya area are lower than the Dutch ones. Whereas Dutch flooding design risks for river flooding range between 1/1250 to 1/10000 years, the current one for Nagoya is in the order of magnitude of 1/200 years. However, this level has not been reached yet, as both planning and construction are still in development. [32] [33]

Current protections have mainly been focused on the downstream reaches of the rivers. Site investigation shows many parts of the river are bordered by either earthen embankments or concrete walls, especially the canals. For the Kiso, Ibi and Nagara in the west, the defences become less restrictive, as the distance between levees increases, giving room for the rivers. Some upstream parts of the Shonai River do not meet the safety standards as of yet, as can be seen in figure A.4.

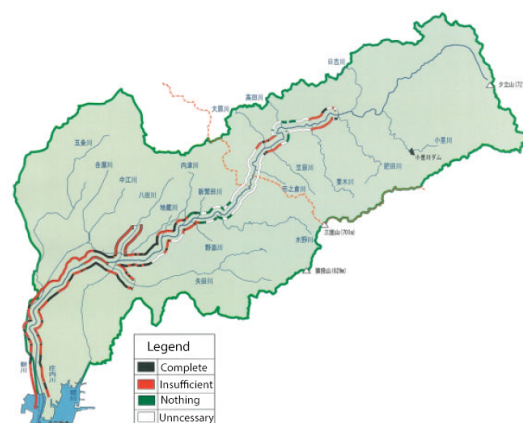


Figure A.4: Current state Shonai River protections [31]

Lastly, the Japanese strategy to deal with disaster seems to also incorporate recovery. In the Netherlands, the main idea is to prevent any flooding from occurring, whereas Japan uses a combination of both preventing damage as well as minimising it, for example by improving evacuation procedures.

# B

## Storm surge characteristics

In the past, storm surges have occurred in Ise bay, for example during typhoon Vera in 1959. During this typhoon, the high tide reached the greatest level in history. The storm tide reached a level of 3.5 m above mean sea level (MSL) [34] (T.P. 3.5 m), the waves had a height up to 3 m [35]. This resulted in flooding the area around the bay, causing 5000 fatalities and 1400 million USD damage [35]. Typhoon Vera became the design typhoon for the Japanese coast to protect against. [36]. This storm surge level became the design level around Ise Bay.

In 2012, Murakami et al. deduced in a research the effects of several scenarios of typhoons. In total, 50 typhoons had been examined. In this examination, future climate change was taken into account. In the end, it was concluded all the scenarios would give a storm surge level higher than the design level, up to a maximum of T.P. +6.9 m. The difference in predicted storm surge level along the bay has been illustrated in figures B.1 and B.2. It is visible, mostly in figure B.2, that storm surge mainly affects the harbour area of Nagoya and Ise Bay estuary.

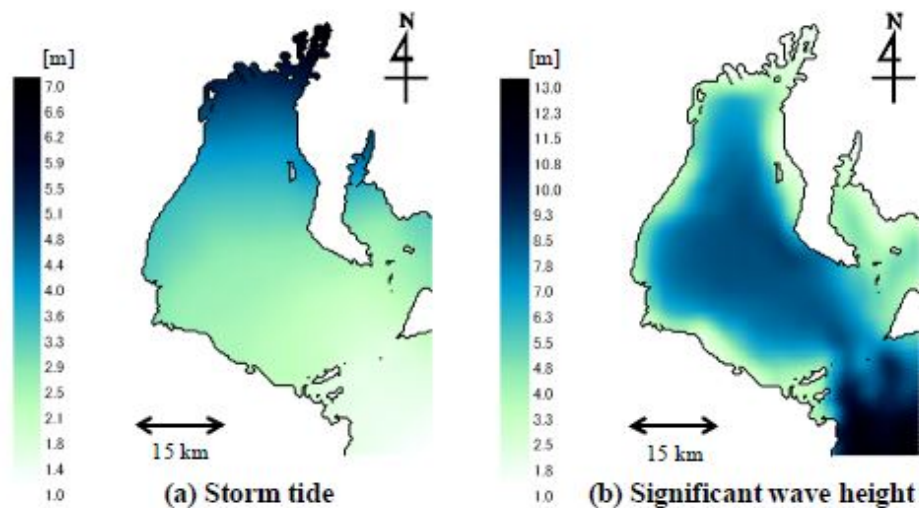


Figure B.1: Map of storm surge tide level and significant wave height in Ise Bay [34]

In the southern part of the bay, the storm surge tides does not exceed T.P. +3.5 m. Flood safety has already either been met or can be done so easily. However, in the northern part, flood safety could pose problems. The more north, the higher the storm surge tide. This has most likely to do with the fact the bay narrows towards the north. To protect the harbour area, it is possible to construct a storm surge barrier. When done, it will be most reasonable to place the barrier at the location given in figure B.3. In this place, the bay is narrow, making construction of a barrier more cost-efficient and easier.



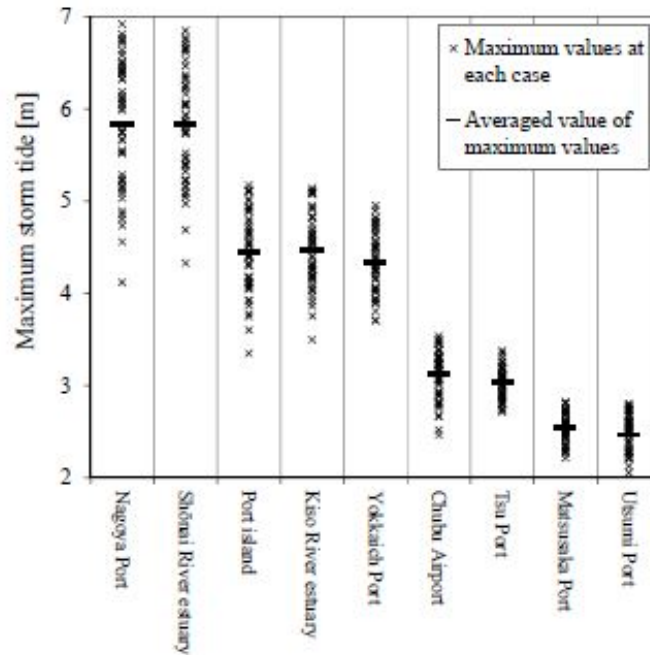


Figure B.2: Graph of storm surge tide level [34]

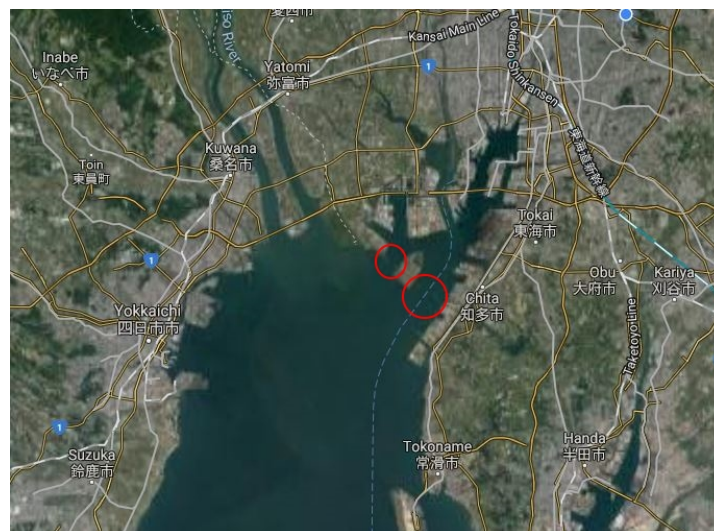
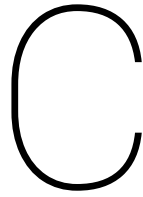


Figure B.3: Possible place for storm surge barrier [4]

For the shorelines between the sea and the location of the port, reinforcement of the flood defences are required. In most cases raising the top of the defence up to the required level should be possible. In the cases where this is not possible, other solutions should be found.

The predicted numbers found above followed from just one report. Shibutani et al. calculated different numbers. They found a storm surge level of T.P. +5 m with a return period of 430 years [37]. In comparison, the storm surge tide of T.P. +3.5 m (design level) has a return period of 150 years [36].

As can be deduced from the above, different numbers are present to use. However, since Murakami et al. do not give any return periods at all, a design storm surge level has not been set yet. Furthermore, the Japanese government does not set requirements on storm surge safety levels. It is advised to carry out more research when designing for the flood safety concerning storm surges.



## Tsunami characteristics

When an earthquake occurs at the Tokai trough with a magnitude occurring every 150 years, simulations reveal that the wave height could be in the order of 8 m at the Aichi coast and 7 m at the Mie coast [38]. As mentioned in appendix F.1, the coastal defence of the Aichi prefecture consist mainly of dunes higher than 40 meters. Therefore, the current protection should be able to stop tsunamis of 8 m height. Subsequently, since the coast of Mie prefecture is rugged and there are no major cities near the coast, the consequences of a tsunami are considered low at this side.

The wave height inside the Ise bay is smaller due to the bay entrance. If a tsunami wave comes in with an angle with respect to the bay axis direction, the wave gets diffracted when it enters the Ise bay. This causes an increase in energy dissipation, resulting in a lowering of the wave height, see figure C.1 [39]. Taking this into account, the maximum height of the tsunami inside the bay is approximately 3 m [38].

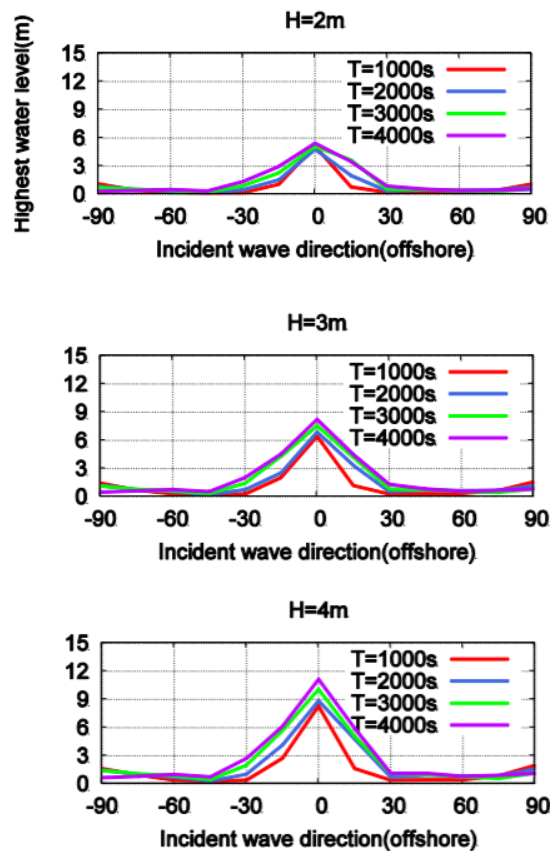


Figure C.1: Maximum water level offshore at the bay entrance [39]



Another important parameter when considering waves is the wave period. Fujita et al. use wave periods ranging from 1000 to 4000 seconds in their simulation of Tsunami propagation at Ise bay [39]. They also mention that a higher wave period enhances the diffraction, thus resulting in more energy dissipation.

Figure C.2 shows the evolution of the water level inside and in front of Ise bay. From this figure it can be seen that the tsunami height in the bay is much smaller than at the coast.

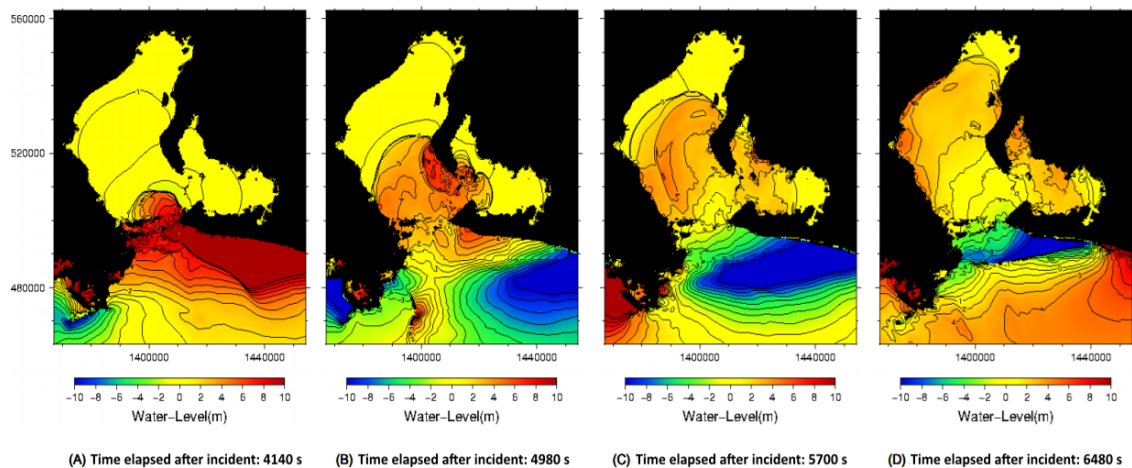


Figure C.2: Time lapse of tsunami height for a wave height of 3 m and period of 3000 s [39]

Additionally, the probability of occurrence of a tsunami attack is of importance. According to the Japan Times [40] large-scale earthquakes at the Tokai trough have occurred once every 100 to 150 years in the past, with the last big quake in 1854. A 70% chance has been predicted of an earthquake taking place in the next 30 years with a magnitude of 8 or more [40].

Therefore, the probability of a tsunami in this area is relatively high. However, since the consequences along the coast are limited, the risk is still low at the adjacent coastal stretches. Inside the bay the consequences will be of more importance, since a flooding of the city Nagoya will have major impact. Yet the wave will be dissipated leading to a relatively small wave and thus less impact resulting in a lower risk. On the other hand, it is also a possibility that the Tokai earthquake triggers the more severe Nankai earthquake due to the interaction with other earthquakes. Due to this the coastal area will be damaged. To minimise this damage, warning systems are used to inform residents so they can evacuate to save places [41].

# D

## Value of region

### D.1. Population density

The greater Nagoya region can be considered as an urbanised region. figure D.1 gives an indication of the population densities in the considered area. From this it can be concluded that the majority lives in the centre of Nagoya. The population density in other regions is substantially less. It has to be mentioned that the numbers are only used to indicate the relative importance of areas due to the fact that the numbers are from the year 2000.

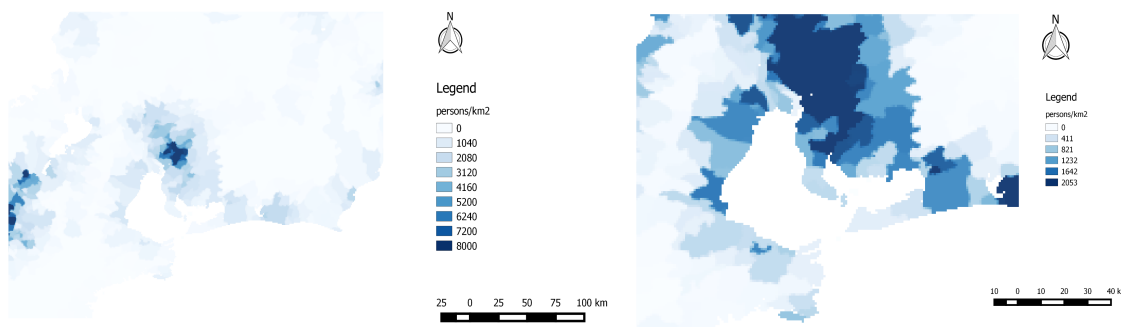


Figure D.1: Left: Population density in the region around Ise bay. Right: Detailed population density for the less populated areas [42]

### D.2. Land usage

The land usage is an important parameter in determining the economic value of a region. Three categories of land usage have been identified as economically valuable:

- Commercial area
- Residential area
- Industrial area

Commercial and residential zones indicate densely populated areas. Figure D.2 gives the type of usage as described in the categories above. The red colour represents commercial area, purple/blue/green is residential area. For the residential area the different colours represent the difference between high- and low-rise residential area, for simplicity these have been grouped into one category. Furthermore, the port of Nagoya is an important area for the region, since the industry is one of the major incomes for the city. The main industry is the automotive, but also other types of industry are present. More land inward, upstream and midstream of the rivers, the area consists more of nature such as forests.

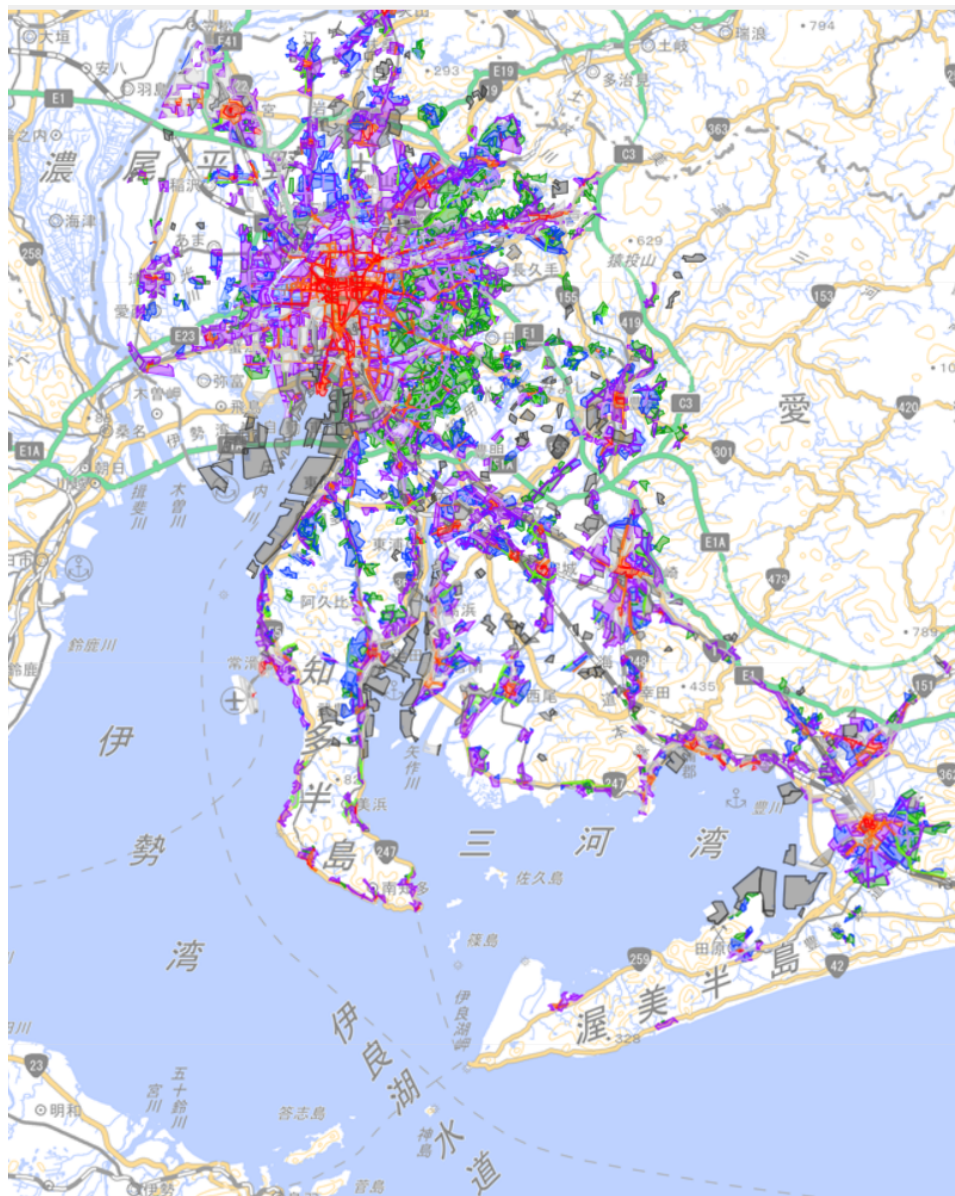


Figure D.2: Land use of the Nagoya area: red = commercial area; purple/blue/green = residential area; grey = industrial area [43]

### D.3. Cultural value

In the city of Nagoya several buildings have special cultural value. An example is the Nagoya Castle, located in the centre of Nagoya, and Ryusenji Castle, which is found along the Shonai River in the northern part of Nagoya centre. Also a shrine is present in the centre of Nagoya which is of great cultural value to the inhabitants. Furthermore, multiple Buddhist temples and altars are present in cities and towns in the observed region. Overall, since Nagoya region is not focused on tourism there are not many touristic attractions in the area. Hence, the cultural value comprises mostly of the above mentioned locations. Especially the Nagoya Castle is of great importance, as already in earlier times river flood management was performed such that the castle was protected.

# E

## Determining project location

As a result of the discussed subjects in the previous sections of this chapter, it has been concluded additional coastal protection is not necessary. Current use of the Tetrapods results in adequate protection against impact of large waves. The steep slope of a small hill protects the towns in the hinterland sufficiently. It can also be concluded that the need of a storm surge barrier is not top-priority. In the past few decades, storm surge floods have not been present, with the last one in the year 1959. Although preventive measures can be taken to protect the city from a disaster like the measurements after North Sea flood of 1953, conditions in Nagoya are different. While protected area from the measurements after the North Sea flood is mostly flat and below sea-level, Nagoya is located on a hill which forms a natural form of protection against sea-side floods. Only areas near the harbour and centre of Nagoya have to be protected.

This argumentation is also valid for tsunamis. Most of the sea side is directly protected with a natural slope, although some place, especially at the coast, are still vulnerable. The harbour is more vulnerable, but is protected by the shape of the bay. The dispersion in the bay reduces the wave height significantly, as elaborated in section C. Therefore, the construction of a massive barrier in the deep entrance of the bay is both otiose and expensive. Rivers have caused major problems in the country. Especially during typhoons, discharge in rivers can increase tremendously. Differences between average discharge and maximum discharge can differ by more than a factor 100. These two orders of magnitude difference create a challenge for the flood protection of the rivers. Because of this all, the rivers through the city are top-priority if it comes to improvement of current flood protection. As a result of the information gathered on recent floods in section A combined with the use of area found in D, the Shonai River will be investigated. An overview of the river has been given in figure E.1, in which four different sections of the 96 km long river are indicated.

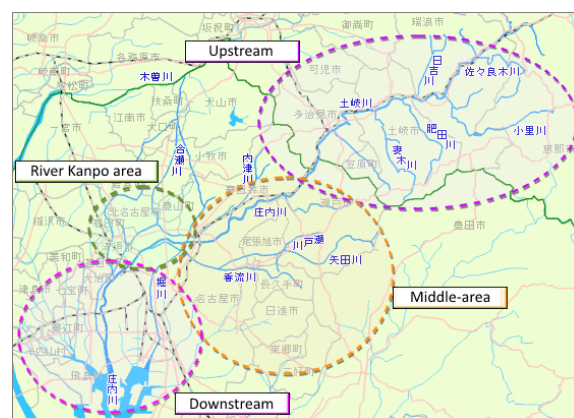


Figure E.1: Sections of the Shonai River [44]

## Current bathymetry and protection

### F.1. Coast

The adjacent coastline can be divided into two sections. The first belongs to the Mie prefecture, and is located at the west of the Ise bay. This section takes into account the coastline running from Toba to Kumano. The second section comprises the coastline of the Aichi prefecture, located in front of the city Tahara at the east of Ise bay. The red lines in figure F.1 point out the location of the considered coastal stretches.

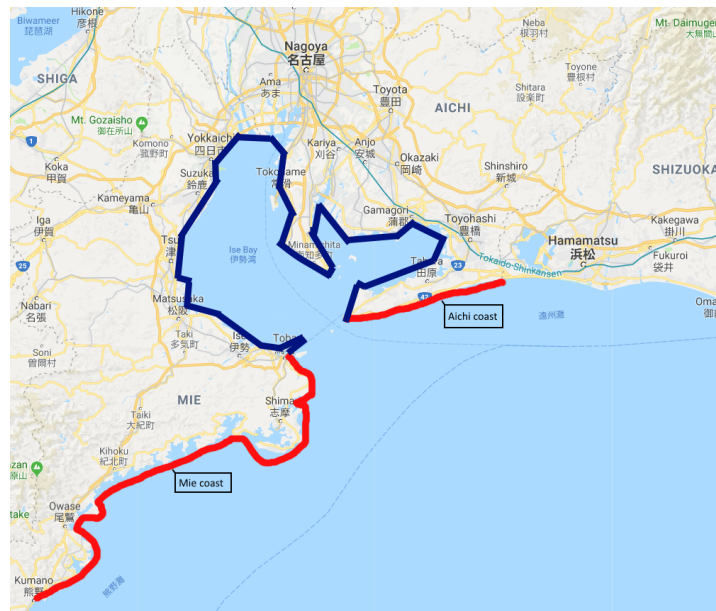


Figure F.1: Locations of the coastlines belonging to Mie and Aichi prefecture [4]

#### F.1.1. Coast of Mie prefecture

In general, the coast of Japan could be characterised as a leading-edge coast. This implies that the coastlines are mostly rugged and cliffed. Furthermore, the continental shelf is narrow, resulting in a fast transition to water depths exceeding 200 m [45]. These coastline characteristics are clearly visible at this part of the coast.

#### Bathymetry

The slope of the coast is rather steep with an average estimated slope of 0.02 (1:55). Since the continental shelf is narrow, the water depth increases fast after approximately 10 km from the coast [46]. Figure F.2 gives the depth contours in front of the considered coastline.



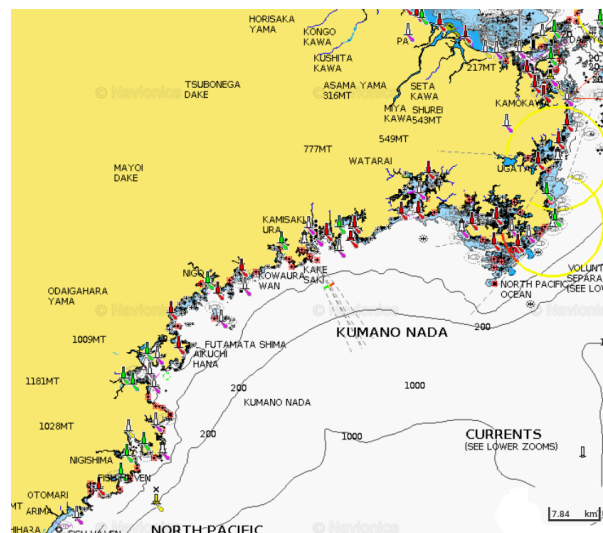


Figure E2: Bathymetry of the Mie coast [46]

### Protection

This part of the coastline does mainly consists out of rocks. There are no major cities close to the coastline. The small cities that are present are situated inside the small inlets, so they are not directly exposed to the sea. Harbours of small cities are protected by caisson breakwaters in combination with concrete elements such as Tetrapods. This type of protection is the case in for example Owase and Kihoku. The part of the cities that is directly located at the coastline, is protected by detached emerged breakwaters made of concrete elements. When approaching the Ise bay, the urbanisation increases. The city of Shima is the largest in the area. The coastline consists of partly rocks and sandy shores. The sandy coasts are protected by detached breakwaters. Between the shore and the city, a wall is often built as protection [4].

### E1.2. Coast of Aichi prefecture

The coastline of the Aichi prefecture is different from the coast of the Mie prefecture. It consists of beaches and does not have the rugged character typical for this area.

### Bathymetry

The coast consists mainly of a sandy shore, while at some places the coast is more made up of rocks. The average estimated slope of the foreshore is 0.007, or 1:140, which is substantially milder than for the Mie prefecture [46]. Figure E3 shows the depth contours in front of the Aichi coastline.

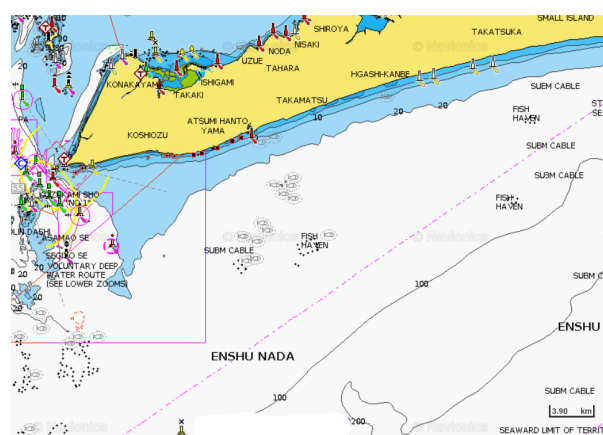


Figure E3: Bathymetry of the Aichi coast [46]

### Protection

At this coastal stretch the protection is mainly caused by reinforced dunes. The city that requires most protection is Toyohashi. Hills with heights exceeding 40 meters are present between the city and the coastline [47]. Any risk posed is from the bay and not the coast. There are no major cities present along the coastal stretch. The small harbours are again protected by caisson breakwaters combined with concrete armour units. Furthermore, at several places along the coast detached breakwaters are present. [4]

## F.2. Ise Bay

Nagoya is situated at a bay, which eventually borders the sea. The shoreline along the bay is shown in blue in figure F.1. Along the bay, some cities are present. Overall, the areas around the bay can be classified as urban to semi-urban with some agricultural land. This use of the area makes protection against flood along the bay necessary.

### F.2.1. Bathymetry Ise Bay

The bathymetry of the bay is quite constant, see also figure F.4. Most part of the bay is 20 m to 30 m deep. The eastern part of the bay tends to be no deeper than 20 m. The slope to the shores differs along the bay. On the western and eastern side, it is on average 0.005, on the eastern side of the north-west part of the bay it is much steeper with parts up to 0.025.



Figure F4: Ise bay bathymetry [46]

### Protection

The protection around the bay consists mainly of dikes or embankments, often covered with stones or concrete. On top of those dikes and embankments, a little wall (in the range of 0.5 m). On some places, like in harbours or in hilly areas, protections are not required or present.

# G

## Seismic identification

Earthquake engineering is an important issue in Japan. In 2017 alone, 6 earthquakes with a magnitude of over 6.0 struck Japan [48]. With 400 earthquakes on a daily basis [49], Japan has created one of the most strict seismic-behaviour design rules of the world. Classification of seismic intensity is determined by the Japan Meteorological Agency (JMA), which separates earthquake into 10 categories which are displayed in table G.1.

Shindo nr.	Description	Peak acceleration	Mercalli Scale
0	Not felt by humans	$< 0.008 \text{ m/s}^2$	I
1	Some people feel slight quake	$0.008 - 0.025 \text{ m/s}^2$	I-II
2	Many people feel quake; Objects start swinging	$0.025 - 0.08 \text{ m/s}^2$	II-IV
3	Most humans feel quake; Objects start moving	$0.08 - 0.25 \text{ m/s}^2$	III-IV
4	People are startled; Objects may fall	$0.25 - 0.80 \text{ m/s}^2$	V-VII
5 – lower	People are frightened; Furniture may move or topple	$0.80 - 1.40 \text{ m/s}^2$	V-VIII
5 – higher	Difficult to walk; Objects move and topple	$1.40 - 2.50 \text{ m/s}^2$	VI-IX
6 – lower	Difficult to stand; Weak houses crack or collapse	$2.50 - 3.15 \text{ m/s}^2$	VIII-X
6 – higher	Impossible to move; Strong buildings crack	$3.15 - 4.00 \text{ m/s}^2$	IX-X
7 and up	Damage to all structures; Lots are tilted or collapsed	$> 4.00 \text{ m/s}^2$	X-XII

Table G.1: JMA Seismic Intensity Scale [50, 51]

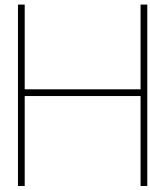
The JMA scale, which reports a figure based on ground acceleration, does measure both intensity and duration. Therefore, acceleration values stated in table G.1 do not always match with the Shindo number. Besides the Shindo number, several international standards for seismic intensity are used as well.

To take this seismic behaviour into account when designing a civil structure, Japan has designed a building code similar to Eurocode 8, but more strict. This so called shin-taishin (implemented in 1981) requires all buildings to be build with a certain seismic standard. Prior to this code, the kyu-taishin rules were followed. The 1995 Great Hanshin earthquake with Shindo number 7 already proved the effect of the implementation of this new code [52]. The largest earthquake measured in Japan - which occurred on March 11<sup>th</sup>, 2011 - had an intensity of 7 on the JMA scale. The acceleration of this earthquake is shown in figure G.1.



Figure G.1: Earthquake of 2011 [53]





## Japanese hydraulic engineering and future vision

In Japan, the history of hydraulic engineering goes back many centuries. From the 17<sup>th</sup> century, relatively large engineering projects started to develop. From the end of the 19<sup>th</sup> century, rivers started to be canalised, especially in the downstream areas. Most of the river banks in the urban areas are made of hard material, like concrete or stones. This leads to less time needed for water to reach the estuary, but also to less nature to develop around the river. [54]

At the sea, there was long time nothing done to protect the land. After several typhoons in the 20<sup>th</sup> century, especially after Vera in 1959, the general opinion changed and flood safety against storm surges was built. Around the specific region of Ise Bay, the storm surge level was set up to T.P. +3.5 m. To protect the regions around it, various type of structures are used. But also here, a lot of hard cover has been used.

In history, the type of structures used on the banks and shores have had quite some impact on the local environment. During the end of 20<sup>th</sup> century, the Japanese government started to see this as a negative consequence. The government is trying to reduce the consequences by improving the environment around the rivers. On top of that, Japan has a lot of dams, with only 3 out of 103 unobstructed. This results in less fish and sediment being able to travel along the river. The government is trying to introduce counter measurements for this problem as well. [54]

To reach a better system, the government has amend the River Law in 1997 (originally from 1896). After the amendment, the rivers were divided into 4 classes, some classes are maintained by the central government, some by the regional governments. With this law, budget became available and so the river restoration could begin. This is done only on some places, by far not in all rivers.

# VI

## Appendices of Phase II

# Shin River + adaptations

## I.1. Description solution

One option to reduce the discharge through the Shonai is reactivating the overflow through the Shin River again. In the year of 2000, this method has led to a major flood around the Shin. After this flood, due to public views, it was decided to not use the Shin River anymore as an overflow for the Shonai River [33]. Only in cases of emergency, when the Shonai has reached its discharge limit, the Shin can be used as an emergency canal [55]. To let water in, a water overflow is constructed at the connection between the Shonai and the Shin as presented in figure I.1 below.

With some updates, the Shin should be able to be used again. This gives that the Shonai can be loaded with less discharge, reducing the risks along the downstream reach of the Shonai. Today, the Shin river is not loaded with discharge from the Shonai River because of public opinions, which should be taken into account when expanding this idea. To reach consensus with the public, extra safety measures should be taken. The use of the Shin River requires a new design for the inlet. When redesigned, one should take a close look at the risk management of the Shin River, since floods will not be accepted by local population. It may be more desirable to use a controllable inlet structure, which can let water pass at all times, but can be (partially) closed at all times as well. When this is implemented, the reinforcement of the defences could be reduced, or might not even be necessary at all. If public opinion is still hard to move because of the history of the Shin, one could also decrease the probability of failure to change the mind of the people.



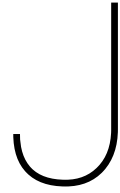
Figure I.1: Current Inlet structure at Shonai River [4]

## I.2. Advantages

- **Reduced discharge through downstream Shonai:** The main advantage is that the areas surrounding the downstream part of the Shonai experience lower risks without extra measures at those locations.

## I.3. Disadvantages

- **Costs of measures to ensure safety:** To ensure the safety of the areas around the Shin, extra measures should be taken, which are likely to be expensive
- **Space required to take measures:** To take the measures, space along the Shin is required. This might be unavailable or lead to the loss of buildings and houses.
- **Adjusting existing structures:** It might be necessary to adjust structures because they are obstacles for the measures. For example, it may be necessary to reconstruct bridges because they do not fit within the measures.
- **Political sensitive measure:** Although the plan proposed in this section may be designed as a safe system, it might feel unsafe for the local population. Public and political resistance may occur. [5]



## Covered version of Shin River

### J.1. Description solution

In appendix I, the reactivation of the Shin was discussed. Reactivation in that way would require measures which would require space which is not present everywhere. In case of unavailable space or public consensus, it is a possibility to cover the Shin with a concrete slab. This would give a maximum to the height the water could reach. Above the top of the slab, which will be on street level, water cannot flow. This creates a canal in a tunnel, with a physically determined maximal water level. For visualisation, see figure J.1. This water level has a maximum, which could form a bottleneck upstream at the start of the tunnel. This bottleneck could cause flooding upstream of the entrance of the tunnel. To prevent this, the influx from the Shonai should be controlled, for example by a controlled inlet structure like in section I.

This options provides less of an increase in discharge capacity when compared to the option discussed in section I. However, this is made up for by the increased safety level provided by the concrete top cover. Flooding is likely only to occur when the structure fails.

Covering the Shin will require a large structure. Especially when the Shin is covered over the full length, costs can become very high. But, since the Shin is covered with a concrete slab on top of the Shin, an open concrete space is created. This could be used for other purposes, as for example a park, real estate, or a combination of both. When developing real estate on the slab, a part of the costs can directly be compensated by the sale of real estate. This will not be part of the report.

### J.2. Advantages

- **Reduced discharge through downstream Shonai:** The areas surrounding the downstream part of the Shonai are protected better without taking extra measurements at that part.
- **Higher safety for the areas around the Shin:** The areas around the Shin will become safer as they are right now, as the concrete cover limits water levels.
- **Real estate development:** New space becomes available for the development of real estate.

### J.3. Disadvantages

- **Costs of measurements to ensure safety:** Such a structure, over the full length or just partly, is expected to be relatively expensive. Although it can also provide future revenue, investment costs are high.
- **Adjusting consisting structures:** It might be necessary to adjust structures because they are obstacles for the measurements. For example, it is very likely some bridges will have to be removed in order to construct the structure.

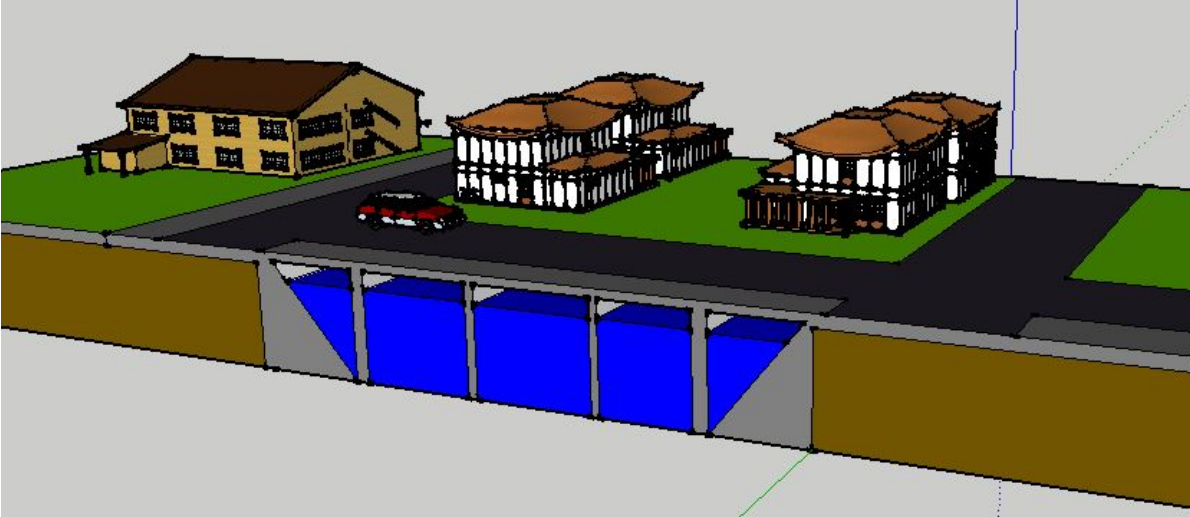
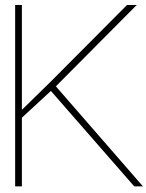


Figure J.1: Rough sketch of new situation with covered Shin river (dimension are not to scale)



## Bottleneck near Biwajima

### K.1. Description solution

Just north of Nagoya, near Biwajima, four bridges span the Shonai River, see figure K.1. Three of those bridges are railway bridges, with two of them next to each other. Furthermore, one of these is used by the Tokaido Shinkansen. The fourth bridge is used by car traffic. The river is narrower than average at this location and cannot be easily widened, due to the bridges. On top of that, the bridge piers decrease the local discharge capacity, by limiting wet cross-sectional area and introducing turbulence. Therefore, the bridges form a bottleneck, causing flooding to occur upstream. This has happened during the flood in September, 2000, when the bridge limited water flow. To prevent this floods in the future, the discharge capacity at the bridges should be increased. The current discharge capacity at Biwajima in the river improvement plan is  $3700 \text{ m}^3/\text{s}$  [56]. [5]



Figure K.1: Bridges across the Shonai River at Biwajima [4]

To increase the capacity, a few possibilities are available. These are presented below.

- Dredging the river around the bridges: requires recalculation of bridge foundation and morphological consequences
- Widening the river: requires either modification or replacement of the bridge, which is unwanted by the railway operators [5]. Furthermore, neighbouring buildings have to be demolished
- Increase bridge height: can be done via either modification or replacement. Requires dike strengthening
- Construct a canal parallel to the Shonai River: might just move the problem, similarly what happened to the Shin River. Some possible trajectories have been given in figure K.3. Constructing this bypass in a tunnel can be a solution



- Construct a tunnel underneath the Shonai River: introduces little additional risk and impact concerning direct environment compared to a canal
- Construct tunnels within the dikes, see figure K.2: requires adjustment of the bridge abutments

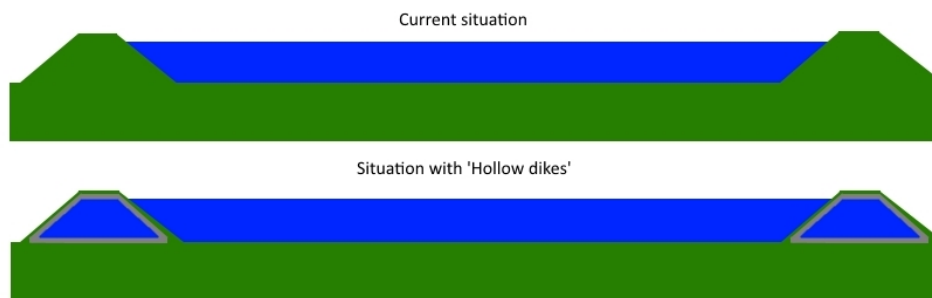


Figure K.2: Option to build a canal within the dikes

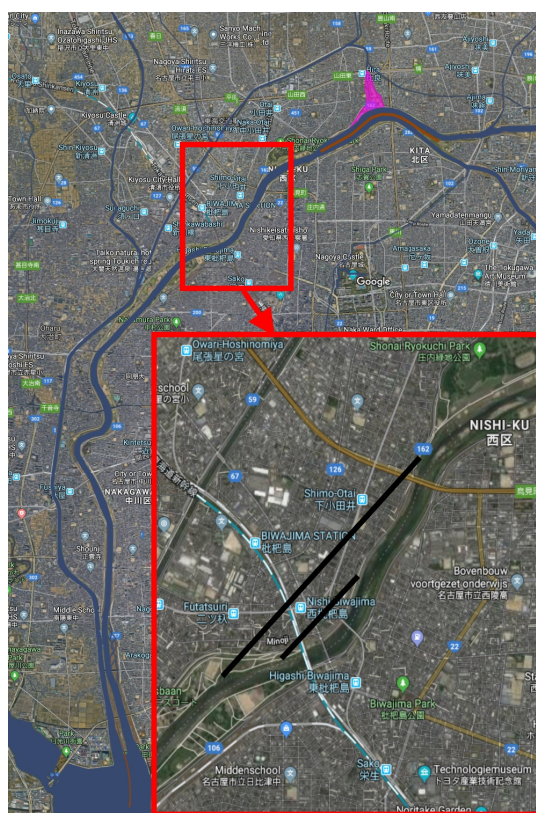


Figure K.3: Possible trajectories of bypass canals [4]

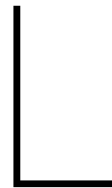
## K.2. Advantages

- **Removes a physical bottleneck:** past events have shown flooding occurred first at the Biwajima bridges. By increasing discharge capacity through one of the methods, flood safety is likely to increase
- **Local instead of general analysis river:** construction works are concentrated around of one area instead of throughout the river basin
- **Easier to verify solution:** because the solution is focused around one location, there is no need for complex analysis of the whole river system

## K.3. Disadvantages

- **Might just move the problem:** it is possible the first flooding will just occur at the next bottleneck





# Use of existing dams upstream

## L.1. Description solution

To decrease the peak discharge in the Shonai River, water could be stored upstream when the discharge becomes critical. This would decrease the discharge downstream. A dam could be used to store the water upstream. By emptying the basins in advance of heavy rain, the capacity of storage in the basins could be increased as much as possible. Several dams are present in the upstream tributaries of the Shonai River. The largest is the Origawa Dam located at the Ori River, a river connected to the upstream Shonai. This dam has a total water storage capacity of 15.1 million  $m^3$ , with an effective water storage capacity of 12.9 million  $m^3$  [57]. Other small dams created for flood control are the Teirinji Dam, Hiyoshi Dam and Tazawa Dam. Those three consist of a sill covered with grass which holds the water and are not controllable. The total capacity of the Teirinji Dam is 295,000  $m^3$  with an effective storage capacity of 244,000  $m^3$  [58]. For the Hiyoshi Dam the total capacity is 317,000  $m^3$ , with an effective storage of 300,000  $m^3$  [59]. Lastly, the Tazawa Dam has a total capacity of 248,000  $m^3$  with 223,000  $m^3$  effective capacity [60]. Since these dam basins do not have large capacity, the flood safety for the Shonai River could be increased by enlarging these small basins. Figure L.1 gives an overview of the locations of these dams.



Figure L.1: Locations of the dams of the Shonai River [4]

Another possibility is to look at the weirs in the Shonai River. In Nagoya city, several weirs are present. Since these are in the city, they cannot be used to hold the water for a long time. More upstream (between Kasugai and Tajimi) a weir is also present in the river system, called the Tamano Dam. If the weirs can be controlled in a more efficient way, this can lead to a reduction in flood damage. As a sufficient enough forecast can be made around 24 hours in advance, the river system can be emptied as much as possible to increase the storage capacity. If this is already implemented, this process could potentially be further optimised.

## L.2. Advantages

- **Reduced discharge:** Since the dams upstream hold the water, the discharge through the Shonai River can be better distributed over time. This reduces the peak discharge and therefore a lower probability of failure in the river.
- **Construction time:** Due to the fact that the dams and weirs are already present in the system, there is already a starting point which could reduce the construction time.
- **Economically interesting:** Since the dams are already present, this solution is relatively cheap. Although deepening or widening of the basins and increasing the dams will cost a substantial amount, it could still be one of the less expensive solutions.

## L.3. Disadvantages

- **Partly effective:** The dams with basins are placed upstream of the river, so all the water that enters the river in mid- and downstream can still lead to a flood in these downstream sections.
- **Storage limited:** The water storage capacity of the existing dams is only limited as mentioned before. This capacity can only be increased for a certain amount, so the storage could still be insufficient.

# M

## Creating new dam/weir upstream

### M.1. Description solution

Instead of adapting the current dams and weirs, a new dam or weir could be constructed as well. Creating a dam with storage basin requires a location with sufficient space and height difference. Therefore, it is most common to place it in the upstream area as the population density is lower and descent is higher there. An option is to place the new basin in the mountains south of Mizunami (see figure M.1), just as the existing Origawa Dam. In this way most discharge coming from this region can be initially stored, resulting in a lower flood discharge. Another option is the mountain range north of Mizunami. In this region only small dams are present. With the construction of a larger basin (like with the Origawa Dam), the ability to store water increases. However, the height differences in the Shonai watershed are relatively low. Therefore, dams could be a less optimal solution for flood protection in this region [5]. Nevertheless, figure M.1 gives an overview of the locations discussed above.



Figure M.1: Possible dam locations [4]

Furthermore, since there are already some weirs present around the city of Nagoya, it is a possibility to construct another weir in this region. Since dams and weirs hold water (thus increasing the water level behind), it is less effective to place them downstream as this will only lead to a heightening of the water level. Therefore, placing a dam in the upstream region could be more efficient. Between Kasugai and Tajimi there is already

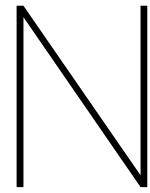
the Tamano Dam. Since this section does not have urbanised area, this area is quite suitable for these kind of structures. Therefore, it is possible to construct a second weir in this river reach, see figure M.1. Compared to other river sections, this part is considered most effective for the placement of one or more weirs. Just as with the Maruyama Dam in the Kiso River, it could also be made multifunctional. If the height of the weir is larger, the weir can hold a larger amount of water and could be used for hydropower. The disadvantage of this location is that it increases the flood problems at Tajimi. This has to be taken into account when considering this option.

## M.2. Advantages

- **Increase flood safety:** Compared to the current situation, weirs and dams will contribute to an increase in flood safety.
- **Relatively low costs:** Creating a weir could be done with relatively low costs, since it does not involve major interventions in densely populated area. However, creating a large dam with basin in mountainous area can be challenging which in turn can increase the costs.

## M.3. Disadvantages

- **Limited effect on discharge:** Especially for the case of creating a weir, this delays the discharge by a small amount. If a flood approaches, this weir has to be open to prevent flooding at the upstream end. In this case it does not contribute to flood safety as it will only increase the vulnerability at the upstream end if it is not opened sufficiently.
- **Limited storage:** Dams and their basins have a limited capacity to store water. In case of heavy rain, one or two extra dams will only diminish the impact slightly. Therefore, it is not a solution on its own but could be combined with other solutions.
- **Difficult to implement:** Since the watershed of the Shonai River does not have high elevations, finding an appropriate location for a dam is difficult. The mentioned locations do still have little height difference and therefore they could be unsuitable [5].



# Construction of new artificial river

## N.1. Description solution

In the past, the Shin River was constructed to transport the discharge of the Shonai River partially. The construction of a new, artificial river is an efficient way to increase the discharge capacity and to decrease the probability of failure. Now, the Shin River has shown its vulnerability in a developed region, after major flooding occurred. As a result, the design value for the outflow of the Shonai River into the Shin river has been set to  $0 \text{ m}^3/\text{s}$  [55]. With modern knowledge and craftsmanship, this can be done better. The Shonai River can diverge part of its discharge to another, new artificial river, which meets modern safety standards and results in a more secure city.

Although the city of Nagoya is build in a very compact manner, the construction of a new artificial river is still possible. Two main ideas will be presented: the first will search for a route within the city of Nagoya, the second will divert around the city borders.

### N.1.1. Extension of the Yamasaki River

The Yamasaki River - which mouth is in the harbour of the Ise Bay - can be extended towards the Shonai river. The river, which is locally only 20 meters wide, can be made more wide and deep. The connection to the Shonai River can be made close to where the Yada River is joining the Shonai River. One could switch the flow direction of the final kilometre of the Yada River to create a nice connection to the Yamasaki River. See figure N.1 for visual reference. In this figure, the Shonai River is indicated in red, the Yada River in blue and the Yamasaki River in green.

### N.1.2. Connection Shonai River to Yahagi River

A connection can be made between the two first class rivers: the Shonai River and the Yahagi River, eastern of Nagoya. In case of high flood in the Shonai River, water can be diverged into the other. Although this area is mainly unused land, it does have the foot of a mountain in it. Complicated civil structures might be needed to realise this concept. The feasibility of such a project should be checked.

## N.2. Advantages

- **Reduced discharge in Shonai:** Since the discharge in the Shonai River is partially diverged into the new river, less water needs to flow through the Shonai.
- **Reduced probability of failure:** Because of this reduced discharge, today's embankment will equal a lower probability of failure.
- **Reduced damage:** If the unfortunate happens and a dike fails, the reduced discharge will result in less damage.
- **New natural environment:** If implemented correctly, the river can create a green environment in the city. Building with nature is the key.

## N.3. Disadvantages

- **Removal of current property:** The new river will replace current existing developed area. Depending on the location of this new river, this might result in needed destruction of buildings and/or roads.



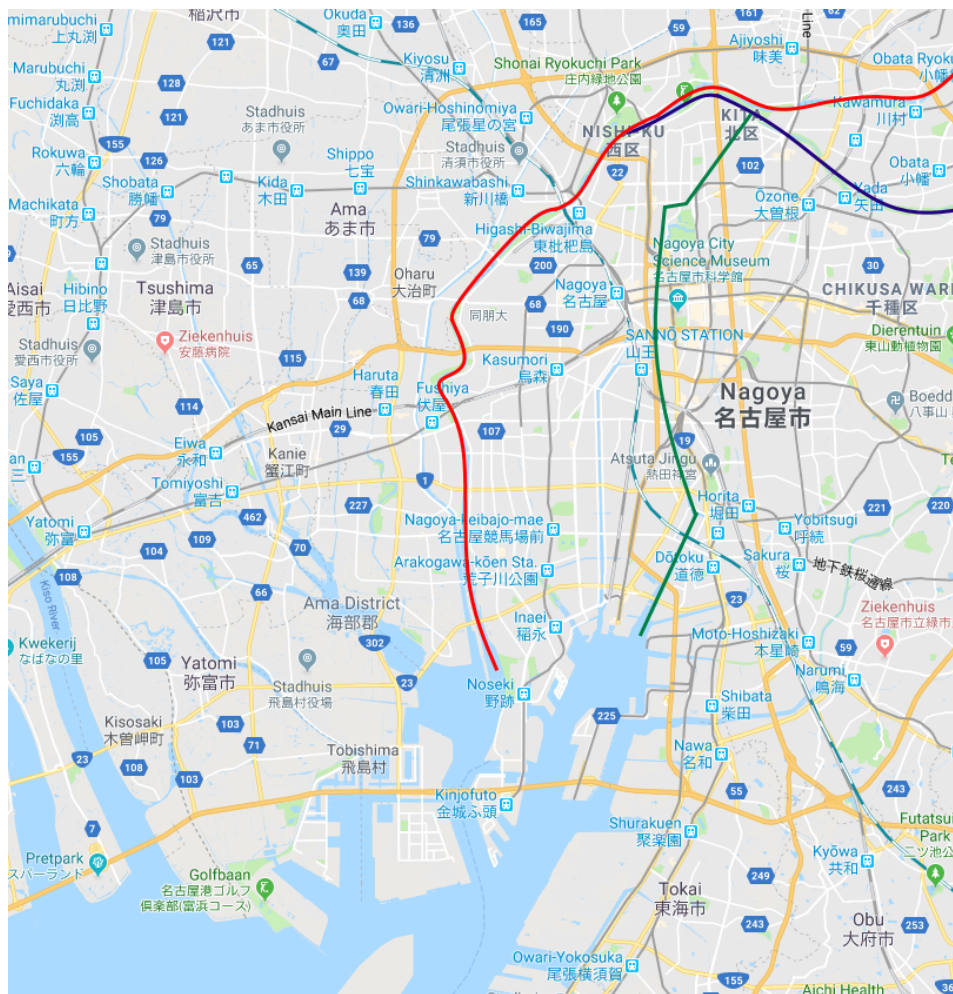
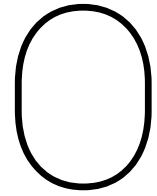


Figure N.1: Use of Yamasaki River to diverge discharge [4]

Besides destruction of property of local residents, it may also be possible that recreational areas need to be transformed.

- **Cost of project:** Although the costs of construction of an artificial river might be severe, the addition of protection around the Shonai River does that as well. A comparison needs to be made.
- **Temporarily hindrance in city:** The construction might result in hindrance, whether it be in a physical form or with noise.
- **New bridges:** The new river might result in the need of new or larger bridges.
- **Nagoya Castle:** One of the options would diverge the water close to Nagoya Castle, which would require additional protection at that specific location to make sure the castle keeps preserved.



## Discharge (metro) tunnel system

### O.1. Description solution

To reduce the discharge through the downstream part of the Shonai River, existing infrastructure could be used. This chapter focuses on the use of existing metro tunnels in the city for redirecting water.

#### O.1.1. Permanent conversion

This option concerns permanently dedicating a part of the metro tunnels to diverting a part of the flood discharge directly to Ise Bay. By doing so, part of the flood discharge is redirected away from the Shonai directly into Ise Bay, via the tunnels. A part of the metro system will permanently be shut of from the rest of the system. An inlet structure has to be designed and constructed where the tunnels connect to the Shonai. Furthermore, an outlet has to be designed as well where the tunnels flow out into Ise Bay. It is possible additional tunnel drilling is required in order to connect to the Shonai and Ise Bay. It can be opted to choose only one or multiple routes. This plan can only be done under the condition that the existing line is descending in elevation and can be missed in the metro system (this is most likely to be not the case). If not, a new tunnel should be created through the city.

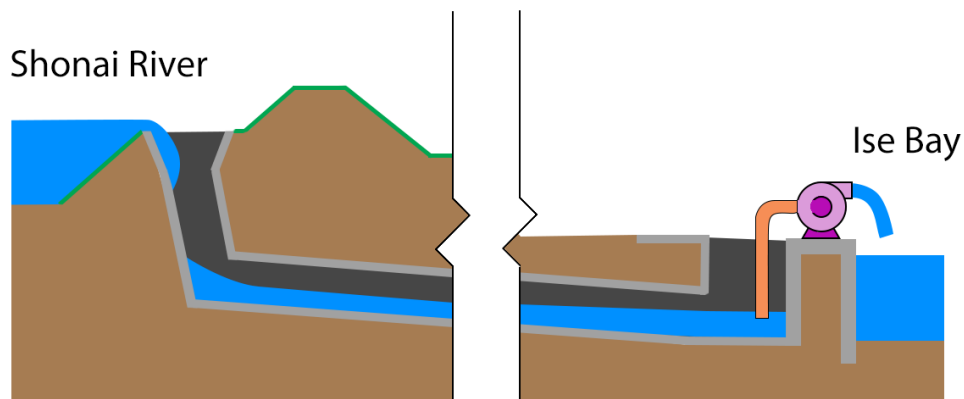


Figure O.1: Flood discharge diversion by converting metro tunnels to drainage pipes

The inlet could be realised using for example a spillway that automatically allows for water to enter the system when high water occurs. This idea is similar to what has been done in the past for the Shonai connecting to the Shin, where a part of the dike was lowered to create a passive inlet (see figure I.1, appendix I). An alternative solution is to create an active system using for example a weir. This would allow for more control over how the discharge is distributed over the river and the tunnels.

For the outlet, a passive spillway can be used as well. If this is not possible, a combination of catchment area and pumps can be used to let out the water.

### O.1.2. Hybrid tunnels

An alternative use of the tunnels is to convert them into a hybrid system. In this system, the tunnels are adjusted to be transformed temporarily into drainage pipes. Metro operations would shut down when a flood warning is given out due to for example an expected typhoon. The corresponding platforms and adjacent tunnels would be shut of. This would yield similar performance compared to the previous solution mentioned above, with the difference being that it does not require permanent closure of a metro line. A similar system has been implemented in Kuala Lumpur SMART tunnel, where a motorway tunnel has been designed to integrate flood safety [61].



Figure O.2: Flood discharge diversion by converting tunnels to drainage pipes [62]

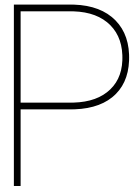
## O.2. Advantages

- **Uses existing structures:** by using existing tunnels, less excavation and construction has to be done, lowering construction costs.
- **Low risk of accidental flooding:** in past floods, diverting flood discharges to for example the Shin caused flooding to occur there. Because the metro tunnels are underground, a low probability of accidental local flooding is expected.
- **Low spatial impact:** because the tunnels are underground, no buildings have to be cleared to make room. The only structures that require space on the surface are the inlet and outlets.

## O.3. Disadvantages

- **Elimination of metro line:** if the permanent option is chosen, this means part of the metro line has to be closed. If the hybrid option is chosen, it is likely the metro has to be closed temporarily for construction, and also when flooding is expected to occur.
- **Limited capacity:** the cross-sectional area of the existing tunnels are relatively low. Therefore, it is expected discharge capacity will be limited. It might be required to widen the tunnels, which would increase costs.





## Multiple-Criteria Decision Analysis

A Multiple-Criteria Decision Analysis (MCDA) has been executed to obtain the most viable solution for the problem. The MCDA is rated in such a way that equation (P.1) will give the highest score for the best option. Weight factors are given between 1 and 10, while category scores are given between -10 and 10 (depending on positive or negative effect). The analysis is shown in table P.1 in which 12 categories are separated:

- **Impact on Shonai River:** This category shows the effect a measurement can have on the discharge distribution of the Shonai River.
- **Destruction of area:** Replacement and destruction of current area to create space for future project.
- **Effect on environment:** Effect of project on global and local environment
- **Additional risks:** The amount of additional risks created by construction of project.
- **Social obstructions:** Social resistance against certain project or project locations.
- **Near important locations:** Whether monumental locations as castles or temples are nearby project location which might need extra safety precautions.
- **Construction hindrance:** The extend to which local residents might find hindrance. Can be noise, light, or physical obstruction.
- **Aesthetics:** The physical appearance of the project.
- **Technical feasibility:** Ease of project.
- **Required maintenance:** Amount of periodic maintenance required to sustain project.
- **Costs:** Total cost of project.
- **Future revenue:** Possibility to create revenue as a side effect of the construction of the project.

$$S_i = \sum_{j=1}^n w_j * s_{i,j} \tag{P.1}$$

Category	Weight	Shin		Shin covered		Bridge cutoff		Existing dams		New dam		New weir		New river 1		New river 2		Metro perm		Metro temp	
		Rating	Score	Rating	Score	Rating	Score	Rating	Score	Rating	Score	Rating	Score	Rating	Score	Rating	Score	Rating	Score	Rating	Score
Impact on Shonai River	10	9	90	8	80	10	100	1	10	2	20	2	20	3	30	5	50	4	40	4	40
Destruction of area	7	-4	-28	-1	-7	-1	-7	-1	-7	-7	-49	-5	-35	-8	-56	-10	-70	-3	-21	-3	-21
Effect on environment	5	-1	-5	-5	-25	-2	-10	-1	-5	-8	-40	-6	-30	3	15	2	10	0	0	0	0
Additional risks	8	-8	-64	-2	-16	-1	-8	-2	-16	-5	-40	-4	-32	-8	-64	-5	-40	-5	-40	-7	-56
Social obstruction	5	-10	-50	-5	-25	-2	-10	-1	-5	-7	-35	-4	-20	-10	-50	-8	-40	-10	-50	-5	-25
Near important locations	8	0	0	0	0	-2	-16	0	0	-3	-24	-2	-16	-8	-64	0	0	0	0	0	0
Construction hindrance	4	-3	-12	-8	-32	-5	-20	0	0	-6	-24	-5	-20	-8	-32	-8	-32	-6	-24	-8	-32
Aestatics	3	0	0	7	21	4	12	0	0	0	0	0	0	3	9	2	6	0	0	0	0
Technical feasibility	3	7	21	5	15	6	18	10	30	4	12	5	15	2	6	1	3	6	18	4	12
Required maintenance	5	-4	-20	-4	-20	-4	-20	-2	-10	-4	-20	-3	-15	-4	-20	-4	-20	-3	-15	-6	-30
Costs	8	-5	-40	-8	-64	-3	-24	-2	-16	-8	-64	-5	-40	-9	-72	-10	-80	-8	-64	-9	-72
Future revenue	6	0	0	10	60	0	0	0	0	3	18	0	0	0	0	0	0	-5	-30	0	0
<b>Total</b>			<b>-108</b>		<b>-13</b>		<b>15</b>		<b>-19</b>		<b>-246</b>		<b>-173</b>		<b>-298</b>		<b>-213</b>		<b>-186</b>		<b>-184</b>

Table P.1: MCDA of different masterplans

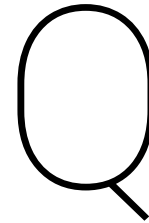
With a score of 15, option 3, the solutions for the bottleneck at the Biwajima bridges, is the best option according to this MCDA. This plan will be elaborated in the following phases. A larger version of the MCDA table can be found on the next page.

Category	Weight	Shin		Shin covered		Bridge cutoff		Existing dams		New dam		New weir		New river 1		New river 2		Metro perm		Metro temp	
		Rating	Score	Rating	Score	Rating	Score	Rating	Score	Rating	Score	Rating	Score	Rating	Score	Rating	Score	Rating	Score	Rating	Score
Impact on Shonal River	10	9	90	8	80	10	100	1	10	2	20	2	20	3	30	5	50	4	40	4	40
Destruction of area	7	-4	-28	-1	-7	-1	-7	-1	-7	-7	-49	-5	-35	-8	-56	-10	-70	-3	-21	-3	-21
Effect on environment	5	-1	-5	-5	-25	-2	-10	-1	-5	-8	-40	-6	-30	3	15	2	10	0	0	0	0
Additional risks	8	-8	-64	-2	-16	-1	-8	-2	-16	-5	-40	-4	-32	-8	-64	-5	-40	-5	-40	-7	-56
Social obstructure	5	-10	-50	-5	-25	-2	-10	-1	-5	-7	-35	-4	-20	-10	-50	-8	-40	-10	-50	-5	-25
Near important locations	8	0	0	0	0	-2	-16	0	0	-3	-24	-2	-16	-8	-64	0	0	0	0	0	0
Construction hindrance	4	-3	-12	-8	-32	-5	-20	0	0	-6	-24	-5	-20	-8	-32	-8	-32	-6	-24	-8	-32
Aestatics	3	0	0	7	21	4	12	0	0	0	0	0	0	3	9	2	6	0	0	0	0
Technical feasibility	3	7	21	5	15	6	18	10	30	4	12	5	15	2	6	1	3	6	18	4	12
Required maintenance	5	-4	-20	-4	-20	-4	-20	-2	-10	-4	-20	-3	-15	-4	-20	-4	-20	-3	-15	-6	-30
Costs	8	-5	-40	-8	-64	-3	-24	-2	-16	-8	-64	-5	-40	-9	-72	-10	-80	-8	-64	-9	-72
Future revenue	6	0	0	10	60	0	0	0	0	3	18	0	0	0	0	0	0	0	0	-5	-30
<b>Total</b>			<b>-108</b>		<b>-13</b>		<b>15</b>		<b>-19</b>		<b>-246</b>		<b>-173</b>		<b>-298</b>		<b>-213</b>		<b>-186</b>		<b>-184</b>

Table P2: MCDA of different masterplans

# VII

## Appendices of Phase III



## Yearly Extreme Discharge Data Shonai River (1960-2016)

Yearly peak discharges at Biwajima have been recorded for a long time. Starting from 1960, yearly maximum has been found on various locations [63–65] and has been collected into the table Q.1.

<b>Year</b>	<b>Discharge [<math>m^3/s</math>]</b>	<b>Year</b>	<b>Discharge [<math>m^3/s</math>]</b>
1960	372	1989	1864
1961	1222	1990	1188
1962	556	1991	2196
1963	389	1992	360
1964	300	1993	671
1965	706	1994	914
1966	572	1995	557
1967	1933	1996	599
1968	722	1997	1056
1969	593	1998	794
1970	1377	1999	1933
1971	1444	2000	3489
1972	1602	2001	778
1973	426	2002	389
1974	707	2003	511
1975	1565	2004	1000
1976	1270	2005	278
1977	560	2006	611
1978	254	2007	667
1979	758	2008	1056
1980	1323	2009	700
1981	764	2010	556
1982	1180	2011	3056
1983	1930	2012	556
1984	946	2013	907
1985	977	2014	457
1986	359	2015	431
1987	508	2016	1553
1988	1602		

Table Q.1: Yearly Extreme Discharge Data Shonai River



## Calculation of discharge values

### R.1. Design discharge

#### R.1.1. Extreme value analysis

The extreme discharge data from table Q.1, page 85 has been collected into the bar graph presented in figure R.1.

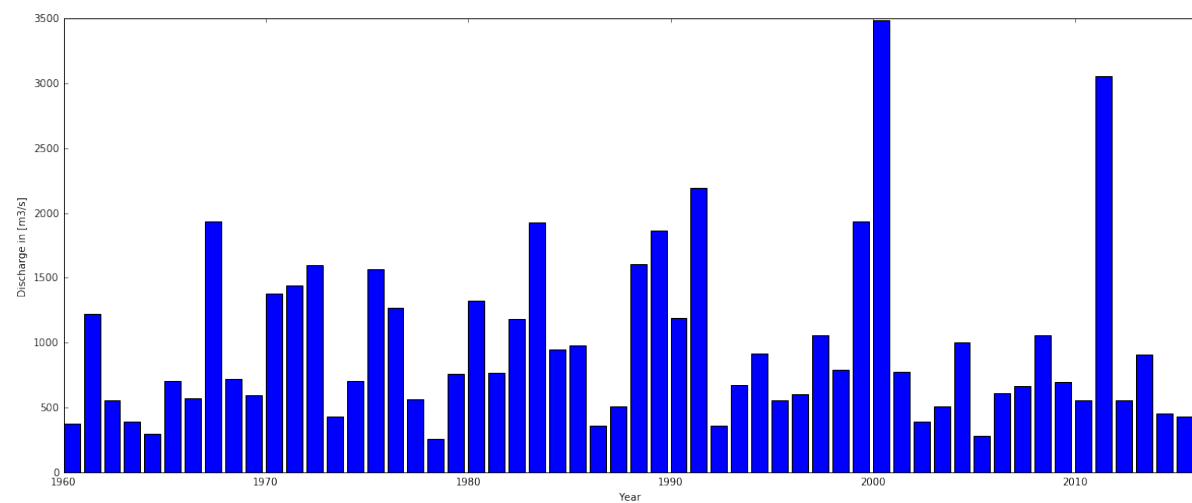


Figure R.1: Yearly maximum discharge

An extreme value analysis has been executed on these yearly peaks. After sorting the data and curve-fitting an exponential distribution, a Gumbel distribution and a Weibull distribution, figure R.2 was obtained.

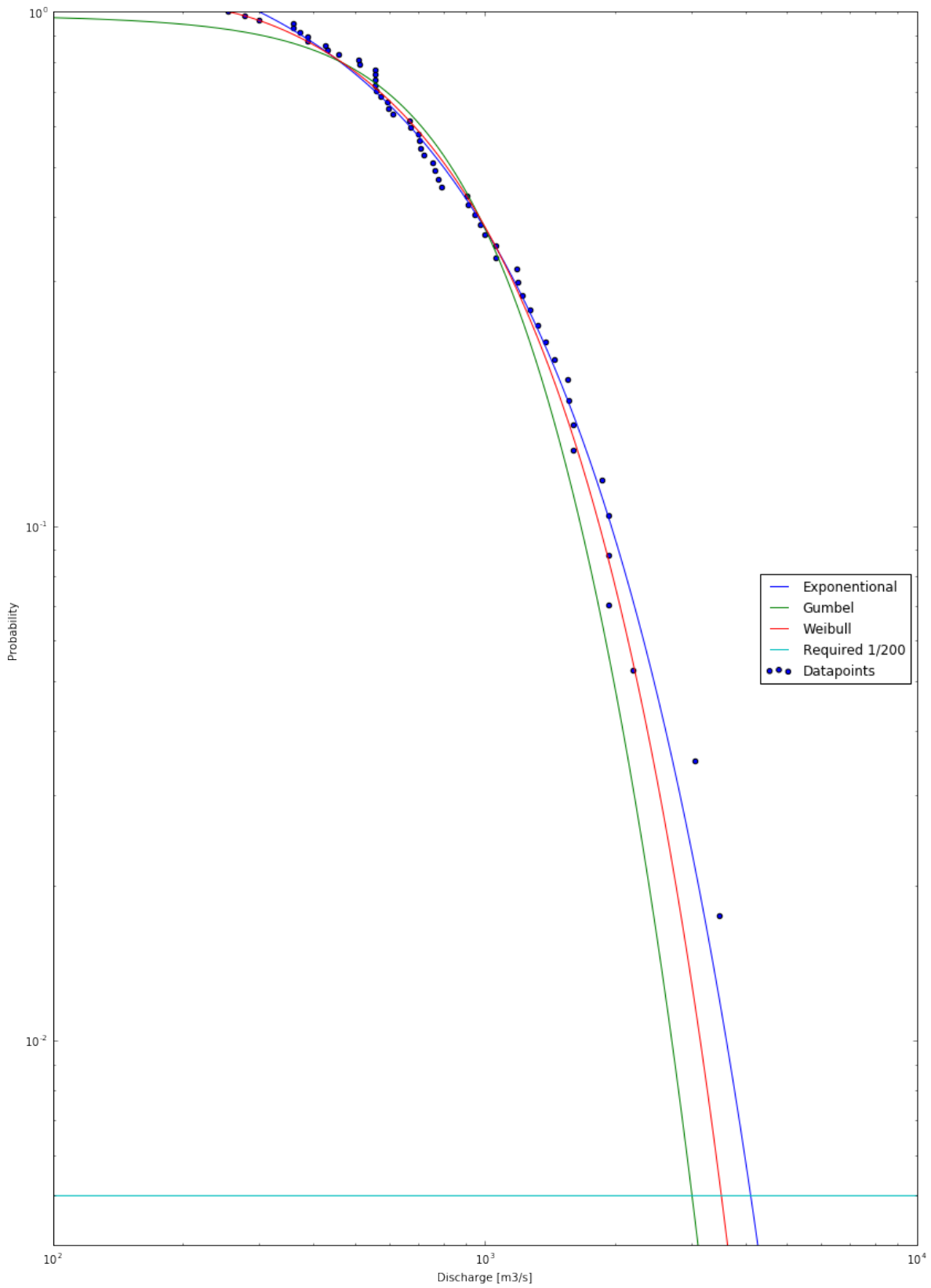


Figure R.2: Discharge probability of exceedance curve for several distributions

The three distributions are characterised by the following expressions:

$$\begin{aligned}
 CDF_{exp} &= 1 - e^{-\lambda_{exp}(Q_{1/200,exp} - \alpha_{exp})} \\
 &= 1 - e^{-0.001387(Q_{1/200,exp} - 300.3)} \\
 CDF_{gum} &= 1 - e^{-e^{\frac{Q_{1/200,gum} - \mu}{\beta}}} \\
 &= 1 - e^{-e^{\frac{Q_{1/200,gum} - 672.3}{442.0}}} \\
 CDF_{wei} &= 1 - e^{-\left(\frac{Q_{1/200,wei} - \alpha_{wei}}{\lambda_{wei}}\right)^k} \\
 &= 1 - e^{-\left(\frac{Q_{1/200,wei} - 253.9}{770.7}\right)^{1.154}}
 \end{aligned} \tag{R.1}$$

The required probability of exceedance in Nagoya has been set to once every 200 years. The probability distributions can now be completed by calculating the  $Q_{1/200}$ . This comes down to values of:

$$\begin{aligned}
 Q_{1/200,exp} &= 4120 \text{ m}^3/\text{s} \\
 Q_{1/200,gum} &= 3013 \text{ m}^3/\text{s} \\
 Q_{1/200,wei} &= 3522 \text{ m}^3/\text{s}
 \end{aligned} \tag{R.2}$$

Visual analysis of figure R.2 shows that the exponential distribution fits best for the extreme values. This distribution is also the governing one of the three, making its value good estimation for a design value for the chosen location.

$$Q_{1/200} = 4120 \text{ m}^3/\text{s} \tag{R.3}$$

The Ministry of Land, Infrastructure and Transport has set a  $Q_{1/200}$  of 4700  $\text{m}^3/\text{s}$ , which would represent a return period of 250 years according to this calculation. The difference between these two outcomes can be explained by the fact that the MLIT calculation only uses data from 1960 until 2002 [66], while these calculations used an additional 14 years of data. If these last 14 years are not included into the calculation presented above, 4700  $\text{m}^3/\text{s}$  is found as well. In figure R.3, a 95 percent upper and lower boundary is given for the curve-fitted exponential distribution. The average value was set to a deterministic value, from which the design capacity has been calculated. Because the exponential distribution gave the highest values from all distribution, this is considered to be a save assumption.



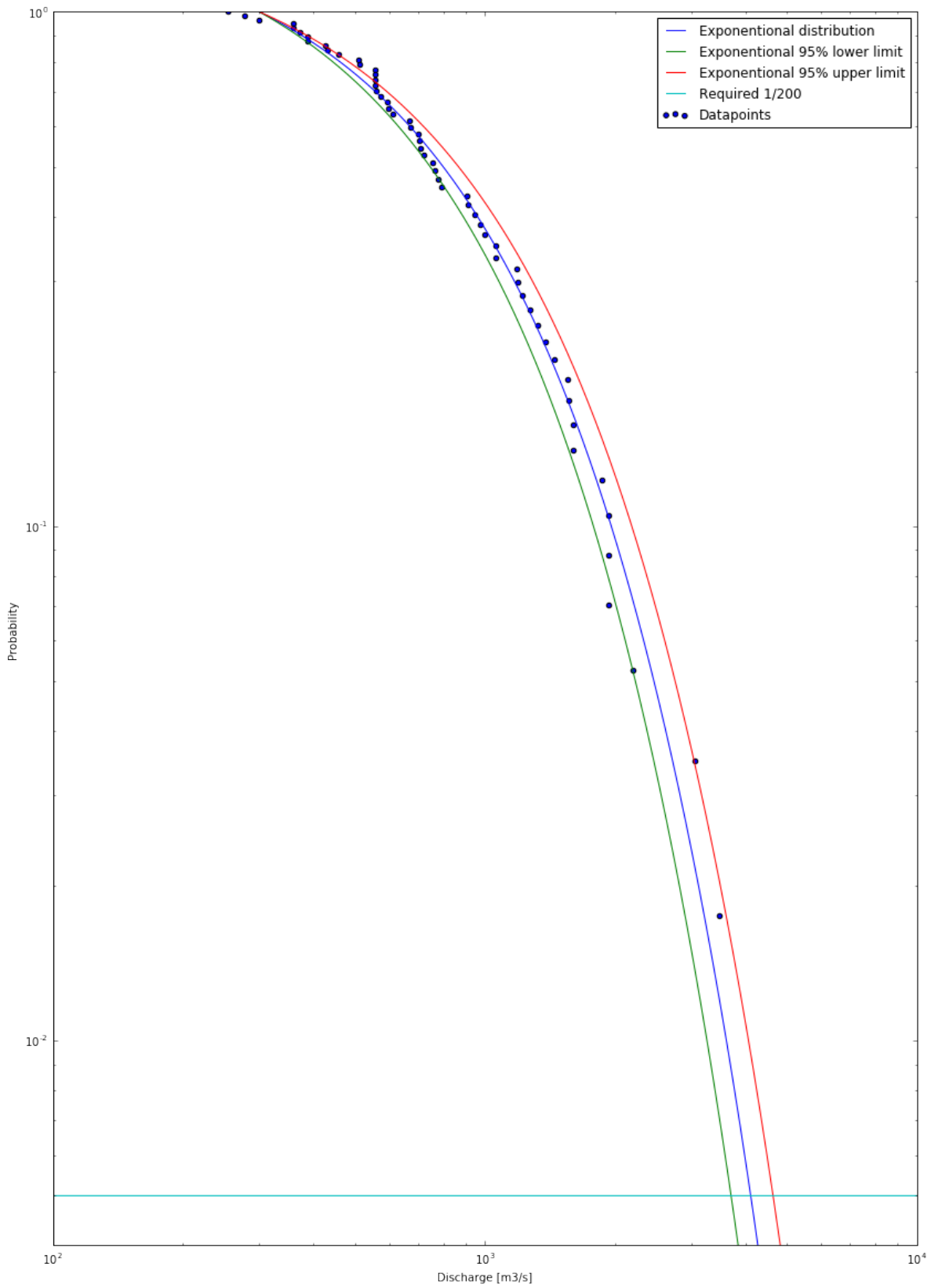


Figure R.3: Discharge probability of exceedance curve with upper and lower boundaries

### R.1.2. Effect of climate change

At the end of the 21<sup>st</sup> century, the river discharge is likely to differ from the current discharge due to climate change. Some expected effects of climate change are an increase in precipitation, rising sea level and higher temperatures leading to more evapotranspiration and less snowmelt, since less snowfall will occur. To retrieve the net effect of climate change, the increase in evapotranspiration should be subtracted from the increase in precipitation. For the Chubu region, the net-water-resources amount is anticipated to decrease by 4-5% at the end of this century [67]. However, this decrease holds for the annual rainfall. When considering the intensity per event, it becomes clear that the precipitation rate is more extreme and that these extreme rates occur more often.

Sato et al. [68] conclude that for most rivers in Japan the monthly discharge in the future will be higher in January to March than for the present situation. Furthermore, the monthly discharge in April to July will slightly decrease at the end of the century. Sato et al. assessed different rivers in their study, including the Nagara River, also located near Nagoya. Since this river is in the same region as the Shonai River and approximately in the same order of magnitude, it gives the best representation for the response of the Shonai River to climate change. However, every river could respond different, so an analysis for the Shonai River should be made to give a more proper conclusion.

Figure R.4 gives the change in discharge according to Sato et al. for the Nagara River [68]. From this it can be clearly seen that in the January until March the discharge is significantly higher in the future scenario. This is due to the increase in winter precipitation. The ratio between future and present discharge for January and February is around 1.6. In the summer months this ratio is around 0.95 [68].

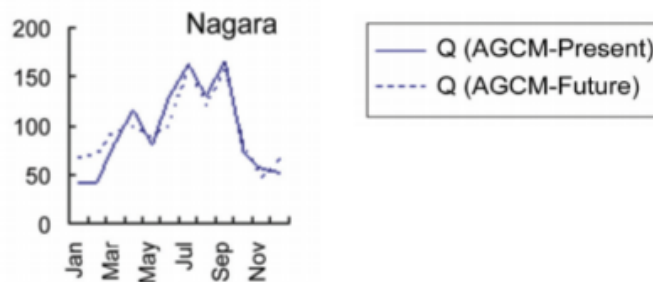


Figure R.4: Average discharge per month at present and at the end of the 21<sup>st</sup> century [68]

In this study the A1B emission scenario has been used. The A1 scenario represents a situation with [69]:

- Rapid economic growth;
- A peak in global population around mid-century with reducing population afterwards;
- Introduction of new and efficient technology occurs rapidly.

The B of A1B describes the situation with a balance between fossil and non-fossil energy sources. In this scenario both forms of energy will still be used.

Concluding the above, the discharge in the Shonai River is likely to show an increase of approximately 60% in the winter months and a slight decrease of 5% in summer. However, this conclusion concerns average discharges. The effect of heavy rainfall at for example a typhoon was not considered. When looking at typhoons, the expectation for the future is that the frequency of landfall will decrease in Japan due to a shift in position of the typhoon tracks. However, the probability that stronger typhoons will arrive increases in the future climate scenario [70]. Higher ocean temperatures lead to lower atmospheric pressure, resulting in more severe typhoons. Although the number will decrease, the impact will become more intense.

Additionally, figure R.5 shows the increase in fluctuation for the annual rainfall in Japan [71]. It can be seen that the average amount of rainfall decreases but the maximum precipitation increases. Therefore, the peak discharge could still increase with a decrease in average rainfall.

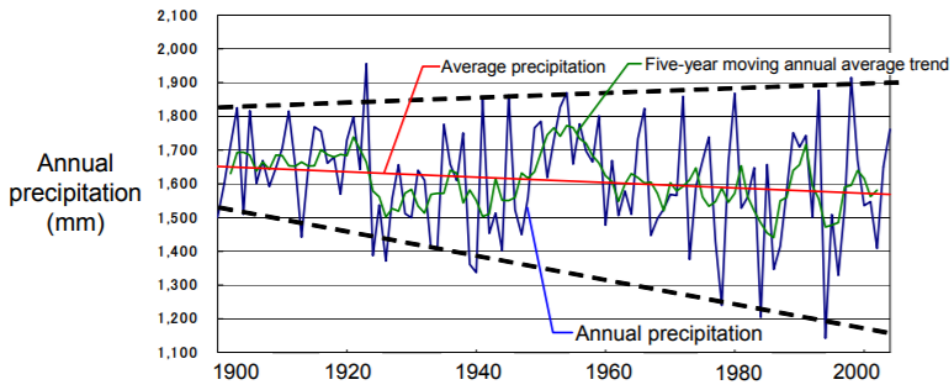


Figure R.5: Increasing fluctuation of the annual precipitation in Japan [71]

To take this increase of maximum precipitation into account into the design discharge, a linear increase has been assumed. This linear increase was determined by assuming a constant ratio between precipitation and discharge. This resulted in an increase of  $130 \text{ m}^3/\text{s}$  for a 100 year time span. Adding this to calculated probability curve, makes for a design discharge of  $4250 \text{ m}^3/\text{s}$ .

## R.2. Discharge capacity

### R.2.1. Cross-sectional profile

Data of the cross-section directly underneath the Tokaido Railway bridges was not available. Therefore, the cross-section has been estimated by using the one from the Biwajima Bridge about 150 m upstream, see figure R.7 below. It has been assumed the depth and shape of the river bed are the same as underneath the Tokaido bridges. The Tokaido bridges cross-section has been obtained by scaling the Biwajima one horizontally until it had the same width. The bottom of the bridge girder is at T.P. +9.07 m [72]. The width of the columns has been estimated to be 2 m for the centre ones, and 1 m for the columns on the ends.

$$\begin{aligned}
 width_{Biwajima} &= 178.5 \text{ m} \\
 width_{Shinkansen} &= 203 \text{ m} \\
 scale \ factor &= \frac{203}{178.5} = 1.1373
 \end{aligned}
 \tag{R.4}$$

This resulted in the following cross-section underneath the Tokaido Bridges:

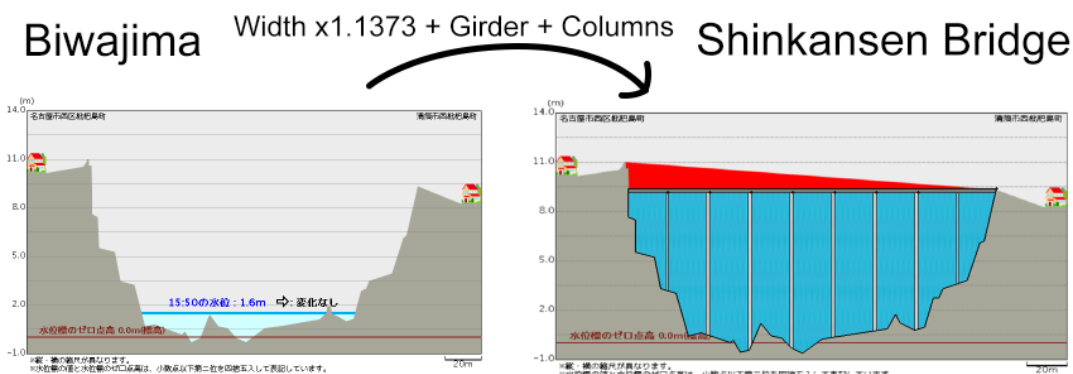


Figure R.6: Left: cross-section at Biwajima Bridge [73]. Right: cross-section underneath Tokaido Bridges. Blue represents wet cross-section taken into account.

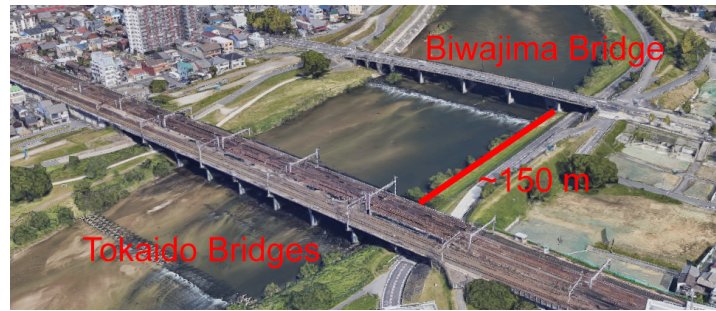


Figure R.7: Distance between Biwajima and Tokaido bridges [4]

### R.2.2. Bed characteristics

To determine the discharge capacity of the Shonai River at the considered section the friction coefficient, bed and water level gradient must be determined. For the friction coefficient, the following relation between Chézy and Manning has been used:

$$C = \frac{1}{n} R^{1/6} \quad (\text{R.5})$$

In which the hydraulic radius  $R$  equals:

$$R = \frac{A}{P} \quad (\text{R.6})$$

The mean and standard deviations of the area  $A$  and wetted perimeter  $P$  have been derived previously. The only remaining unknown is the Manning roughness coefficient. The Manning coefficient of the Shonai equals on average  $0.0184 \text{ s/m}^{1/3}$ . This is an average value calculated by combining the concrete, sand and overgrown sections of the cross-section and averaging them. A standard deviation of 5 %, equal to  $0.00092 \text{ s/m}^{1/3}$ , has been chosen. The individual Manning roughness coefficients for the three categories are given in table R.1.

Material	Value [ $\text{s/m}^{1/3}$ ]
Concrete	0.014
Sand	0.022
Overgrown	0.050

Table R.1: Manning values for individual materials [74]

### R.2.3. Single flood characteristics

Continuous measurements between 2002 and 2016 [63] have been used to generate an overview of the characteristics of the discharge. As a mean, a value of  $25.25 \text{ m}^3/\text{s}$  has been found. However, this value can heavily fluctuate as will be shown in section R.1.1. The median value will prove to be  $15 \text{ m}^3/\text{s}$ , which indicates that the river will be near empty most of the time.

On September 20<sup>th</sup> 2011, the largest flood in this data set occurred. The discharge of this showed a shape similar to a log-normal shape over time, which is illustrated in figure R.8. In this graph,  $t = 0$  equals 06:00 AM of September 20<sup>th</sup> 2011. Other floods show similar characteristics as the one shown below. This data has been used to simulate the design flood to be calculated later.

### R.2.4. Design capacity

The design discharge is determined by the capacity of water that can flow beneath the bridges. This discharge is equal to:

$$Q_u = AC\sqrt{Ri} \quad (\text{R.7})$$

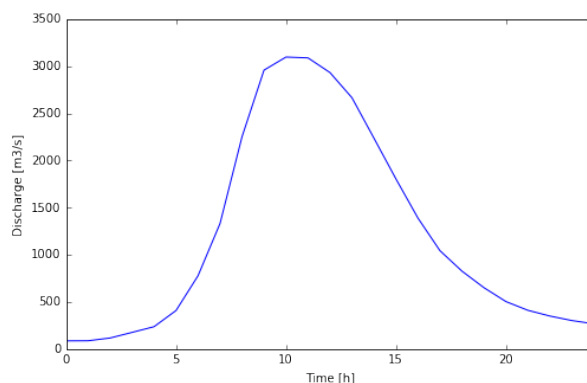


Figure R.8: Discharge over time of single flood

This is the Chézy equation, which is valid for steady uniform flow. In case of a flood wave, the flow will be non-uniform. Since the capacity is only exceeded in case of a flood wave, the non-uniform flow regime should be taken into account. Furthermore, the pillars of the bridges will cause extra turbulence and enhance the non-uniformity of the flow. For simplicity, this effect of extra turbulence has not been taken into account in this stage. Additionally the resistance term is large compared to the local inertia. Hence, steady flow will be assumed. These assumptions lead to the following equation:

$$Q = Q_u \sqrt{1 - i_b^{-1} \frac{\partial d}{\partial s}} \tag{R.8}$$

The bed level gradient ( $i_b$ ) equals the design gradient for the Shonai with a value of  $1/1313 = 7.6E-04$  [75]. The gradient of the water depth over distance could be determined by taking the flood shown in figure R.8. The maximum slope occurs after approximately 8 to 9 hours. The corresponding discharges at that time are 1332 and 2251  $m^3/s$  respectively. The flood wave that was used for this had a maximum discharge of 3096  $m^3/s$  instead of the design discharge of 4250  $m^3/s$ . To account for this, the discharges have been linearly extrapolated to 1829 and 3090  $m^3/s$  respectively. By use of iteration of the Chézy formula it was found that the water depths at  $t_1$  and  $t_2$  are 6.6 and 8.9 m respectively. Table R.2 gives these values together with the area and wetted perimeter.

Time	Discharge	Water depth	Area	Perimeter
$t_1$	1829 $m^3/s$	6.6 m	829 $m^2$	263 m
$t_2$	3090 $m^3/s$	8.9 m	1245 $m^2$	311 m

Table R.2: The discharge, water depth, area and wetted perimeter of a flood after  $t_1 = 8$  hours and  $t_2 = 9$  hours

From the water depths it follows that the change in water depth in one hour equals 2.3 m. To determine the travelled distance the flow velocity is needed, this has been obtained using equation R.9. With this velocity the travelled distance can be determined, since the observed time was 1 hour the travelled distance is 8537 meters. From this it follows that the gradient of the water depth over the travelled distance equals  $2.7E-04$ .

$$u = \frac{\frac{Q_1+Q_2}{2}}{\frac{A_1+A_2}{2}} = 2.4 \text{ m/s} \tag{R.9}$$

With equation R.8 the discharge becomes 3756  $m^3/s$ . For calculating this discharge capacity, multiple assumptions have been made. Therefore, the capacity was taken normally distributed with a standard deviation of 187  $m^3/s$ . Table R.3 gives an overview of all the parameters used in this chapter with their corresponding distributions.

Figure R.9 gives the distribution of the discharge capacity given by the red colour. The blue line shows the design discharge of 4250  $m^3/s$ . It can be observed that the current capacity of the Shonai River at the bridge location is substantially less than the needed capacity. Hence, the current capacity is insufficient and a measure is needed to account for this lacking capacity.

Direction	Abbreviation	Distribution	Mean	Std	Unit
Manning coefficient	$n$	Normal	$1.84E-02$	$9.2E-04$	$s/m^{1/3}$
Area	$A$	Normal	1235	12.35	$m^2$
Wetted perimeter	$P$	Normal	310	3.1	$m$
Bed slope	$i_b$	Normal	$7.6E-04$	$2.3E-05$	–
Discharge	$Q$	Normal	3765	209.6	$m^3/s$

Table R.3: Distributions of the used parameters

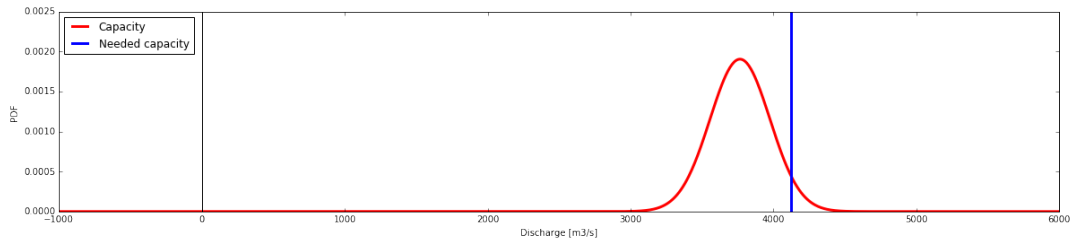


Figure R.9: Probability curve of discharge capacity

### R.3. Discharge capacity new structure

As seen in section R.1 and R.2, the capacity of the Shonai River must be increased at the Biwajima cross-section. Figure R.10 shows the required capacity. The increase of the mean value to the right is an effect of the structure that will be designed in this report. This can be realised by an increase in cross-section, or the creation of a bypass. To have a safety level of  $\beta = 4.3$ , the probability of failure of the capacity must be  $0.85E-04$ . This beta-value represents the probability that a design value will be exceeded in an unfavourable way. To calculate the representing value in this proposal, a limit state probability curve has been created, which is shown in figure R.11. According to Dutch standards, the mean of this function ( $\mu$ ) should be '4.3 \*  $\sigma$ ' away from the y-axis. As a result of all the calculations above, the capacity of the Shonai River should be increased by  $1400 m^3/s$ . This value has been verified using the expression given in (R.10).

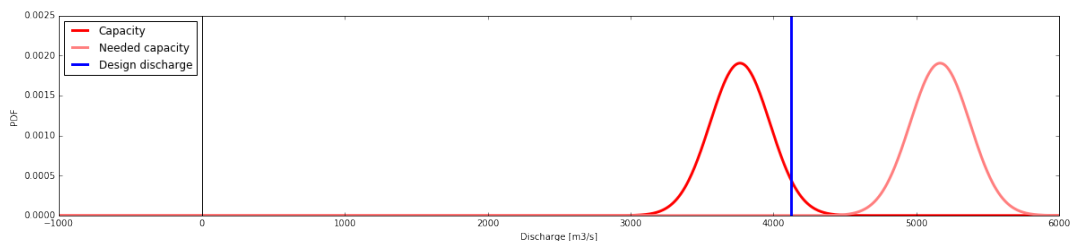


Figure R.10: Probability curve of discharge load and capacity

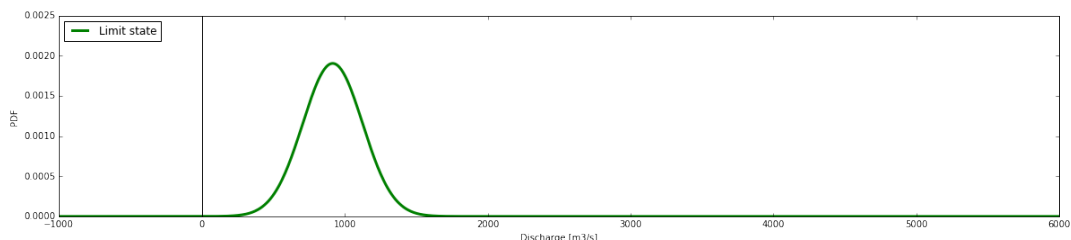


Figure R.11: Limit state probability curve

$$\begin{aligned}
 Q_{bypass} &= Q_{1/200} - (\mu_Q - \beta * \sigma_Q) \\
 &= 4250 - (3765 - 4.3 * 209.6) \\
 &= 1386 m^3/s
 \end{aligned}
 \tag{R.10}$$

# S

## Soil characteristics

Soil properties near the construction site have been based on the data on the following pages [76]. The data has been translated and interpreted as presented in table S.1. The values have been based on Eurocode 7, table 2.b (characteristic values of soil parameters).

	<b>Sand, Slightly silty clayey</b>	<b>Sand, Greatly silty clayey</b>	<b>Sand, Clean moderate</b>	<b>Gravel, slightly silty solid</b>
Layer (m to T.P)	+4.3 m to +2.4 m -7.4 m to -10.4 m	+2.4 m to -0.3 m -	-0.3 m to -7.4 m -10.4 m to -13.9 m	-13.9 m to -21.2 m -
$\gamma_{unsat}(kN/m^3)$	18	18	18	20
$\gamma_{sat}(kN/m^3)$	20	20	20	20
Young's modulus (MPa)	35	20	45	90
Angle of friction (°)	30	25	32.5	40
Poisson's ratio	0.25	0.3	0.2	0.25

Table S.1: Characteristics of subsoil

Based on soil data originated from a location further away, it has been assumed the soil below the bottom layer consists of gravel.



BEDCB52366639002.XML (0 - 15 m)

ボーリング柱状図

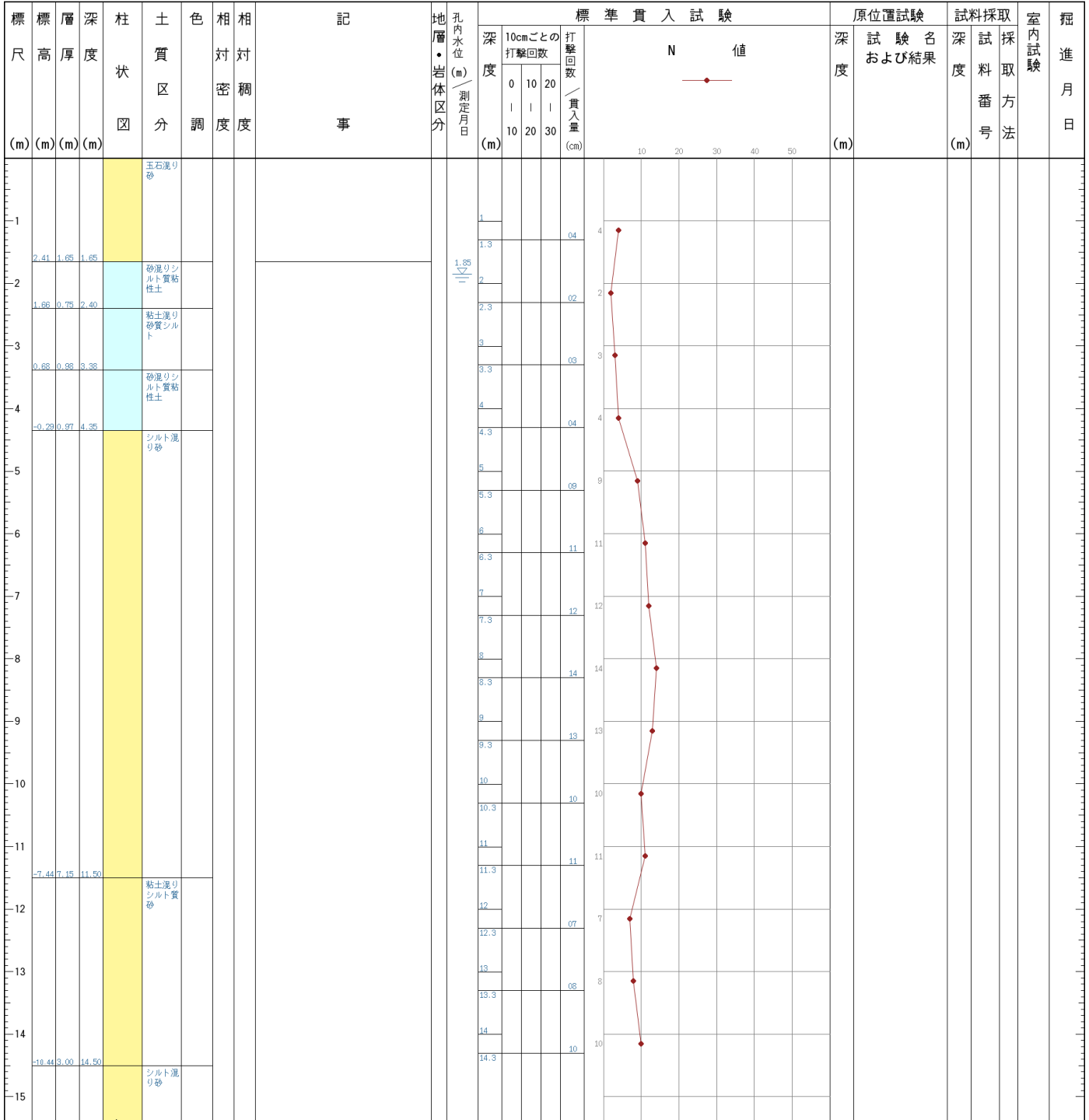
調査名 枇杷島陸橋拡巾設計委託の内地質調査

ボーリングNO.										
----------	--	--	--	--	--	--	--	--	--	--

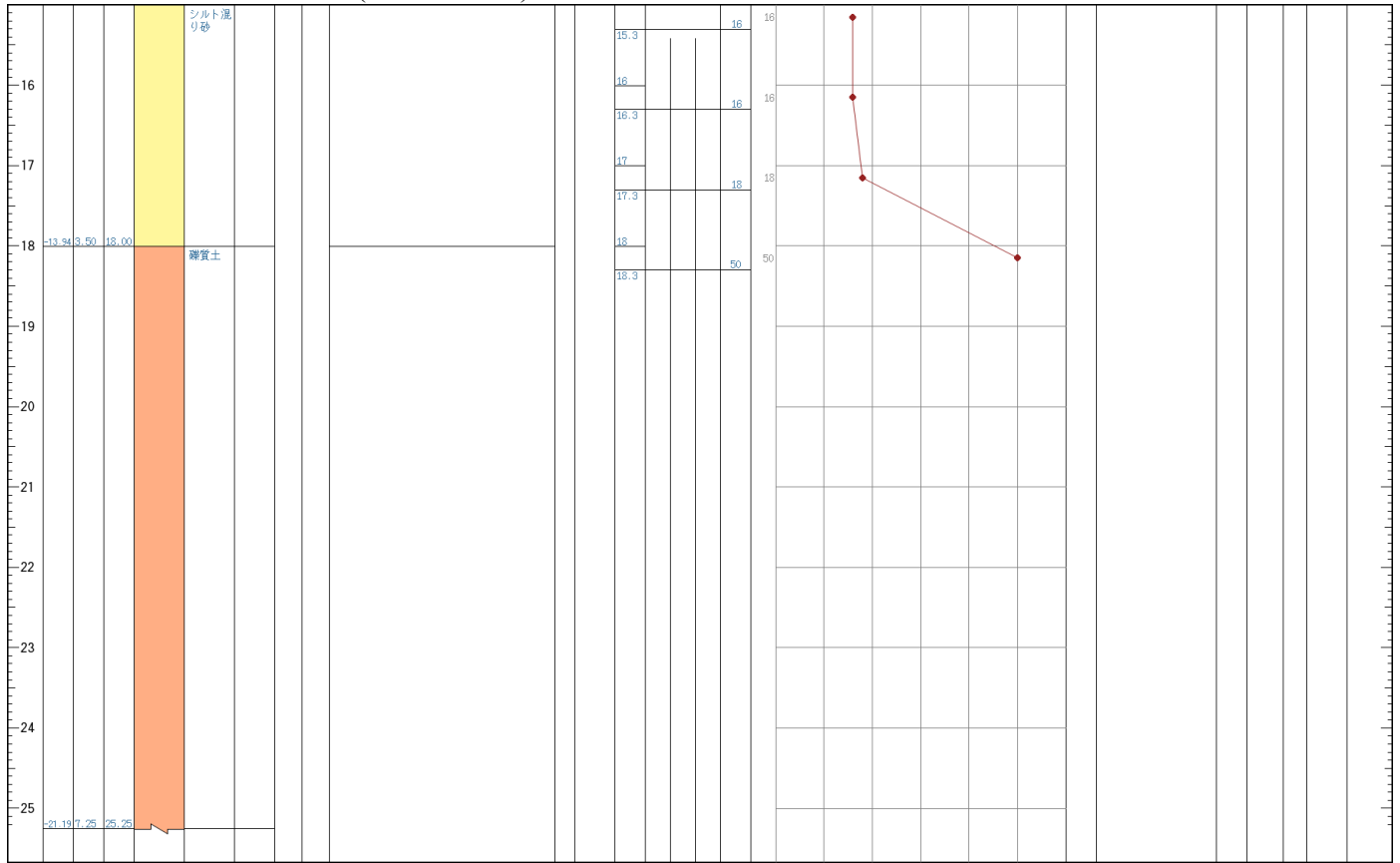
事業・工事名

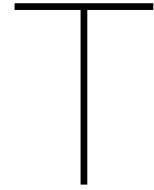
シートNO.

ボーリング名					調査位置					北緯	35° 11' 42.576"
発注機関	国土交通省 中部地方整備局 中部技術事務所				調査期間	~ 1978-03				東経	136° 51' 57.754"
調査業者名	*		主任技師		現場代理人			コア鑑定者	ボーリング責任者		
孔口標高	4.06 m	角度	180°上 90°下	方 向			地盤勾配	水平	使用機種	試験機	ハンマー 落下用具
総掘進長	25.25 m	ポンプ									



BEDCB52366639002.XML (15 - 25.25 m)





# Design calculation of bypass tunnel

Almost all calculations in this appendix have been performed for the long tunnel variant to get a good comparison between the variants. Therefore, the length of the tunnel is 2.5 km. The exception is the in-situ tunnel, for which the short tunnel variant with a length of 1200 m has been used due to the construction method.

## T.1. Bored Tunnel

### T.1.1. Calculation of required dimensions using Chézy

According to Chézy, the flow velocity can be calculated as follows:

$$u = \frac{i^{0.5} R^{2/3}}{n} \quad (\text{T.1})$$

Where:

$i$  = slope = 7.6E-04 (-)

$R$  = hydraulic radius =  $\frac{A}{P}$

$n$  = Manning's number = 0.014 (-)

$A$  = cross-sectional area =  $\pi r^2$  (m<sup>2</sup>)

$P$  = wet perimeter =  $2\pi r$  (m)

$r$  = radius of the tunnel (m)

The discharge, which should equal 1400 m<sup>3</sup>/s, can be found by:

$$Q = u * A = \frac{i^{0.5} R^{2/3}}{n} * A \quad (\text{T.2})$$

Solving those equations for the use of one tunnel results in a diameter of 19.1 m. Since the largest TBM ever used as of writing had a diameter of 19 m, it can be concluded that this radius is too large and more tunnels are needed. Using two tunnels, the inner radius becomes about 7 m. This gives a concrete thickness  $t$  of 0.7 m, using a rule of thumb of 5% of the inner diameter. This results in an outer diameter of 15.4 m, equal to an outer radius  $r$  of 7.7 m.

### T.1.2. Calculation of required dimensions

Energy losses are generated by friction inside the tunnels, turbulence at the inlet and outlet, and losses at the bends. The in- and outlet as well as the bends are not taken into account when using Chézy. Therefore, using Chézy gives an underestimation of the required dimensions. Thus, making use of energy head losses is recommended.

The roughness of concrete determines the energy lost due to friction. The friction coefficient for turbulent flow can be calculated using equation T.3. The complete calculation has been done in an iterative manner from which it was concluded that the velocity equals 4.3 m/s when a diameter of 16.8 m is used. The calculations below have been performed with these values. In here, the  $k_s$  is the roughness height, which is between 0.3-3.0 mm for concrete pipes [14]. It has been assumed that smooth concrete will be used in the design,

therefore a value of 0.3 mm was chosen.  $L$ , the length of the tunnel, is equal to 2.5 km.

$$Re = \frac{uD}{\nu} = \frac{4.3 * 16.8}{1E-06} = 7.22E + 07$$

$$f = \frac{0.25}{\left[ \log_{10} \left( \frac{k_s}{3.7D} + \frac{5.74}{Re^{0.9}} \right) \right]^2} = \frac{0.25}{\left[ \log_{10} \left( \frac{0.0003}{3.7 * 16.8} + \frac{5.74}{(7.22E+07)^{0.9}} \right) \right]^2} = 0.0090 \quad (T.3)$$

$$H_f = f \left( \frac{L}{D} \right) \left( \frac{u^2}{2g} \right) = 0.0090 * \left( \frac{2500}{16.8} \right) \left( \frac{4.3^2}{2 * 9.8} \right) = 1.27 \text{ m}$$

For the head losses at the inlet and the two bends, standard loss coefficients have been used. Assuming a funnel shaped entrance, the transition from river to tunnel is relatively smooth ( $r/D > 0.2$ ). Therefore, the loss coefficient,  $K_e$ , becomes 0.03. At the outlet, there is an expansion for which the transition is made smooth, leading to a loss coefficient of  $K_E = 0.3$ . For a 90° smooth bend with  $r/D = 4$  the loss coefficient becomes  $K_b = 0.16$  [14]. This 90° bend will be a large overestimation since a 30° turn will be probably be sufficient. The energy loss due to these transitions becomes:

$$H_t = \sum K \left( \frac{u^2}{2g} \right) = (0.03 + 0.3 + 2 * 0.16) \left( \frac{4.3^2}{2 * 9.8} \right) = 0.61 \text{ m} \quad (T.4)$$

Adding the losses due to friction and transitions gives the total energy loss in the bypass. This head loss should be approximately equal to the head loss in the Shonai River. The water level change in the Shonai River is more or less equal to the loss in energy head. Over a length of 2.5 km with a slope of 1/1313, the change in water level elevation is approximately 1.90 m. With the discussed velocity and diameter, the total head loss inside the tunnel becomes:

$$H_{total} = H_f + H_t = 1.27 + 0.61 = 1.88 \text{ m} \quad (T.5)$$

The cross-sectional area of the tunnel is as follows:

$$A = \frac{D^2}{4} \pi = \frac{16.8^2}{4} \pi = 222 \text{ m}^2 \quad (T.6)$$

The total capacity of the tunnels is:  $Q = 1400 \text{ m}^3/s$ . Therefore, the required area becomes:

$$A_{required} = \frac{Q}{u} = \frac{1400}{4.3} = 326 \text{ m}^2 \quad (T.7)$$

Hence, two tunnels are necessary. As expected, the required diameter is higher than was computed using the Chézy equation. When excluding the losses found at the entrance and the bends, the final result from the calculations above match the Chézy equation relatively well.

In conclusion, the energy calculation has been used to give a better representation of reality. Therefore, two tunnels with an inner diameter of 16.8 m are necessary to create enough capacity. This also ensures that the energy loss is not too high. Since the wall thickness is approximately 5% of the inner diameter, the thickness now becomes 0.85 m, resulting in an outer diameter of 18.5 m. See table T.1 for an overview of the dimensions.

Dimension	Value
Inner diameter	16.8 m
Concrete thickness	0.85 m
Outer diameter	18.5 m
Outer radius	9.25 m
Number of tunnels	2

Table T.1: Dimensions of the bored tunnel

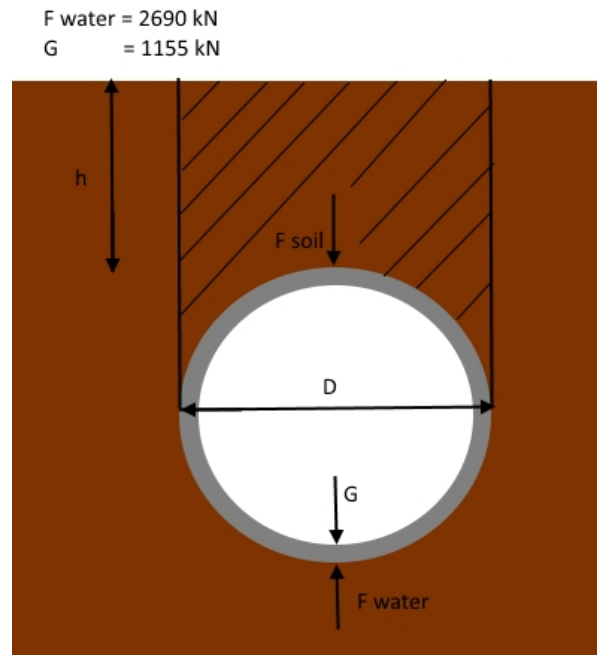


Figure T.1: Principle of buoyancy of the tunnel

### T.1.3. Depth of tunnel

The tunnel should be at sufficient depth to prevent uplift of the tunnel due to upward water forces. This uplift can be prevented when the effective weight of the tunnel and the soil above is larger than the upward water pressure. Archimedes' principle shows that the upward water force is equal to the volume of the tunnel multiplied with the water density.

The tunnel diameter equals 18.5 m, giving the whole a volume of 269 m<sup>3</sup>/m and an upward force of 2690 kN. An average weight of 24.5 kN/m<sup>3</sup> is used for the concrete tunnel. The concrete part of the tunnel has a volume of 47.1 m<sup>3</sup>/m, equal to an own weight of 1155 kN/m.

The downward forces by the soil and the tunnel are favourable acting forces. A safety factor of 0.9 has been used for this favourable force. The unfavourable force due to the water density is well known. Therefore, the safety factor for the upward water force is set to 1.0. Using the results above, one can find that the weight of the soil should equal 1834 kN, as seen in figure T.1

Soil data can be found in appendix S. It can be seen that the soil consists mainly of gravel and sand up to a depth of 29.5 m. Since the calculations in this phase are not much in detail yet, a constant saturated specific weight of 20 kN/m<sup>3</sup> has been assumed, resulting in an effective density  $\gamma'_{\text{soil}}$  of 10 kN/m<sup>3</sup>. The volume above the tunnel can be described by:

$$\begin{aligned}
 V_{\text{soil}} &= 0.5 * D^2 * h - 0.5 * \frac{D^2}{4} * \pi + D * h \\
 &= 0.5 * 18.5^2 * h - 0.5 * \frac{18.5^2}{4} * \pi + 18.5 * h = 36.7 + 18.5 * h \\
 F_{\text{soil}} &= \gamma'_{\text{soil}} * V_{\text{soil}} = 367 + 185 * h
 \end{aligned}
 \tag{T.8}$$

The weight of the soil  $F_{\text{soil}}$  above should be equal to 1834 kN. This results in a minimum depth of 8 m below surface level, for the top of the tunnel.

### T.1.4. Calculation of forces and strength of concrete lining

In this phase, forces within the concrete lining have been determined with the method of Duddeck. This method takes the deformation of the concrete lining into account. Because of this, a new distribution of forces will be found. This is done by taking the factors  $C_{n0}$ ,  $C_{n2}$  and  $C_m$  into account. The calculation of the normal forces and bending moments within the concrete lining can be shown as follows:

$$\begin{aligned}
 N &= -C_{n0} * \frac{\sigma_v + \sigma_h}{2} * r + C_{n2} * \frac{\sigma_v - \sigma_h}{2} * r * \cos(2 * \theta) \\
 M &= C_m * \frac{\sigma_v - \sigma_h}{4} * r^2 * \cos(2 * \theta) \\
 C_{n0} &= \frac{2}{2 + 1.54\beta} \\
 C_{n2} &= \frac{2(1 + 0.064\alpha)}{2 + 0.171\alpha} \\
 C_m &= \frac{4}{4 + 0.342\alpha} \\
 \alpha &= \frac{E_{soil} * r^3}{E_{concrete} * I_{concrete}} = \frac{E_{soil} * r^3}{E_{concrete} * \frac{1}{12} t^3} \\
 \beta &= \frac{E_{soil} * r}{E_{concrete} * A_{concrete}} = \frac{E_{soil} r^3}{E_{concrete} * t}
 \end{aligned} \tag{T.9}$$

The stress used in the Duddeck formulas are the stresses at the centre of the tunnel. The centre of the tunnel is at a depth  $d$  of 17.25 m. Furthermore, based on figure R.6 it can be stated that the maximum water depth  $h$  is 9.5 m. The soil stresses are calculated below. For the horizontal stress, a value of 0.5 was initially assumed for the neutral soil stress factor.

$$\begin{aligned}
 \sigma'_v &= d * \gamma'_{sat} = 17.25 * 10 = 172.5 \text{ kPa} \\
 \sigma_v &= \sigma'_v + (d + h) * \gamma_{water} = 172.5 + (17.25 + 9.5) * 10 = 440 \text{ kPa} \\
 \sigma_h &= K_0 * \sigma'_v + (d + h) * \gamma_{water} = 0.5 * 172.5 + (17.25 + 9.5) * 10 = 353.75 \text{ kPa}
 \end{aligned} \tag{T.10}$$

For the variables  $\alpha$  and  $\beta$  in equation T.9, the following values have been used:

$$\begin{aligned}
 E_{soil} &= 50 \text{ MPa} \\
 E_{concrete} &= 30 \text{ GPa} \\
 r &= 9.25 \text{ m} \\
 t &= 0.85 \text{ m}
 \end{aligned}$$

This gives the following values for the formulas T.9:

$$\begin{aligned}
 \alpha &= 25.77 \text{ (-)} \\
 \beta &= 0.018 \text{ (-)} \\
 C_{n0} &= 0.986 \text{ (-)} \\
 C_{n2} &= 0.827 \text{ (-)} \\
 C_m &= 0.312 \text{ (-)} \\
 N &= -3950 \text{ kN/m} \\
 M &= 576 \text{ kNm/m}
 \end{aligned}$$

The strength of the concrete lining will be discussed briefly. As mentioned earlier, the thickness of the concrete tunnel equals 0.85 m. The stress due to normal force and bending moment becomes:

$$\begin{aligned}
 \sigma &= \frac{N}{A} = \frac{-3950E + 03}{850 * 1000} = -4.5 \text{ N/mm}^2 \\
 \sigma &= \frac{M}{W} = \frac{M}{\frac{1}{6}bh^2} = \frac{576E + 06}{\frac{1}{6} * 1000 * 850^2} = 4.8 \text{ N/mm}^2
 \end{aligned} \tag{T.11}$$

Reinforcement is required to resist the tensile forces in the concrete. Because the used model only gives the maximum forces and not its location, the normal force at the maximal bending moment is unknown. Therefore, this will not be taken into account in the reinforcement calculations.

$$M_{Rd} = A_s * f_{yd} * z \quad (\text{T.12})$$

Where:

- $A_s$  = cross-sectional area of reinforcement
- $f_{yd}$  = Design yield strength of reinforcement
- $z$  = distance between longitudinal reinforcement and centre of concrete compressive zone
- $z = d - 0.39 * x_u$
- $d = h - c - \varnothing_{stirrups} - \frac{1}{2} \varnothing_{long.reinfor.}$
- $c = \text{cover} = 25 \text{ mm}$
- $h = 1500 \text{ mm}$  for the vertical slabs,  $1000 \text{ mm}$  for the bottom and top slab.

Derivation of  $x_u$ :

$$\begin{aligned} N_s &= N_c \\ A_s * f_{yd} &= 0.75 * b * x_u * f_{cd} \\ x_u &= \frac{A_s * f_{yd}}{0.75 * b * f_{cd}} \end{aligned} \quad (\text{T.13})$$

- $f_{cd} = 30 \text{ N/mm}^2$
- $\varnothing_{reinforcement} = 16 \text{ mm}$
- $\varnothing_{stirrups} = 8 \text{ mm}$
- $c = 25 \text{ mm}$
- $h = 850 \text{ mm}$
- $d = 809 \text{ mm}$
- $\rho \approx 0.24 \%$
- number of reinforcement bars = 10/m
- $A_s = 1942 \text{ N/mm}^2/\text{m}$
- $x_u = 38 \text{ mm}$
- $z = 794 \text{ mm}$
- $M_{Rd} = 671 \text{ kNm/m}$

## T.2. Pneumatic caisson tunnel

This option looks at the feasibility of pneumatic caissons. Due to the restriction of the bridge pillars, the width of the caissons is limited to 10 m. The tunnel follows the Shonai River, leading to a tunnel length of 2.5 km.

### T.2.1. Calculation of required dimensions using energy loss

Extra energy losses are expected at the transitions. The head loss due to friction is shown in equation T.14. Since a non-circular cross-section is used, use has been made of the hydraulic diameter  $D_h$ . Iteration shows that a height of 15 m is sufficient. These dimensions allow a velocity of 3.7 m/s. The computation of this value



are shown below.

$$\begin{aligned}
 D_h &= \frac{2 * h * w}{h + w} = \frac{2 * 15 * 10}{15 + 10} = 12 \text{ m} \\
 Re &= \frac{uD_h}{\nu} = \frac{3.7 * 12}{1E-06} = 4.4E + 07 \\
 f &= \frac{0.25}{\left[ \log_{10} \left( \frac{k_s}{3.7D_h} + \frac{5.74}{Re^{0.9}} \right) \right]^2} = \frac{0.25}{\left[ \log_{10} \left( \frac{0.0003}{3.7 * 12} + \frac{5.74}{(4.4E+07)^{0.9}} \right) \right]^2} = 0.0095 \\
 H_f &= f \left( \frac{L}{D_h} \right) \left( \frac{u^2}{2g} \right) = 0.0095 * \left( \frac{2500}{12} \right) \left( \frac{3.7^2}{2 * 9.8} \right) = 1.39 \text{ m}
 \end{aligned} \tag{T.14}$$

The losses due to the bends, the inflow and the outflow have been approximated by using the coefficients for pipes. This is not correct, but for this phase assumed to give a sufficient representation. The head loss due to these transitions is as follows:

$$H_t = \sum K \left( \frac{u^2}{2g} \right) = (0.03 + 0.3 + 2 * 0.16) \left( \frac{3.7^2}{2 * 9.8} \right) = 0.45 \text{ m} \tag{T.15}$$

The total energy loss becomes:

$$H_{total} = H_f + H_t = 1.39 + 0.45 = 1.84 \text{ m} \tag{T.16}$$

As discussed earlier, the total energy loss in the Shonai River is equal to 1.90 m. This value matches the calculated value above quite well. The effective area of the tunnel is equal to:

$$A = w * h = 10 * 15 = 150 \text{ m}^2 \tag{T.17}$$

The total capacity of the tunnels should be  $Q = 1400 \text{ m}^3/\text{s}$ , therefore the required area becomes:

$$A_{required} = \frac{Q}{u} = \frac{1400}{3.7} = 378 \text{ m}^2 \tag{T.18}$$

This concludes that three caissons will be sufficient. The design gives a redundant 19% extra capacity. This computation has been done in a deterministic way, thus when performing a probabilistic calculation this extra area may be needed to still fulfil requirements. A thickness of 1.0 and 1.5 m for the horizontal walls and vertical walls has been assumed initially. See table T.2 for a summary of the dimensions.

Dimension	Value
Height	15 m
Width	10 m
Concrete thickness bottom and top slab	1 m
Concrete thickness vertical slabs	1.5 m
Number of tunnels	3

Table T.2: Dimensions of a pneumatic caisson tunnel

### T.2.2. Depth of caisson

When the tunnel is empty and in position, a buoyancy force will be present. The outer width becomes 13 m, the outer height 17 m. A buoyancy force of 2210 kN/m will be the result of these dimensions. This has to be compensated by the downward forces, the own weight  $G$  and the weight of the soil above the tunnel  $F_{soil}$ . Since those forces are acting favourably, a load factor of 0.9 has been applied. For the soil force, the specific weight of the soil is assumed to be  $20 \text{ kN/m}^3$ . From formula T.20, it can be concluded that the top of the structure should be at least 5.5 m below the river bed. This is equal to T.P. -6 m.

$$V_{concrete} = (15 * 1.5 + 13 * 1) * 2 = 71$$

$$G_{concrete} = V_{concrete} * \gamma_{concrete} \\ = 71 * 24.5 = 1740 \text{ kN}$$

(T.19)

$$F_{soil} = width * \sigma'_{soil}$$

$$= 13 * h * \gamma'_{soil}$$

$$= 13 * h * 10 = 130 * h$$

$$0.9 * (G + F_{soil}) > F_{buoyancy}$$

(T.20)

### T.2.3. Structural analysis

Three loads are acting on the structure: the own weight, the effective soil pressure and water weight. The governing load combination is when the water outside the tunnel is at a maximal level, T.P. +9.5 m, and is absent inside the present. For the soil pressure, in this phase, it has been assumed that all the soil present is sand or gravel. The corresponding soil parameters are  $\gamma' = 10 \text{ kN/m}^3$ ,  $K_0 = 0.5$  and a Young's modulus = 25 MPa. The concrete used is of class C45/55.

The following elevations are of relevance:

- Water level: T.P. +9.5 m
- River Bed level: T.P. -0.5 m
- Top of Structure: T.P. -6 m
- Bottom of Structure: T.P. -23 m

These levels give the following pressures:

- P at top of structure: 155 kPa
- P at bottom of structure: 325 kPa
- $\sigma'_v$  at top of structure: 55 kPa
- $\sigma'_h$  at top of structure: 27.5 kPa
- $\sigma'_v$  at bottom of structure: 225 kPa
- $\sigma'_h$  at top of structure: 112.5 kPa

The capacity for shear and for bending moment has been checked in the following sections.

#### Shear capacity without shear reinforcement

The shear capacity without shear reinforcement has been calculated as follows:

$$V_{Rd,c} = (C_{Rd,c} * k * (100 * \rho * f_{ck})^{1/3} + k_1 * \sigma_{cp}) * b * d$$

(T.21)

$$V_{Rd,c,min} = (0.035 * k^{3/2} * f_{ck}^{1/2} + k_1 * \sigma_{cp}) * b * d$$

Where:

- $C_{Rd,c} = 0.12$
- $k = 1 + \sqrt{\frac{200}{d}}$
- $f_{ck} = 45 \text{ N/mm}^2$
- $\rho$  = ratio of longitudinal reinforcement
- $k_1 = 0.15$
- $\sigma_{cp}$  = compressive stress

## Shear capacity with shear reinforcement

$$V_{Rd,c} = \frac{A_{sw}}{s} * z * f_{yd} * \cot(\theta)$$

$$V_{Rd,c,max} = \frac{\alpha_{cw} * b * z * v_1 * f_{cd}}{\cot(\theta) + \tan(\theta)}$$
(T.22)

Where:

- $A_{sw}$  = cross-sectional area of of shear reinforcement
- $s$  = distance between shear reinforcement
- $v_1 = 0.6(1 - \frac{f_{ck}}{250})$
- $\theta$  = angle of shear reinforcement = 45°
- $\alpha_{cw}$  = coefficient

## Bending moment capacity with longitudinal reinforcement

$$M_{Rd} = A_s * f_{yd} * z$$
(T.23)

Where:

- $A_s$  = cross-sectional area of reinforcement
- $f_{yd}$  = Design yield strength of reinforcement
- $z$  = distance between longitudinal reinforcement and centre of concrete compressive zone
- $z = d - 0.39 * x_u$
- $d = h - c - \emptyset_{stirrups} - \frac{1}{2} * \emptyset_{long.reinfor.}$
- $c$  = cover = 25 mm
- $h$  = 1500 mm for the vertical slabs, 1000 mm for the bottom and top slab.

Derivation of  $x_u$ :

$$N_s + N_{ed} = N_c$$

$$A_s * f_{yd} + N_{ed} = 0.75 * b * x_u * f_{cd}$$

$$x_u = \frac{A_s * f_{yd} + N_{Ed}}{0.75 * b * f_{cd}}$$
(T.24)

The reinforcement has been calculated for each location where the bending moments are at its maximum. This maximum value can be found at the end or in the middle of the element. The following general parameters have been used:

- $f_{ck} = 45 \text{ N/mm}^2$
- $f_{cd} = 30 \text{ N/mm}^2$
- Reinforcement steel = B500B
- $f_{yk} = 500 \text{ N/mm}^2$
- $f_{yd} = 435 \text{ N/mm}^2$

A summary of all strength calculations is given in tables T.3 and T.4 below.

<b>Parameter</b>	<b>End of bottom slab</b>	<b>End of vertical slab</b>	<b>End of top slab</b>
$M_{Ed}$ (kNm/m)	3560	3560	2760
$V_{Ed}$ (kN/m)	1940	1900	1350
$N_{Ed}$ (kN/m)	1900	1940	1160
Calculation longitudinal reinforcement			
$\emptyset_{long.reinfor.}$ (mm)	32	32	16
$\emptyset_{stirrups}$ (mm)	16	16	16
d (mm)	943	1443	943
$\rho_{estimation}$ (%)	1.1	0.45	0.85
$A_{s,estimation}$ (mm <sup>2</sup> / m)	10373	6494	8016
Number of reinforcement bars used	13	8	10
$A_s$ (mm <sup>2</sup> )	10455	6434	8042
$N_s$ (kN)	4548	2799	3498
$x_u$ (mm)	287	211	207
z (mm)	831	1361	862
$M_{Rd}$ (kNm/m)	3779	3809	3015
Calculation shear capacity without shear reinforcement			
k (-)	1.46	1.37	1.46
$\rho$ (%)	1.1	0.67	0.85
$\sigma_{cp}$ (N/mm <sup>2</sup> )	1.9	1.3	1.116
$V_{Rd,c}$ (kN/m)	3084	3709	2742

Table T.3: Reinforcement calculations at the element ends

<b>Parameter</b>	<b>End of bottom slab</b>	<b>End of vertical slab</b>	<b>End of top slab</b>
$M_{Ed}$ (kNm/m)	1400	1910	1150
$V_{Ed}$ (kN/m)	0	0	0
$N_{Ed}$ (kN/m)	1900	1670	1160
Calculation longitudinal reinforcement			
$\emptyset_{long.reinfor.}$ (mm)	32	32	32
$\emptyset_{stirrups}$ (mm)	16	16	16
d (mm)	943	1443	943
$\rho_{estimation}$ (%)	0.4	0.25	0.35
$A_{s,estimation}$ (mm <sup>2</sup> / m)	3772	3608	3300
Number of reinforcement bars used	5	5	4
$A_s$ (mm <sup>2</sup> )	4021	4021	3217
$N_s$ (kN)	1749	1749	1399
$x_u$ (mm)	162	152	114
z (mm)	880	1384	899
$M_{Rd}$ (kNm/m)	1539	2420	1258

Table T.4: Reinforcement calculations at the location of the maximum bending moment between the element ends

### T.3. In-situ tunnel

#### T.3.1. Calculation of required dimensions

As before, friction losses are present in the tunnel. These have been calculated in equation T.25 below. Iteration of the computations shows that a width of 10 m and a height of 9 m corresponds with a velocity equal to 3.3 m/s. This value was already implemented into the calculations below. Therefore, it shows the answers for the last iteration. Since the short tunnel variant will be applied for this tunnel type, the length of the tunnel is 1200 m.

$$\begin{aligned}
 D_h &= \frac{2 * h * w}{h + w} = \frac{2 * 9 * 10}{9 + 10} = 9.47 \text{ m} \\
 Re &= \frac{uD_h}{\nu} = \frac{3.3 * 9.47}{1E-06} = 3.13E + 07 \\
 f &= \frac{0.25}{\left[ \log_{10} \left( \frac{k_s}{3.7D_h} + \frac{5.74}{Re^{0.9}} \right) \right]^2} = \frac{0.25}{\left[ \log_{10} \left( \frac{0.0003}{3.7 * 9.47} + \frac{5.74}{(3.13E+07)^{0.9}} \right) \right]^2} = 0.0099 \\
 H_f &= f \left( \frac{L}{D_h} \right) \left( \frac{u^2}{2g} \right) = 0.0099 * \left( \frac{1200}{9.47} \right) \left( \frac{3.3^2}{2 * 9.8} \right) = 0.70 \text{ m}
 \end{aligned} \tag{T.25}$$

Since the bottom of the inlet/outlet of the tunnel is at the same level as the river bed, the inlet/outlet can be seen as a side channel. At the bifurcation point (inlet) and the confluence (outlet) energy losses are present. Since no exact values are known, it has been assumed that at the inflow of the tunnel the loss coefficient equals  $K_e = 0.03$ . The loss coefficient at the outflow has been assumed to be  $K_E = 0.3$ . In this stage these values have been assumed to be equal to the loss coefficients of the bored tunnel.

$$H_t = \sum K \left( \frac{u^2}{2g} \right) = (0.03 + 0.3) \left( \frac{3.3^2}{2 * 9.8} \right) = 0.18 \text{ m} \tag{T.26}$$

The total energy loss inside the pneumatic tunnel then becomes:

$$H_{total} = H_f + H_t = 0.70 + 0.18 = 0.88 \text{ m} \tag{T.27}$$

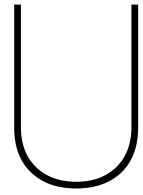
The total energy loss in the Shonai River is equal to  $1200/1313 = 0.91$  m. The calculated value in the equation above is approximately equal to this 0.91. The effective area of one pneumatic caisson becomes:

$$A = w * h = 9 * 10 = 90 \text{ m}^2 \tag{T.28}$$

The total capacity of the tunnels should be  $Q = 1400 \text{ m}^3/\text{s}$ , therefore the required area becomes:

$$A_{required} = \frac{Q}{u} = \frac{1400}{3.3} = 424 \text{ m}^2 \tag{T.29}$$

In conclusion, according to the energy loss approach, six tunnels are required with a width of 10 m and a height of 9 m. In the deterministic approach the design has a redundant capacity of 27%, which accounts for uncertainties in the probabilistic calculation.



# Design calculations of Shinkansen bridge

## U.1. Effect of reducing piers

As shown in section R.2, the discharge capacity is approximately  $3750 \text{ m}^3/\text{s}$  in the current situation. In order to check whether the construction of a new bridge would create sufficient discharge capacity, a rough calculation has been executed first. In this first calculation, it had been assumed that the cross-section of the river will have no piers. This situation has characteristics as in table U.1:

Variable	Value	Unit
A	1479	$\text{m}^2$
P	204	$\text{m}$
n	0.0184	$\text{s}/\text{m}^{1/3}$

Table U.1: Cross-sectional characteristics of proposed 3x70 span bridge

This results in a capacity of  $6711 \text{ m}^3/\text{s}$  if calculated with a deterministic approach. Calculations are done similarly to the calculations in R.2. This value is significantly more than needed, which is  $4250 \text{ m}^3/\text{s}$ . Although this is a massive overestimation of the capacity since piers will definitely be needed, it does prove the viability of this idea.

The total span of the bridge is 210 m. Also, the bottom of the bridge is to be raised to 12 m above the river bed to increase the capacity even more. This is above the planned dike level.

## U.2. Common Shinkansen bridges

Investigation of all Shinkansen bridges in Japan shows that the majority of the bridges are continuous box-girder bridges with short spans of about 30 meters. When larger spans need to be realised, two options are used:

- The use of a double (warren) truss design.
- The construction of a tunnel, primarily found when connecting different main islands;

The use of a truss design is an efficient way to limit the maximum deflection, which will most likely be the governing criterion for the bullet train. Two reference projects have been found when investigating this option: the Tohoku Shinkansen Tonekawa Bridge and the Tokaido Shinkansen Fujikawa Bridge, both are shown in figure U.1. The former has a span of 80 meters, while the latter has a span of 60 meters. Both bridges (and the current Tokaido Shinkansen Shonaikawa Bridge) are 12 meters in width. These values have been taken for an initial estimate of dimensions.



(a) Tohoku Shinkansen Tonekawa Bridge [4]

(b) Tokaido Shinkansen Fujikawa Bridge [4]

Figure U.1: Shinkansen bridges with larger spans

### U.3. Conceptual design structure

Three spans of 70 meters will be used for the conceptual design of the Shinkansen bridge. The use of a warren truss will be used, since all Shinkansen truss bridges are constructed with this type of truss. Also, the bottom of the bridge will be placed at T.P. +12 m above river bed, while only T.P. +11 m is initially required. This is to allow room for future dike raising.

The railway track is placed on a concrete slab. This slab is connected to the bottom of the truss. The steel truss is to be constructed using S235. In order to create a easy to construct grid, a repetitive length of 10 m has been used. The same steel cross-section is used for all truss elements. See figure U.2 for the chosen design.

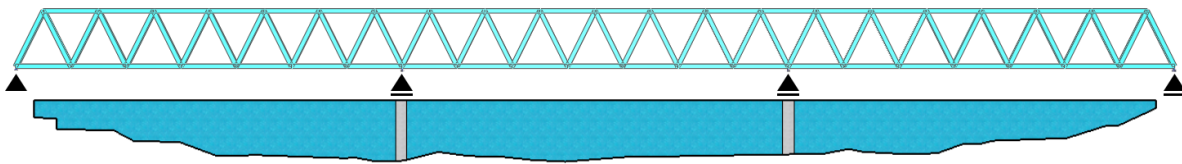


Figure U.2: Conceptual truss layout 3x70 m

### U.4. Concrete slab verification

In this conceptual design, loads have been limited to basic static cases. Self weight of the steel truss, the concrete slab and the rails have been taken into account and have been multiplied with a load factor of 1.2. Besides this permanent load, the load of the bullet train has been taken into account, which has been multiplied with a load factor of 1.5. Other loads have been neglected for this design phase. All loads have been summarised in table U.2. The train load has been calculated as follows on the next page:



$$\begin{aligned}
F_{train,total} &= F_{empty} + F_{passengers} \\
F_{empty} &= 7150 \text{ kN [77]} \\
F_{passengers} &= capacity * F_{one passenger} \\
capacity &= 1323 \\
F_{one passenger} &= 600 \text{ N} \\
F_{passengers} &= 1323 * 600 \\
&= 793.8 \text{ kN} \\
F_{train,total} &= 7150 + 793.8 \\
&= 7944 \text{ kN} \\
F_{train,wheel} &= F_{train,total} / n_{wheels} \\
n_{wheels} &= 128 \\
F_{train,wheel} &= 7944 / 128 \\
&= 62.06 \text{ kN}
\end{aligned} \tag{U.1}$$

The rail track load has been calculated as follows:

$$\begin{aligned}
q_{track} &= \frac{G_{track}}{A_{track}} \\
G_{track} &= 50 \text{ kN[78]} \\
A_{track} &= 2.340 \text{ m} * 4.950 \text{ m} \\
&= 11.58 \text{ m}^2 \\
q_{track} &= \frac{50}{11.58} \\
&= 4.32 \text{ kN/m}
\end{aligned} \tag{U.2}$$

Load	Load type	Value	Unit	Load factor
Bullet train per wheel	Variable	62.06	kN	1.5
Rail track	Dead load	4.32	kN/m <sup>2</sup>	1.2
Concrete slab	Dead load	24.5	kN/m <sup>3</sup>	1.2
Truss elements	Dead load	78	kN/m <sup>3</sup>	1.2

Table U.2: Loads taken into account

The loads are placed according to figure U.3, where the red dots indicate the placement of the wheels of the bullet train, the brown elements indicate the placement of the rail track slabs. The complete area is loaded by the concrete slabs. At the four edges, the slab is connected to the truss design.

Stresses in the concrete slab have been calculated using the finite element method in MatrixFrame, using a mesh density factor of 5. The loads as schematised in figure U.3 have been implemented into the software, resulting in various shear- and moment-distribution graphs. These graphs are presented in figure U.4 and figure U.5. Larger versions of these figures can be found in appendix V. A thickness of 700 mm has been used, determined by the maximum deflection criterion, which is equal to 1:800. Using the proposed thickness, deflections of 1:923 are found. An E-modulus of 36,000 MPa has been used.

The  $m_{xy}$  distribution graph can now be used to calculate the support reactions, which is equal to two times the  $m_{xy}$  at that location. Due to the fact that MatrixFrame makes the graph at this singularity point smooth,

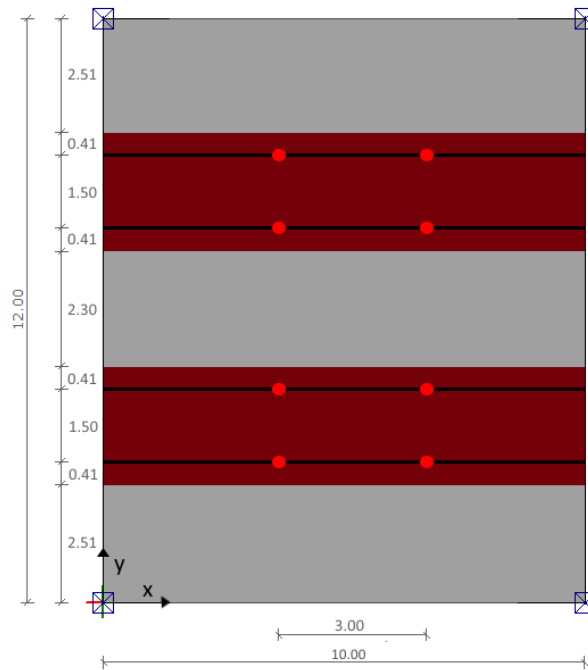


Figure U.3: Loads on bridge. Red: wheel loads. Brown: rail track load. Entire concrete slab is loaded by self-weight.

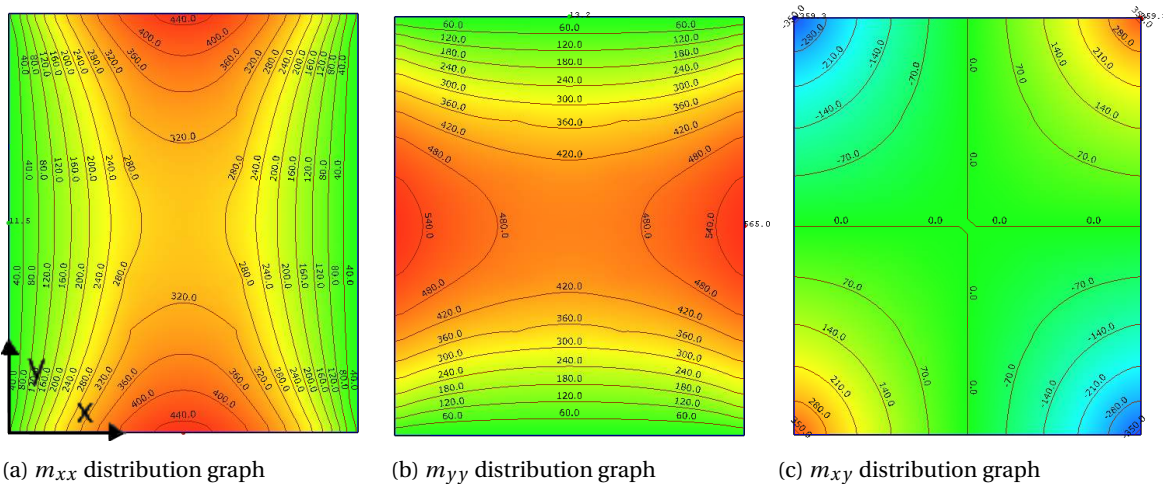


Figure U.4: Moment-distribution graphs

a small error has been found. Equilibrium of vertical forces (U.3) show that the support reaction should be 791.5 kN per corner.

$$\begin{aligned}
 \Sigma F_v = 0 &= 8F_{wheel} + 12 * 10 * Q_{plate} + 2 * 10 * 2.34 * Q_{rail} - 4F_{support} \\
 0 &= 8 * 62.06 + 120 * 20.58 + 46.8 * 4.27 - 4F_{support} \\
 \rightarrow F_{support} &= 791.5kN
 \end{aligned}
 \tag{U.3}$$

### U.4.1. Resistance

The bending moment resistance has been designed by schematising the plate as a beam. First, the  $m_{ii}$  has been integrated over the width using Matrixframe. Then, required reinforcement has been calculated based on the beam model. The procedure has been carried out for both directions. The following values have been found, see table U.3.

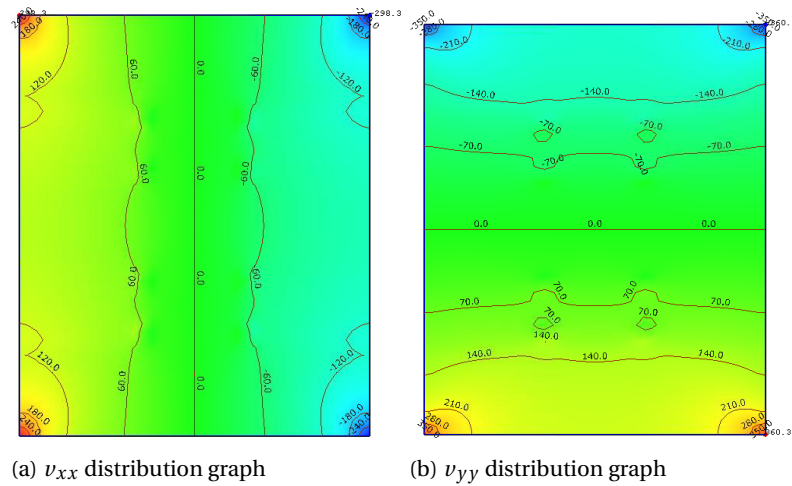


Figure U.5: Shear-distribution graphs

Direction	Length [m]	Width [m]	$M_{Ed}$ [kNm]
X	10	12	4180
Y	12	10	4957

Table U.3: Resulting bending moments concrete slab using beam theory

The total amount of required reinforcement has been based on the bending moment obtained in this manner. The spacing of the bars has not been calculated in this phase. However, reinforcement has to be more concentrated near the edges, as the bending stresses are higher there, as seen in the graphs above. The bending moment resistance has been calculated as follows:

$$\begin{aligned}
 M_{Rd} &= N_c * lever \\
 N_c &= N_s \\
 N_s &= n_{bars} * \frac{\pi}{4} * \phi * f_{yd} \\
 f_{yd} &= f_{yk} / \gamma_s \\
 lever &= t - c - \phi / 2 - \beta * x_u \\
 x_u &= \frac{N_c}{\alpha * w * f_{cd}} \\
 f_{cd} &= f_{ck} / \gamma_c
 \end{aligned} \tag{U.4}$$

With the parameters presented in table U.4, the bending moment capacities have been calculated. The capacities have been noted in table U.5.

The calculated capacity of the slab is significantly higher than the occurring bending moment. It is suggested to explore different ways of reinforcing the slab. For the feasibility design, the current calculations have been deemed sufficient.

## U.5. Steel truss verification

According to Eurocode EN1990 Annex A-2, maximum allowable deflections of high speed rail bridges are limited to a function of the speed and the span, see figure U.6. As the Shinkansen line is designed to handle a speed of 285 km/h [77] and the spans have been determined to be 70 meter, maximum allowable deflection has been set to 1:1800.

Parameter	Symbol	Value	Unit
Thickness	t	700	mm
Cover	c	40	mm
Yield stress rebar steel (B500B)	$f_{yk}$	500	N/mm <sup>2</sup>
Yield stress concrete (C45/55)	$f_{ck}$	45	N/mm <sup>2</sup>
Material factor rebar steel	$\gamma_s$	1.15	-
Material factor concrete	$\gamma_c$	1.5	-
Shape factor area compressive zone	$\alpha$	0.75	-
Shape factor centre of gravity	$\beta$	0.39	-

Table U.4: Parameters bending moment capacity concrete slab

Direction	$\phi$ [mm]	Number of bars	$M_{Rd}$ [kNm]	$M_{Ed}$ [kNm]	u.c.
X	40	23	7312	4180	0.572
Y	40	20	6786	4957	0.730

Table U.5: Parameters bending moment capacity concrete slab

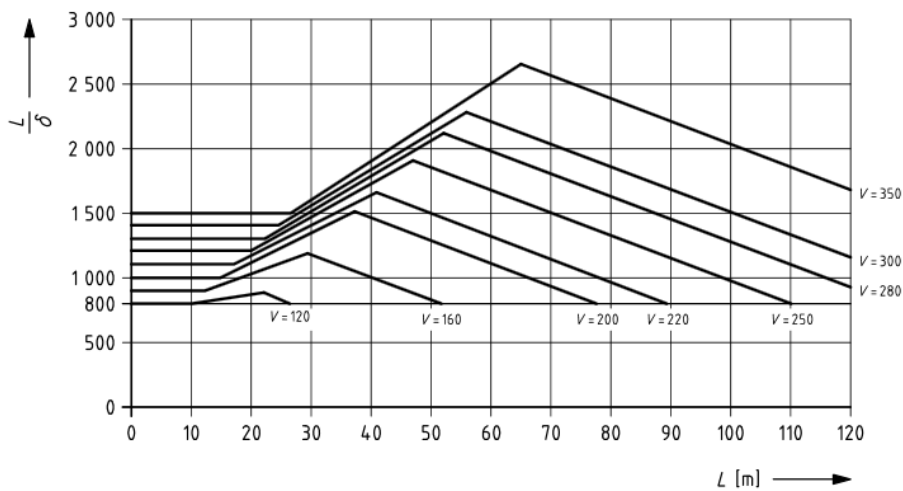


Figure U.6: Maximum allowed deflection of high speed train bridges [79]

### U.5.1. Loads

To account for the fact that not every plate is loaded as calculated in section U.4 at all time, the weight of the train has been distributed over the entire bridge. Equation (U.5) shows the support reaction from the slabs given as implemented into this calculation. Besides this force, self weight of the primary load bearing construction has been taken into account. Factors 0.9 and 1.2 have been applied on unfavourable and favourable loads respectively.

$$\begin{aligned}
 \Sigma F_v = 0 &= \frac{2 * \frac{3*70}{25} * 8 * F_{wheel}}{21} + 12 * 10 * Q_{plate} + 2 * 10 * 2.34 * Q_{rail} - 4F_{support} \\
 0 &= \frac{2 * \frac{3*70}{25} * 8 * 62.06}{21} + 120 * 20.58 + 46.8 * 4.27 - 4F_{support} \\
 \rightarrow F_{support} &= 765.9kN
 \end{aligned}
 \tag{U.5}$$

In this calculation has been assumed that all elements of the truss are constructed with the same shape. A rectangular pipe profile has been taken for this design be 10 meters high. A MatrixFrame analysis shows that the use a rectangular 500 mm profile with 60 mm is sufficient for the structural integrity of all elements. Also, deflections have been limited to 39 mm, which represent a deflection 1:1800. A figure of a cross-section of an element and the connection is shown in figure U.7. In table U.6, maximum axial element forces are given.

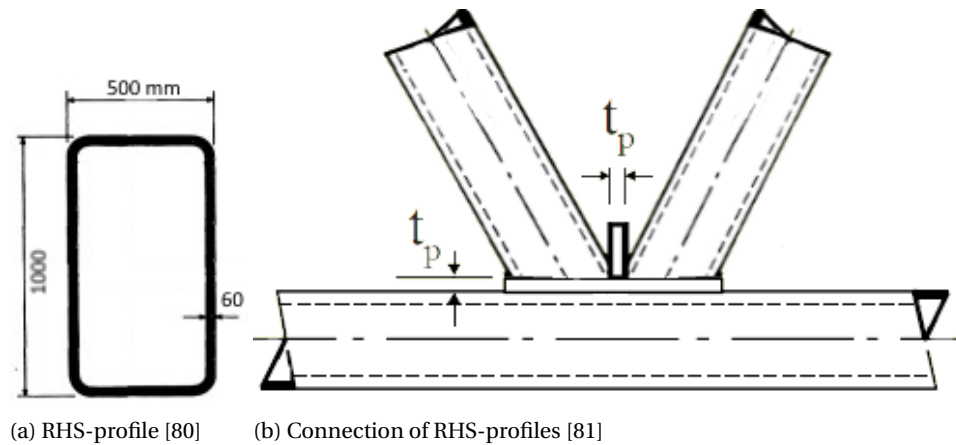


Figure U.7: Truss profile

Description	Value	Unit
Tension beam	+11627.1	<i>kN</i>
Horizontal compression beam	-10607.1	<i>kN</i>
Diagonal compression beam	-10495.4	<i>kN</i>

Table U.6: Extreme truss elements

Strength checks have been carried out for each element of the truss. For the tensile elements, the following strength check has been carried out:

$$A = 500 * 1000 - (500 - 120) * (1000 - 120) = 165600 \text{ mm}^2 \quad (\text{U.6})$$

$$N_{Rd} = A * \sigma = 165600 * 235 = 38916 \text{ kN} > 11627.1 \text{ kN}$$

The elements in compression have been checked for buckling. This has been separated into two sections. First, the horizontal beams with a length of 10 m have been checked, then the beams with a length of 12.73 m. These calculations are presented below.

$$I_{cr} = \frac{1}{12} (b^3 * h - (b - 2t)^3 * (h - 2t))$$

$$= \frac{1}{12} (500^3 * 1000 - (500 - 2 * 60)^3 * (1000 - 2 * 60)) \quad (\text{U.7})$$

$$= 6.39E + 09 \text{ mm}^4$$

$$\begin{aligned}
N_{cr} &= \frac{\pi * E_s * I_{cr}}{L^2} \\
&= \frac{\pi * 210000 * 6.39E + 09}{10^2} \\
&= 132 \text{ MN} \\
\lambda &= \sqrt{\frac{A * f_y}{N_{cr}}} \\
&= \sqrt{\frac{247500 * 235}{132E + 06}} \\
&= 0.542 \\
\Phi &= 0.5 * (1 + \alpha * (\lambda - 0.2) + \lambda^2) \\
&= 0.5 * (1 + 0.21 * (0.542 - 0.2) + 0.542^2) \\
&= 0.683 \\
\chi &= \min\left(1; \frac{1}{\Phi + \sqrt{\Phi^2 - \lambda^2}}\right) \\
&= \min\left(1; \frac{1}{0.683 + \sqrt{0.683^2 - 0.542^2}}\right) \\
&= 0.911 \\
N_{Rd} &= A * f_{yd} * \chi \\
&= 165600 * 235 * 0.911 \\
&= 35.4 \text{ MN} > 10.6 \text{ MN}
\end{aligned} \tag{U.8}$$

$$\begin{aligned}
N_{cr} &= \frac{\pi * E_s * I_{cr}}{L^2} \\
&= \frac{\pi * 210000 * 6.39E + 09}{\sqrt{125}^2} \\
&= 106 \text{ MN} \\
\lambda &= \sqrt{\frac{A * f_y}{I} N_{cr}} \\
&= \sqrt{\frac{247500 * 235}{I} 106E + 06} \\
&= 0.606 \\
\Phi &= 0.5 * (1 + \alpha * (\lambda - 0.2) + \lambda^2) \\
&= 0.5 * (1 + 0.21 * (0.606 - 0.2) + 0.606^2) \\
&= 0.726 \\
\chi &= \min\left(1; \frac{1}{\Phi + \sqrt{\Phi^2 - \lambda^2}}\right) \\
&= \min\left(1; \frac{1}{0.726 + \sqrt{0.726^2 - 0.606^2}}\right) \\
&= 0.888 \\
N_{Rd} &= A * f_{yd} * \chi \\
&= 165600 * 235 * 0.888 \\
&= 34.5 \text{ MN} > 10.5 \text{ MN}
\end{aligned} \tag{U.9}$$

An axial compressive resistance of 35.4 and 34.5 MN has been found for the members of 10 m and 12.37 m respectively. With occurring compressive forces being 10.6 MN and 10.5 MN, both elements fulfil the strength criterion.

## U.6. Pier verification

As a result of the proposed construction, support reactions can be calculated. See figure U.8 for the support reactions.

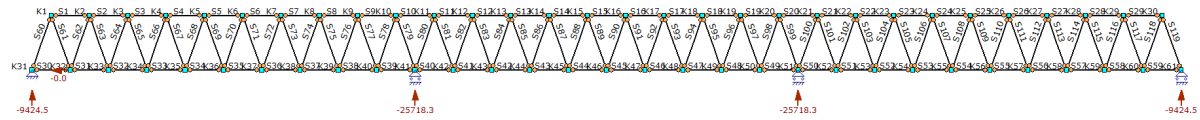


Figure U.8: Support reactions of truss design

A feasibility design has been made for the centre bridge piers, presented in figure U.9 below. The pier consists of one solid wall. By using one wall instead of a set of columns, the total amount of turbulence in the flow is relatively lower, thus increasing discharge capacity. Furthermore, it has been aimed to minimise the thickness of the wall. This increases the cross-sectional area of the river and therefore the discharge capacity.

Crude calculations have been made to check the feasibility of the design. Further calculations and detailing are to be carried out in the next design phase, if this option was chosen.



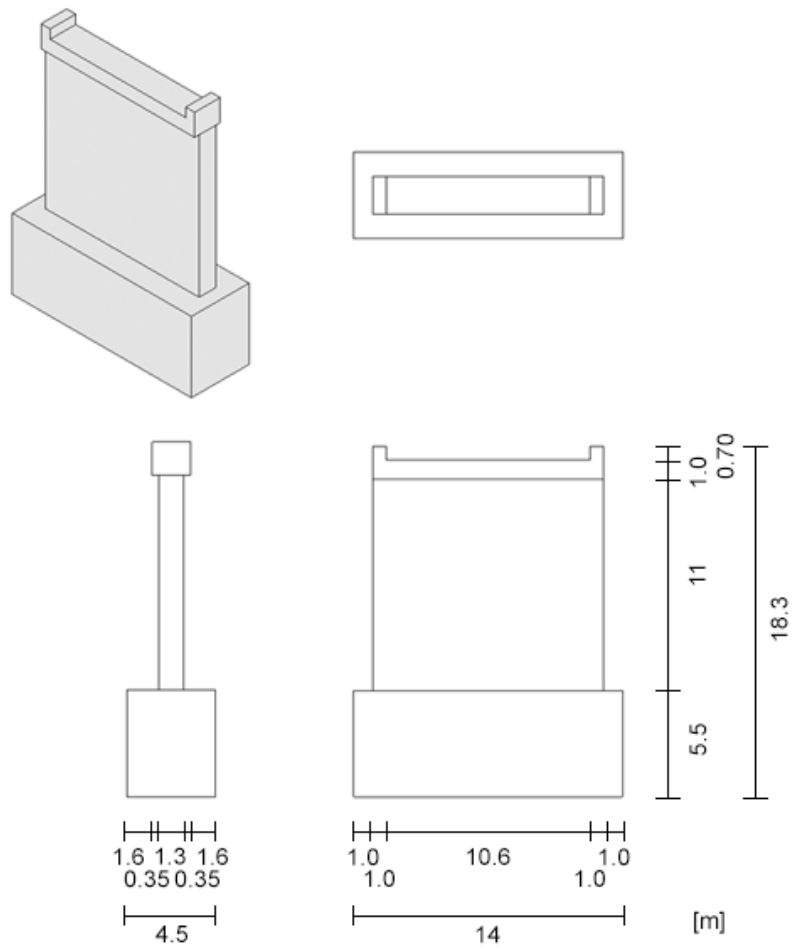


Figure U.9: Design bridge pier - structure

### U.6.1. Truss-Pier connection

The truss beam rests on the concrete notches at both ends of the pier. A draft of the connection is presented in figure U.10.

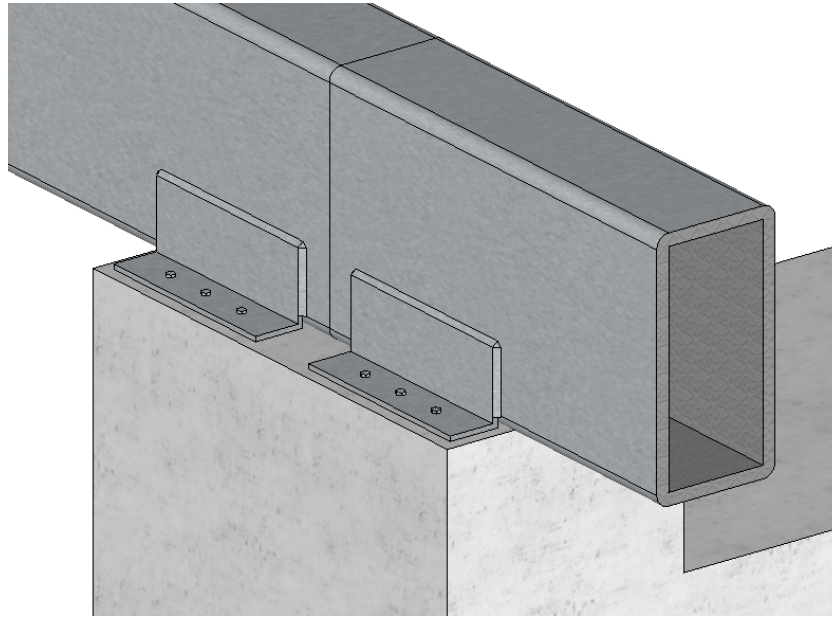


Figure U.10: Connection truss to pier

The length and width of the concrete support have been based on the beam dimensions, to allow for an even stress distribution. The width is 1000 mm, which given that the truss beam is 500 mm wide, provides 250 mm on both sides for mounting. The length is 2000 mm, equal to two times the beam height. This provides surface area to evenly transfer the forces from the beams into the concrete. The concrete support has been checked in the cross-section where uniform stresses are present. The following parameters have been used:

Parameter	Symbol	Value	Unit
Load from truss	$N_{Ed}$	1.915E+07	N
Cross-sectional area concrete	A	700*2000 = 1.4E+06	mm <sup>2</sup>
Design strength concrete (C30/37)	$f_{cd}$	30 / 1.5 = 20	N/mm <sup>2</sup>

Table U.7: Parameters truss-pier connection calculations

$$N_{Ed} = 1.915E + 07 \text{ N}$$

$$N_{Rd} = A * f_{cd}$$

$$= 1000 * 2000 * 20$$

$$= 4.00E + 07 \text{ N}$$

(U.10)

$$u.c. = N_{Ed} / N_{Rd}$$

$$= 1.915E + 07 / 4.00E + 07 = 0.479$$

At cross-sections with uniform stress distribution, the support has sufficient strength. Further detailing is required for the zone at the top, where forces are introduced.

### U.6.2. Pier

The pier has been checked for strength in a similar manner as the connection in the previous section. Calculations are presented below.

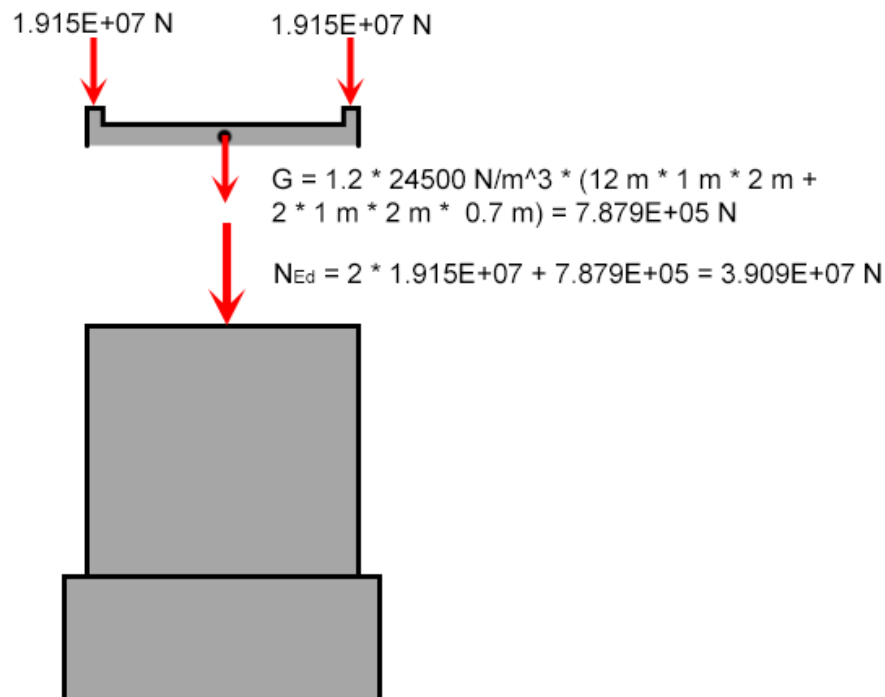


Figure U.11: Load schematisation bridge pier

Parameter	Symbol	Value	Unit
Load	$N_{Ed}$	$2 * 1.915E+07 + 7.879E+05 = 3.909E+07$	N
Cross-sectional area	$A$	$1300 * 12000 = 1.56E+07$	$\text{mm}^2$
Design strength concrete (C30/37)	$f_{cd}$	$30 / 1.5 = 20$	$\text{N/mm}^2$

Table U.8: Parameters bridge pier calculations, strength criterion

$$\begin{aligned}
 N_{Rd} &= A * f_{cd} \\
 &= 1300 * 12000 * 20 \\
 &= 3.120E+08 \text{ N} \\
 & \hspace{15em} \text{(U.11)}
 \end{aligned}$$

$$\begin{aligned}
 u.c. &= N_{Ed} / N_{Rd} \\
 &= 3.909E+07 / 3.120E+08 = 0.125
 \end{aligned}$$

The pier fulfils the strength criterion based on maximum allowable stress. However, stability or buckling has not yet been taken into account. Therefore, a slenderness criterion has been used, as by NEN-EN 1992-1-1+C2. The criterion is as follows on the next page:

$$\begin{aligned}
\lambda &< \lambda_{lim} \\
\lambda_{lim} &= 20 * \frac{A * B * C}{\sqrt{n}} \\
n &= N_{Ed} / N_{Rd} \\
\lambda &= L_{buc} / i \\
i &= \sqrt{\frac{I}{A}} \\
&= h / 3.464
\end{aligned} \tag{U.12}$$

When this criterion is met, no second order calculations have to be taken into account. For this feasibility design phase, this has been deemed sufficient to check for stability of the plate. For the buckling length  $L_{buc}$ , hinged connections on both ends have been assumed. The following parameters have been used, with corresponding calculations:

Parameter	Symbol	Value	Unit
Load	$N_{Ed}$	3.909E+07	N
Resistance	$N_{Rd}$	3.120E+08	N
Height cross-section	$h$	1300	mm
Buckling length	$L_{buc}$	11000	mm
Creep factor	$A$	0.7	-
Reinforcement factor	$B$	1.1	-
End bending moments factor	$C$	0.7	-

Table U.9: Parameters bridge pier calculations, slenderness criterion

$$\begin{aligned}
n &= N_{Ed} / N_{Rd} \\
&= 3.909E + 07 / 3.120E + 08 \\
&= 0.1253 \\
\lambda_{lim} &= 20 * \frac{A * B * C}{\sqrt{n}} \\
&= 20 * \frac{0.7 * 1.1 * 0.7}{\sqrt{0.1252}} \\
&= 30.44 \\
i &= \sqrt{\frac{I}{A}} \\
&= h / 3.464 \\
&= 1300 / 3.464 \\
&= 375.3 \text{ m} \\
\lambda &= L_{buc} / i \\
&= 11000 / 375.3 \\
&= 29.31 \\
&< 30.46
\end{aligned} \tag{U.13}$$

The pier fulfils the slenderness criterion. Therefore, no additional second order calculations are required.

## U.7. Foundation verification

For the foundation of the bridge pier, it has been decided to use a shallow foundation. Cone penetration tests, as seen in appendix S, show the bed consists of sand. The foundation consists of a massive concrete block, as illustrated in figure U.12. The top of the block is 0.5 m above the river bed. The embedded depth is 0.5 m more than has been calculated, to take into account uncertainties in bed level and possible scour.

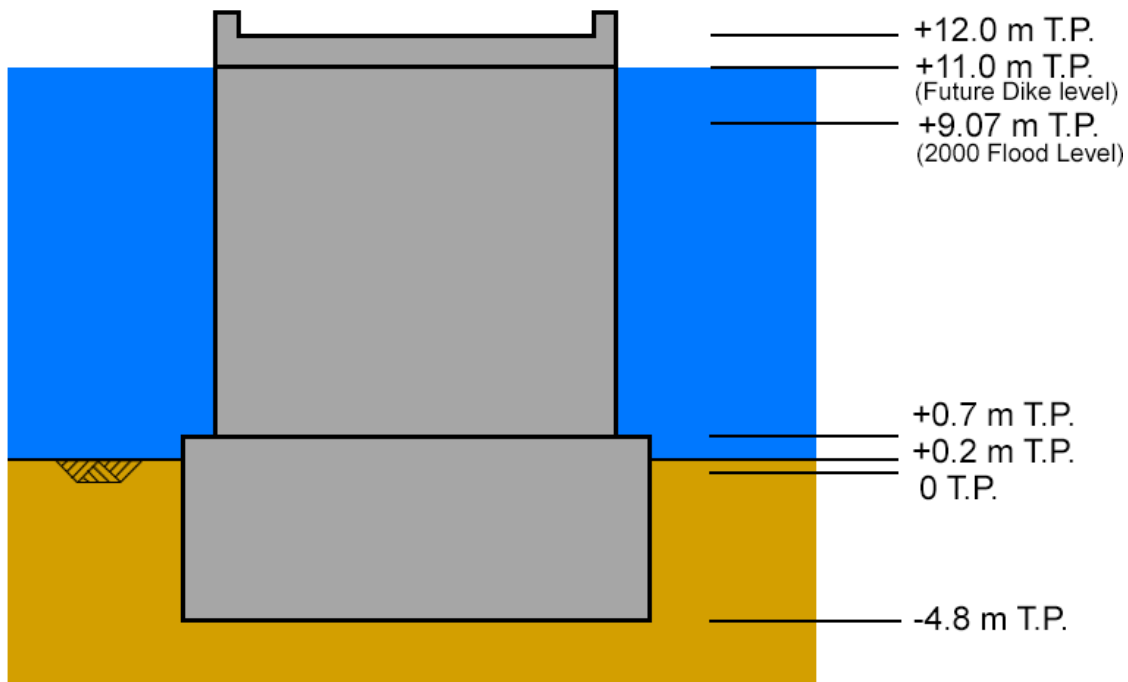


Figure U.12: Design bridge pier, foundation

The maximum bearing capacity of the foundation is the sum of the toe resistance and the shaft resistance. For the toe resistance, Brinch-Hansen has been used, and for the shaft resistance, the slip method. The Brinch-Hansen method for a foundation in cohesion-less sand and loaded by only a vertical force is as follows:

$$\begin{aligned}
 N_{Rd,shaft} &= A * p'_{max,drained} \\
 p'_{max,drained} &= \sigma'_q N_q s_q + 0.5 \gamma' B N_\gamma s_\gamma \\
 N_q &= \frac{1 + \sin(\phi')}{1 - \sin(\phi')} * e^{\pi * \tan(\phi')} \\
 N_\gamma &= (N_q - 1) * \tan(1.32\phi') \\
 s_q &= 1 + \frac{B}{L} \sin(\phi') \\
 s_\gamma &= 1 - 0.3 \frac{B}{L} \\
 \sigma'_q &= d * \gamma'
 \end{aligned} \tag{U.14}$$

The slip method is as follows:

$$\begin{aligned}
 N_{Rd,shaft} &= P * d * p_{r,shaft,max} \\
 &= P * d * \int_0^d \gamma'_s * z dz \\
 &= \frac{1}{2} * P * K_s * \gamma'_s * \tan(\delta) * d^2 \\
 \delta &= \frac{2}{3} \phi'
 \end{aligned}
 \tag{U.15}$$

For this foundation type, soil is removed during installation. After installation, it has been assumed horizontal displacements are small enough to use neutral soil pressure. Because the foundation is in a river, it has been assumed all soil is under water level. A minimum factor of safety of 1.5 has been used. The parameters used are presented in table U.10.

Parameter	Symbol	Value	Unit
Load	$N_{Ed}$	4.907E+04	kN
Submerged weight sand	$\gamma'$	8.0	kN/m <sup>3</sup>
Internal friction angle sand	$\phi'$	32	°
Width foundation	B	4.5	m
Length foundation	L	14	m
Embedded depth foundation	d	4.5	m
Horizontal soil pressure coefficient	$K_s$	0.5	-

Table U.10: Parameters bridge foundation

With the total load  $N_{Ed}$  calculated as follows:

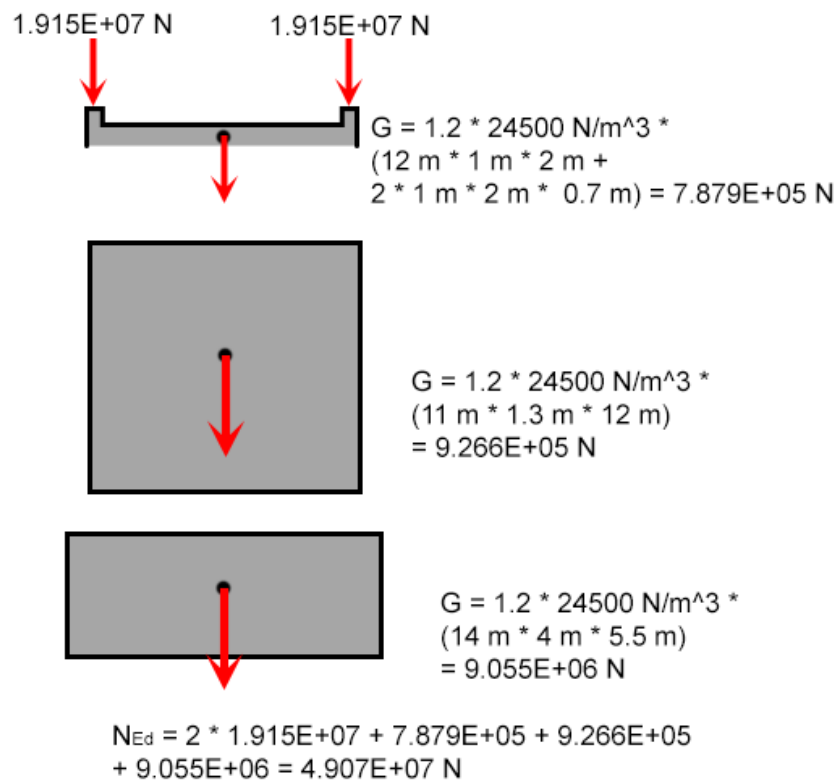


Figure U.13: Total load on foundation

With the given parameters, the following bearing capacity has been calculated:

$$\begin{aligned}
 N_q &= \frac{1 + \sin(\phi')}{1 - \sin(\phi')} * e^{\pi * \tan(\phi')} \\
 &= \frac{1 + \sin(32)}{1 - \sin(32)} * e^{\pi * \tan(32)} \\
 &= 23.18 \\
 N_\gamma &= (N_q - 1) * \tan(1.32\phi') \\
 &= (N_q - 1) * \tan(1.32\phi') \\
 &= 20.14 \\
 s_q &= 1 + \frac{B}{L} \sin(\phi') \\
 &= 1 + \frac{4.5}{14} \sin(32') \\
 &= 1.170 \\
 s_\gamma &= 1 - 0.3 \frac{B}{L} \\
 &= 1 - 0.3 \frac{4.5}{14} \\
 &= 0.9036 \\
 \sigma' &= d * \gamma' \\
 &= 4.5 * 8 \\
 &= 36 \text{ kPa}
 \end{aligned}
 \tag{U.16}$$

$$\begin{aligned}
 p'_{max,drained} &= \sigma'_q N_q s_q + 0.5 \gamma' B N_\gamma s_\gamma \\
 &= 36 * 23.18 * 1.170 + 0.5 * 8 * 4.5 * 20.14 * 0.9036 \\
 &= 1304 \text{ kPa}
 \end{aligned}$$

$$\begin{aligned}
 N_{Rd,toe} &= A * p'_{max,drained} \\
 &= 4.5 * 14 * 1304 \\
 &= 8.215E + 04 \text{ kN}
 \end{aligned}$$

$$\begin{aligned}
 \delta &= \frac{2}{3} \phi' \\
 &= \frac{2}{3} * 32 \\
 &= 21.33^\circ
 \end{aligned}
 \tag{U.17}$$

$$\begin{aligned}
 N_{Rd,shaft} &= \frac{1}{2} * P * K_s * \gamma'_s * \tan(\delta) * d^2 \\
 &= \frac{1}{2} * (2 * 4.5 + 2 * 14) * 0.5 * 8 * \tan(21.33) * 4.5^2 \\
 &= 5.852E + 02 \text{ kN}
 \end{aligned}$$

$$\begin{aligned}
 N_{Rd,total} &= N_{Rd,shaft} + N_{Rd,toe} \\
 &= 8.215E + 04 + 5.852E + 02 \\
 &= 8.274E + 04 \text{ kN}
 \end{aligned}$$

$$\begin{aligned}
 \text{Factor of Safety} &= N_{Rd,total} / N_{Ed} \\
 &= 8.274E + 04 / 4.907E + 04 \\
 &= 1.68 \\
 &> 1.50
 \end{aligned}
 \tag{U.18}$$

The foundation fulfils the strength criterion, as the factor of safety is large enough.

## U.8. Discharge capacity with proposed plan

Now that the supports of the bridge have been estimated, a new discharge capacity can be estimated with the measurement introduced in this chapter. As a result of the piers, characteristics of the cross-section can be described as following:

Variable	Value	Unit
A	1785	$m^2$
P	252	$m$
n	0.02004	$s/m^{1/3}$

Table U.11: Cross-sectional characteristics of proposed 3x70 m span bridge

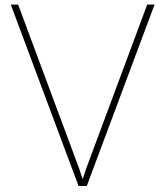
Again, using the same calculations as elaborated in section R.2, one can conclude that the cross-section with two bridge piers and embankment enlargement has a discharge capacity of  $7341 m^3/s$  with a standard deviation of  $485 m^3/s$ . Using the beta-value of 4.3 again, this is sufficient as shown in equation (U.19) as used in previously mentioned section. This shows that replacement of the Shinkansen bridge gives a desired outcome since there is residual capacity.

$$\begin{aligned}
 Q_{bypass} &= Q_{1/200} - (\mu_Q - \beta * \sigma_Q) \\
 &= 4250 - (7341 - 4.3 * 485) \\
 &= -1007 m^3/s
 \end{aligned}
 \tag{U.19}$$

## U.9. Construction

This proposal can be realised by several erection methods. However, due to the limited space around the construction site, some are not feasible. Constructing the bridge besides on shore to roll in onto the piers later, is not advisable because of the needed space. Construction of three 70 m long sections further down-stream in the park, or making use of a cranes to directly manufacture the elements on location is advised.





## Concrete slab FEM results

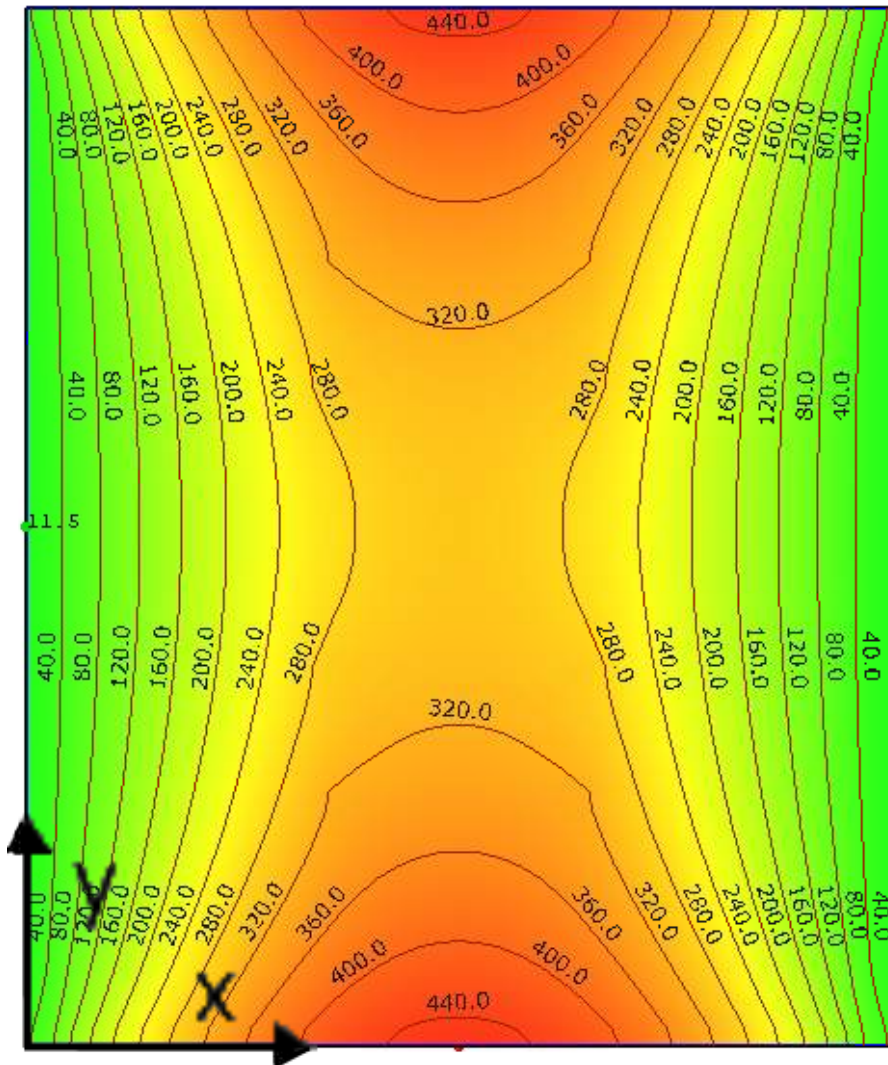
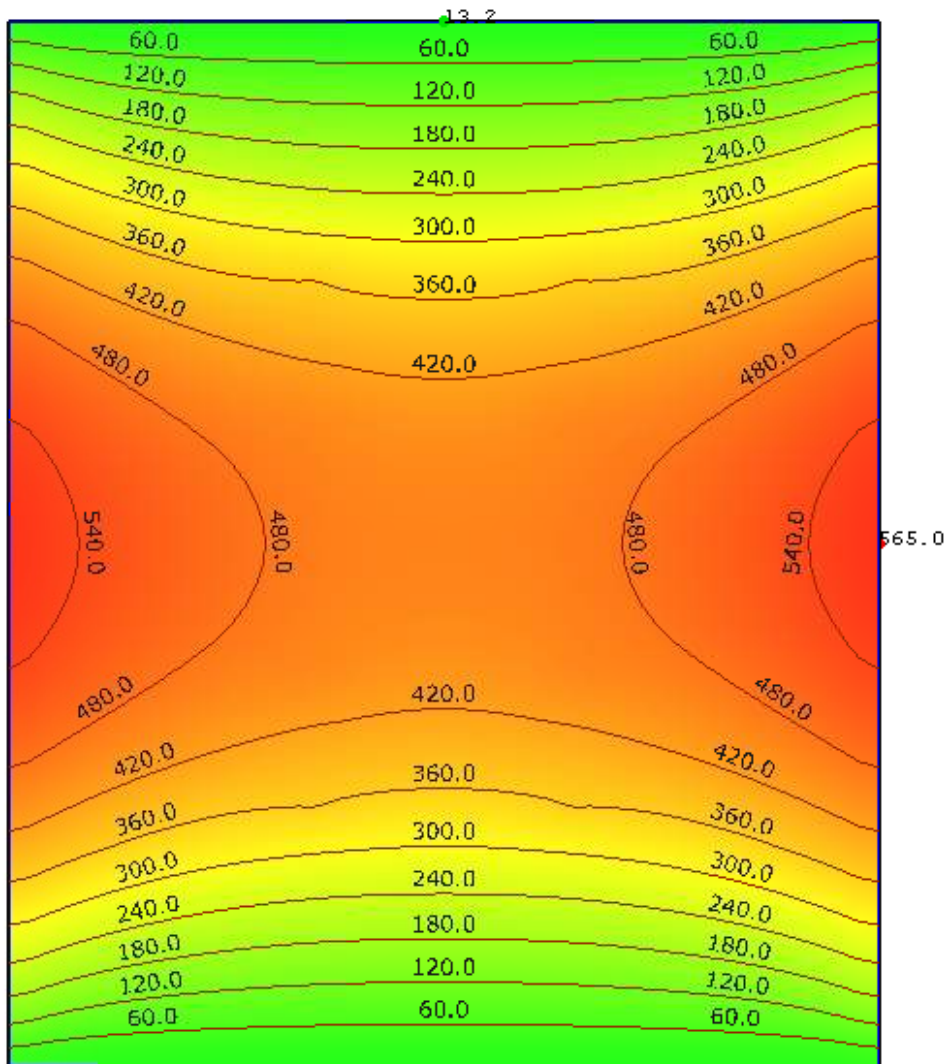


Figure V.1:  $m_{xx}$  distribution graph

Figure V.2:  $m_{yy}$  distribution graph

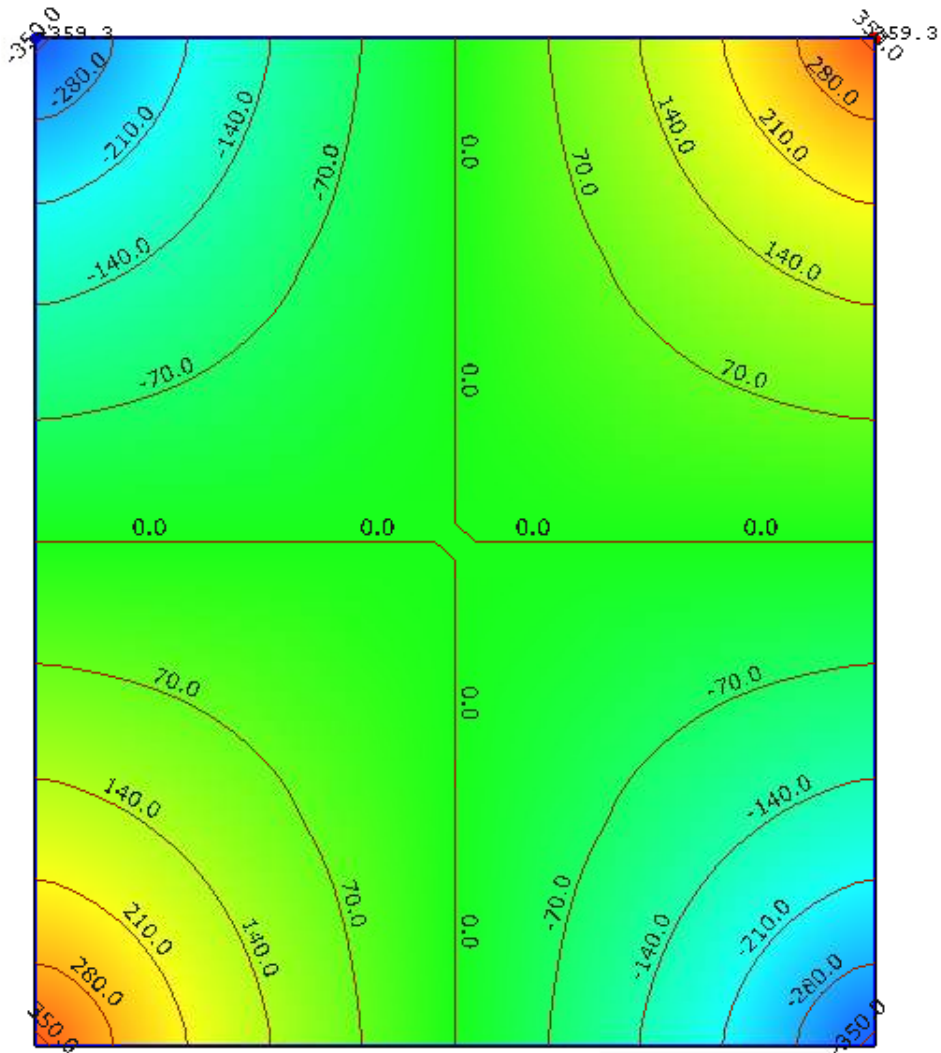
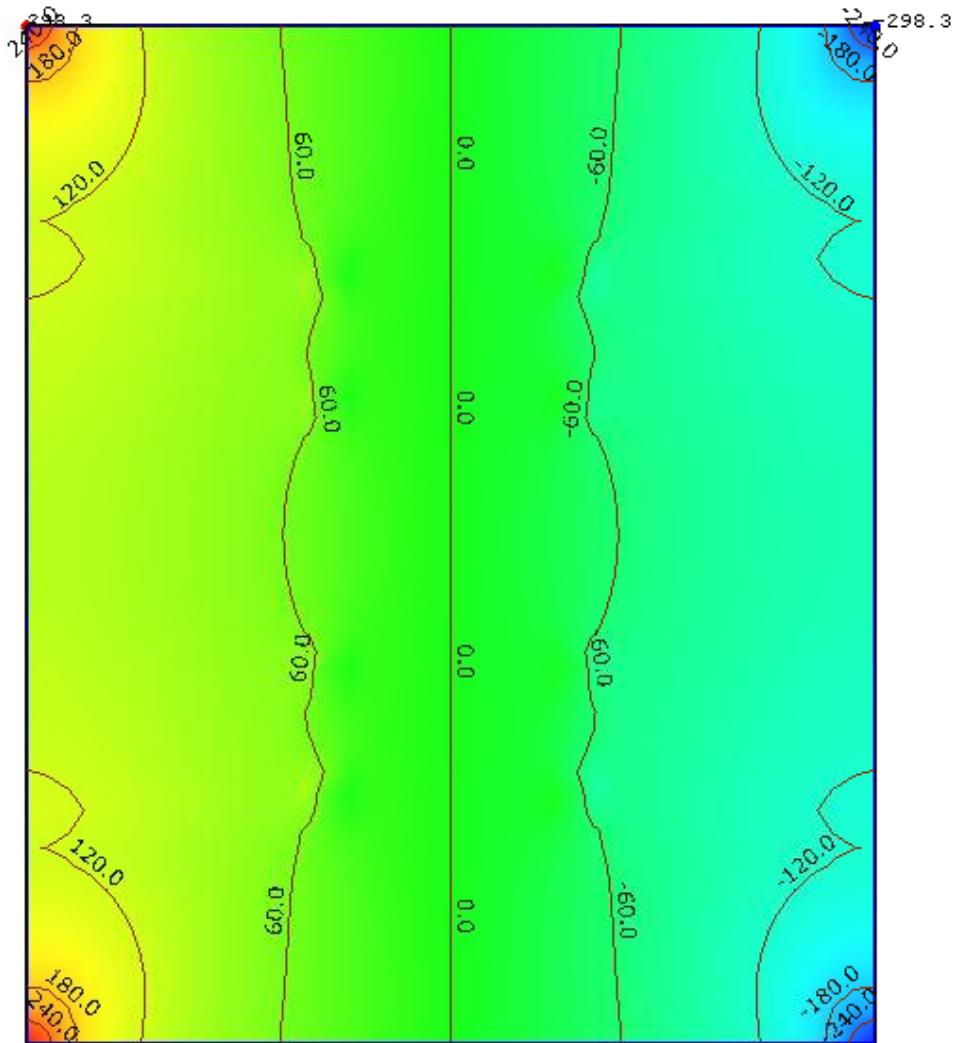
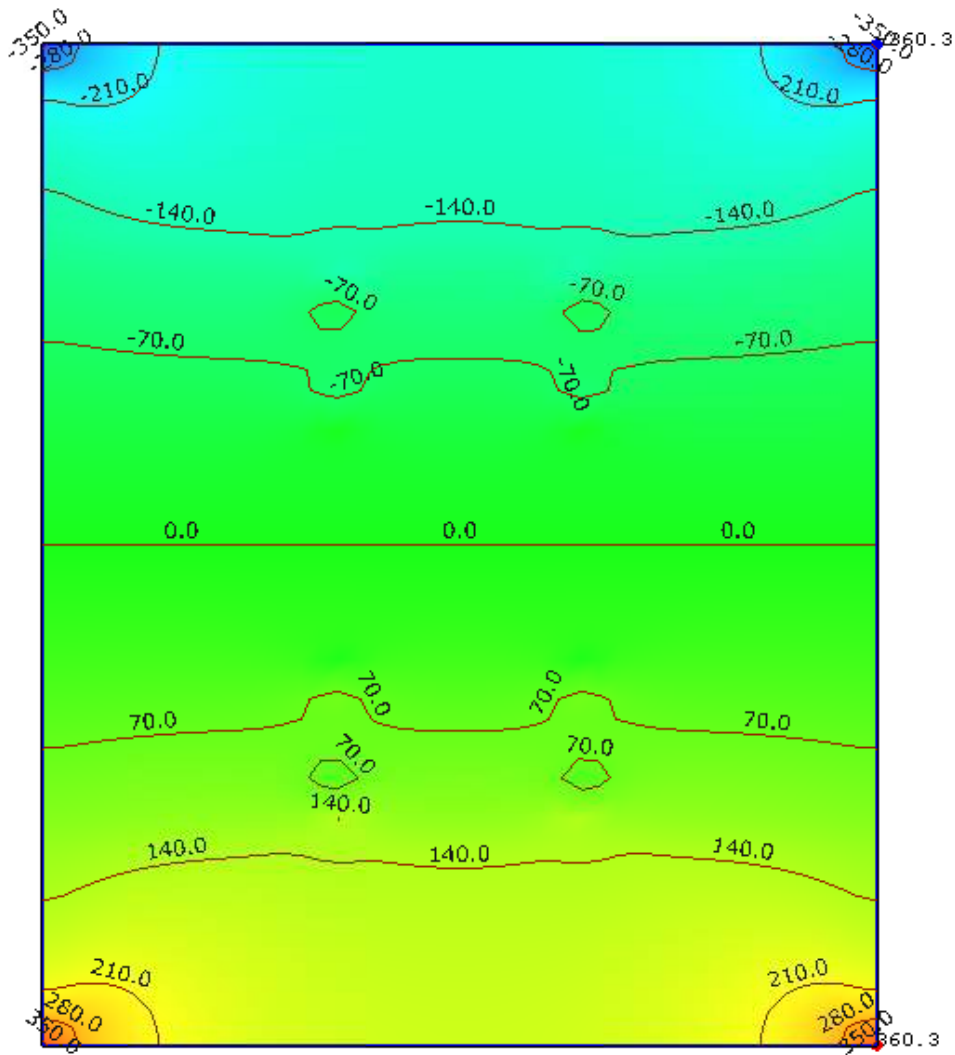
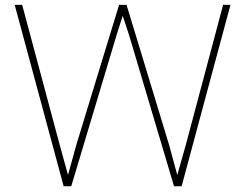


Figure V.3:  $m_{xy}$  distribution graph

Figure V.4:  $v_{xx}$  distribution graph

Figure V.5:  $v_{yy}$  distribution graph



## Calculations of the Shinkansen tunnel

### W.1. Buoyancy

#### W.1.1. Bored tunnel

To calculate the minimum depth of the bored tunnel and thus of the railway, the force acting downward on the tunnel should be larger than the upward buoyancy force. Because the downward forces are acting favourably, a load factor of 0.9 has been applied. The downward forces are the own weight  $G$  of the tunnel and  $F_{soil}$ . The tunnel has an inner diameter  $D$  of 10 m and the thickness of the concrete  $t$  is 0.5 m.

$$\begin{aligned}G &= V_{concrete} * \gamma_{concrete} \\V_{concrete} &= (D + t) * \pi * h \\G &= (10 + 0.5) * \pi * 24.5 = 404 \text{ kN} \\V_{soil} &= 0.5 * D^2 * h - 0.5 * \frac{D^2}{4} * \pi + D * h \\&= 0.5 * 10^2 * h - 0.5 * \frac{10^2}{4} * \pi + 10 * h \\&= 10.7 + 10 * h \\F_{soil} &= \gamma'_{soil} * V_{soil} = 107 + 100 * h \\F_{up} &= V_{tunnel} * \gamma_{water} \\V_{tunnel} &= (0.5 * D + t)^2 * \pi \\F_{up} &= (5 + 0.5)^2 * \pi * \gamma_{water} = 950 \text{ kN} \\0.9 * (G + F_{soil}) &> F_{up}\end{aligned} \tag{W.1}$$

Solving the last equation, it can be concluded that the tunnel should be at a depth of 4.8 m below the river bed. See figure W.1 for a schematisation.

#### W.1.2. Rectangular tunnel

For the Buoyancy test of the tunnel with the rectangular cross-section, the ballast bed of the rail track has been taken into account as well. The ballast has a thickness of 1 m, has a density of  $20 \text{ kN/m}^3$  and is applied over 30 m of the cross-section.

This bed is 1 m thick and has an assumed density of  $20 \text{ kN/m}^3$ .

Upward water force:

$$\begin{aligned}V &= b * h = 34 * 10 = 340 \text{ m}^3 \\F_{up} &= V * \gamma_{water} \\&= 340 * 10 = 3400 \text{ kN}\end{aligned} \tag{W.2}$$

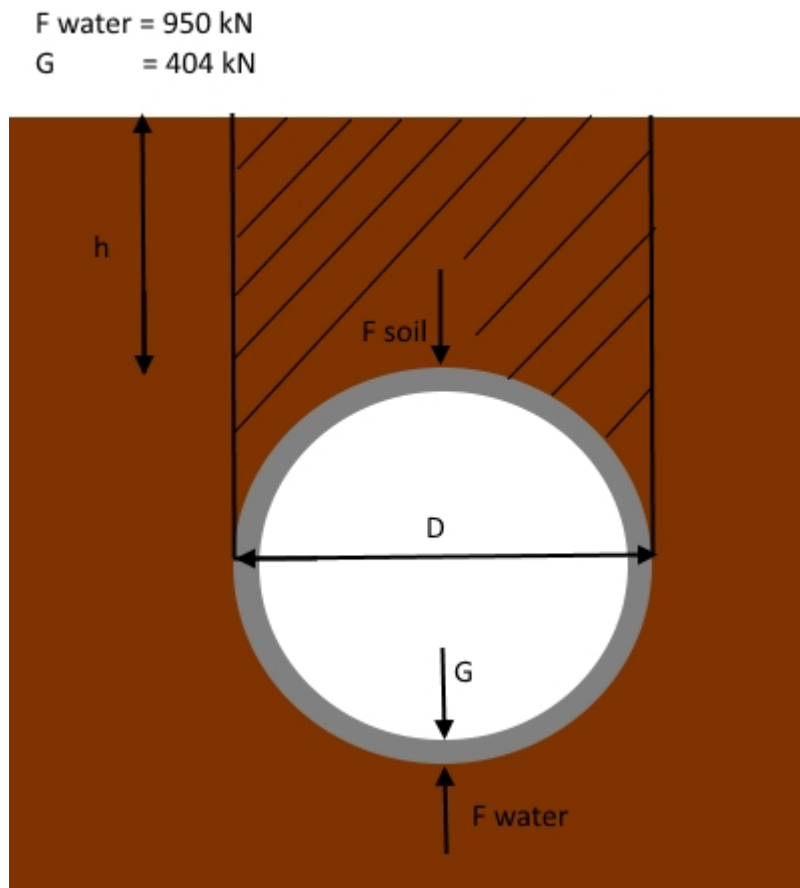


Figure W.1: Principle of buoyancy of the tunnel

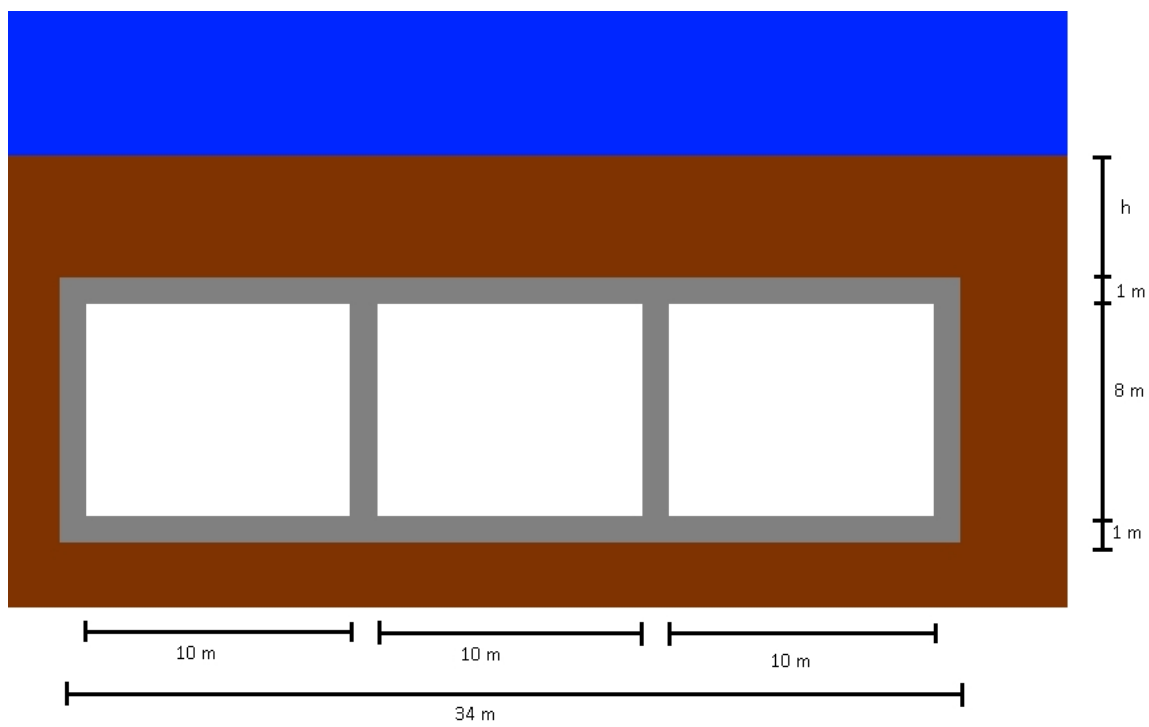


Figure W.2: cross-section of the rectangular tunnel below the river

Downward force, consisting of ballast B, own weight G and soil weight  $F_s$ :

$$\begin{aligned}F_{down} &= B + G + F_s \\B &= V_{ballast} * \gamma_{ballast} = 30 * 20 = 600 \text{ kN} \\G &= V * \gamma_c = 100 * 24.5 = 2450 \text{ kN} \\F_{soil} &= h * b * \gamma'_{soil} = 340 * h\end{aligned}\tag{W.3}$$

Where:

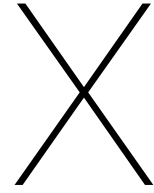
- h = thickness of soil layer above the tunnel
- b = width of tunnel = 34 m

A load factor of 0.9 has been taken for the downward force, since it acts in a favourable direction. It has been found that the thickness of the soil layer should be 2.15 m thick. Because the river bed is inconsistent in depth and prone to erosion, the depth is rounded up to 2.5 m. This has as a result that the top of the structure is at T.P. -3 m.



# VIII

## Appendices of Phase IV



## Calculation of flow velocity in bypass

### X.1. Parameters

For the calculations, several assumptions have been made for the used parameters. Firstly, the roughness of the concrete is approximately  $k_s = 1$  mm, due to the joints present in the tunnel. This would lead to too much friction, therefore the concrete will be coated using epoxy. This reduces the roughness and thus the friction inside the tunnel. Despite the fact that this will increase the costs of the project, it is expected to be less expensive than creating larger or extra tunnels.

The energy loss at the river equals the length of the section divided by the water surface slope at this location. This slope is on average equal to  $1/1867$  [82], with a river length of 1.4 km the head loss of the river becomes 0.75 m.

The energy losses at the bends near the inlet and outlet depend on the angle and radius of the bend as well as the tunnel diameter. The loss coefficients are known for a bend angle of  $22.5^\circ$  and  $45^\circ$  [83]. The inlet has been designed so that the radius of the bend divided by the diameter of the tunnel, or  $r/D$ , equals 6. The height difference that needs to be covered by the two bends is in total 27 m. Following geometry and the height difference, it was found that the bend angle should be  $30.75^\circ$  for one bend. Interpolation between the angles for which the loss coefficients are known gives a bend loss coefficient of 0.056, as seen in table X.1. This table shows the distribution types of all used parameters in the calculation. In here also the tunnel diameter, number of tunnels and flow velocity are given. These will be used in the upcoming calculations, which will show that these are indeed the correct values.

Description	Abbreviation	Distribution	Mean	Std	Unit
Gravitational constant	$g$	Deterministic	9.8	-	$m/s^2$
Kinematic viscosity	$\nu$	Deterministic	1E-06	-	$m^2/s$
Design capacity single tube	$Q$	Deterministic	700	-	$m^3/s$
Bend ratio	$r/D$	Deterministic	6	-	-
Total tunnel length	$L$	Deterministic	1200	-	$m$
Equivalent roughness	$k_s$	Normal	0.1E-04	0.1E-05	$m$
Flow velocity river	$u_{river}$	Normal	1.70	0.085	$m/s$
Head loss coefficient $22.5^\circ$	$K_{b,22.5^\circ}$	Normal	0.045	0.00675	-
Head loss coefficient $45^\circ$	$K_{b,45^\circ}$	Normal	0.075	0.01125	-
Head loss coefficient bend $30.75^\circ$	$K_b$	Deterministic	0.056	-	-
Head loss coefficient contraction	$K_{cont}$	Deterministic	0.06	-	-
Head loss river	$\Delta H_{river}$	Deterministic	0.75	-	$m$
Diameter	$D$	Deterministic	16.0	-	$m$
Number of tunnels	$n$	Deterministic	2	-	-
Flow velocity	$u$	Deterministic	3.70	-	$m/s$

Table X.1: Description of the used parameters

## X.2. Small Losses

Head losses will be found in three sections of the bypass: the inlet, the tube itself and the outlet. Small losses for these three categories have been separated and investigated in three different subsections. In all calculations shown, deterministic values have been used. Probabilistic calculations have been done using software and will not be elaborated.

### X.2.1. Inlet

The inlet has three factors which contribute to the head loss. The first is the separation of flow from the river into the bypass. This separation has been set to zero, since only very minor losses will be found here.

$$H_{sep} = 0 \quad (X.1)$$

Secondly, the separated flow needs to be accelerated into the tube. Head losses due to contraction are defined as shown in the equation below. In this equation, the loss coefficient has been set to 0.06. This is according to research done with a contraction angle of 60 °[14].

$$\begin{aligned} H_{cont} &= \frac{K_{cont} * u^2}{2 * g} \\ &= \frac{0.06 * 3.70^2}{2 * 9.8} \\ &= 0.0418 \text{ m} \end{aligned} \quad (X.2)$$

Lastly, losses will occur because of the two bends to get the tunnel to the required depth. The maximum head loss which will be found in the pipes is:

$$\begin{aligned} H_b &= \frac{K_b * u^2}{2 * g} \\ &= \frac{0.056 * 3.70^2}{2 * 9.8} \\ &= 0.0390 \text{ m} \end{aligned} \quad (X.3)$$

Total inlet head loss was found with:

$$\begin{aligned} H_{inlet} &= H_{sep} + H_{cont} + 2 * H_b \\ &= 0 + 0.0418 + 2 * 0.0390 \\ &= 0.1199 \text{ m} \end{aligned} \quad (X.4)$$

### X.2.2. Friction in pipe

The head loss as a consequence of pipe friction has been calculated using the following steps:

$$\begin{aligned} Re &= \frac{u * D}{\nu} = \frac{3.70 * 16}{1E-06} = 592E+05 \\ f &= \frac{0.25}{\left( \log_{10} \left( \frac{k_s}{3.7 * D} + \frac{5.74}{Re^{0.9}} \right) \right)^2} \\ &= \frac{0.25}{\left( \log_{10} \left( \frac{0.01/1000}{3.7 * 16} + \frac{5.74}{(591E+05)^{0.9}} \right) \right)^2} \\ &= 0.0067 \\ H_f &= \frac{f * L * u^2}{D * 2 * g} \\ &= \frac{0.0067 * 1200 * 3.70^2}{16 * 2 * 9.8} \\ &= 0.3485 \text{ m} \end{aligned} \quad (X.5)$$

### X.2.3. Outlet

The head losses in the outlet are a sum of two contributions; the loss of flow velocity by mixing with the river and the two bends as used in the inlet. The mixing head loss has been calculated using the following formula:

$$\begin{aligned} H_{mix} &= \frac{(u - u_{river})^2}{2 * g} \\ &= \frac{(3.70 - 1.70)^2}{2 * 9.8} \\ &= 0.2034 \text{ m} \end{aligned} \quad (\text{X.6})$$

Head loss in the bends has again been calculated as follows:

$$\begin{aligned} H_b &= \frac{K_b * u^2}{2 * g} \\ &= \frac{0.056 * 3.70^2}{2 * 9.8} \\ &= 0.0390 \text{ m} \end{aligned} \quad (\text{X.7})$$

The total outlet head loss sums up to:

$$\begin{aligned} H_{outlet} &= H_{mix} + 2 * H_b \\ &= 0.2034 + 2 * 0.0390 \\ &= 0.2816 \text{ m} \end{aligned} \quad (\text{X.8})$$

### X.2.4. Discharge in bypass

The summation of all losses should be equal to the loss in the river, which is equal to 0.75 m. Using this value, the flow velocity in the tube can be calculated.

$$\begin{aligned} H_{total} &= H_{inlet} + H_f + H_{outlet} = \Delta H_{river} \\ &= 0.1199 + 0.3485 + 0.2816 = 0.75 \end{aligned} \quad (\text{X.9})$$

It can be concluded that the flow velocity of 3.70 m/s matches the required head difference. The discharge in the two pipes can now be calculated with the following expression:

$$\begin{aligned} Q_{bypass} &= n * \frac{1}{4} * D^2 * \pi * u \\ &= 2 * \frac{1}{4} * 16^2 * \pi * 3.70 \\ &= 1487 \text{ m}^3/\text{s} \end{aligned} \quad (\text{X.10})$$

This discharge value is slightly more than the required 1400 m<sup>3</sup>/s.

### X.3. Flow profile in tunnel

The Reynolds number inside the tunnel following from equation X.5 equals 592E+05. Since the Reynolds number is much larger than 3000, the flow through the tunnel can be considered turbulent. For developed turbulent flow through a pipe, the time-averaged velocity distribution can be described by means of the power law formula:

$$\begin{aligned} \frac{u(r)}{u_{max}} &= \left( \frac{r_0 - r}{r_0} \right)^m \\ u(r) &= u_{max} \left( \frac{r_0 - r}{r_0} \right)^m \end{aligned} \quad (\text{X.11})$$

In here  $r_0$  is the radius of 8 m and  $u_{max}$  is the maximum velocity that occurs in the tunnel. The variable  $m$  is depending on the Reynolds number, in this case  $m = 1/10$  [14]. The ratio of maximum velocity to mean velocity is for the calculated Reynolds number equal to 1.16 [14]. Using the mean velocity of 3.70 m/s, the maximum velocity becomes 4.29 m/s.

This formula gives the velocity distribution in longitudinal direction shown in figure X.1. The left figure shows the distribution of the velocity over the diameter at one location. The right figure shows a longitudinal section of 1 m length of the tunnel, in which the colour indicates the velocity.

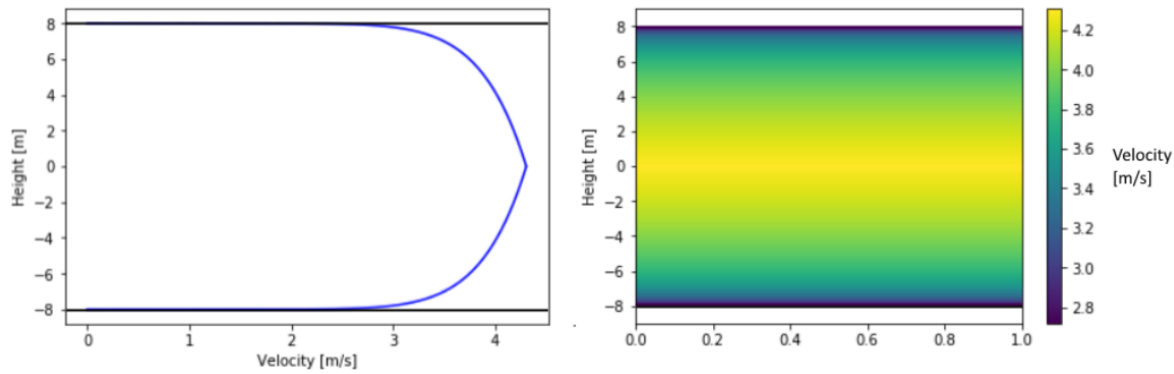


Figure X.1: Longitudinal profile of velocity in the tunnel. Left: 1D velocity profile at a certain location in the tunnel, right: velocity profile along the tunnel axis

This method provides an accurate general view of the velocity distribution, but describes the behaviour near the wall poorly. The velocity and thus the shear stress near the wall need to be approximated using different methods. In the boundary layer the velocity is better approximated using the logarithmic velocity distribution and the distribution for the viscous sub layer, see equation X.13. For this,  $u_*$  should first be determined, see equation X.12 below. In here,  $c_f$  is the friction coefficient calculated by the equation for smooth-walled pipes [84]. From this equations it follows that the wall shear stress equals 10.9 N/m<sup>2</sup> with a  $u_*$  of 0.10 m/s.

$$\begin{aligned}
 \frac{1}{\sqrt{c_f}} &= 4.0 \log_{10} \left( \frac{Re \sqrt{c_f}}{1.26} \right) \\
 \frac{1}{\sqrt{c_f}} &= 4.0 \log_{10} \left( \frac{592E + 05 \sqrt{c_f}}{1.26} \right) \\
 &\rightarrow c_f = 0.0016 \\
 \tau_0 &= c_f \rho \frac{u_0^2}{2} \\
 &= 0.0016 * 1000 * \frac{3.70^2}{2} \\
 &= 10.9 \text{ N/m}^2 \\
 u_* &= \sqrt{\frac{\tau_0}{\rho}} \\
 &= \sqrt{\frac{10.9}{1000}} \\
 &= 0.10 \text{ m/s}
 \end{aligned} \tag{X.12}$$

Now that  $u_*$  is known, the velocity distribution becomes:

$$\begin{aligned}
u(r) &= \frac{(r_0 - r)u_*^2}{\nu} && \text{for } 0 < \frac{(r_0 - r)u_*}{\nu} < 11.84 \\
u(r) &= u_* \left( \frac{1}{\kappa} \ln \frac{(r_0 - r)u_*}{\nu} + 5.56 \right) && \text{for } 11.84 < \frac{(r_0 - r)u_*}{\nu} < 500 \\
&= u_* \left( 2.44 \ln \frac{(r_0 - r)u_*}{\nu} + 5.56 \right) && \\
u(r) &= u_{max} \left( \frac{r_0 - r}{r_0} \right)^m && \text{for } \frac{(r_0 - r)u_*}{\nu} > 500
\end{aligned} \tag{X.13}$$

This gives the velocity profile close to the wall for  $\frac{(r_0 - r)u_*}{\nu} < 500$  as shown in figure X.2. The figure shows the velocity near the bottom wall of the tunnel, which is in this case located at a height of -8.0 m relative to the centre of the tube.

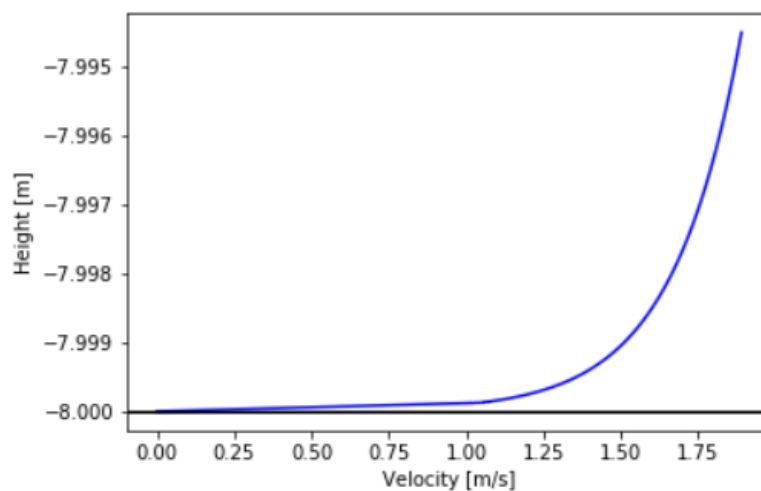


Figure X.2: Velocity in stream wise direction at the turbulent boundary layer

Subsequently, the cross-sectional velocity profile can also be obtained using these equations, since  $u$  is only dependent on  $r$ . Thus, the following distribution for the velocity was made:

It is clearly visible that the velocity gradient near the wall is high, as is expected for turbulent flow. Furthermore, the low velocities are almost invisible in the figure due to the large dimensions of the tunnel compared to the size of the boundary layer.

In conclusion, the maximum flow velocity in the tunnel occurs in the middle part of the tunnel with a value of 4.29 m/s. Due to the turbulent flow the velocity gradient at the boundary layer is high, resulting in a shear stress at the wall equal to  $10.9 \text{ N/m}^2$ .

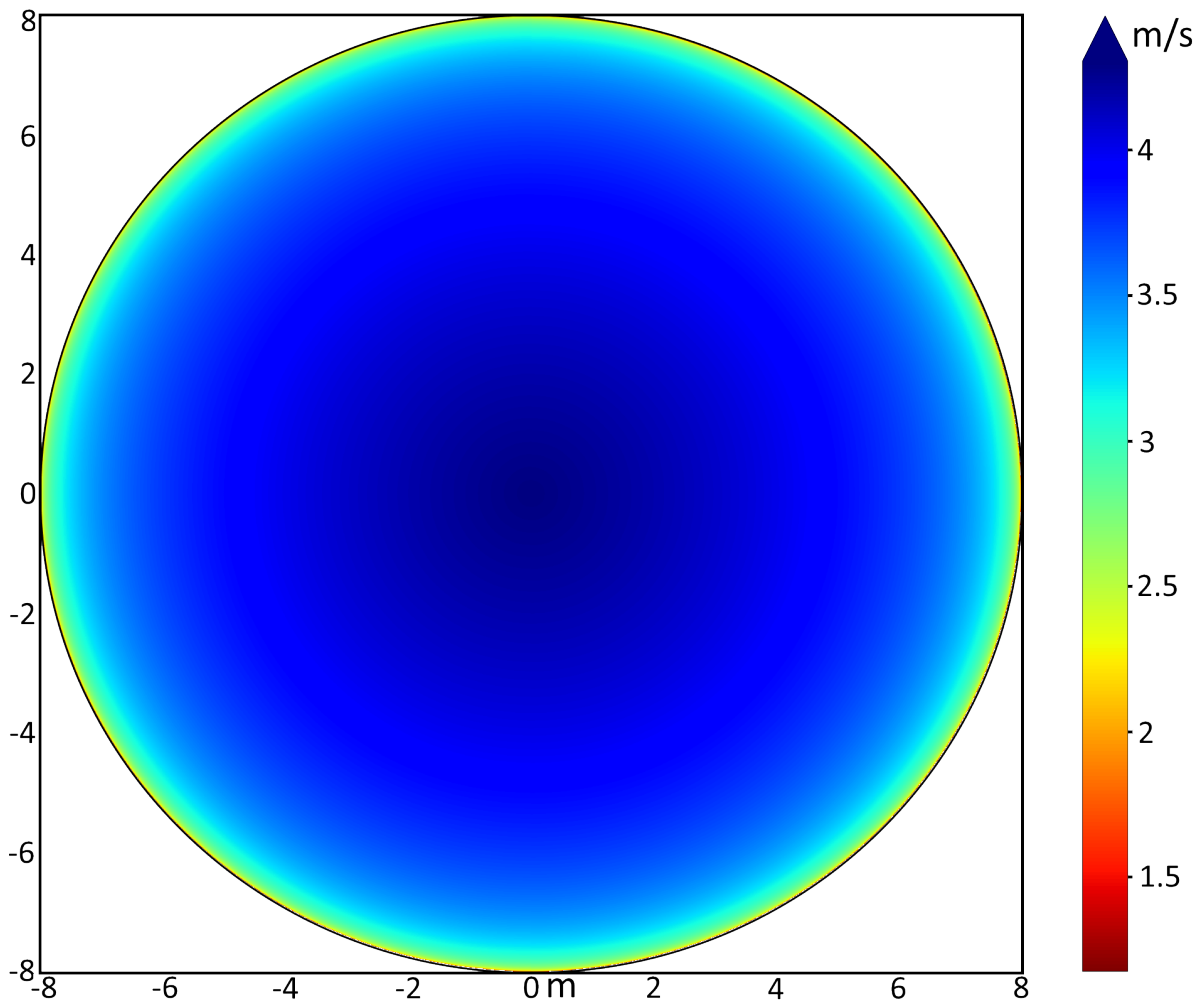
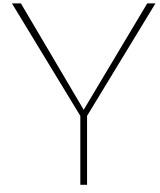


Figure X.3: Velocity distribution in the cross-section of the tunnel



## Effect on river

### Y.1. Deriving backwater curve expression

The proposed construction will have an effect on the river. Not only at the location of the bypass, but further upstream as well. Using (classified) cross-sectional information provided by Chubu Regional Development Bureau, an estimation of the water level at several longitudinal location has been made. To assess this, a derivation for the water level has been defined first. See figure Y.1 for the initial setup for the momentum balance. In here  $F_f$  accounts for the friction,  $F_g$  for gravity,  $F_p$  is the pressure term and  $Q_0$  represents momentum flow.

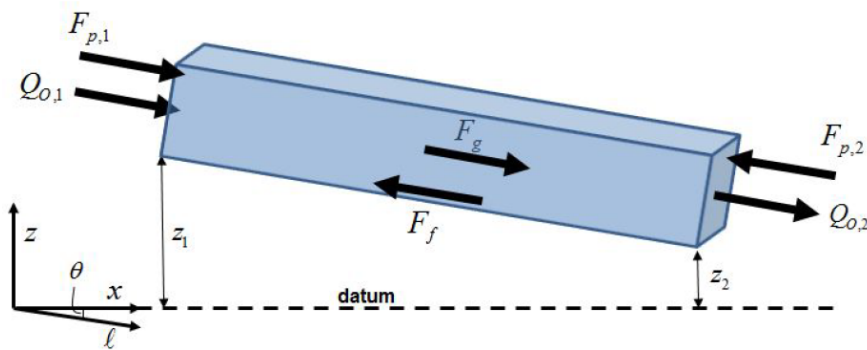


Figure Y.1: Momentum balance of a river [85]

The following momentum balance can now be given:

$$\begin{aligned}
 0 &= Q_{O,1} - Q_{O,2} + F_{p,1} - F_{p,2} + F_g - F_f \\
 &= \rho \frac{\beta_1 Q_1^2}{A_1} + \rho \frac{\beta_2 Q_2^2}{A_2} + \left( \rho g b \frac{y_1^2}{2} + \rho g m \frac{y_1^3}{3} \right) - \left( \rho g b \frac{y_2^2}{2} + \rho g m \frac{y_2^3}{3} \right) + i_b \rho g A \Delta l - S_f \rho g A \Delta l
 \end{aligned} \tag{Y.1}$$

Dividing the momentum balance by  $\rho$  and  $\Delta l$  and letting  $\Delta l \rightarrow 0$  gives:

$$0 = -\frac{d}{dl} \frac{\beta Q^2}{A} - g A \frac{dy}{dl} + i_b g A - S_f g A \tag{Y.2}$$

The first term of the expression above can be rewritten to:

$$\begin{aligned}
 \frac{d}{dl} \frac{\beta Q^2}{A} &= \beta \left( \frac{2Q}{A} \frac{dQ}{dl} - \frac{Q^2}{A^2} \frac{dA}{dl} \right) \\
 &= -\beta \frac{Q^2}{A^2} \frac{dA}{dl}
 \end{aligned} \tag{Y.3}$$



Now, expression (Y.2) can be solved for  $dy/dl$ , resulting in the following equation for the backwater curve:

$$\frac{dy}{dl} = -\beta \frac{Q^2}{A^2} \frac{dA}{dl} - S_f + i_b \quad (\text{Y.4})$$

## Y.2. Deriving cross-sectional parameters

The individual terms in this equation shall be defined now. The cross-sectional values used are classified as confidential information and can therefore not be mentioned. Firstly, the cross-sectional constants Chézy and Strickler coefficients have been determined for every location in longitudinal directions. The coefficients have been calculated using:

$$C = \frac{Q}{A * \sqrt{\frac{A}{P} * i}} \quad (\text{Y.5})$$

$$k = \frac{C}{\left(\frac{A}{P}\right)^{1/6}}$$

The values used for the area and wetted perimeter are known parameters for a discharge of 4400 m<sup>3</sup>/s, since these are directly depended on the water level. Also the width of the river at the water surface, B, is known in this way. The A- and P-values have been determined with the mentioned discharge of 4400 m<sup>3</sup>/s since this comes closest to the discharge used in this evaluation. The Chézy relation has been used to find equivalent A and P values for the discharges of 4250 and 2763 (4250 - 1487) m<sup>3</sup>/s. This has been done by iterating a deviation in water level, finding a corresponding A- and P-value and checking whether these values do indeed give the desired discharge capacity. The final check has been done using equation (Y.5) again. The deviation of the A-, P-, and B-values have been calculated using the trapezoidal equations shown in equation (Y.6).

$$A = A_{4400} + (B + m * \Delta y) \Delta y$$

$$P = P_{4400} + 2\Delta y \sqrt{1 + m^2} \quad (\text{Y.6})$$

$$B = B_{4400} + 2\Delta y * m$$

Using an m-value of 2.5 gave results closest to the data. First, these equations were used to find the stable water depth for the given discharges. The expressions in equation (Y.6) could then be used to calculate the magnitude of the backwater effect. The deviation of  $\Delta y$  has been assumed to be the difference between the stable water depth (without backwater effect) and the water depth estimate with backwater effect, which has been derived from the cross-section downstream. The magnitude of this estimation will be expressed later in this appendix.

The derivative of the cross-sectional area as function of longitudinal direction has been split into three sections, to find the value as precise as possible. For the most upstream and most downstream cross-section, forward Euler and backward Euler have been used respectively. For all cross-sections in between, central Euler has been used. The expressions are given in equation (Y.7).

$$\frac{dA_i}{dl} = \frac{A_i - A_{i+1}}{\Delta l} \quad (\text{Forward Euler})$$

$$\frac{dA_i}{dl} = \frac{A_{i-1} - A_{i+1}}{2\Delta l} \quad (\text{Central Euler}) \quad (\text{Y.7})$$

$$\frac{dA_i}{dl} = \frac{A_{i-1} - A_i}{\Delta l} \quad (\text{Backward Euler})$$

The parameters  $i_b$  and  $S_f$  are defined as follows:

$$i_b = i = 1/1860$$

$$S_f = \frac{Q^2 P^{4/3}}{k^2 A^{10/3}} \quad (\text{Y.8})$$

### Y.3. Backwater magnitude estimation

The change in depth per length  $\frac{dy}{dl}$ , as described in equation (Y.4), can now be calculated. This value can be used to estimate the height of the backwater curve at the next cross-section upstream, which is used in the  $\Delta y$  value as mentioned before. The magnitude can be calculated with:

$$y_{i+1} = y_i + \frac{dy}{dl} * \Delta l \tag{Y.9}$$

Computation of these formulas result in figure Y.2. Please note that between location 13.6 km and 15.0 km, the bypass is present and a lower equilibrium depth has been found.

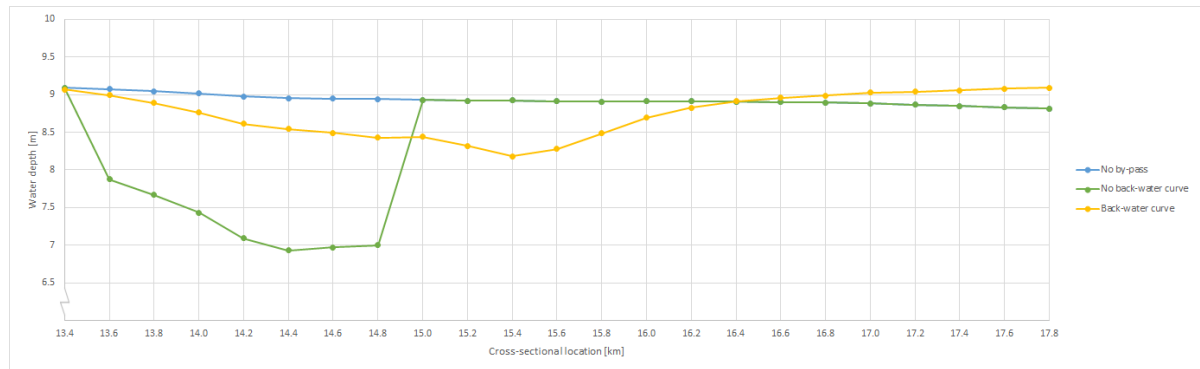


Figure Y.2: Backwater curve at location of bypass

It is remarkable that the backwater curve exceeds the green line upstream of location 16.4 km, and that the curve makes a dip around location 15.4 km. Both effects can be explained when taking a look at the graph in figure Y.3. The unexpected behaviour is a result of the large jumps in cross-sectional area, resulting in another backwater effect on top of the backwater effect as a result of the bypass. Making the grid more fine should make the unexpected behaviour less severe.

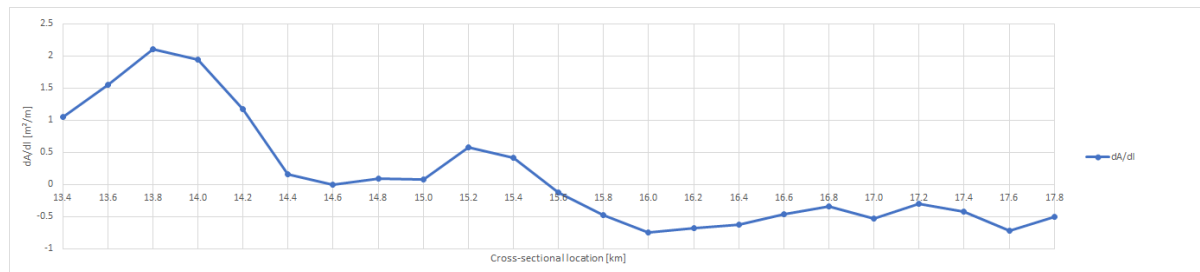
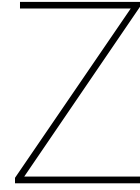


Figure Y.3: Derivative of cross-sectional area

It has been concluded that the bypass results in a water level drop of approximately 0.50 m at the bypass. Also, effects can be found further upstream of the bypass.



## Sediment settlement

### Z.1. Sediment discharge of Shonai River

During the design flood, the sediment discharge can become significant in the Shonai River. The sediment discharge has been calculated with the design discharge of  $4250 \text{ m}^3/\text{s}$ . Information of the Nippon Koei Corporation gives a so called L-Q equation that relates the sediment discharge to the flow discharge. This information is classified and is therefore not allowed to be published. This relation was fitted to measured data from the Shonai River at the Biwajima Bridge. Using this relation together with the fact that the design flow discharge equals  $4250 \text{ m}^3/\text{s}$  leads to a sediment discharge  $Q_s$  of  $13.45 \text{ m}^3/\text{s}$ .

### Z.2. Sediment discharge distribution

The water and sediment discharge is divided over the river branch and the bypass, thus it can be seen as a bifurcation. Since the water discharges differ per branch, the sediment discharge will also be different. The problem has been taken as a simple 1D case, hence the nodal point relation for bifurcations was used, see equation Z.1 below [86].

$$\frac{Q_{s,river}}{Q_{s,bypass}} = \left( \frac{B_{river}}{B_{bypass}} \right) \left( \frac{Q_{river}}{Q_{bypass}} \right)^k \quad (\text{Z.1})$$
$$Q_{s,total} = Q_{s,bypass} + Q_{s,river}$$

In here,  $k$  is a coefficient that should be larger than  $5/3$ . Lower values give more sediment discharge into the tunnel, therefore the minimum value of  $5/3$  was chosen to get the maximum sediment discharge into the tunnels. Also, the sum of the sediment discharge in the bypass and the river branch should be equal to the total sediment discharge in the river just before the bifurcation. With these two equations, the distribution of the sediment discharge over both branches has been determined, resulting in  $Q_{s,bypass} = 1.71 \text{ m}^3/\text{s}$  and  $Q_{s,river} = 11.74 \text{ m}^3/\text{s}$ . Hence, 13 % of the sediment discharge from the main river enters the bypass.

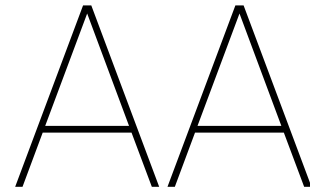
This simplification just gives a first estimate, since the bifurcation angle and other bend effects have not been taken into account. Also the influence of the sill in front of the bypass was not included in this estimate.

### Z.3. Settling after flood

The sediment discharge inside the tunnel equals  $1.71 \text{ m}^3/\text{s}$  corresponding to a flow rate of  $1486 \text{ m}^3/\text{s}$ , as calculated in previous section. Furthermore, the suspended sediment concentration of the Shonai River has been determined in the data of the Nippon Koei Corporation. Extrapolating the data led to a concentration of  $11 \text{ g/L}$  in the river corresponding to a flow rate of  $4250 \text{ m}^3/\text{s}$ . Using the fact that 13 % of the sediment is transported into the bypass, the suspended sediment concentration in the bypass becomes  $1.44 \text{ g/L}$  at peak flow. It has been assumed that the flow and sediment is equally split between the two tunnels, therefore the suspended sediment concentration is  $1.44 \text{ g/L}$  in each tunnel. The maximum amount of sediment inside a tunnel can be calculated if the tunnel volume is known. This volume has been calculated as in equation Z.2.

$$\begin{aligned} V &= \pi \frac{D^2}{4} L \\ &= \pi * \frac{16^2}{4} * 1200 \\ &= 2.41E+05 \text{ m}^3 = 2.41E+08 \text{ L} \end{aligned} \tag{Z.2}$$

The maximum amount of sediment that can stay in a tunnel equals:  $2.41E+08 \text{ L} * 1.44 \text{ g/L} = 347E+03 \text{ kg}$ . Per unit length of the tunnel this amount becomes  $289 \text{ kg/m}$ . This is the maximum amount that corresponds to the peak flow rate. In reality less sediment is likely to stay in the tunnel when the water becomes stagnant, since the flow rate at the end of a flood is already less than at the peak.



## Morphology and scour protection

### AA.1. Initial morphological response in river

Due to the sudden reduction in discharge in the Shonai River, the morphological response to a flood in the river changes. In this section this effect has been assessed qualitatively. For simplicity it was assumed that the width of the river is constant along the considered stretch. The equilibrium depth is in this case equal to:

$$d_e^3 = \frac{c_f q^2}{i_b g} \quad (\text{AA.1})$$

$$= \frac{q^2}{i_b C^2}$$

With the equilibrium depth, the velocity can be determined using  $q/d_e$ . Subsequently, the sediment discharge can again be calculated using the Engelund-Hansen method, see equation AA.2.

$$q_s = m u^n \quad (\text{AA.2})$$

Lastly, the change in bed elevation over time can be determined using the Exner equation, see equation AA.3.

$$c_b \frac{\partial z_b}{\partial t} = - \frac{\partial q_s}{\partial x} \quad (\text{AA.3})$$

These equations have been used to create the graphs in figure AA.1. In here,  $x = 0$  is at the downstream end of the bypass and  $x$  increases upstream. Due to the bypass the discharge reduces in the river branch. This leads to a reduction in equilibrium depth and thus a M1 backwater curve will be created. Upstream of the tunnel the water depth converges to the original depth again, leading to a M2 backwater curve.

Finally, the bottom right graph shows the change in bottom elevation over time. Upstream of the bypass, the bed will degrade. Then, at the entrance of the bypass, a hump will form, leading to deposition of sediment at this location. Between the inlet and outlet of the bypass some aggregation could occur due to the reduced discharge. Lastly, at the outlet of the bypass, a scour pit will form due to the sudden increase of discharge and thus sediment capacity.

The duration of a flood wave is in the order of one day and the peak discharge will only be reached for about three hours. In the remaining time, the discharge is much lower and the bypass will not be used. Therefore, there is no long term morphological response due to the bypass. Scour and degradation created during a flood will partly or completely disappear during times that the bypass is not used.

On the other hand, since the discharge and thus the flow velocity during a flood is much higher than during normal flow conditions, the amount of sediment transported during a flood is much higher. Thus, in the short term the morphological response will be significant and in the way figure AA.1 suggests. However, the bypass will not have major impact on the long term morphological behaviour.

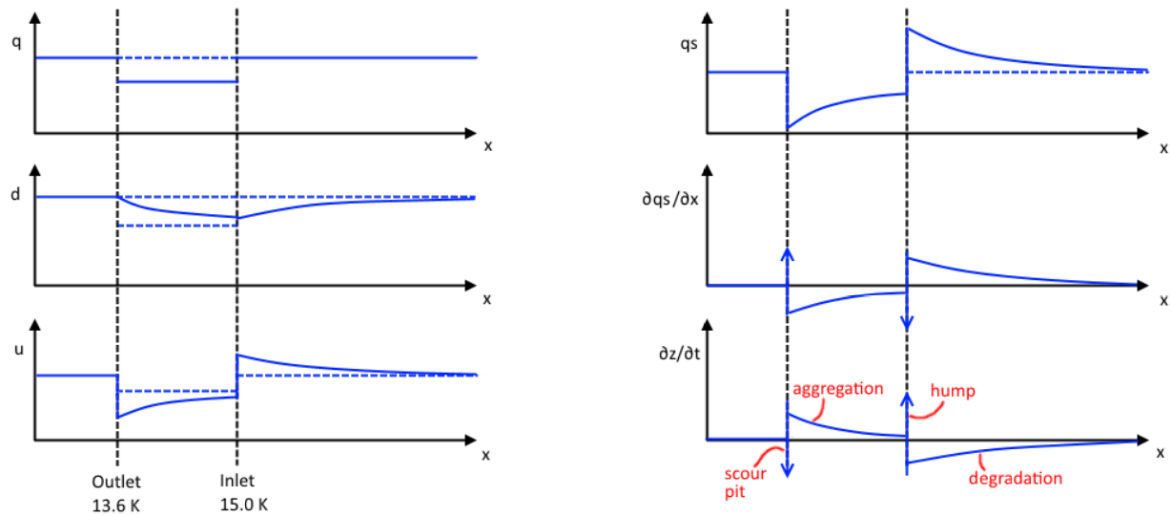


Figure AA.1: Initial morphological response during a flood when using the bypass

## AA.2. Scour protection

### AA.2.1. Erosion river

As mentioned, erosion is expected to occur in the river at the sill of the outlet. The scour depth with bed protection over time can be described using equation AA.4.

$$h_s(t) = \frac{(\alpha \bar{u} - \bar{u}_c)^{1.7} h_0^{0.2}}{10 \Delta^{0.7}} t^{0.4} \quad (\text{AA.4})$$

$$\alpha = 1.5 + 5r$$

$$\bar{u}_c = u + 3r$$

In this equation,  $h_0$  is the original water depth in the river at this location, equal to 9.2 m. Due to the deceleration from the water coming from the sill, the turbulent fluctuation  $r$  was set to 0.3 [21]. This results in an  $\alpha$  value equal to 3. The depth averaged velocity in the river at the location equals 1.7 m/s, resulting in a critical velocity,  $u_c$ , of 2.6 m/s. Lastly the relative density,  $\Delta$ , has been taken to be 1.65. With these values the development of the scour depth over time has been plotted in figure AA.2.

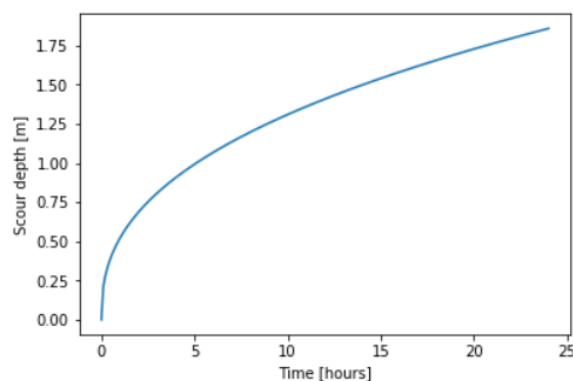


Figure AA.2: Development of scour depth over time

This plot has been made with the circumstances present in case of peak flow. However, these high discharges will only be reached for about one to three hours. After three hours and under these conditions, the scour hole has a depth of 0.82 m. In total, the scour hole at design flood has been estimated to have a depth of 1.2

m, taking the varying discharge into account.

Because of this scour hole, bed protection is to be applied. The bed protection will be made of rocks placed on fascine mattresses to prevent instability due to lifting forces. The stability of the protection is described by equation AA.5.

This Izbash type of equation has been used to determine the diameter,  $d_{50}$ , of the used rocks. With a relative density of 1.65 the  $d_{50}$  becomes 0.22 m. According to EN13383, this corresponds to stone class  $LM_A$  5-40 with a range of 5-40 kg [21].

$$\begin{aligned}\frac{\bar{u}_c}{\sqrt{\Delta g d_{50}}} &= 1.7 \\ \bar{u}_c &= \bar{u}(1 + 3r) \\ &= 1.7 * (1 + 3 * 0.3) \\ &= 3.23 \text{ m/s}\end{aligned}\tag{AA.5}$$

### AA.2.2. Inlet and outlet structure

To prevent erosion at the inlet funnel of the bypass, protection is required. Obstacles should be minimised as much as possible, since they hinder the flow and cause extra turbulence and energy losses. Therefore, the most optimal solution in terms of hydraulics would be to protect the ground with concrete. However, this is a rather expensive and unaesthetic solution. Only near the tunnels where the flow contraction starts concrete protection is needed to cope with the high flow velocities. The same goes for the outlet structure, where flow velocity is maximal just before expansion takes place.

Before the contraction of the inlet and after the expansion of the outlet, the area could be made in such a way that the citizens can use it in case of low water in the river. Therefore, a baseball field will be made together with tennis courts. Rubber tiles could be used to cover the soil of the sport fields [87]. These will have a low roughness and prevent the underlying soil to erode. Also, grass is used to cover the soil surrounding the fields. Moderate grass is able to withstand flow velocities of around 2.1 m/s for 10 hours [21]. During the design flood the flow velocity is higher and the grass will erode. Since high flow velocities do not occur regularly, grass is still a good and relatively affordable solution. After a larger flood, the grass that has eroded can be replanted. Figure AA.3 gives an overview of the layout of the inlet structure.

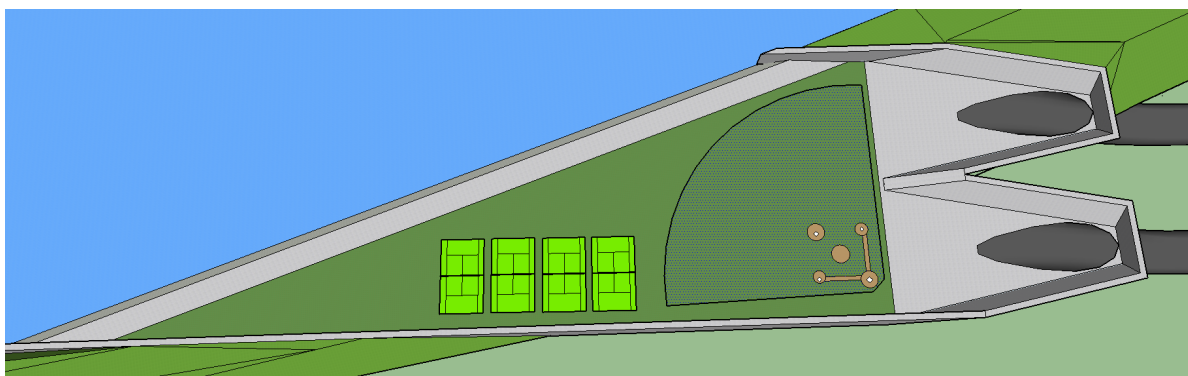


Figure AA.3: Recreational use of inlet and outlet structure

# AB

## Creating a bored tunnel

Boring a tunnel with a TBM, or Tunnel Boring Machine, will induce some loads on the tunnel. In this chapter, the construction steps will be elaborated. First, the type of TBM is discussed. Secondly, the steps of the general boring process will be discussed, followed by the process to get into the ground from the starting shaft and out of the ground to the reception shaft. Buoyancy will not be discussed in this chapter. This is because the depth is determined by face stability, not by buoyancy.

### AB.1. Type of TBM

All TBMs suitable for soft soil are quite similar. Big difference between the types of TBMs are found when looking at type of bore shield, or the method to keep the cut soil surface stable. Because the tunnel is below the phreatic water level, only two methods can be used: The EPB, or Earth Pressure Balance, or a slurry shield. With the EPB shield, the soil face is kept stable by the excavated soil in the shield and the cutting wheel itself. A problem with this method is that boulders may damage the cutting wheel. Since the soil is sandy and gravelly, collision with boulders are likely to occur. With a slurry shield, boulders cause less damage to the cutting wheel. Therefore, the slurry shield is most appropriate to use and therefore, this method will be used. The soil face is kept stable by a bentonite slurry in the shield. In order to generate enough pressure in the shield, the bentonite slurry is pressurised.

Once the soil is excavated and the bore shield has moved forward, the concrete lining has not been placed yet. To keep the soil around the excavated area stable, a steel shell is attached on the shield (see figure AB.1). This shell is called the tail of the shield. The tail is long enough to be able to construct the concrete lining. Once the lining is in place, the TBM can move forward again. A sketch of the front of the TBM is given in figure AB.1.

The inner diameter is 16 m (see chapter 2). The thickness is assumed to be 5% of the inner diameter, so 0.8 m. That brings the outer diameter of the tunnel to 17.6 m. To give some space the tail, the outer diameter of the TBM is set to be 18 m.

### AB.2. Boring steps

#### AB.2.1. Step 1: Stability bore shield

The first step of the TBM is to excavate the soil. When the soil is excavated, it will fall into the bore shield, see figure AB.1. This is removed from the bore shield in an airlock. To prevent soil falling into the shield, the shield pressure should exceed the horizontal soil pressure. However, when the overpressure exceeds the vertical soil stress at the top of the bore shield, it will blow out the soil above the TBM.

The overpressure is generated behind the shield. Because the shield is moving forward constantly, the volume of the bore shield and thus the pressure are not constant. Therefore, the pressure has to be able to fluctuate with a magnitude of 50 kPa. On top of that, it usual to add another 20 kPa on the horizontal pressure [88] to account for uncertainties. Figure AB.2 shows this process. To reach both requirements, the TBM should be at sufficient depth.



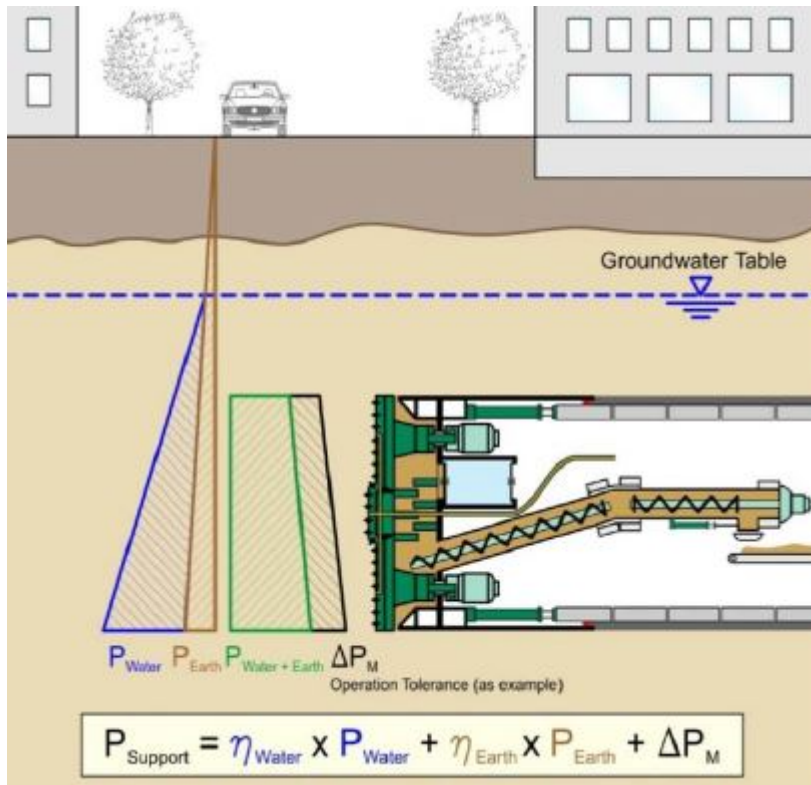


Figure AB.1: Front of TBM, with principle of face stability [13]

## Pressure Fluctuations

- Rules of thumb
  - Minimal =  $p + 20 \text{ kPa}$
  - Maximal = overburden or more
  - Difference at least 50 kPa

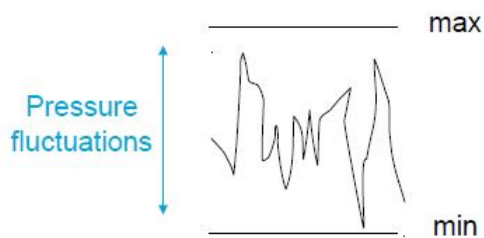


Figure AB.2: Slide of lecture by dr. ir. W. Broere [88]

In figure AB.3, the pressure distribution is given. The figure is based on a TBM diameter of 18 m and a depth of 12 m below surface, at T.P. -9 m. It was concluded that the vertical pressure at the top of the TBM was 236 kPa. The maximum overpressure was set to 230 kPa. To allow the fluctuation in the pressure in the bentonite, the minimum overpressure is 180 kPa. At the bottom of the TBM, at T.P. -27 m, the active horizontal soil pressure is 379 kPa. With the extra safety of 20 kPa, the minimum pressure in the shield should be 400 kPa at the bottom. The minimum pressure in the shield, using bentonite with a density of  $13 \text{ kN/m}^3$ , values 414 kPa.

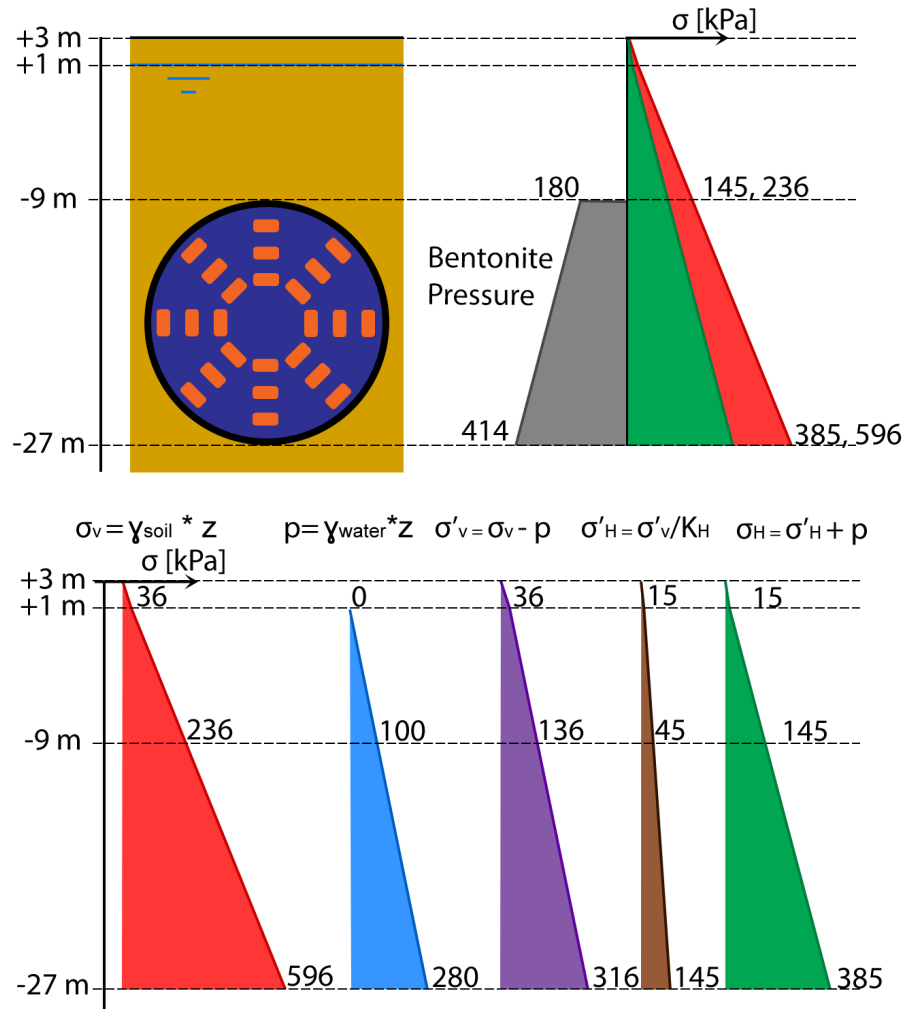


Figure AB.3: Top: pressure distribution soil. Gray: bentonite. Green: total horizontal pressure. Red: vertical soil pressure. Bottom: calculations soil pressures. Red: vertical soil pressure. Blue: water pressure. Purple: effective vertical soil pressure. Brown: effective horizontal soil pressure. Green: horizontal soil pressure.

### AB.2.2. Step 2: Movement of the TBM

To move the TBM forward, it needs a longitudinal force. To create this force, it needs to push itself away against the concrete lining. To allow this, hydraulic jacks are placed between the bore shield at the front of TBM and the lining. The total force given by the jacks can reach a value of 250 MN for a 18 m diameter tunnel [13].

### AB.2.3. Step 3: Placement of the concrete lining

Once the soil has been removed, the space for the tunnel is free. To place the concrete lining, three steps are required. First, the jacks need to be removed. Secondly, the lining needs to be placed. Finally, the jacks need to be placed again to support the new lining. To keep a force on the bore shield, only the jacks which are at the location of the to be placed segment are removed. Normally, bored tunnels have 6 to 10 segments and keystone, see stone A in figure AB.4. In this case, 12 segments and 1 keystone will be used, due to the relative

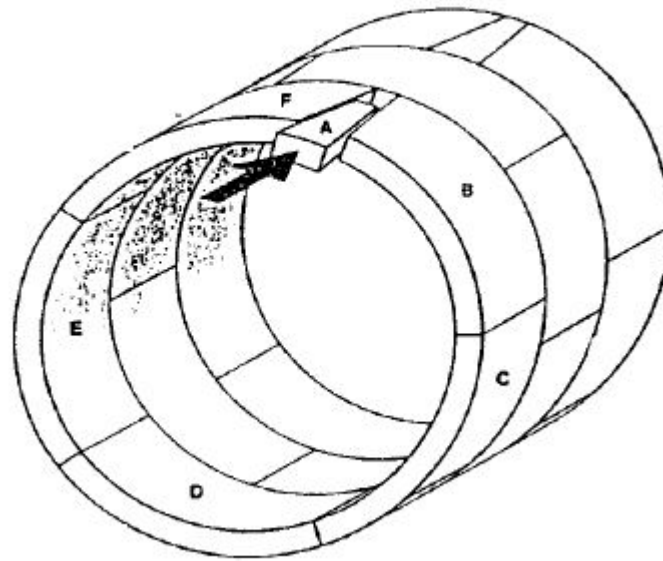


Figure AB.4: Full ring of tunnel segments

large size of the tunnel.

#### **AB.2.4. Step 4: Grouting the tail void**

Once the tail of the TBM has passed a section, a void will be created between the lining and the ground. To prevent unstable ground and settlements, this space is filled up with grout. Because of the same reason as with the bore shield, the grout is kept under the same pressure as the bentonite slurry when hardening. Once the grout has been hardened, it will keep the soil stable during the life-time of the tunnel.

#### **AB.3. TBM at the first and last metres**

Once the TBM starts boring and gets through the wall of the starting shaft, the soil and subsoil is exposed to the hole in the wall. This might lead to settlements. To prevent this, the soil behind the wall should be improved in order to keep it stable and water tight. One option is to second concrete wall to the end of the pit. The space between the two walls can be filled with improved soil. However, since the depth is 31 m, sheet piles are not applicable. Therefore, this method cannot be used. A second option is to improve the soil behind the wall with grouting. It is advised to use this method.

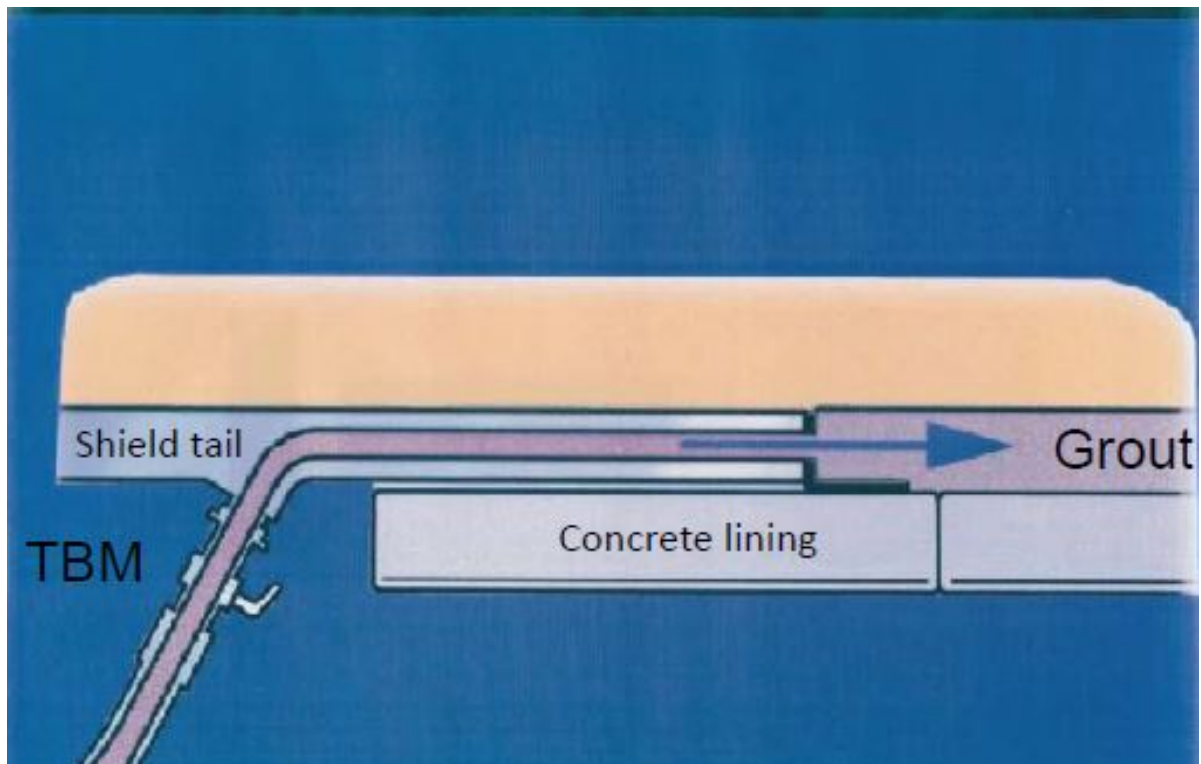


Figure AB.5: Grouting the void behind the tail

# AC

## Structural design of tunnel

### AC.1. Structural design of the tunnel

For the design of the tunnel, the values presented in table AC.1 have been used. For the calculations of the resistance capacity formulas AE.2 until AE.4 have been used. These are the same as already used in previous calculations. For the concrete class C55/67 has been used. Because of the high bending moments, reinforcement bars with a diameter of 40 mm were used as a first estimation.

Force	Deterministic value	Design value
Minimum Normal Force (kN)	-2171	-3257
Maximum Normal Force (kN)	-479	-719
Minimum Shear Force (kN)	471	707
Maximum Shear Force (kN)	-401	-602
Minimum Bending Moment (kNm)	-1686	-2529
Maximum Bending Moment (kNm)	1496	2244

Table AC.1: Internal forces within concrete lining

#### Moment capacity

$$M_{Rd} = A_s * f_{yd} * z \quad (\text{AC.1})$$

Derivation of  $x_u$ :

$$\begin{aligned} N_s + N_{Ed} &= N_c \\ A_s * f_{yd} + N_{Ed} &= 0.75 * b * x_u * f_{cd} \\ x_u &= \frac{A_s * f_{yd} + N_{Ed}}{0.75 * b * f_{cd}} \end{aligned} \quad (\text{AC.2})$$

- C55/67 -  $f_{cd} = 36.67 \text{ N/mm}^2$  -  $\varnothing_{\text{reinforcement}} = 40 \text{ mm}$
- $\varnothing_{\text{stirrups}} = 12 \text{ mm}$
- $c = 25 \text{ mm}$
- $h = 800 \text{ mm}$
- $d = 743 \text{ mm}$
- $\rho \approx 1.25 \%$  (rough estimation)
- number of reinforcement bars = 8/m
- $A_s = 10052.8 \text{ mm}^2/\text{m}$  -  $x_u = 276 \text{ mm}$
- $z = 635 \text{ mm}$
- $M_{Rd} = 2778 \text{ kNm/m}$

8 reinforcement bars are required per metre. The bars are to be applied on both sides of the cross-section, to resist both the positive as the negative bending moment. This gives an reinforcement ratio of 2.7%.

The shear capacity of the lining has been calculated as follows:

$$V_{Rd,c} = (C_{Rd,c} * k * (100 * \rho * f_{ck})^{1/3} + k_1 * \sigma_{cp}) * b * d$$

$$V_{Rd,c,min} = (0.035 * k^{3/2} * f_{ck}^{1/2} + k_1 * \sigma_{cp}) * b * d$$
(AC.3)

With:

- $C_{Rd,c} = 0.12$
- $k = 1 + \sqrt{\frac{200}{d}} = 1.52$
- $f_{ck} = 55 \text{ N/mm}^2$
- $\rho = 2.7\%$
- $k_1 = 0.15$
- $\sigma_{cp} = 4 \text{ N/mm}^2$
- $V_{Rd,c} = 1168 \text{ kN}$

To guarantee the safety of the structure, the total strength should be checked according to formula AE.6 below. After checking for each cross-section, a maximum value of 1.14 was found. Therefore, more reinforcement was added. When applying 10 bars of 40 mm diameter, a maximum check of 0.99 was found, which is sufficient.

$$U.C. = \frac{M_{Ed}}{M_{Rd}} + \frac{V_{Ed}}{V_{Rd}} \leq 1.0$$
(AC.4)

# AD

## Use of Plaxis FEM program

In this appendix, all the input parameter used for the FEM program Plaxis are given. If a parameter isn't given, this was kept to the standard parameters determined by the program itself.

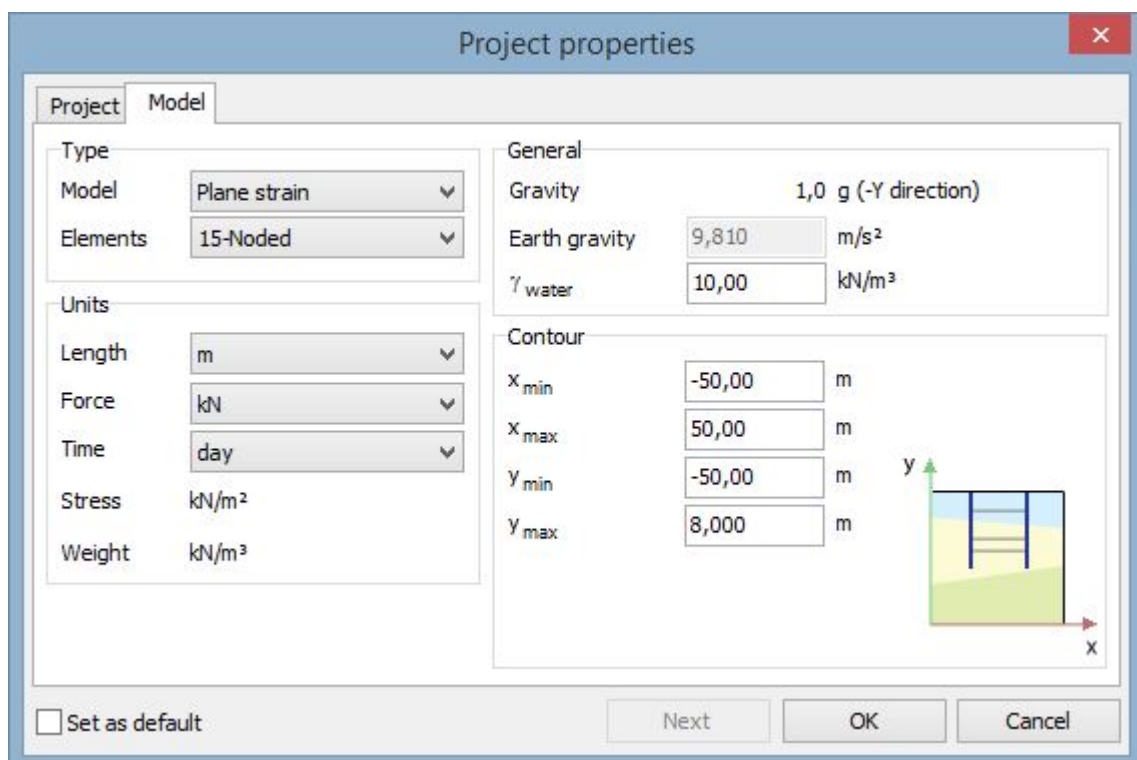


Figure AD.1: Project properties

Soil data used:

	<b>Sand, Slightly silty clayey</b>	<b>Sand, Greatly silty clayey</b>	<b>Sand, Clean moderate</b>	<b>Gravel, slightly silty solid</b>
Layer (m to T.P.)	+5 m to +2.4 m -7.4 m to -10.4 m	+2.4 m to -0.3 m -	-0.3 m to -7.4 m -10.4 m to -13.9 m	-13.9 m to -21.2 m -
$\gamma_{unsat}$ (kN/m <sup>3</sup> )	18	18	18	20
$\gamma_{sat}$ (kN/m <sup>3</sup> )	20	20	20	20
Young's modulus (Mpa)	35	20	45	90
Angle of friction°	30	25	32.5	40
Poisson's ratio	0.25	0.3	0.2	0.25
Water level T.P. (m)	1			

Table AD.1: Characteristics of subsoil

The screenshot shows the 'Soil - Mohr-Coulomb - Sand, slightly silty clayey' dialog box. It is divided into several sections:

- General**: Contains tabs for 'General', 'Parameters', 'Flow parameters', 'Interfaces', and 'Initial'.
- Material set**: A table with columns 'Property', 'Unit', and 'Value'.
 

Property	Unit	Value
Identification		Sand, slightly silty clayey
Material model		Mohr-Coulomb
Drainage type		Drained
Colour		RGB 161, 226, 232
Comments		
- General properties**: A table with columns 'Property', 'Unit', and 'Value'.
 

Property	Unit	Value
$\gamma_{unsat}$	kN/m <sup>3</sup>	18,00
$\gamma_{sat}$	kN/m <sup>3</sup>	20,00
- Advanced**: A section with a 'Void ratio' sub-section.
 

Property	Value
Dilatancy cut-off	<input type="checkbox"/>
$e_{init}$	0,5000
$e_{min}$	0,000
$e_{max}$	999,0

At the bottom of the dialog box, there are three buttons: 'Next', 'OK', and 'Cancel'.

Figure AD.2: Soil data: Sand, Slightly silty clayey



Soil - Mohr-Coulomb - Gravel

General Parameters Flow parameters Interfaces Initial \*

Property	Unit	Value
<b>Stiffness</b>		
$E'$	kN/m <sup>2</sup>	35,00E3
$\nu'$ (nu)		0,2500
<b>Alternatives</b>		
$G$	kN/m <sup>2</sup>	14,00E3
$E_{oed}$	kN/m <sup>2</sup>	42,00E3
<b>Strength</b>		
$c'_{ref}$	kN/m <sup>2</sup>	0,000
$\phi'$ (phi)	°	30,00
$\psi$ (psi)	°	0,000
<b>Advanced</b>		
Set to default values		<input checked="" type="checkbox"/>
<b>Stiffness</b>		
$E'_{inc}$	kN/m <sup>2</sup> /m	0,000
$\gamma_{ref}$	m	0,000
<b>Strength</b>		

Next OK Cancel

Figure AD.3: Soil data: Sand, Slightly silty clayey

Soil - Mohr-Coulomb - Sand, Greatly silty clayey

General Parameters Flow parameters Interfaces Initial

Property	Unit	Value
<b>Material set</b>		
Identification		Sand, Greatly silty clayey
Material model		Mohr-Coulomb
Drainage type		Drained
Colour		RGB 161, 226, 232
Comments		
<b>General properties</b>		
$\gamma_{unsat}$	kN/m <sup>3</sup>	18,00
$\gamma_{sat}$	kN/m <sup>3</sup>	20,00
<b>Advanced</b>		
<b>Void ratio</b>		
Dilatancy cut-off		<input type="checkbox"/>
$e_{init}$		0,5000
$e_{min}$		0,000
$e_{max}$		999,0

Next OK Cancel

Figure AD.4: Soil data: Sand, Greatly silty clayey

Soil - Mohr-Coulomb - Gravel

General Parameters Flow parameters Interfaces Initial

Property	Unit	Value
<b>Stiffness</b>		
$E'$	kN/m <sup>2</sup>	20,00E3
$\nu'$ (nu)		0,3000
<b>Alternatives</b>		
G	kN/m <sup>2</sup>	7692
$E_{oed}$	kN/m <sup>2</sup>	26,92E3
<b>Strength</b>		
$c_{ref}$	kN/m <sup>2</sup>	0,000
$\phi'$ (phi)	°	25,00
$\psi$ (psi)	°	0,000
<b>Advanced</b>		

Next OK Cancel

Figure AD.5: Soil data: Sand, Greatly silty clayey

Soil - Mohr-Coulomb - Sand, Clean moderate

General Parameters Flow parameters Interfaces Initial

Property	Unit	Value
<b>Material set</b>		
Identification		Sand, Clean moderate
Material model		Mohr-Coulomb
Drainage type		Drained
Colour		RGB 161, 226, 232
Comments		
<b>General properties</b>		
$\gamma_{unsat}$	kN/m <sup>3</sup>	18,00
$\gamma_{sat}$	kN/m <sup>3</sup>	20,00
<b>Advanced</b>		
<b>Void ratio</b>		
Dilatancy cut-off		<input type="checkbox"/>
$e_{init}$		0,5000
$e_{min}$		0,000
$e_{max}$		999,0

Next OK Cancel

Figure AD.6: Soil data: Sand, Clean moderate

Soil - Mohr-Coulomb - Gravel

General Parameters Flow parameters Interfaces Initial \*

Property	Unit	Value
<b>Stiffness</b>		
$E'$	kN/m <sup>2</sup>	45,00E3
$\nu'$ (nu)		0,2000
<b>Alternatives</b>		
G	kN/m <sup>2</sup>	18,75E3
$E_{oed}$	kN/m <sup>2</sup>	50,00E3
<b>Strength</b>		
$c'_{ref}$	kN/m <sup>2</sup>	0,000
$\phi'$ (phi)	°	32,50
$\psi$ (psi)	°	0,000
<b>Advanced</b>		

Next OK Cancel

Figure AD.7: Soil data: Sand, Clean moderate

Soil - Mohr-Coulomb - Sand, Greatly silty clayey

General Parameters Flow parameters Interfaces Initial

Property	Unit	Value
<b>Material set</b>		
Identification		Sand, Greatly silty clayey
Material model		Mohr-Coulomb
Drainage type		Drained
Colour		RGB 161, 226, 232
Comments		
<b>General properties</b>		
$\gamma_{unsat}$	kN/m <sup>3</sup>	18,00
$\gamma_{sat}$	kN/m <sup>3</sup>	20,00
<b>Advanced</b>		
<b>Void ratio</b>		
Dilatancy cut-off		<input type="checkbox"/>
$e_{init}$		0,5000
$e_{min}$		0,000
$e_{max}$		999,0

Next OK Cancel

Figure AD.8: Soil data: Gravel, slightly silty solid

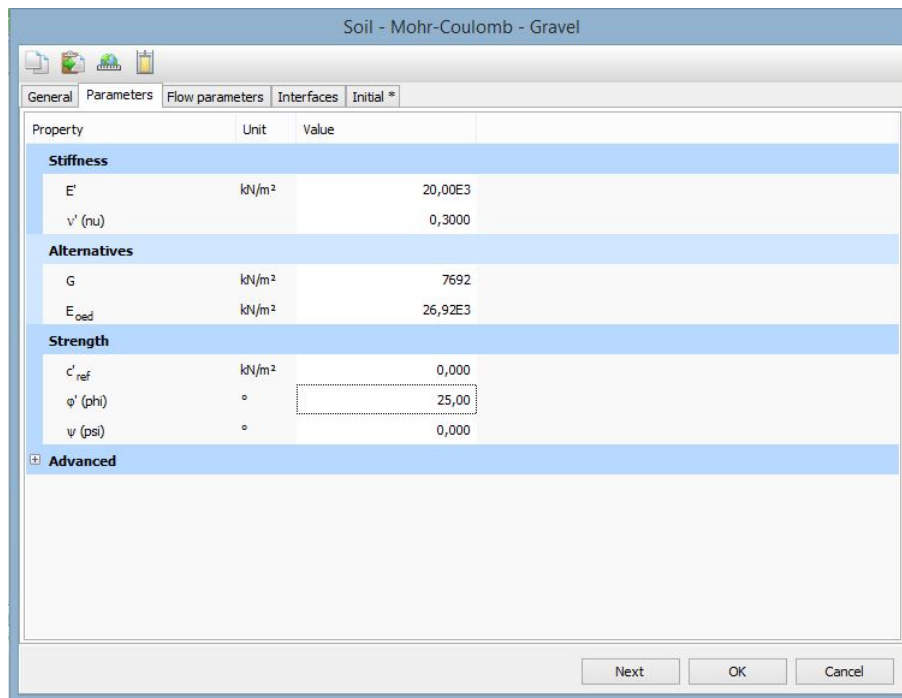


Figure AD.9: Soil data: Gravel, slightly silty solid

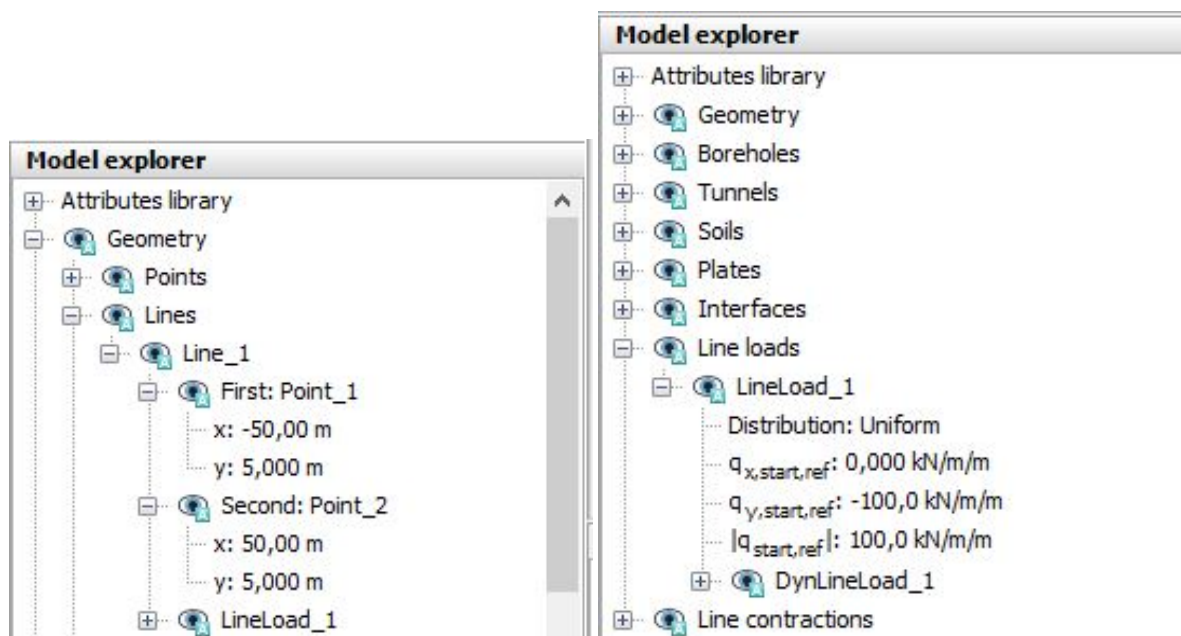


Figure AD.10: Left: coordinates of Line load; Right: Value of line load

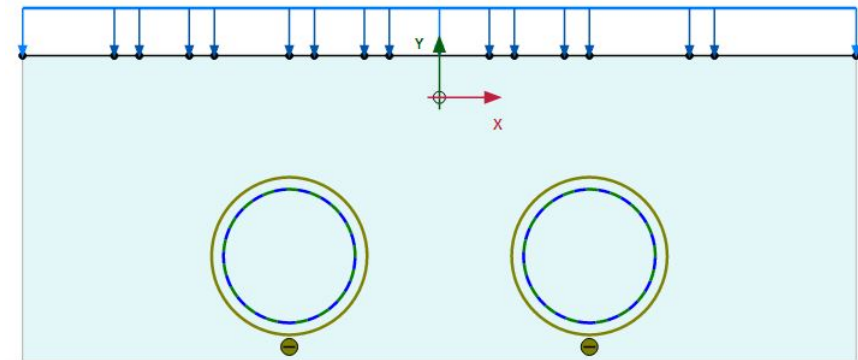


Figure AD.11: Loads given by trains (point of 62 kN loads at -39, -36, -30, -27, -18, -15, -9, -6, 6, 9, 15, 18, 30 and 33 m)

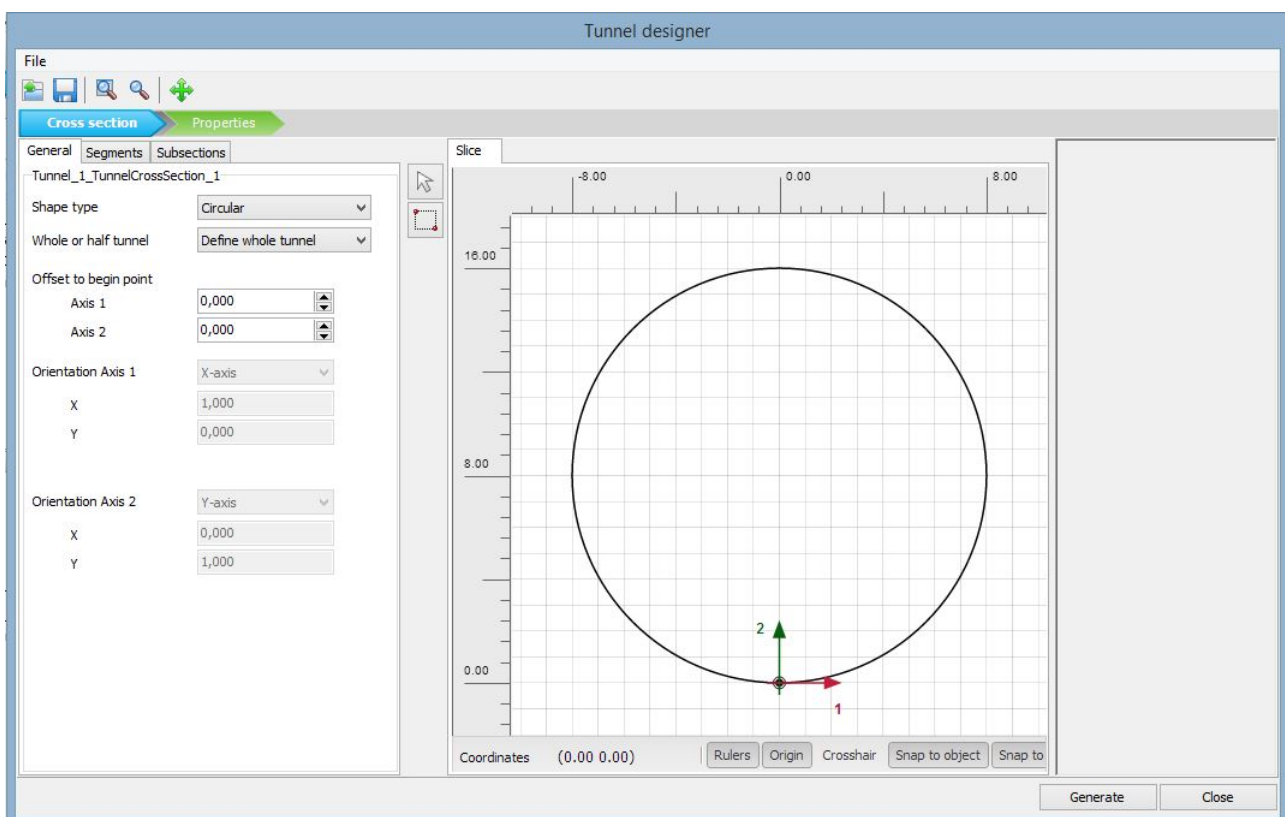


Figure AD.12: Left tunnel coordinates input

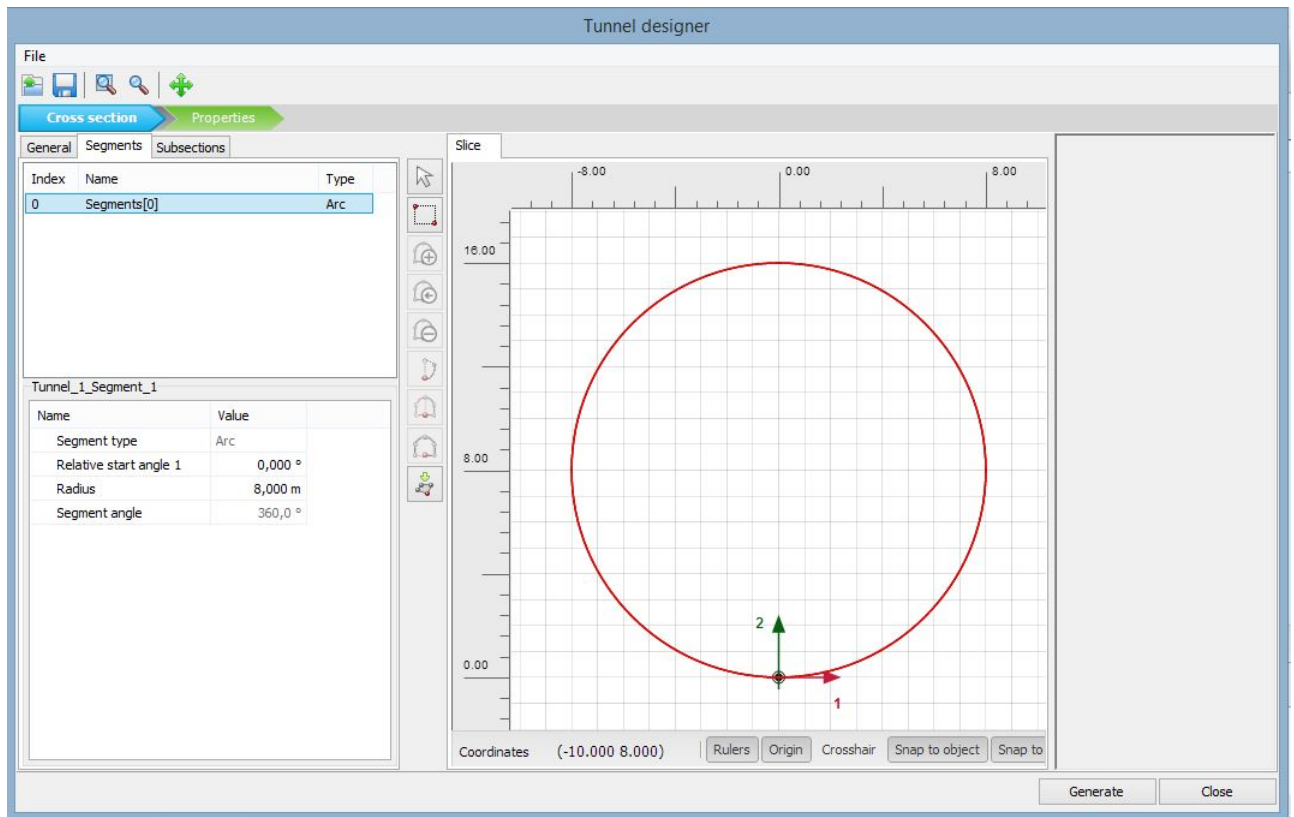


Figure AD.13: Left tunnel segment input

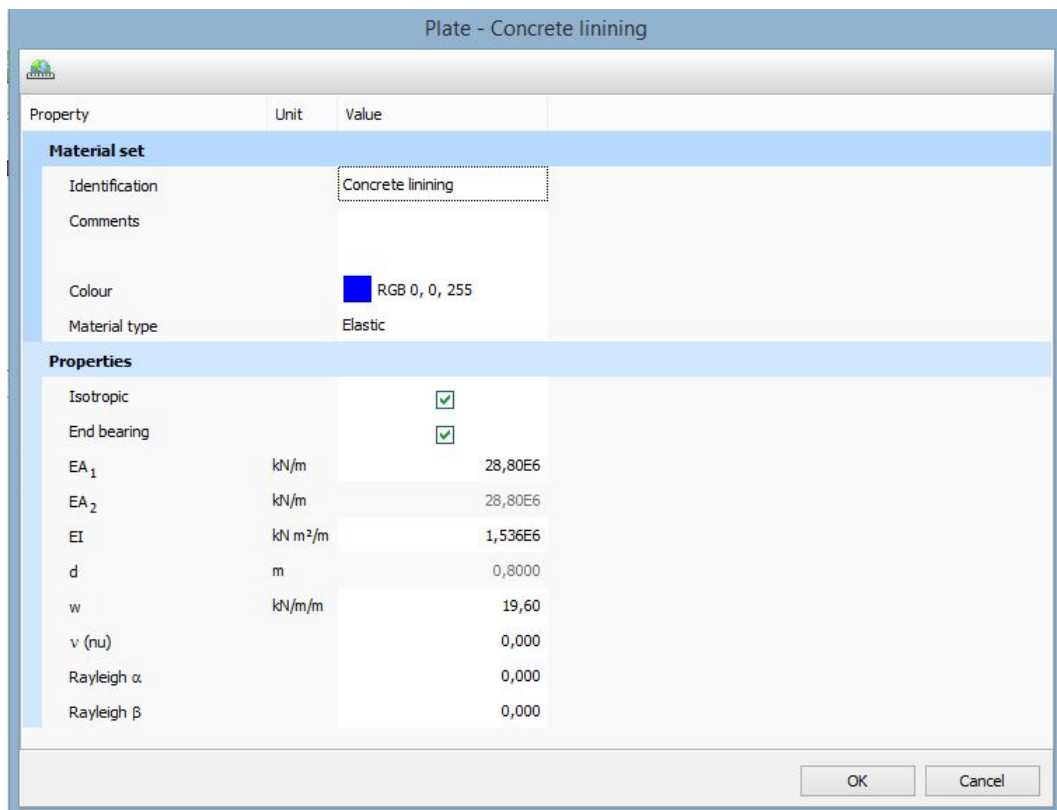


Figure AD.14: Tunnel lining input

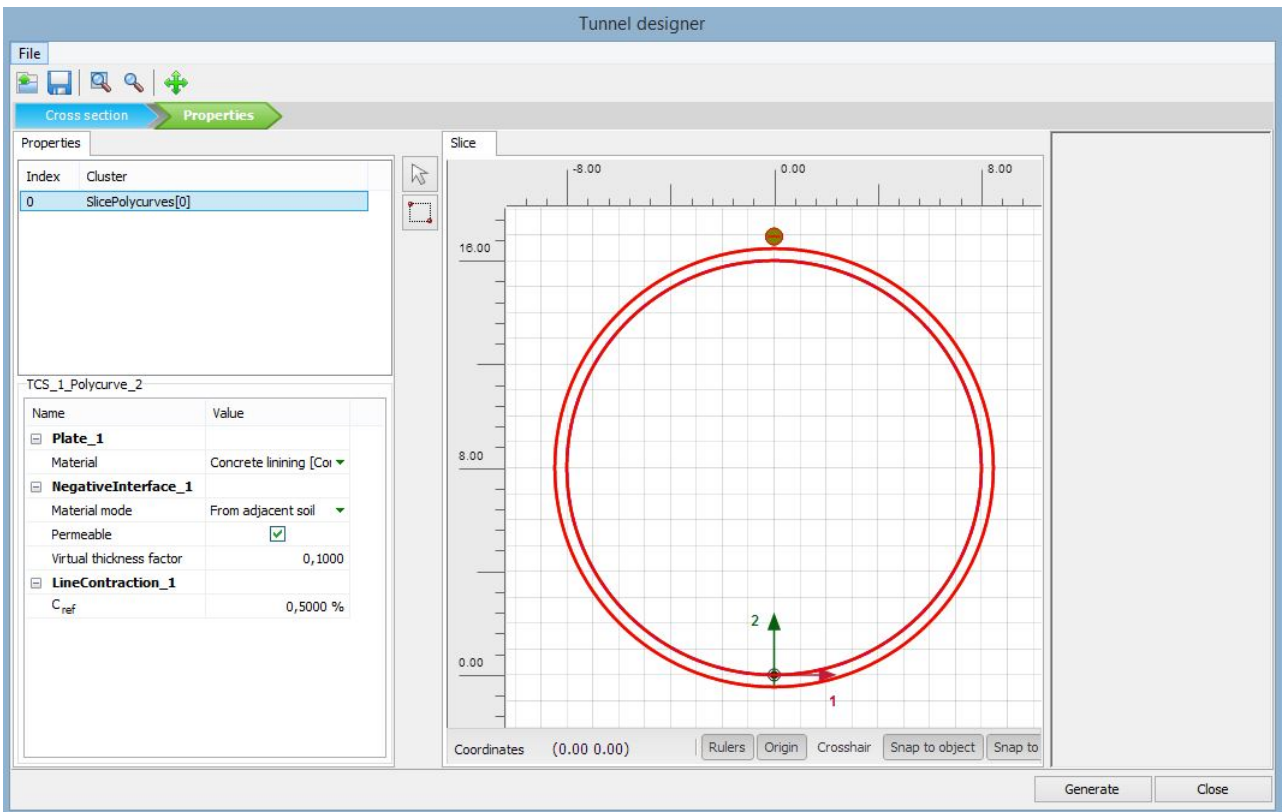


Figure AD.15: Left tunnel properties input

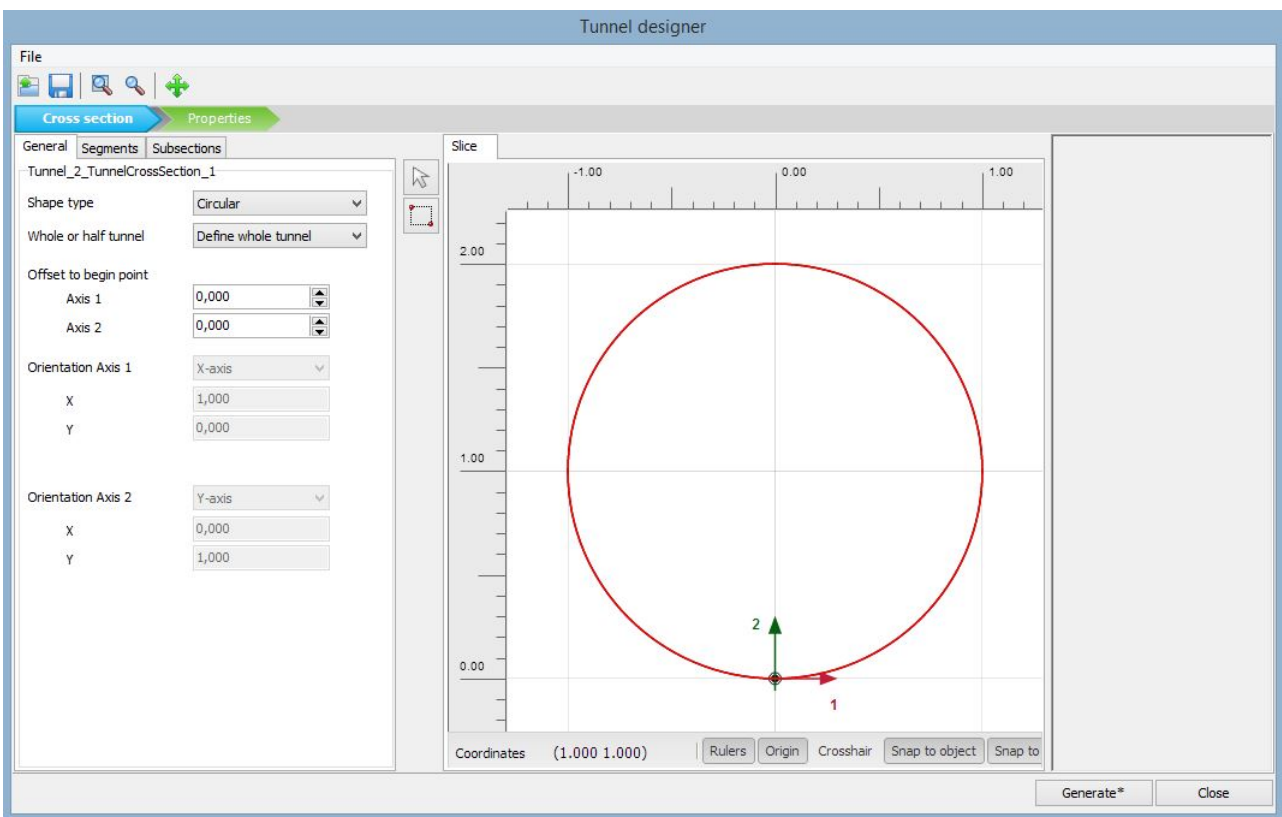


Figure AD.16: Right tunnel coordinates

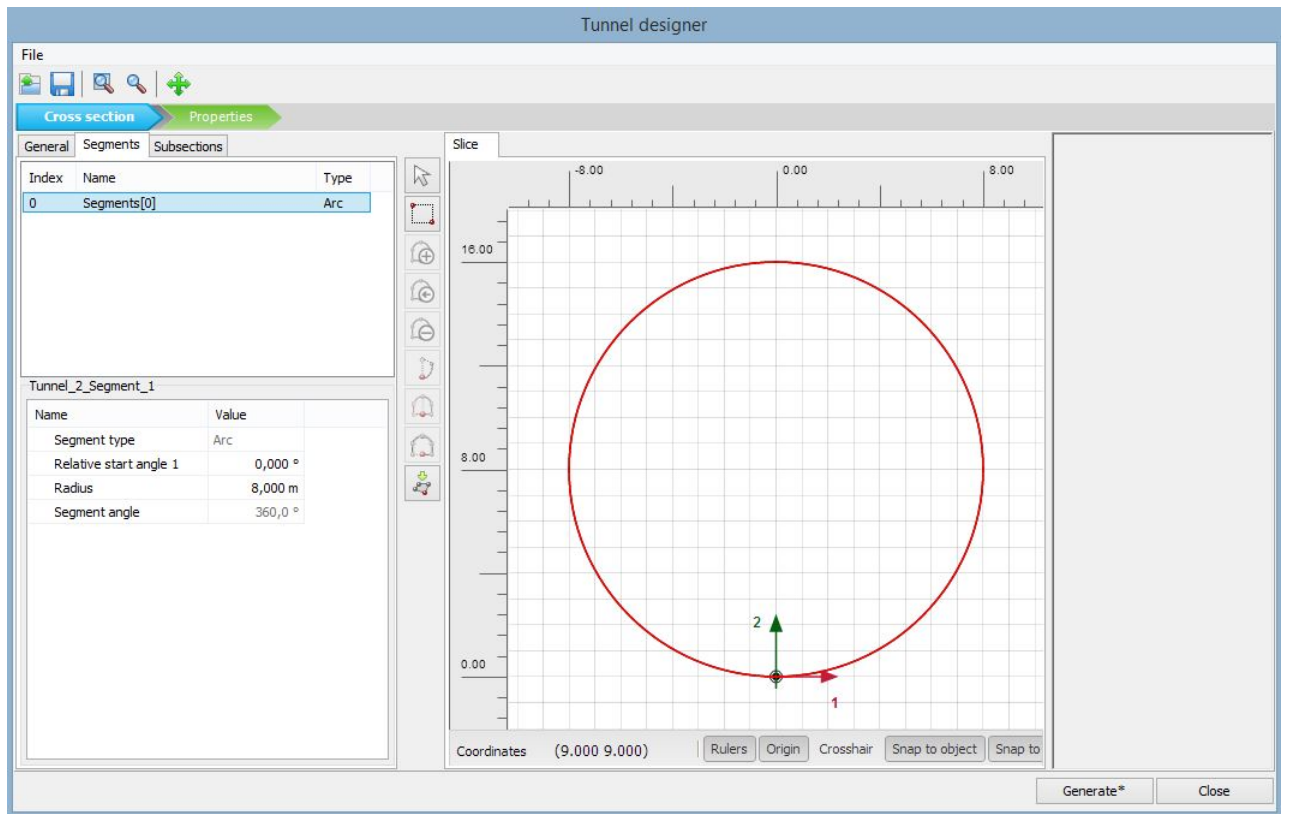


Figure AD.17: Right tunnel segment input

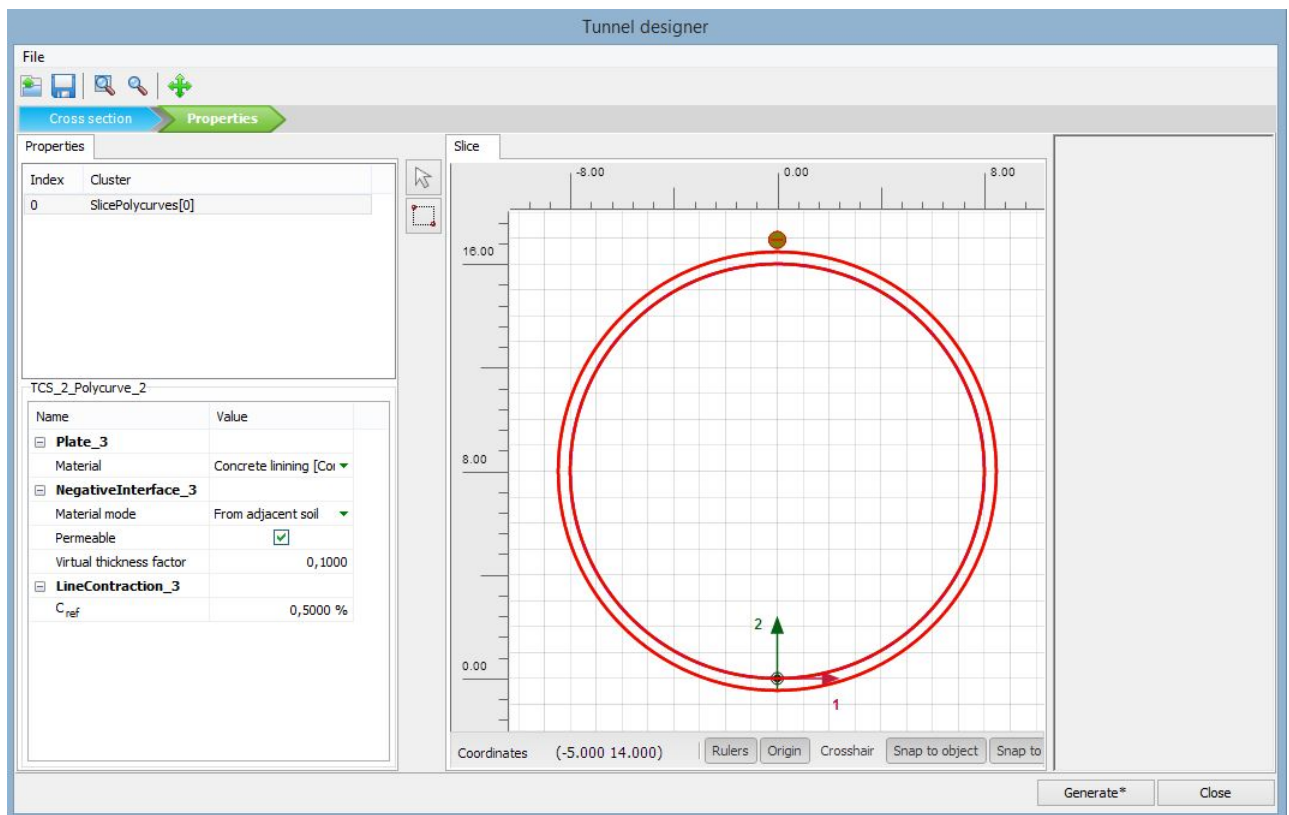


Figure AD.18: Right tunnel properties input



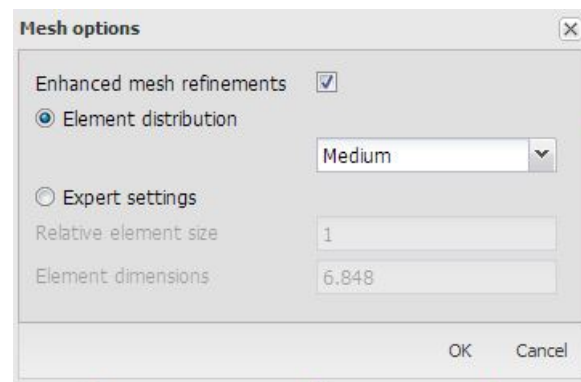


Figure AD.19: Mesh settings

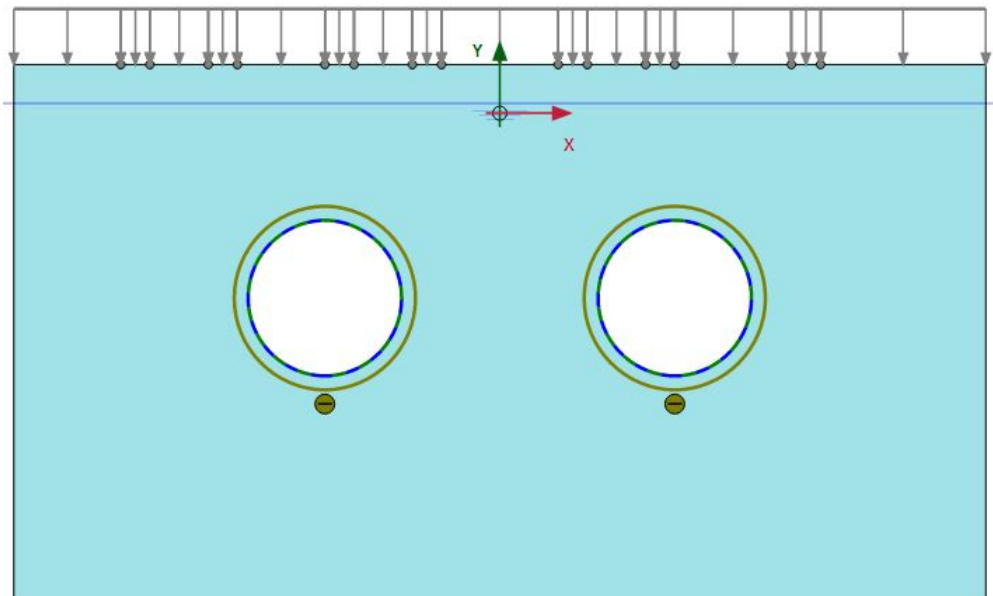


Figure AD.20: Cross view of excavated tunnel

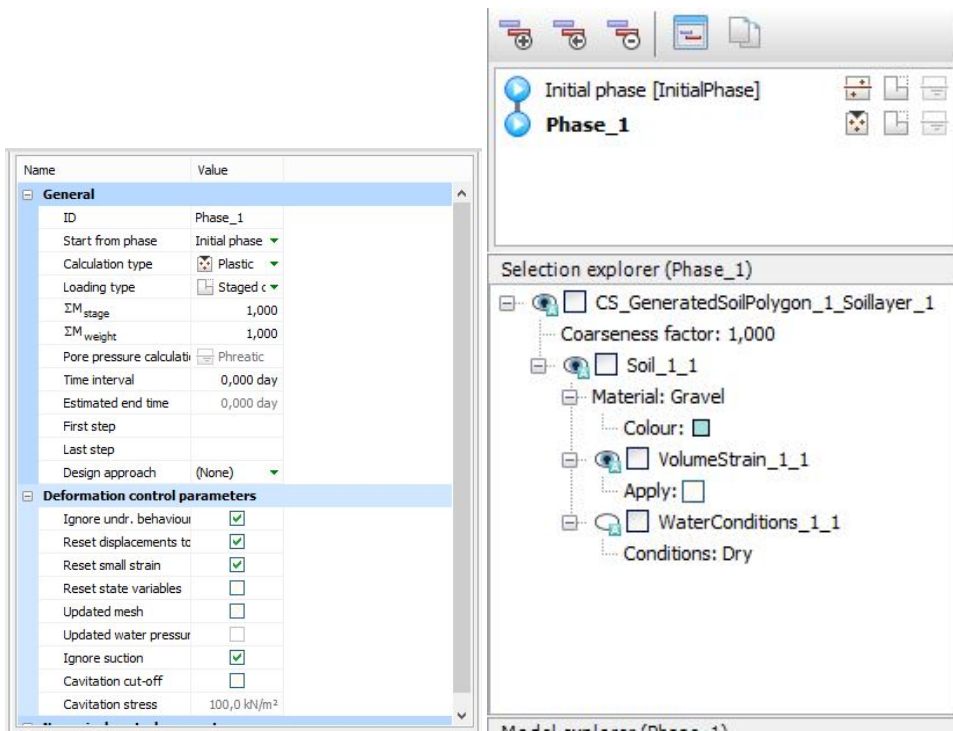


Figure AD.21: Left: General soil conditions phase 1; Right: Conditions of excavated soil phase 1

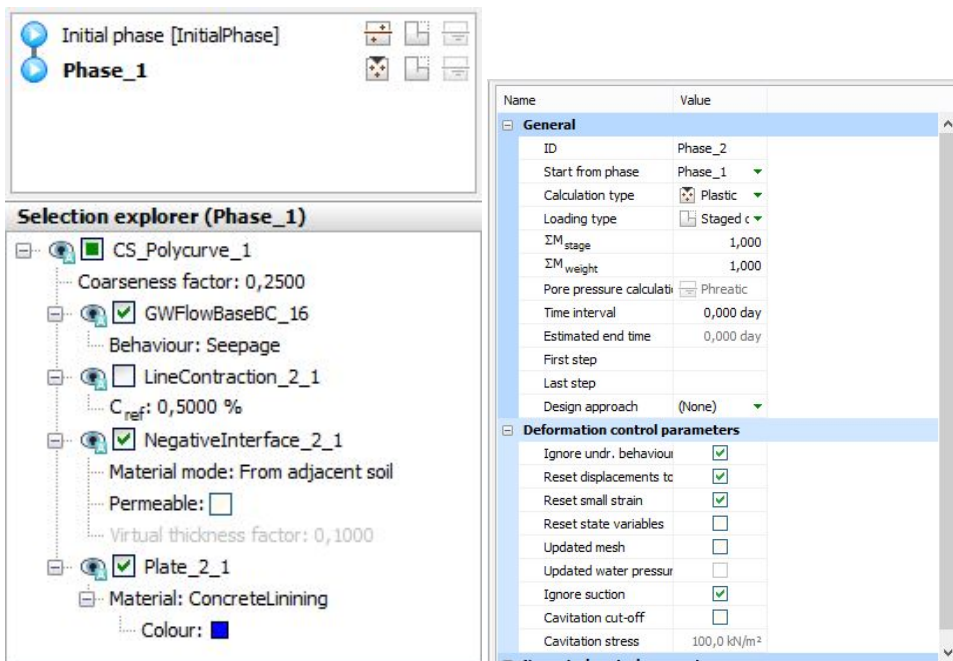


Figure AD.22: Left: Tunnel lining conditions phase 1; Right: General soil conditions phase 2;

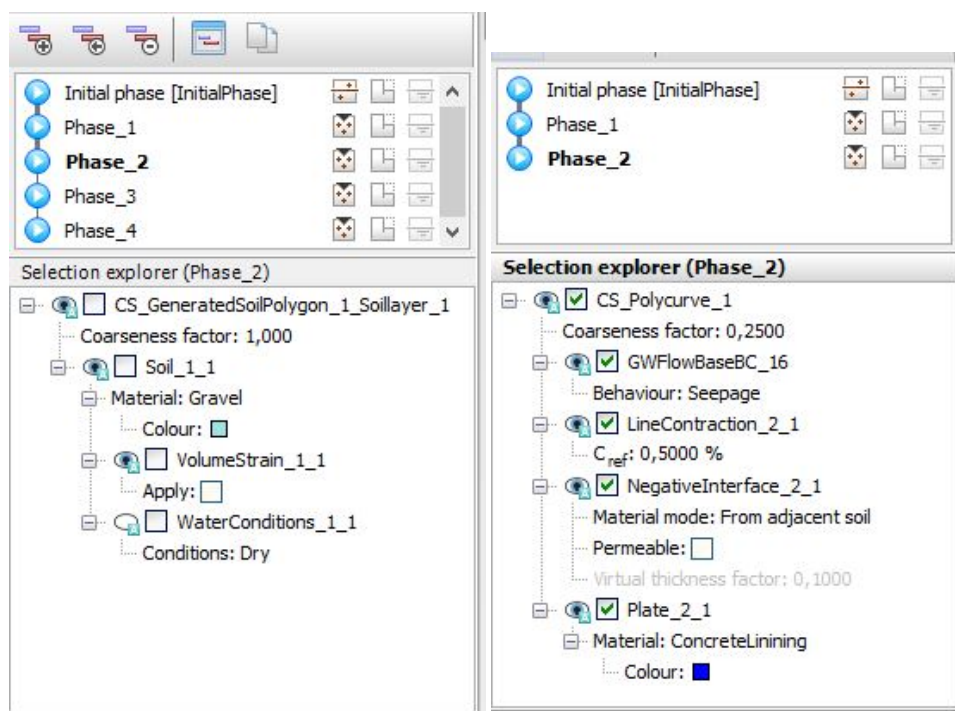


Figure AD.23: Left: Conditions of excavated soil phase 2;Right: Tunnel lining conditions phase 2;

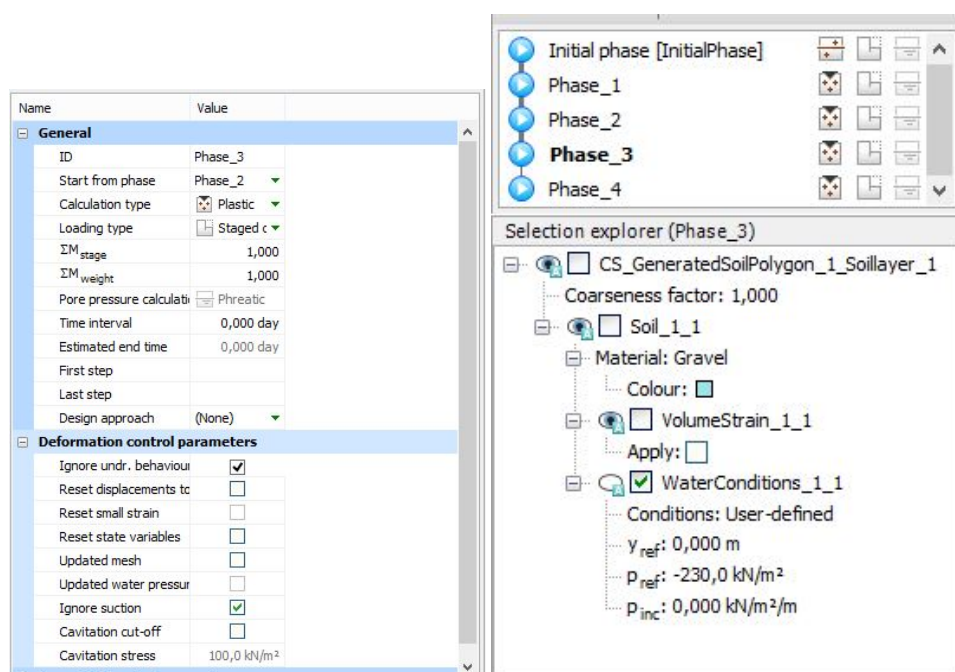


Figure AD.24: Left: General soil conditions phase 3; Right: Conditions of excavated soil phase 3

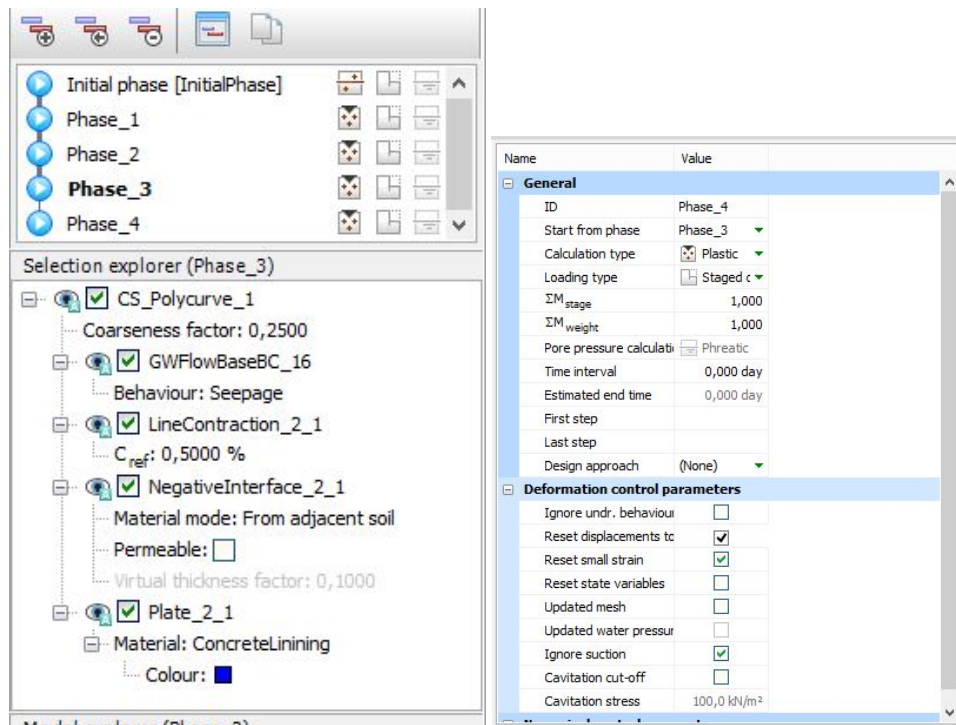


Figure AD.25: Left: Tunnel lining conditions phase 3;Right: General soil conditions phase 4;

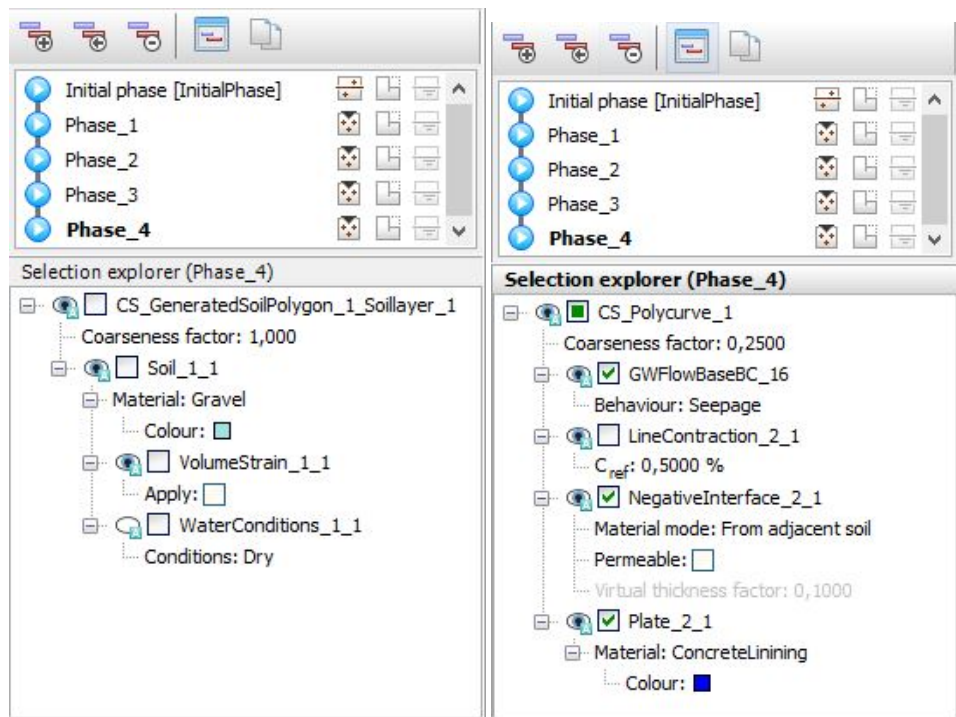


Figure AD.26: Left: Conditions of excavated soil phase 4 ;Right: Tunnel lining conditions phase 4;



## Structural design building pit

In order to construct the inlet and outlet of the tunnel a building pit should be created. Because the TBM has to start at its final depth, the pit should be deep enough. There are solutions to start the TBM at a smaller depth, but that would require more space above ground, which is unavailable on this location. In this section, the building pit will be designed.

### AE.1. Type of building pit

To construct the pit with a depth of 31 m, a large soil retaining wall is required. For this case, a few types have been considered: a pneumatic caisson, diaphragm walls and sheet pile walls. One important criterion is whether a TBM is able to bore through the walls of the pit. Table AE.1 shows the advantages and disadvantages of each type. The sheet pile wall can be ruled out, as its many disadvantages show that it is near impossible to use this method. The pneumatic caisson has been ruled out as well, as no anchors can be installed when using this method, resulting in extremely thick walls. Furthermore, expected costs are relatively high. Therefore, the application of diaphragm walls will be used in this design.

Wall type	Advantage	Disadvantage
Pneumatic caisson	Much applied method within Japan Can reach large depth	Expensive method Requires a lot of power
Diaphragm wall	TBM can bore through concrete walls Can reach large depths	Applying anchors not possible semi-expensive
Sheet piles	Easy and cost effective method	Depth of excavation limited Prone to deflection in gravelly soil TBM cannot penetrate wall

Table AE.1: Different types of building pits

### AE.2. Dimensions of building pit

The bottom of the TBM is at T.P. -27 m. Special structures are required between the bottom of the pit and the TBM in order to place the TBM between in the pit. See figure AE.1 for a depiction of a starting shaft. An extra metre is reserved for this proposal. Therefore, the top of the floor is at T.P. -28 m. The surroundings of the pit are at T.P. +3 m, which means the total depth becomes 31 m.

The width of the building pit has been based on the tunnel diameter, the space between two tunnels and the space between the side walls of the pit and the tunnel. See figure AE.2 for a sketch of the building pit. The space between the side walls and the pit has been based on the amount of working space required. The more space, the better. However, that would also be more expensive. The space required has been estimated to be 8 m. When the space in between the tunnels is set to 14 m, the total width becomes 66 m. The width in between has to be around 1 times the diameter of the TBM in order to reduce the influence of the tunnels to each other. Also, when the in- and outlet are created, some space between both in- and outlet pipes is



Figure AE.1: Starting structure of TBM in the starting shaft (Location: Rotterdamsebaan The Hague)

required.

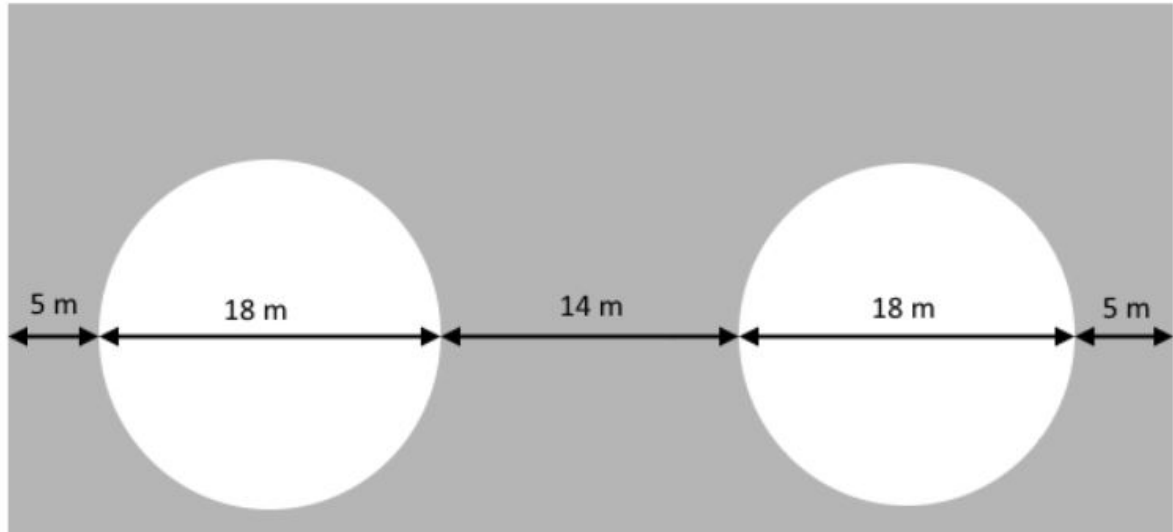


Figure AE.2: Width dimensions of building pit

The length of the building pit is partly defined by the length of the TBM, but mainly by the length of the in- and outlet structure. A length of 100 m is assumed, see appendix AG for a more detailed analysis of the inlet. Usually, a TBM has a length of 100 m including all the installations. However, not all the elements have to be necessarily in one line. The minimum of the two will be chosen, hence a length of 100 m is applied.



### AE.3. Pressure on diaphragm walls

In this section, the loads given by the soil and water have been calculated and given for each characteristic point in the soil profile.

$$\begin{aligned}\sigma'_h &= K_a * \sigma'_v \\ \sigma'_v &= \sigma_v - P_{water} \\ \sigma_v &= \gamma_{soil} * \text{depth} \\ P_{water} &= \gamma_{water} * (\text{depth} - \text{water head}) \\ K_a &= \frac{1 - \sin(\phi)}{1 + \sin(\phi)}\end{aligned}\tag{AE.1}$$

Using the soil data in appendix S, one can find the data in table AE.2 for the active soil pressure. The passive horizontal soil pressure develops to 92 kPa at the tip of the wall, which is at a depth of 34 m.

<b>Soil layer</b>	<b>Top level (depth) (m)</b>	<b>Vertical soil pressure (kPa)</b>	<b>Water pressure (kPa)</b>	<b>Active horizontal soil pressure factor (-)</b>	<b>Effective horizontal soil pressure (kPa)</b>
Sand, Slightly silty clayey, first layer	0	0	0	0.33	0
Sand, Greatly silty clayey	0.6	10.8	0	0.41	4.43
Pressure at water level	2	36	0	0.41	14.76
Sand, Clean moderate, first layer	3.3	62	13	0.3	14.7
Sand, Slightly silty clayey, second layer	10.4	204	84	0.33	39.6
Sand, Clean moderate, second layer	13.4	264	114	0.3	45
Gravel, slightly silty solid	16.9	334	149	0.22	40.7
<b>Soil layer</b>	<b>Bottom level (depth) (m)</b>	<b>Vertical soil pressure (kPa)</b>	<b>Water pressure (kPa)</b>	<b>Active horizontal soil pressure factor (-)</b>	<b>Effective horizontal soil pressure (kPa)</b>
Sand, Slightly silty clayey, first layer	0.6	10.8	0	0.33	3.6
Sand, Greatly silty clayey	3.3	62	13	0.41	20.1
Sand, Clean moderate, first layer	10.4	204	84	0.3	36
Sand, Slightly silty clayey, second layer	13.4	264	114	0.33	50
Sand, Clean moderate, second layer	16.9	334	149	0.3	55.5
Gravel, slightly silty solid	34	676	320	0.22	78.32

Table AE.2: Active soil along the diaphragm wall



## AE.4. Structural calculations

### AE.4.1. Conventional reinforcement

**Moment capacity** Below, the capacity and required reinforcement in the diaphragm wall have been calculated.

$$M_{Rd} = A_s * f_{yd} * z \quad (\text{AE.2})$$

Derivation of  $x_u$ :

$$\begin{aligned} N_s &= N_c \\ A_s * f_{yd} &= 0.75 * b * x_u * f_{cd} \\ x_u &= \frac{A_s * f_{yd}}{0.75 * b * f_{cd}} \end{aligned} \quad (\text{AE.3})$$

- $M_{Ed} = 3420 \text{ kNm}$
- Concrete class C55/67
- $f_{cd} = 36.67 \text{ N/mm}^2$
- $\varnothing_{\text{reinforcement}} = 40 \text{ mm}$
- $\varnothing_{\text{stirrups}} = 12 \text{ mm}$
- $c = 25 \text{ mm}$
- $h = 1500 \text{ mm}$
- $d = 1443 \text{ mm}$
- $\rho \approx 0.5 \%$  (rough estimation)
- number of reinforcement bars = 6/m
- $A_s = 7540 \text{ mm}^2/\text{m}$
- $x_u = 120 \text{ mm}$
- $z = 1396 \text{ mm}$
- $M_{Rd} = 4579 \text{ kNm/m}$

6 reinforcement bars are required. The bars will be applied on both sides of the cross-section, to resist both the positive as the negative bending moment. This gives an reinforcement ratio of 1%.

**For shear capacity without shear reinforcement:**

$$\begin{aligned} V_{Rd,c} &= (C_{Rd,c} * k * (100 * \rho * f_{ck})^{1/3} + k_1 * \sigma_{cp}) * b * d \\ V_{Rd,c,min} &= (0.035 * k^{3/2} * f_{ck}^{1/2} + k_1 * \sigma_{cp}) * b * d \end{aligned} \quad (\text{AE.4})$$

Where:

- $C_{Rd,c} = 0.12$
- $k = 1 + \sqrt{\frac{200}{d}} = 1.37$
- $f_{ck} = 55 \text{ N/mm}^2$
- $\rho = 1\%$
- $k_1 = 0.15$
- $\sigma_{cp} = 0 \text{ N/mm}^2$
- $V_{Rd,c} = 902 \text{ kN}$
- $V_{Ed} = 1860 \text{ kN}$

In the calculations above, it is shown that shear reinforcement is required. How much is required, has been calculated below. It has been assumed bars of 24 mm are placed every 100 mm.

$$V_{Rd,s} = \frac{A_{sw}}{s} * z * f_{yd} * \cot(\theta) \quad (\text{AE.5})$$

Where:

- $A_{sw}$  = cross-sectional area of reinforcement per meter ( $\text{mm}^2/\text{m}$ )
- $s$  = c.t.c. distance between two reinforcement bars (mm)
- $\theta$  = Angle of reinforcement =  $21.8^\circ$
- $V_{Rd} = 7100$  kN

### Unity Check

To guarantee the safety of the structure, the total strength should be checked according to formula AE.6. It was found that applying 6 bars at each side, a value of exactly 1 is found.

$$U.C. = \frac{M_{Ed}}{M_{Rd}} + \frac{V_{Ed}}{V_{Rd}} = 1 \leq 1.0 \quad (\text{AE.6})$$

### AE.4.2. Glass fibre reinforcement

For the soft eye, glass fibre reinforcement is to be applied. This reinforcement has to resist the same forces, but will show another behaviour compared steel reinforcement. It has been chosen to use glass fibre bars from the company SchöckComBAR. This manufacturer has provided a document with guidelines about glass fibre reinforcement [23]. All the formulas given for the calculation of the glass fibre reinforcement are derived from this specific document. This document provides a table (table AE.3) which shows the minimum ratio of reinforcement required. The entrance value for the table for this design is 42 (AE.7). With this value one can find:

- $k * \omega_{gl} = 4.42$
- $k = 8.77$
- $\omega_{gl} = 0.5\%$
- $A_{gl} = 7215 \text{ mm}^2/\text{m}$

$$\frac{M_u}{b * d * f_{cd}} = 42 \quad (\text{AE.7})$$

7215  $\text{mm}^2/\text{m}$  of glass reinforcement is required to resist the bending moment. This is equal to 9 bars with a diameter of 32 mm. It will be applied to both sides, since there is a negative as well as a positive bending moment.

Furthermore, it can be stated that:

$$x_u = k_x * d = 0.15 * 1443 = 216 \text{ mm}$$

$$z = k_z * d = 0.95 * 1443 = 1371$$

The shear reinforcement has been calculated using shear stresses, allowable concrete stresses and shear reinforcement. The shear reinforcement consists of dowels of 16 mm or 32 mm thick.

$$\tau_d = \frac{V_{Ed}}{b * d} = \frac{1860E3}{1443 * 1000} = 1.29 \text{ N/mm}^2 \quad (\text{AE.8})$$

$$\tau_1 = \max(0.4 * f_{ctk;0.05} * k_\lambda * k_h * \omega_0^{1/3}; 0.4 * f_{ctk;0.05})$$

- Concrete class C55/67
- $f_{ctk;0.05} = 3.0$
- $k_\lambda = 1$
- $k_h = 1$
- $\omega_0 = 0.3 * \omega_{gl} = 0.167\%$
- $\tau_1 = 1.2 \text{ N/mm}^2$

$$\tau_{gl} = \tau_d - \tau_1 = 0.09 \text{ N/mm}^2$$

$$A_{shearrein.} = \frac{\tau_{gl} * b * d}{z * 0.0022 * E_{gl}} \quad (\text{AE.9})$$

$$E_{gl} = 60 \text{ GPa}$$

$$A_{shearrein.} = 0.72 \text{ mm}^2/\text{mm} = 720 \text{ mm}^2/\text{m}$$

Applying two 16 mm dowels per meter at each side of the cross-section should be sufficient.

$\frac{h_0}{f_{yk} \cdot b \cdot d^2}$	$k \cdot \omega_{gl}$	$k_x$	$k_y$	$\eta_{mu}$	$\sigma_{gl}$	$\frac{h_0}{f_{yk} \cdot b \cdot d^2}$	$k \cdot \omega_{gl}$	$k_x$	$k_y$	$\eta_{mu}$	$\sigma_{gl}$	$\frac{h_0}{f_{yk} \cdot b \cdot d^2}$	$k \cdot \omega_{gl}$	$k_x$	$k_y$	$\eta_{mu}$	$\sigma_{gl}$
[H]	[%]	[H]	[H]	[H]	[N/mm <sup>2</sup> ]	[H]	[%]	[H]	[H]	[H]	[N/mm <sup>2</sup> ]	[H]	[%]	[H]	[H]	[H]	[N/mm <sup>2</sup> ]
20	2,29	0,11	0,96	1,00	342	110	11,94	0,24	0,92	1,00	342	200	26,80	0,37	0,86	0,87	297
22	2,29	0,11	0,96	1,00	342	112	12,17	0,24	0,92	1,00	342	202	32,22	0,40	0,85	0,80	254
24	2,50	0,12	0,96	1,00	342	114	12,39	0,24	0,92	1,00	342	204	33,28	0,40	0,84	0,80	249
26	2,71	0,12	0,96	1,00	342	116	12,62	0,24	0,92	1,00	342	206	34,37	0,41	0,84	0,80	244
28	2,92	0,13	0,96	1,00	342	118	12,85	0,24	0,92	1,00	342	208	35,49	0,41	0,84	0,80	239
30	3,14	0,13	0,96	1,00	342	120	13,08	0,25	0,92	1,00	342	210	36,65	0,42	0,84	0,80	234
32	3,35	0,13	0,96	1,00	342	122	13,31	0,25	0,92	1,00	342	212	37,85	0,42	0,84	0,80	229
34	3,56	0,14	0,95	1,00	342	124	13,54	0,25	0,92	1,00	342	214	39,08	0,43	0,83	0,80	225
36	3,78	0,14	0,95	1,00	342	126	13,77	0,25	0,92	1,00	342	216	40,35	0,43	0,83	0,80	220
38	3,99	0,14	0,95	1,00	342	128	14,00	0,25	0,91	1,00	342	218	41,67	0,44	0,83	0,80	216
40	4,21	0,15	0,95	1,00	342	130	14,23	0,26	0,91	1,00	342	220	43,03	0,44	0,83	0,80	211
42	4,42	0,15	0,95	1,00	342	132	14,46	0,26	0,91	1,00	342	222	44,43	0,45	0,83	0,80	207
44	4,64	0,16	0,95	1,00	342	134	14,69	0,26	0,91	1,00	342	224	45,88	0,45	0,82	0,80	203
46	4,86	0,16	0,95	1,00	342	136	14,93	0,26	0,91	1,00	342	226	47,38	0,46	0,82	0,80	199
48	5,07	0,16	0,95	1,00	342	138	15,16	0,26	0,91	1,00	342	228	48,93	0,46	0,82	0,80	194
50	5,29	0,16	0,95	1,00	342	140	15,40	0,27	0,91	1,00	342	230	50,53	0,47	0,82	0,80	190
52	5,51	0,17	0,94	1,00	342	142	15,63	0,27	0,91	1,00	342	232	52,19	0,47	0,82	0,80	186
54	5,73	0,17	0,94	1,00	342	144	15,87	0,27	0,91	1,00	342	234	53,91	0,48	0,81	0,80	182
56	5,94	0,17	0,94	1,00	342	146	16,10	0,27	0,91	1,00	342	236	55,68	0,48	0,81	0,80	179
58	6,16	0,18	0,94	1,00	342	148	16,34	0,27	0,91	1,00	342	238	57,52	0,49	0,81	0,80	175
60	6,38	0,18	0,94	1,00	342	150	16,58	0,28	0,90	1,00	342	240	59,43	0,50	0,81	0,80	171
62	6,60	0,18	0,94	1,00	342	152	16,82	0,28	0,90	1,00	342	242	61,41	0,50	0,81	0,80	167
64	6,82	0,18	0,94	1,00	342	154	17,06	0,28	0,90	1,00	342	244	63,45	0,51	0,80	0,80	164
66	7,04	0,19	0,94	1,00	342	156	17,30	0,28	0,90	1,00	342	246	65,58	0,51	0,80	0,80	160
68	7,26	0,19	0,94	1,00	342	158	17,54	0,29	0,90	1,00	342	248	67,78	0,52	0,80	0,80	157
70	7,48	0,19	0,94	1,00	342	160	17,78	0,29	0,90	1,00	342	250	70,07	0,52	0,80	0,80	153
72	7,70	0,20	0,93	1,00	342	162	18,02	0,29	0,90	1,00	342	252	72,44	0,53	0,79	0,80	150
74	7,92	0,20	0,93	1,00	342	164	18,27	0,29	0,90	1,00	342	254	74,91	0,53	0,79	0,80	146
76	8,14	0,20	0,93	1,00	342	166	18,51	0,29	0,90	1,00	342	256	77,48	0,54	0,79	0,80	143
78	8,36	0,20	0,93	1,00	342	168	18,75	0,30	0,90	1,00	342	258	80,15	0,55	0,79	0,80	140
80	8,59	0,20	0,93	1,00	342	170	19,00	0,30	0,89	1,00	342	260	82,93	0,55	0,79	0,80	137
82	8,81	0,21	0,93	1,00	342	172	19,24	0,30	0,89	1,00	342	262	85,82	0,56	0,78	0,80	133
84	9,03	0,21	0,93	1,00	342	174	19,49	0,30	0,89	1,00	342	264	88,84	0,56	0,78	0,80	130
86	9,25	0,21	0,93	1,00	342	176	19,74	0,30	0,89	1,00	342	266	91,98	0,57	0,78	0,80	127
88	9,48	0,21	0,93	1,00	342	178	20,11	0,31	0,89	0,99	340	268	95,26	0,58	0,78	0,80	124
90	9,70	0,22	0,93	1,00	342	180	20,55	0,31	0,89	0,99	337	270	98,69	0,58	0,77	0,80	121
92	9,92	0,22	0,93	1,00	342	182	21,02	0,32	0,89	0,98	334	272	102,3	0,59	0,77	0,80	118
94	10,15	0,22	0,93	1,00	342	184	21,50	0,32	0,88	0,97	331	274	106,0	0,59	0,77	0,80	115
96	10,37	0,22	0,93	1,00	342	186	22,01	0,32	0,88	0,96	328	276	109,9	0,60	0,77	0,80	112
98	10,59	0,22	0,93	1,00	342	188	22,54	0,33	0,88	0,95	324	278	114,0	0,61	0,76	0,80	109
100	10,82	0,23	0,92	1,00	342	190	23,11	0,33	0,88	0,94	321	280	118,3	0,61	0,76	0,80	106
102	11,04	0,23	0,92	1,00	342	192	23,72	0,34	0,87	0,93	317	282	122,8	0,62	0,76	0,80	103
104	11,27	0,23	0,92	1,00	342	194	24,37	0,34	0,87	0,91	312	284	127,6	0,63	0,76	0,80	101
106	11,49	0,23	0,92	1,00	342	196	25,09	0,35	0,87	0,90	308	286	132,6	0,63	0,75	0,80	98
108	11,72	0,23	0,92	1,00	342	198	25,89	0,36	0,86	0,88	303	288	137,8	0,64	0,75	0,80	95

k-waarden voor de berekening van  $\omega_b$

Schöck ComBAR* $f_{yk} = 342 \text{ N/mm}^2$	C12/15 $f'_b = 9 \text{ N/mm}^2$	C20/25 $f'_b = 15 \text{ N/mm}^2$	C28/35 $f'_b = 21 \text{ N/mm}^2$	C35/45 $f'_b = 27 \text{ N/mm}^2$	C45/55 $f'_b = 33 \text{ N/mm}^2$	C53/65 $f'_b = 39 \text{ N/mm}^2$
$k = \frac{f_{yk}}{f'_b}$	38,00	22,80	16,29	12,67	10,36	8,77

Table AE.3: Table for bending moment for glass fibre reinforcement

# AF

## Structural design in- and outlet tube

The transition from the surface to the tunnel consists of an S-curved tube, as presented in figure AF1. This structure will be used on both ends of the tunnel.

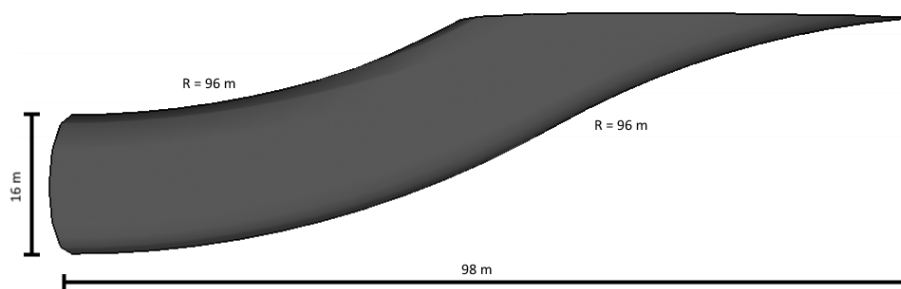


Figure AF1: Transition tube surface to tunnel

The tube consists of concrete rings, that is assembled from four segments. The segments are to be bolted together. The same thickness, concrete type and tangential reinforcement as for the bored tunnel are to be used. This is because the bottom section of the tube is subjected to similar load conditions as the regular tunnel. Sketches of a segment and tube ring are presented in figures AF2 and AF3.

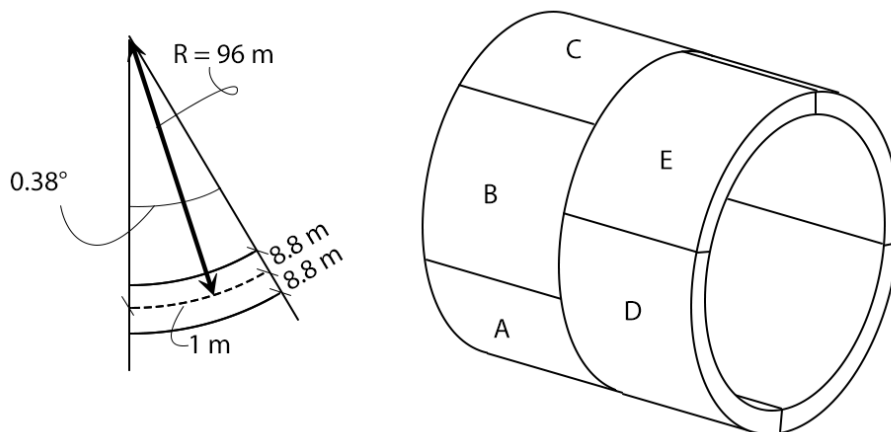


Figure AF2: Sketches tube ring and curvature

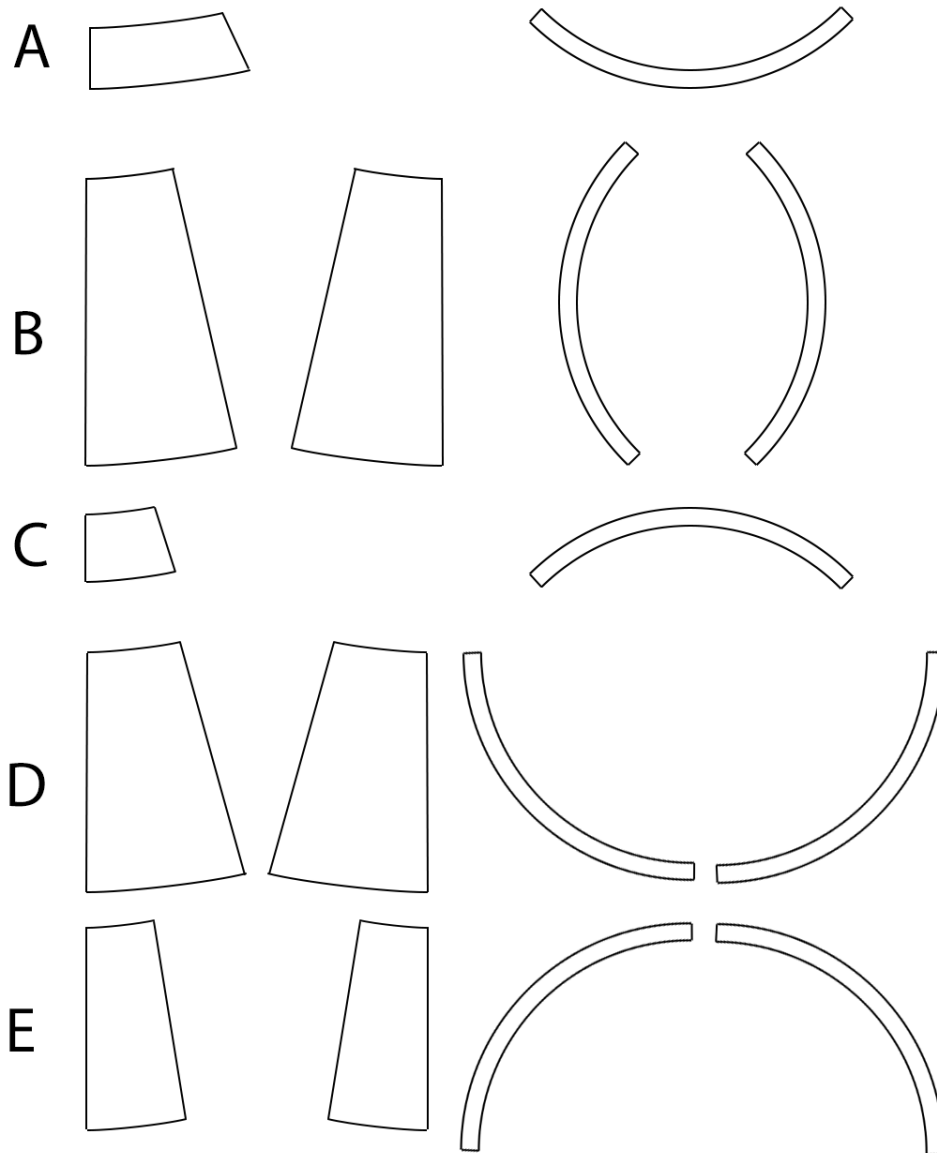


Figure AE3: Sketches individual segments

### AF1. Construction process

Construction of the tube is to start after both tunnels have been bored. First, the segments will be bolted to the existing tunnel one by one, as well as to each other. The next step consists of supplying soil until the tunnel rests on the bed. This process is repeated for each ring. When the next ring is applied, the previous ring will settle into the soil, until forces are fully transferred to the subgrade. This process has been illustrated in figure AF4. The construction process will be elaborated in appendix AH.4.

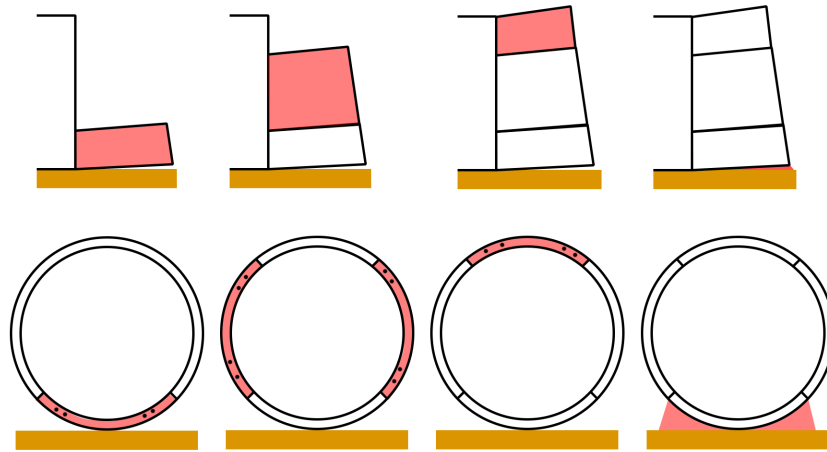


Figure AF4: Construction process transition tube. Red parts indicate the step, black dots indicate bolts.

### AF2. Structural design

For the structural design, the following two situations have been considered:

- Bottom segment hanging free - start tube
- One ring hanging free - start tube
- Bottom segment hanging free - centre tube
- One ring hanging free - centre tube

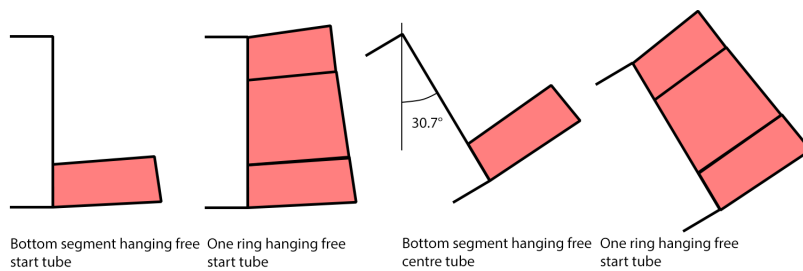


Figure AF5: Situations checked on strength

Both situations have been checked through the usage of Diana Finite Element Analysis software. The following parameters have been used for modelling the structural elements:

Parameter	Value	Unit
Concrete type	C55/63	-
Density concrete	2450	kg/m <sup>3</sup>
Young's modulus steel	210E+09	N/m <sup>2</sup>
Poisson's ratio steel	0.3	-
Element size	0.200	m
Mesher type	Hexa/Quad	-
Mesh order	Linear	-

Table AF.1: Parameters Diana FEA tube models

The reaction forces in the bolted connections have been checked for all situations. For the situation at the start of the ring, the bending moments have been checked as well. This calculations assumed that the start of the shaft is the governing situation. This is because the segment is rotated upwards. Therefore, the load component perpendicular to the segment decreases, as well as the lever arm.

For the bending moments, a 'regular curved shell' model has been used. The reaction forces haven been calculated using a 3D solid model. The concrete elasticity, plasticity and cracking has been taken into account according to European CEB-FIP 1990 model code using C55/63. Young's modulus and Poisson's ratio have also been calculated by the software using this model.

### AF2.1. Bottom segment

#### Bending capacity

For the bending moments, the segment has been modelled as follows:

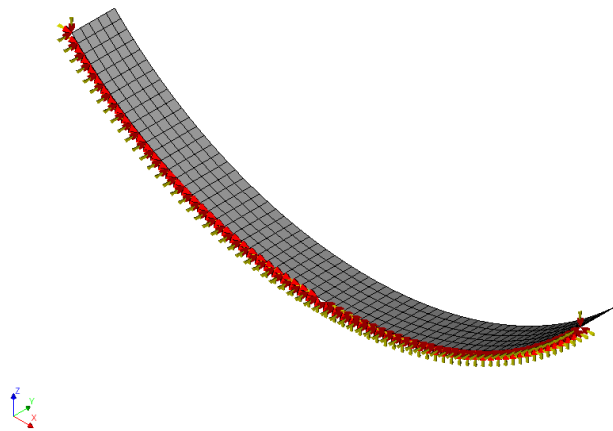


Figure AF.6: Bottom segment bending moment model

The segment is a quarter circle with a radius of 8.4 m, the centre of the tube to the centre of the concrete lining. The segment curves upward in the y-z plane, around an arch with radius of 104.4 m and an angle of 0.3790°. The supported side, which is shown by the red arrows, is a clamped support. When the segment is attached to the tunnel, there is little to no rotation possible at this point. The results are presented in the following figures.



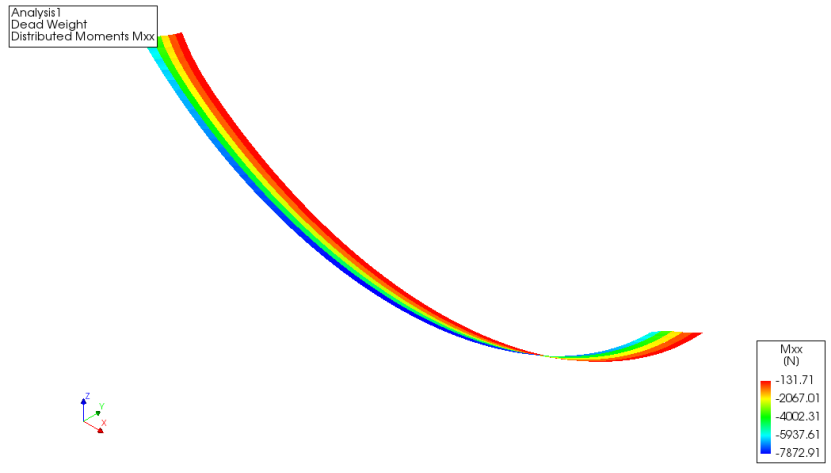


Figure AF7: Bottom segment - start tube, Mxx

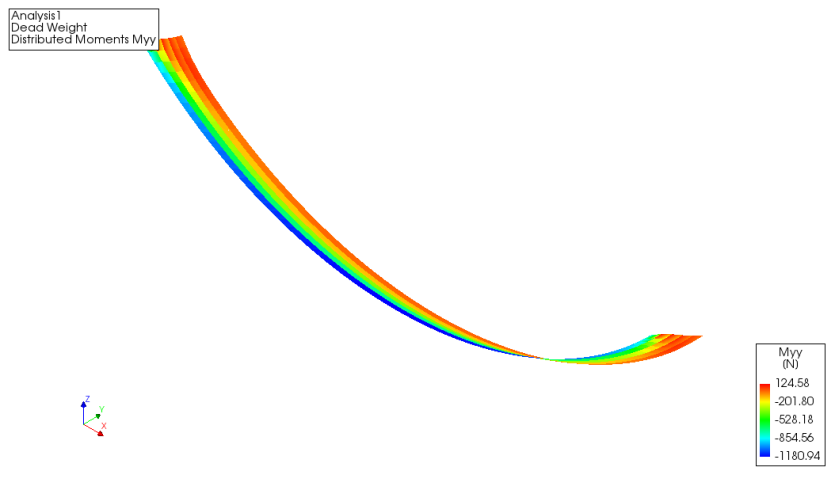


Figure AF8: Bottom segment - start tube, Myy

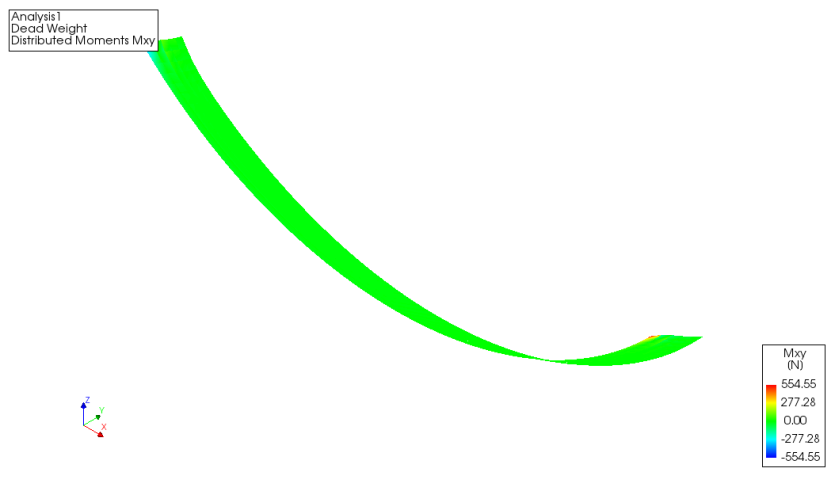


Figure AF9: Bottom segment - start tube, Mxy

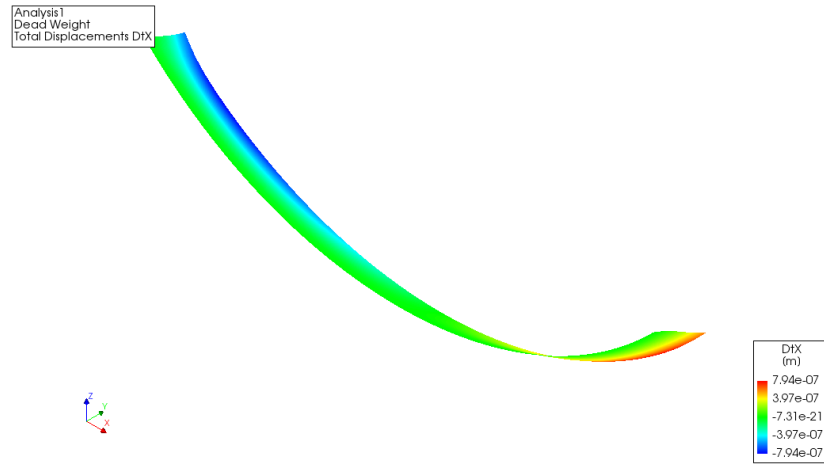


Figure AF.10: Bottom segment - start tube, X displacements

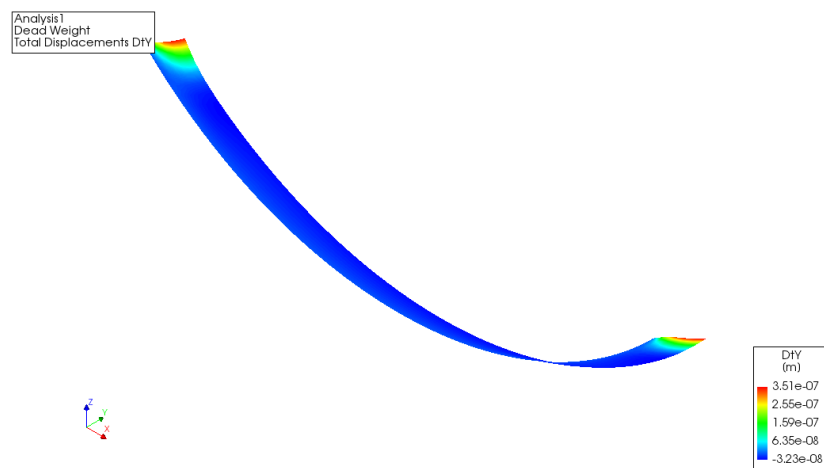


Figure AF.11: Bottom segment - start tube, Y displacements

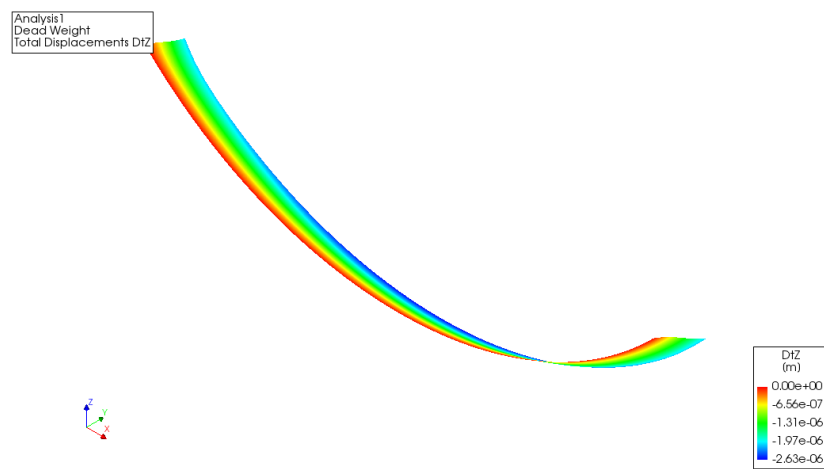


Figure AF.12: Bottom segment - start tube, Z displacements

Figure AF9 shows there is little to no torsional bending, only concentrated bending in the corners where the supports ends. These are singularities and have been neglected.

Design bending moments have been determined by integrating over 1 m at the maximums. Results are presented in table AF2.

Direction	$M_E$ [kNm]	$M_{Ed}$ [kNm]
$M_{xx}$	4.002	4.803
$M_{yy}$	5.905	7.086

Table AF2: Bending moments - start tube, bottom segment

The bending moment capacity in xx-direction has already been determined in section AC.1 and equals 2778 kNm/m. The bending moment capacity in yy-direction has been determined on a non-reinforced concrete cross-section, with parameters as used in table AF3.

Parameter	Symbol	Value	Unit
Characteristic axial tensile strength C55/67	$f_{ct,0.05}$	3.0	MPa
Thickness	$t$	0.8	m
Material factor concrete	$\gamma_c$	1.5	-

Table AF3: Parameters bottom segment bending capacity

$$\begin{aligned}
 M_{Rd,ct} &= f_{ctd} * W_{yy} \\
 f_{ctd} &= f_{ct,0.05} / \gamma_c \\
 &= 3.0 / 1.5 \\
 &= 2.0 \text{ MPa} \\
 W_{yy} &= \frac{1}{6} * 1 \text{ m} * t^2 \\
 &= \frac{1}{6} * 1 * 0.8^2 \\
 &= 0.1067 \text{ m}^3 / \text{m} \\
 M_{Rd,ct} &= 2.0 * 0.1067 \\
 &= 213.3 \text{ kNm/m}
 \end{aligned} \tag{AF.1}$$

Direction	$M_{Ed}$ [kNm/m]	$M_{Rd}$ [kNm/m]	u.c.
$M_{xx}$	4.803	2778	1.73E-03
$M_{yy}$	7.086	213.3	0.03

Table AF4: Bending moments and capacities bottom segment - start tube

No additional reinforcement is required for the bending moments that occur when the bottom segment is installed. This is because the bending moments found in that stage, are of less magnitude than in an earlier stage.

### Connection

The tube segments are to be bolted to the existing tunnel. To check whether the bolted connection can hold, the following model has been used:

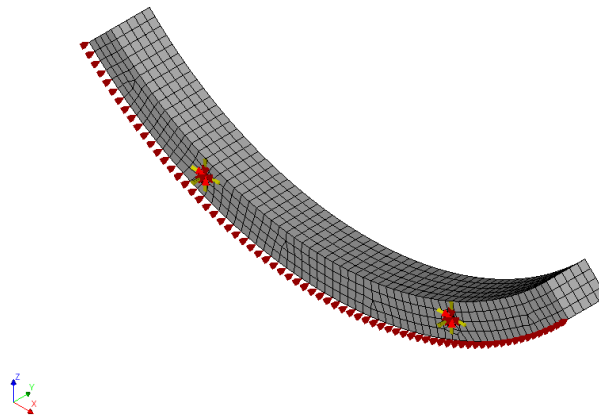


Figure AF13: Bottom segment connection model

The model describes part A in figures AF3 on page 178 and AF2 on page 177. It consists of a quarter circle with inner radius of 8.0 m and an outer radius of 8.8 m. The focal point curves upwards in the y-z plane along an arch with radius of 96 m and an angle of  $0.3790^\circ$ , similar to AF6, which can be found on page 180.

The bolts have been modelled as circular supports that restrict translation. Each bolt group has been modelled as one circle with diameter of 27 mm. Furthermore, the bottom line has been modelled as a support that resists translation in the y-direction. This is because the segment will rotate slightly, trying to pull out the bolts and resting at the bottom. The coordinates of each bolt group are presented in table AF5.

Bolt	x [m]	y [m]	z [m]
A1	-3.2	0	-7.7
A2	3.2	0	-7.7

Table AF5: Bottom segment - start tube, centre coordinates bolt groups, with origin in the centre of the tube.

The results are presented in the following figures:

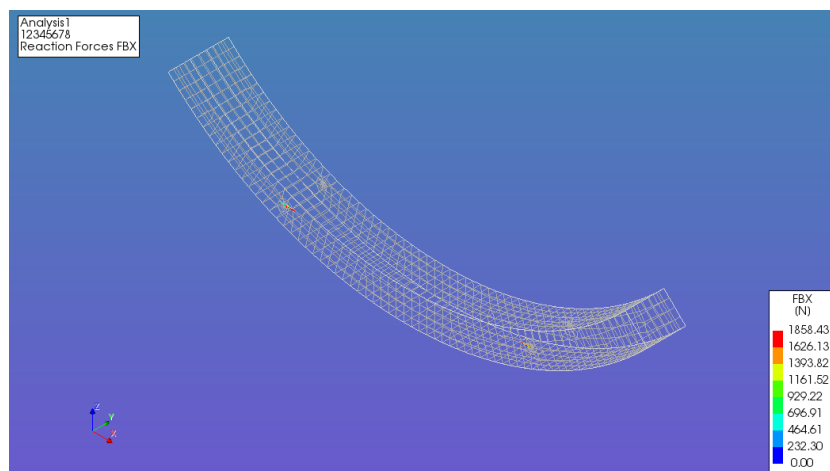


Figure AF14: Bottom segment - start tube, reaction forces X direction

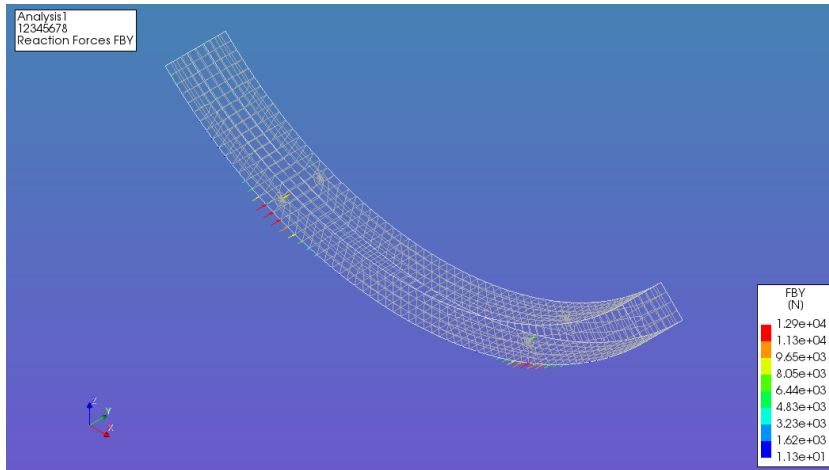


Figure AF.15: Bottom segment - start tube, reaction forces Y direction

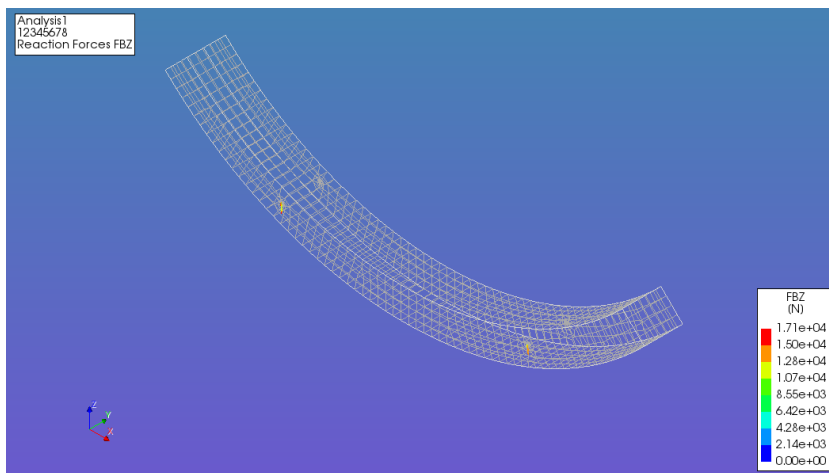


Figure AF.16: Bottom segment - start tube, reaction forces Z direction

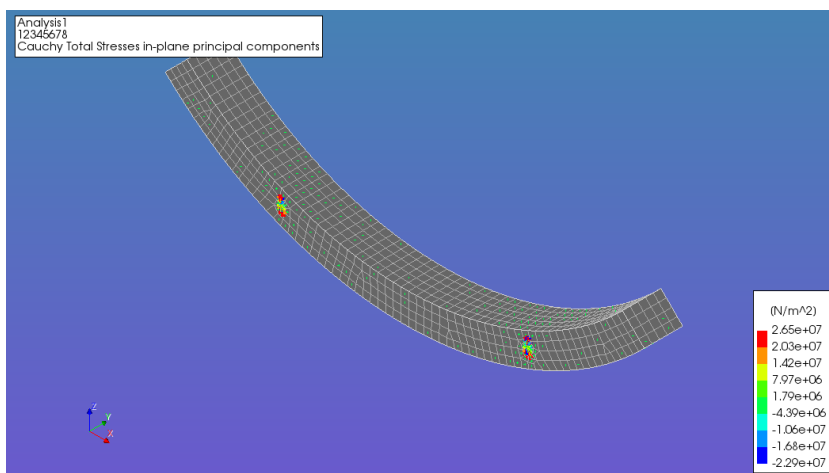


Figure AF.17: Bottom segment - start tube, principle stresses

The bottom of the segment had been modelled as a support, but it can only take compressive forces. Figure AF15 shows only compressive forces occur at the bottom of the segment. Therefore, the modelling of the bottom as a support is valid.

The results have been summarised in table AF6. A load factor of 1.2 has been applied. Table AF6 shows the forces per bolt group, with a bolt group being one pair of two bolts.

Force component	$F_E$ [kN]	$F_{Ed}$ [kN]
X	8.780	10.54
Y	84.93	101.9
Z	126.8	152.2

Table AF6: Reaction force components per connection. X and Z are perpendicular to shaft, Y is parallel to the shaft.

For the connection, it has been assumed to use 2 M24 8.8 bolts per group, with two groups per segment. This has been set as a minimum; if the tunnel design requires more bolts or a stronger connection, that would be governing. This phase solely checks whether it is feasible to construct the tube concerning the connection. The bolts required for the final situation are likely to have larger capacities. However, these bolts have been assumed for the calculations. The following parameters have been used for the design check:

Parameter	Symbol	Value	Unit
Shaft cross-sectional area M24	$A_s$	353	mm <sup>2</sup>
Material factor steel connections	$\gamma_{M2}$	1.25	-
Ultimate tensile strength	$f_{ub}$	800	N/mm <sup>2</sup>
Shear resistance factor	$k_2$	0.9	-
Tensile resistance factor	$\alpha_v$	0.6	-
Number of bolts	$n$	2	-

Table AF7: Parameters bolted connection

The tensile resistance per joint has been calculated as follows:

$$\begin{aligned}
 F_{t,Rd} &= \frac{n * k_2 * f_{ub} * A_s}{\gamma_{M2}} \\
 &= \frac{2 * 0.9 * 800 * 353}{1.25} \\
 &= 406.7 \text{ kN}
 \end{aligned}
 \tag{AE.2}$$

The shear resistance per joint has been calculated as follows:

$$\begin{aligned}
 F_{v,Rd} &= \frac{n * \alpha_v * f_{ub} * A_s}{\gamma_{M2}} \\
 &= \frac{2 * 0.6 * 800 * 353}{1.25} \\
 &= 271.1 \text{ kN}
 \end{aligned}
 \tag{AE.3}$$

The strength has been checked as follows:

$$\begin{aligned}
 u.c. &= \sqrt{\left(\frac{F_{t,Ed}}{F_{t,Rd}}\right)^2 + \left(\frac{F_{v,Ed}}{F_{v,Rd}}\right)^2} \\
 &= \sqrt{\left(\frac{F_{y,Ed}}{F_{t,Rd}}\right)^2 + \left(\frac{\sqrt{F_{x,Ed}^2 + F_{z,Ed}^2}}{F_{v,Rd}}\right)^2} \\
 &= \sqrt{\left(\frac{101.9}{406.7}\right)^2 + \left(\frac{\sqrt{10.54^2 + 152.2^2}}{271.1}\right)^2} \\
 &= 0.51 \\
 &< 1.00
 \end{aligned}
 \tag{AF4}$$

The bolts are strong enough to transfer the force. However, as seen in figure AF17 stress concentrations occur near the bolts. It is advised to apply sufficient transfer lengths for the bolt, with possible additional reinforcement.

### AF2.2. One ring - start tube

#### Bending capacity

For the bending moments, the ring has been modelled as follows:

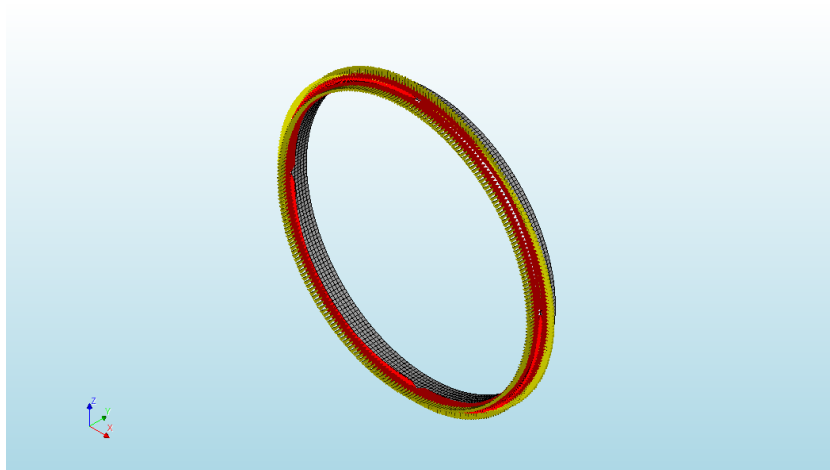


Figure AF18: Bottom segment bending moment model

The ring has a radius of 8.4 m. Its centre curves along an arch with radius 96 m and an angle of 0.3790°. The support, the line with the red arrows, is a clamped support. When the segment is attached to the tunnel, there is little to no rotation possible at this point. The results are presented in the figures below.

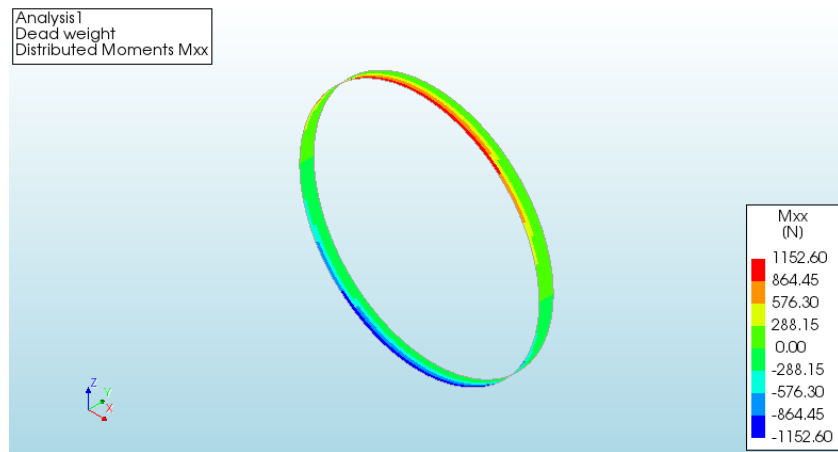


Figure AF19: One ring - start tube, Mxx

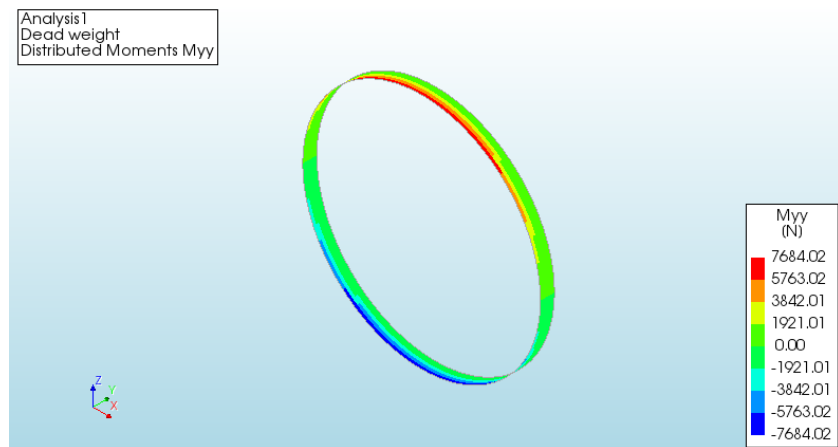


Figure AF20: One ring - start tube, Myy

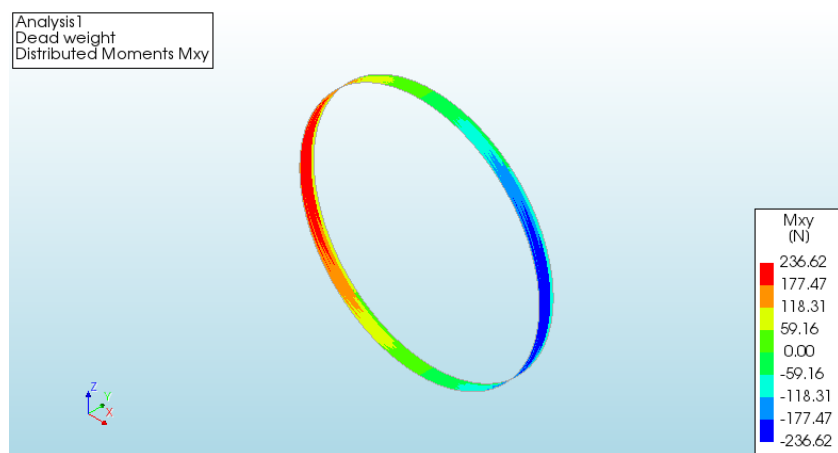


Figure AF21: One ring - start tube, Mxy



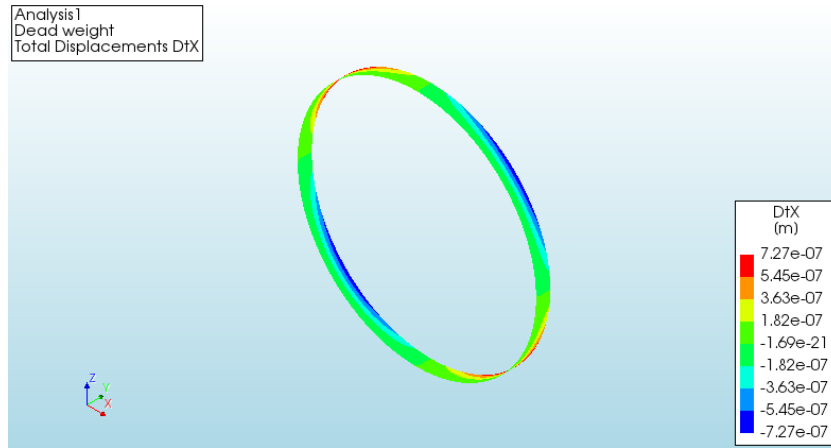


Figure AF22: One ring - start tube, X displacements

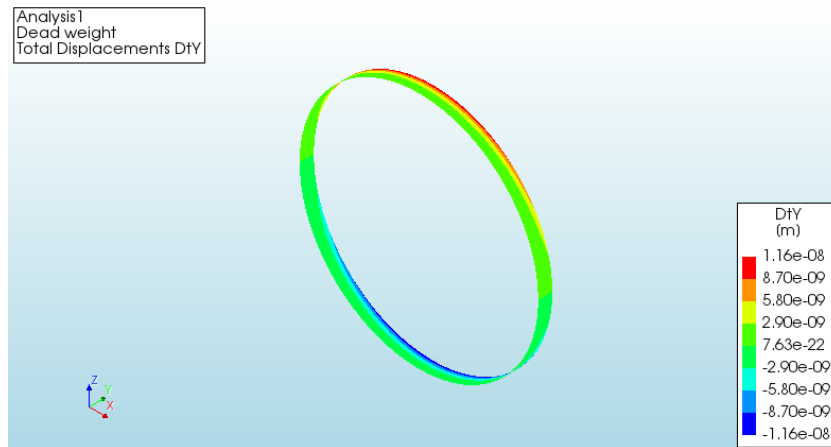


Figure AF23: One ring - start tube, Y displacements

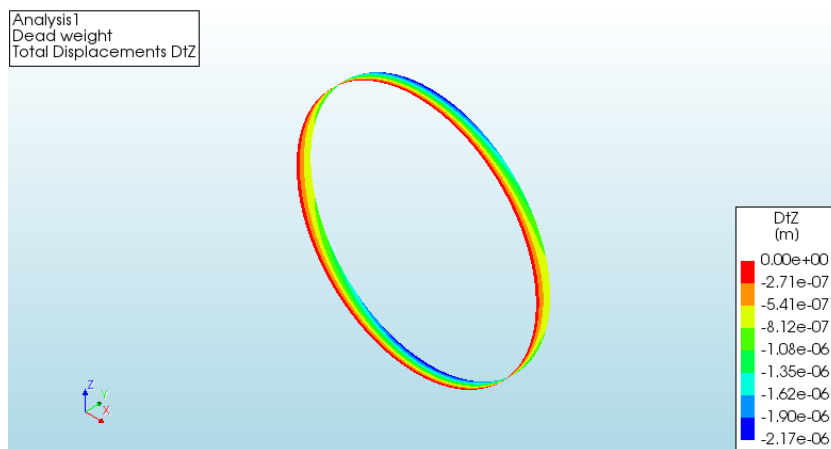


Figure AF24: One ring - start tube, Z displacements

Similar operations have been carried out as in the previous section AE2.1 to obtain the bending moments. To check the strength, the same calculations have been carried out as in previously mentioned section. The results are presented in table AF8.

Direction	$M_E$ [kNm]	$M_{Ed}$ [kNm]	$M_{Rd}$ [kNm]	u.c.
$M_{xx}$	0.5763	0.6916	2778	2.49E-04
$M_{yy}$	7.684	9.221	213.3	0.0432

Table AF8: Bending moments - start tube, one ring

The ring fulfils the strength criterion. No additional reinforcement is required for this construction stage.

### Connection

To check the connection, the following model has been used:

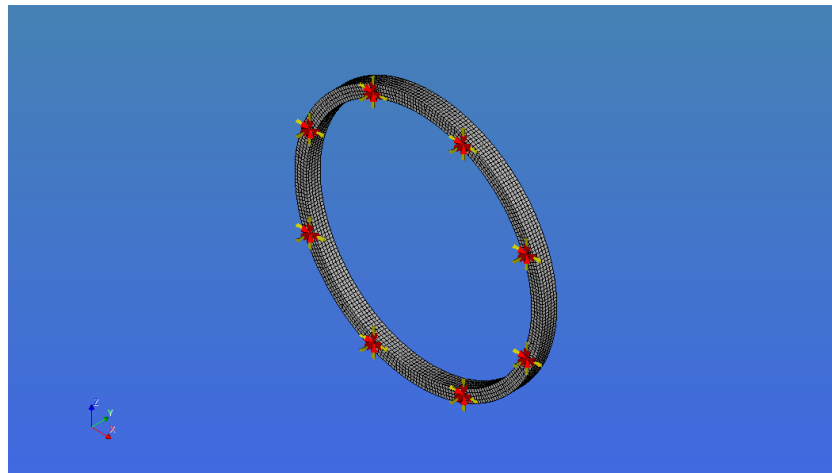


Figure AF25: One ring connection model

The ring has an inner radius of 8.0 m and an outer radius of 8.8 m. The centre of the ring curves along an arch with radius of 96 m and an angle of 0.3790°. The coordinates of each bolt group are presented in table AF9.

Bolt	x [m]	y [m]	z [m]
A1	-3.2	0	-7.7
A2	3.2	0	-7.7
B1	-7.7	0	-3.2
B2	7.7	0	-3.2
C1	-7.7	0	3.2
C2	7.7	0	3.2
D1	-3.2	0	7.7
D2	3.2	0	7.7

Table AF9: Bottom segment - start tube, centre coordinates bolt groups, with origin in the centre of the tube.

To check the strength of the bolts, similar calculations have been carried out as in the previous section AE2.1. The results of the modelling are presented in the following figures.

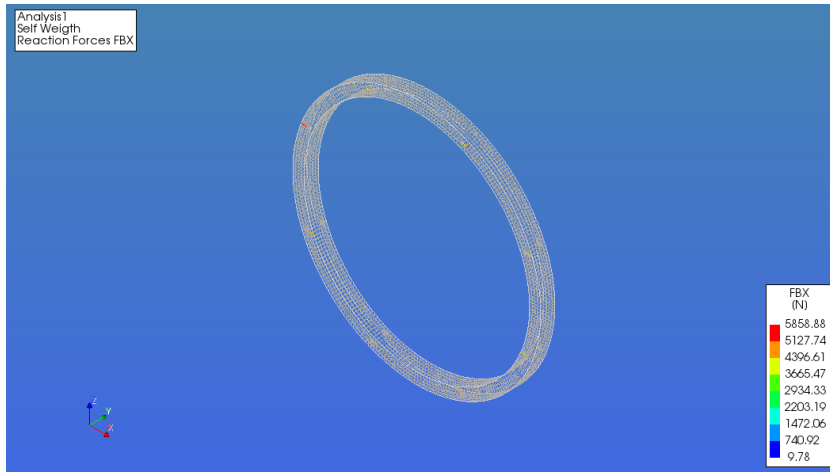


Figure AF26: Bottom segment - start tube, reaction forces X direction

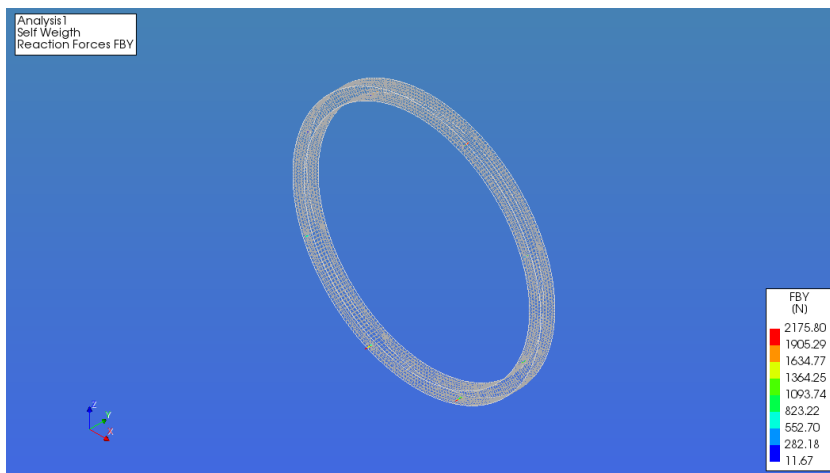


Figure AF27: Bottom segment - start tube, reaction forces Y direction

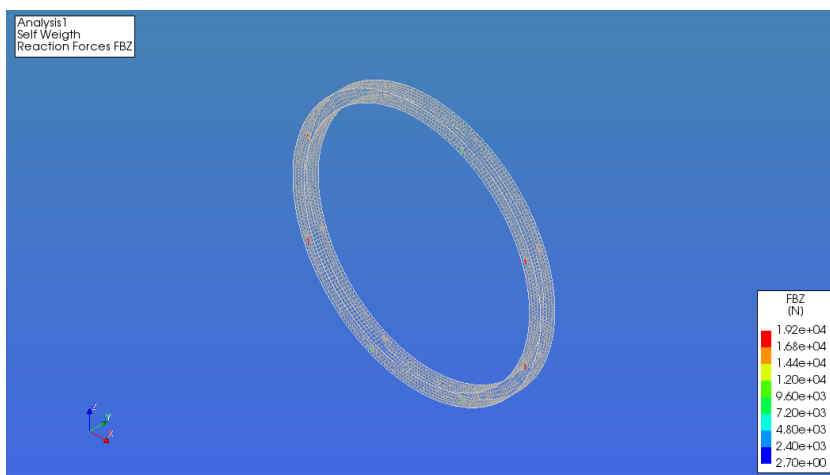


Figure AF28: Bottom segment - start tube, reaction forces Z direction

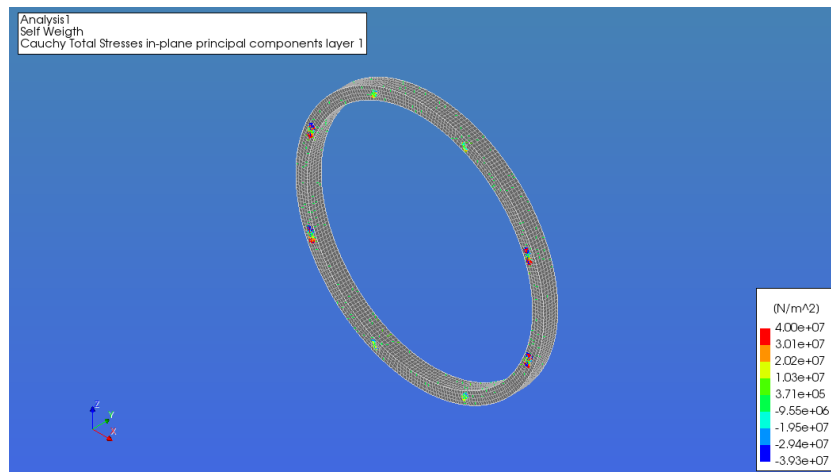


Figure AF29: Bottom segment - start tube, principle stresses

The results of the modelling and design calculations have been summarised in table AF.10.

<b>Bolt group</b>	<b>F<sub>x,E</sub> [kN]</b>	<b>F<sub>x,Ed</sub> [kN]</b>	<b>F<sub>y,E</sub> [kN]</b>	<b>F<sub>y,Ed</sub> [kN]</b>	<b>F<sub>z,E</sub> [kN]</b>	<b>F<sub>z,Ed</sub> [kN]</b>
A	44.25	53.10	0	0	83.07	99.68
B	44.09	52.91	0	0	169.9	203.9
C	43.80	52.56	5.660	6.790	171.4	205.7
D	45.03	54.04	14.16	16.99	83.01	99.61

<b>Bolt group</b>	<b>F<sub>t,Rd</sub> [kN]</b>	<b>F<sub>v,Rd</sub> [kN]</b>	<b>u.c.</b>
A	406.7	271.1	0.42
B	406.7	271.1	0.78
C	406.7	271.1	0.78
D	406.7	271.1	0.42

Table AF10: Reaction force components per connection. X and Z are perpendicular to shaft, Y is parallel to the shaft. \*Compressive forces have been set to zero, as the bolts are designed to only transfer shear and tensile forces. Bolt groups go A through D from bottom to the top.

The connection fulfils the strength criterion, as all unity checks are smaller than 1.

### AF2.3. Bottom segment - centre tube

#### Connection

The occurring forces in the connection have been obtained by rotating those at 0°30.7° upwards, as illustrated in figure AF30. The 30.7° is rotation of the centre segment compared to the first segment of the whole tube. Rotating of the forces in this manner is deemed to be on the conservative side, as it does not take into the account that part of the load will rest on the previous segment.

The forces have been transformed as follows:

$$\begin{aligned}
 F_{x,Ed,local} &= F_{x,Ed,global} \\
 F_{y,Ed,local} &= F_{y,Ed,global} * \cos(30.7^\circ) + F_{z,Ed,global} * \sin(30.7^\circ) \\
 F_{z,Ed,local} &= F_{z,Ed,global} * \cos(30.7^\circ) - F_{y,Ed,global} * \sin(30.7^\circ)
 \end{aligned}
 \tag{AF.5}$$

The strength check has been performed as done in previous sections. The results are presented in table AF11.

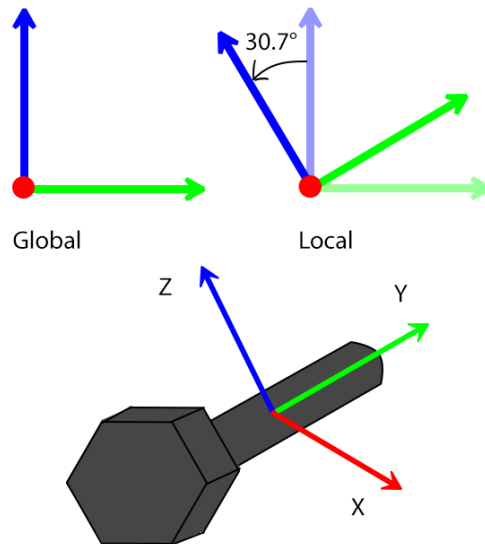


Figure AF30: Rotation reaction forces

$F_{x,Ed,global}$ [kN]	$F_{x,Ed,local}$ [kN]	$F_{y,Ed,global}$ [kN]	$F_{y,Ed,local}$ [kN]	$F_{z,Ed,global}$ [kN]	$F_{z,Ed,local}$ [kN]
10.54	10.54	101.9	165.4	152.2	78.85
$F_{t,Rd}$ [kN]	$F_{v,Rd}$ [kN]	<b>u.c.</b>			
406.7	271.1	0.50			

Table AF11: Reaction force components per connection. X and Z are perpendicular to shaft, Y is parallel to the shaft. \*Compressive forces have been set to zero, as the bolts are designed to only transfer shear and tensile forces

### AF2.4. One ring - centre tube

#### Connection

Bolt capacity has been checked in a similar way as in the previous section, by rotating the forces from table AF10 and rotating them over 30.7° in the y-z plane, as described in figure AF30. Strength calculations similar to previous sections have been carried out and are presented in the following table.

Bolt group	$F_{x,E}$ [kN]	$F_{x,Ed}$ [kN]	$F_{y,E*}$ [kN]	$F_{y,Ed}$ [kN]	$F_{z,E}$ [kN]	$F_{z,Ed}$ [kN]
A	53.10	53.10	0	50.89	99.68	85.71
B	52.91	52.91	0	104.1	203.9	175.3
C	52.56	52.56	6.790	110.9	205.7	173.4
D	54.04	54.04	16.99	76.98	99.61	76.98
Bolt group	$F_{t,Rd}$ [kN]	$F_{v,Rd}$ [kN]	<b>u.c.</b>			
A406.7	271.1	0.39				
B406.7	271.1	0.72				
C406.7	271.1	0.72				
D406.7	271.1	0.38				

Table AF12: Reaction force components per connection. X and Z are perpendicular to shaft, Y is parallel to the shaft. \*Compressive forces have been set to zero, as the bolts are designed to only transfer shear and tensile forces

The connection fulfils the strength criterion.

### AF.3. Uplift

The tube has been tested on uplift. The following scenario has been considered:

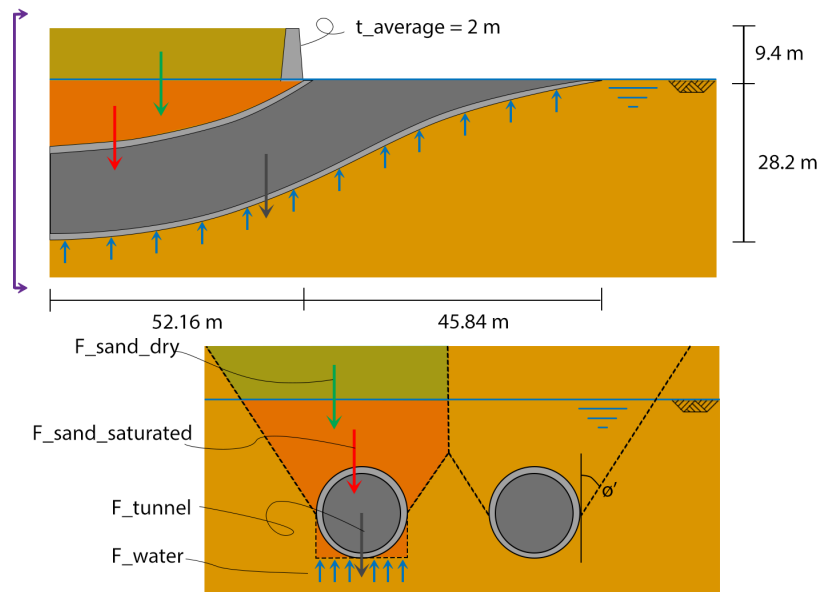


Figure AF.31: Load scheme uplift

This scenario has been considered governing. If the water level drops, upwards pressure decreases faster than the downward ones. If the water level rises, water will first flow into the tube and fill it up, before groundwater pressure increases. When the tube is filled with water, the resistance to uplift has increased, whereas the uplift force itself has not.

The following parameters have been used in the calculation on uplift safety:

Parameter	Symbol	Value	Unit
Specific weight saturated sand	$\gamma_{sand,sat}$	20.0	kN/m <sup>3</sup>
Specific weight dry sand	$\gamma_{sand,dry}$	18.0	kN/m <sup>3</sup>
Specific weight water	$\gamma_{water}$	10.0	kN/m <sup>3</sup>
Specific weight concrete	$\gamma_c$	24.5	kN/m <sup>3</sup>
Internal friction angle sand	$\Phi'$	30.0	°

Table AF.13: Parameters transition tube uplift

The volumes of the soil elements and the tube have been obtained from the Sketchup model as presented in figures AG.1, page 196, and AG.3, page 197. These volumes are presented in table AF.14.

Body	Volume [m <sup>3</sup> ]
Tube	2651
Dry sand	15998
Saturated sand	9378
Wall	330.9

Table AF.14: Volumes bodies for uplift

The total weight of the soil has been obtained by multiplying the volumes with the corresponding specific weights. The total upward water pressure has been obtained by integrating the water pressure over the bottom of the tube and multiplying it with the width. The forces can be found in table AF.15.

<b>Body</b>	<b>Force [kN]</b>
Tube	64950
Dry sand	287964
Saturated sand	187560
Wall	8106
Total downward	548580
Uplift force	451243

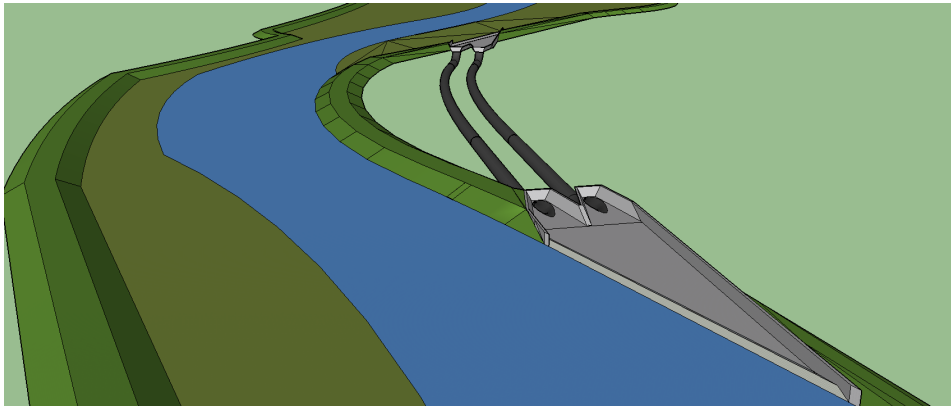
Table AF.15: Selfweight and uplift forces

For the downward force, a total of 548,580 kN has been calculated. For the uplift force, a total of 451,243 has been calculated. This results in a uplift factor of safety of  $548,580 / 451,243 = 1.22$ . The tube meets the uplift criterion, but it is advised to further investigate the uplift of the tube with a 3D FEM software.

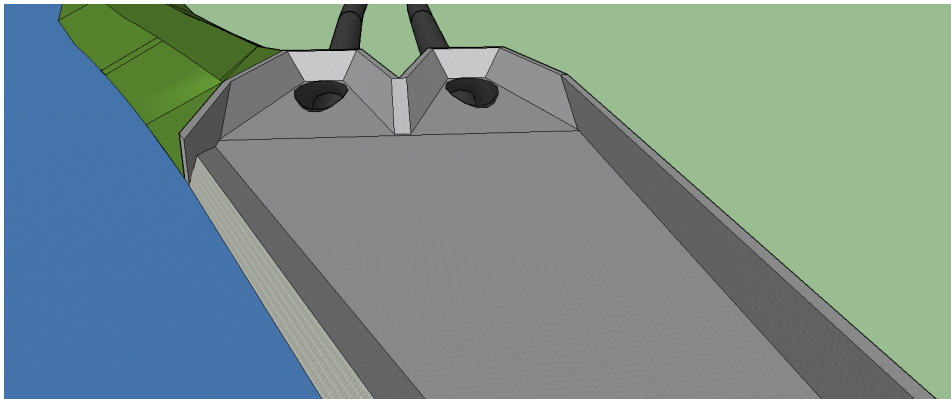
## Design inlet and outlet structure

### AG.1. Shape

Both the inlet and outlet structure have been designed as presented in figure AG.1. The high concrete walls are proposed to have a diagonally inclining shape, enabling a streamlined flow into the pipe.



(a) Inlet/outlet structure



(b) Structure close up

Figure AG.1: Outline of inlet/outlet structure

The structure consists of a sill with the top at T.P. +4.7 m and a funnel to guide the water into the tunnels. The sill acts as a threshold, allowing water only to flow into the tunnels when the flood levels exceed the top. The funnels provide a smooth transition between the sill and the tunnels, to reduce flow losses and increase discharge capacity.



## AG.2. Separation sill

A sill has been introduced to limit the amount of flow going into the tunnels. The tunnels are only to be used during peak discharges. This has been decided to ensure sufficient water flows through the Shonai River to sustain the natural habitats. Furthermore, by making less usage of the tunnel, the required amount of maintenance decreases. Additionally, the maintenance can be performed during normal discharge conditions, as there is no inflow into the tunnels.

It has been decided to use a passive inlet instead of an active one. A passive inlet has been considered to require no human input to allow water flow into the tunnel, for example with the chosen sill. An active inlet does require human input, an example would be a gate. A gate would provide more control over the water flow. However, the cost is expected to be relatively larger compared to a sill. Not only construction costs would be higher, a gate requires more maintenance than a sill.

The dimensions of the about 250 meter wide sill have been determined as presented in figure AG.2. This shape allows the design capacity of the tubes to flow over the sill. Dimensions are given in figure AG.3.

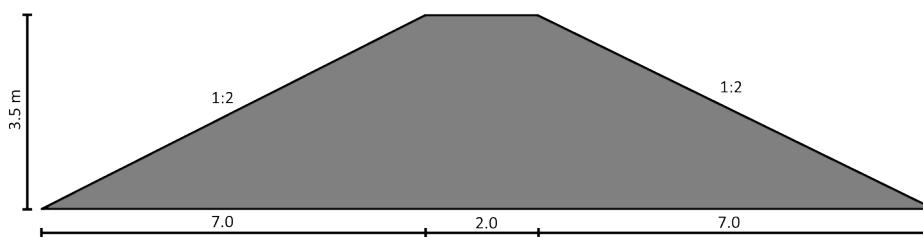


Figure AG.2: Sill of inlet/outlet structure

The integration of this design with the surroundings and nature can be realised when vegetation is allowed to grow on the concrete walls. This measure will increase the aesthetic appearance of the structure. However, adding vegetation to the structure will also increase the wall friction, which has a negative influence on the discharge capacity of the tunnels.

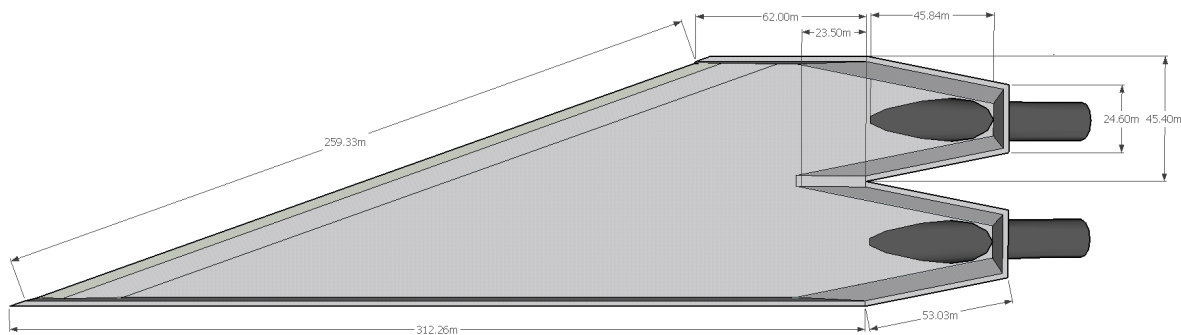


Figure AG.3: Dimensions of inlet/outlet structure

## AG.3. Flow over sill

To get an indication of the flow velocities at the sill, use has been made of a 2DV flow model in the application SWASH. The model was configured for the outlet sill, however the differences between the sills at inlet and outlet are negligible. Thus, the model also shows the situation at the inlet. It has to be mentioned that the output is only an indication since the 3D mixing effects with the river have not been taken into account.

At the outlet the flow approaches the sill under an angle. To take this into account, the dimensions of the sill in the model were increased to get a better representation of the path the flow follows. The grid was made as shown in table AG.1. The x and y are in horizontal direction, with x perpendicular to the sill and y parallel (2DV model so y is not taken into account). The total length of the model in x direction equals 100 m. The z

is in the vertical direction and is represented by 300 layers. The layers are equidistant and a percentage of the water depth.

Direction	number of meshes	mesh width
x	300	33
y	0	0
z	300	0.33d

Table AG.1: Grid characteristics of the sill model

The applied boundaries are a discharge boundary at the tunnel side and a water depth boundary at the river side of the outlet sill. The discharge at the tunnel side equals  $1487 \text{ m}^3/\text{s}$ . Having a width of  $86.8 \text{ m}$ , this results in a specific discharge of  $17.1 \text{ m}^2/\text{s}$ . The water depth during peak flow in the river at the outlet equals  $9.2 \text{ m}$ . In the model the reference level is set to an elevation of  $9.2 \text{ m}$ , thus the water level at the river side becomes zero with the bed level at  $-9.2 \text{ m}$ .

The  $k-\epsilon$  model has been used for the turbulence model together with the logarithmic wall law for determining the friction. Furthermore, to get a better approximation of the variation in the vertical direction, the non-hydrostatic pressure part has been included in the equations of the model.

Figure AG.4 gives the final result of the model, in here the flow is taken from left to right. It can be seen that the flow on top of the sill is larger, in the order of  $3.5 \text{ m/s}$ , and there is a small depression in water level on top of the sill. Right behind the sill at the bottom the flow velocity is relatively low. These results are also what is expected from literature.

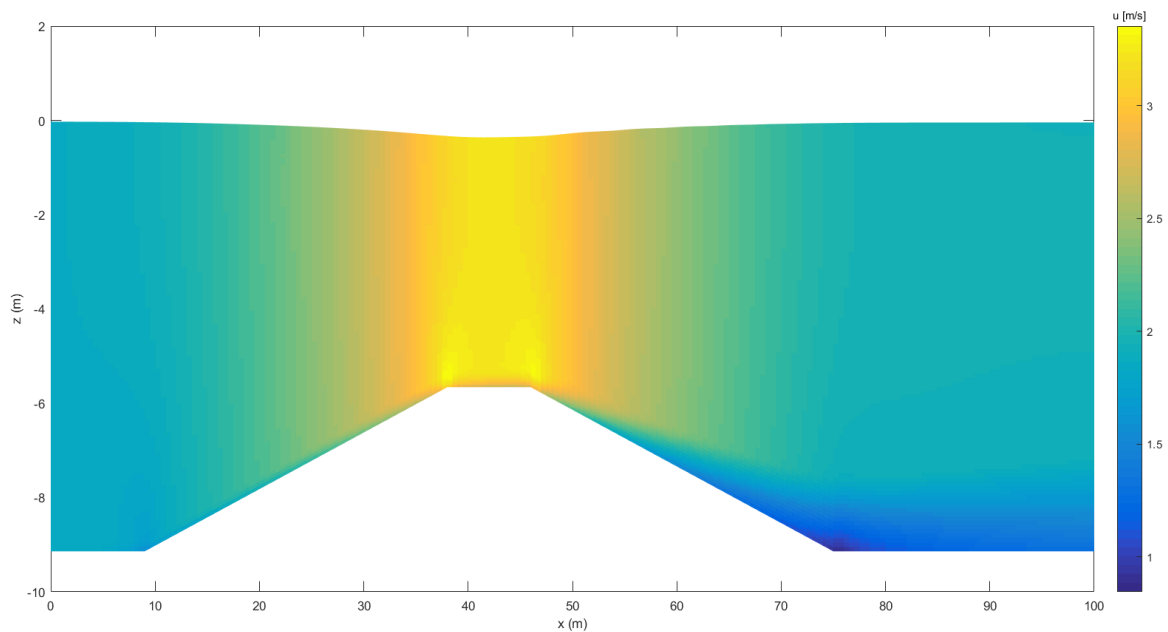


Figure AG.4: Flow profile over the sill

#### AG.4. Construction method

After a building pit has been constructed and dredged, a connection between tunnel and inlet/outlet can be constructed, see appendix AE for elaboration. Then, the connection to the river will be made. This can be most practically realised by creating a small wall around the dike which will be the future sill, dredging the dike and creating a sill. This should be no problem since water levels in the river are normally below  $2 \text{ m}$ .



## Construction Process

This appendix describes the whole construction process of the project. The process has been split up into the following steps:

1. Construction site
2. Excavation starting and reception shaft
3. Bored tunnel
4. In- and outlet tubes
5. Sill and funnel

For each of these steps, the construction process has been described. Furthermore, a planning has been made, giving a time indication of the corresponding step. Last, a cost estimate has been made for each step. For a list of all costs taken into account, see appendix AI on page 218.

### AH.1. Construction site

This section will focus on the design of the construction site, both at the inlet as the outlet structure. This section will only focus on what it will cost to create a clear building site. Cost for aspects such as the lowering of the area to create the inlet and outlet itself, are described in section AH.5. First, the inlet will be discussed. After that, the outlet will be discussed.

#### AH.1.1. Construction process of the construction site, inlet

Figure AH.1 shows the area which will be used as construction site for the inlet. As can be seen, the inlet will be constructed within an urban area. As a result, the costs to construct the inlet will be relatively high. First, the properties in the area will have to be bought. Once that has finished, the demolishing of the property can start. In total, an area of 42,000 m<sup>2</sup> will have to be cleared. It has been assumed that 90% of this area is filled with housing. When the area is clear, the construction of the building pit can start.

#### AH.1.2. Planning of the construction site, inlet

It has been estimated that removal of properties and disconnection of all utilities can be finished in 12 weeks. These utilities include power lines, water pipes, gas pipes and sewage.

#### AH.1.3. Costs of the construction site, inlet

As mentioned earlier, the area which has to be cleared equals 37,800 m<sup>2</sup>. The current price of property in this region has been estimated to be about €3000 / m<sup>2</sup> [89]. This results in a total value of €115,000,000. However, once construction is completed, an empty area is left which can be redeveloped. About 40% of the site is left unused after construction. Economic rest value can be found when this area is reused for new properties. If 90% of the area is used for new property, 15,000 m<sup>2</sup> can be sold. Of course, this will have less value than the mentioned €3000. An estimation of €1000 / m<sup>2</sup> will be used. The total rest value will be €15,000,000. This gives that the total costs of the construction site are €100,000,000.

#### AH.1.4. Construction process of the construction site, outlet

The area where the outlet has to be constructed consists of a floodplain (see figure AH.2). Because the area is not occupied by property and part of the river, it is already available without costs. However, because the

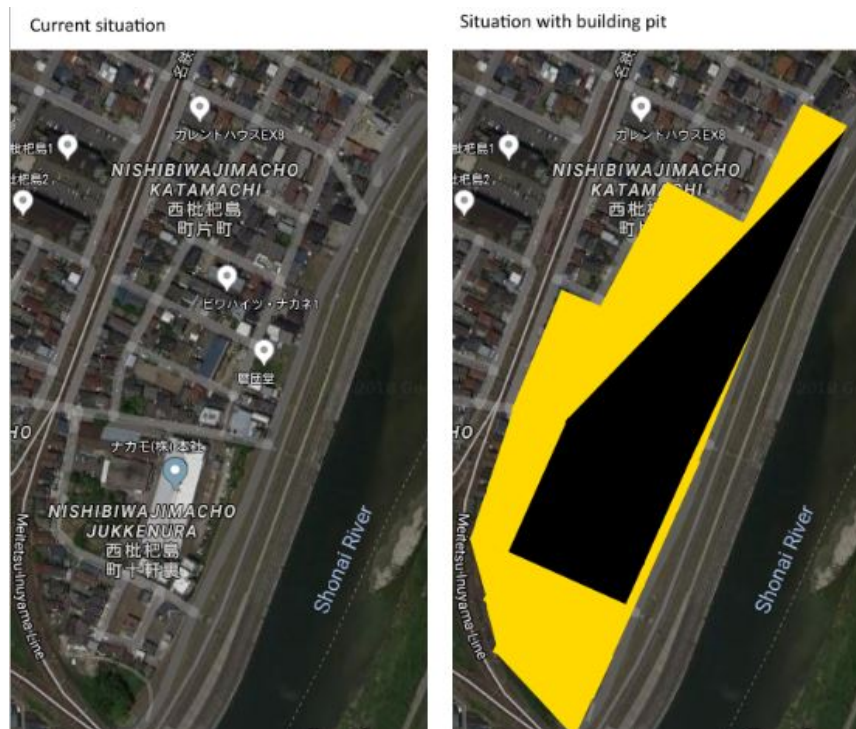


Figure AH.1: Area of building site Inlet. Left: current situation; Right: Situation with building pit; Black: Future structure; Yellow: Construction site

	<b>Dimension</b>
Crest level	T.P. +9.5 m
Height	4.5 m
Slope	30°
Volume	36 m <sup>3</sup> /m
Length	700 m

Table AH.1: Dimensions of temporary dike

area is part of the river, there is a danger of flooding. Temporary dikes should be installed around the outlet building pit, to prevent overflow into the building pit and destruction of building equipment.

The dikes will be constructed as temporary dikes (see figure AH.2). Since the building site has to be lowered to reach river bed level, soil for constructing a dike is available on site.

#### **AH.1.5. Planning of the construction site, outlet**

To estimate how long it will take to create the dike, dimensions need to be known. The crest will be constructed at a level of T.P. +9.5 m, just as the other dikes around the outlet. The current floodplain is at T.P. +5 m, resulting in dikes of 4.5 m high. When applying slopes of 30°, the width becomes 16 m. The volume of the dike becomes 36 m<sup>3</sup>/m. If the trajectory as presented in figure AH.2 is used, a 700 m long dike needs to be constructed. In total, 25200 m<sup>3</sup> of dike has to be created. Assuming 4 sets of workers, 40 hour workweeks and an estimated speed of 50 m<sup>3</sup>/h, three weeks are needed to construct this dike. In total, this equals 960 man hours.

#### **AH.1.6. Costs of the construction site, outlet**

It will cost approximately €40,-/m<sup>3</sup> to construct the dike, including labour costs. This results in a total of €1,000,000.



Figure AH.2: Area of building site outlet. Top: current situation; Bottom: Situation with building pit; Black: Future structure; Green: Temporary dike

## AH.2. Excavation starting and reception shaft

The first act in construction will be the creation of the construction shaft. The way this can be done will be discussed in the first paragraph. Process and planning will be discussed as well. The costs of the excavation stage will be discussed separately. In total there are 12 phases, which will be discussed separately.

### AH.2.1. Construction process

#### Phase 0

During phase 0, depicted in AH.3, nothing is constructed. The building site is just being cleared. The materials and machines required for the first steps will be installed in the weeks before construction. For example, it will take some time to install the bentonite plant required for the diaphragm walls. In total, 4 weeks are reserved for this phase.

#### Phase 1

In phase 1, see figure AH.4, conducting structures are placed on top of the future diaphragm wall. This will help the soil cutter to cut the wall out at the correct location. It is estimated it will take a week to place all those structures, covered by two workers, equal to 80 work hours. This will be done simultaneously with the last week of phase 0.

#### Phase 2

In week 5, phase 2 can start. In this phase, all diaphragm walls can be constructed. See figure AH.5 for a depiction of this phase. The soil excavation will be done with a wall cutter, see figure AH.6. It has been estimated that this can cut a wall of 5 m within a day. The walls will reach a depth of 34 m and are 1.5 m wide, which means that  $255 \text{ m}^3/\text{day}$  has to be excavated. The building pit is 66 m wide and 100 m long, so in total 340 m of wall have to be cut. Therefore, it will take 68 days (14 weeks) to cut out the walls. Once the walls are cut out, the reinforcement has to be installed. The soil cutter needs to be lifted by a crane due to its size. Therefore, a crane, needs to be present during this whole phase.

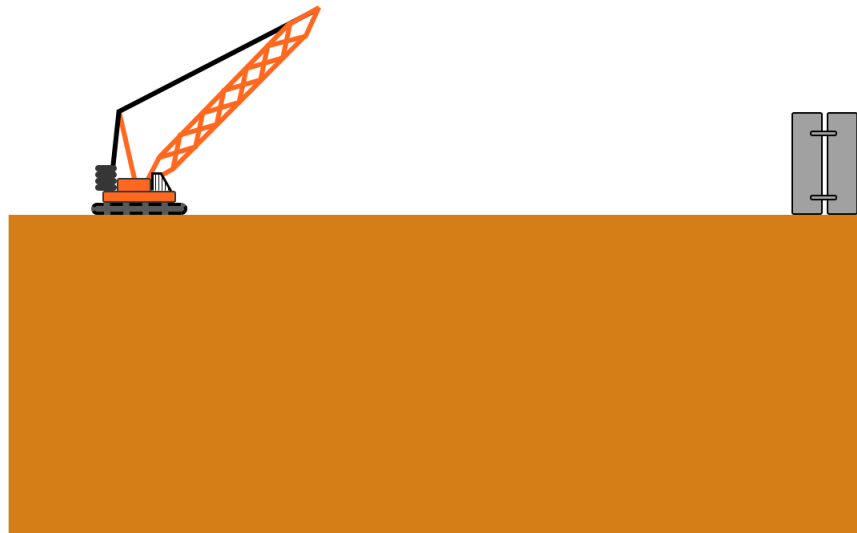


Figure AH.3: Phase 0, clear construction site, installations installed

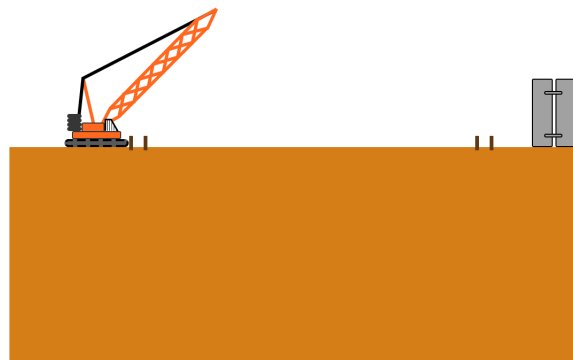


Figure AH.4: Phase 1, placing conducting structures

No concrete has been installed yet at this phase. To keep the excavated shaft stable, the bentonite is injected while excavating. During the whole phase, the bentonite plant has to be active.

Once the soil has been excavated, the reinforcement as to be installed. To do this, the crane will release its cutter, lift up the reinforcement, and let it down into the bentonite. This concludes that the crane needs a minimum height of 34 m.

As mentioned before, it will take 68 days to construct all the walls. In total, 14 weeks will be planned for this phase. It has been assumed the crew can dig the wall with 5 workers. In the end, this phase will require 2800 work hours.

### Phase 3

In week 19, the excavation of the pit can start. The total surface which has to be excavated is  $6600 \text{ m}^2$ . The surface is at T.P. +3 m. The water level is expected to be at T.P. +1 m. This means that the first 3 m can be excavated using an ordinary excavator. The subsoil consists of sand and gravel, so lowering the ground water table by pumping is not an option. From this level on, the pit has to be excavated using excavators with a very long reach. If this will be done from the sides, the longest reach such an excavator has to do is 35 m. Since the required length will increase in the next phases, this cannot be done from the side of the pit. It has to be done from a pontoon. In this phase, 7 m has to be excavated this way, to reach a level of T.P. -10 m. It is estimated this excavator can excavate  $1000 \text{ m}^3/\text{day}$ . Using two excavators, it will take 33 days to fulfil this phase. 33 days are rounded up to 7 weeks. It has been assumed that it will cost 6 workers full-time, in total 1680 work hours.



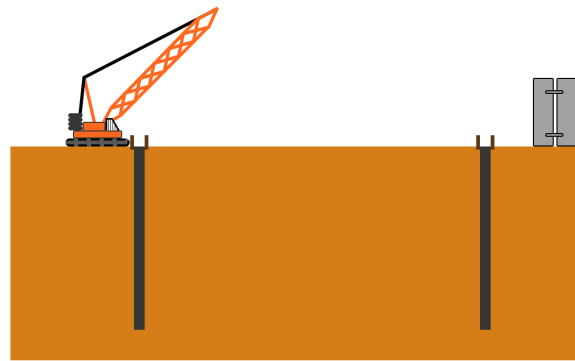


Figure AH.5: Phase 2, constructing diaphragm walls

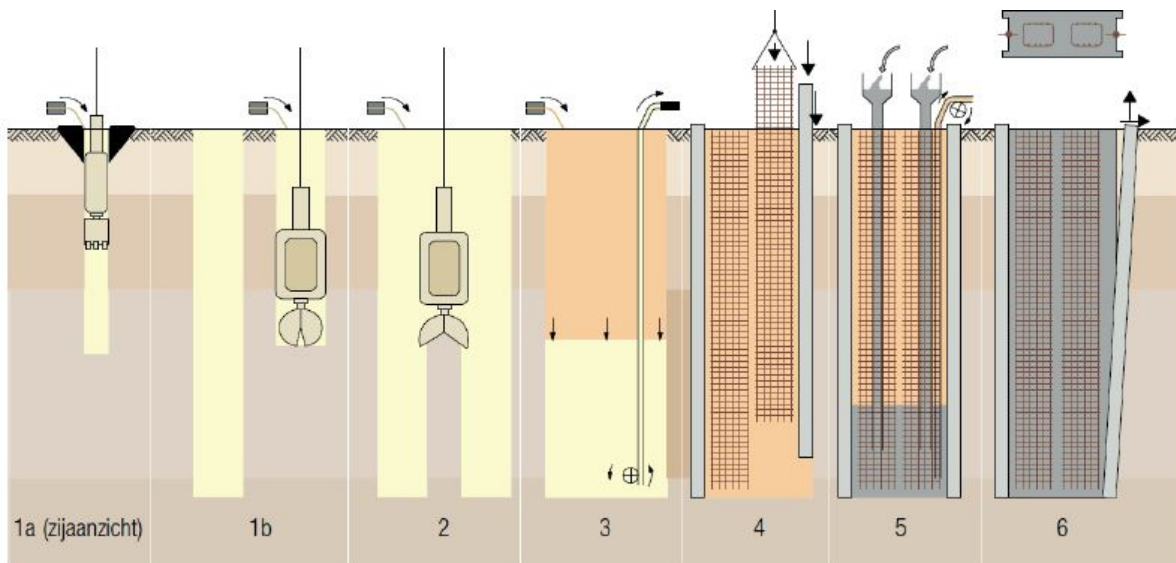


Figure AH.6: Steps to create a diaphragm wall

This phase will end in week 26.

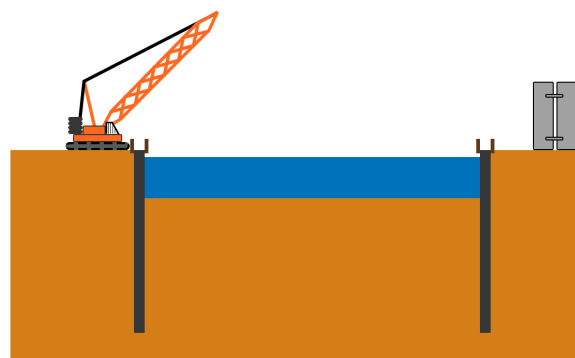


Figure AH.7: Phase 3, excavating the pit

**Phase 4**

The diaphragm walls are still unsupported in phase 3. The first anchor wall was planned at T.P. -5 m. The anchors will be installed from the pontoon as well. The anchors have a centre to centre distance of 2 m, so there are 166 anchors per row required. It has been estimated that one machine can install one anchor every hour. Using two machines, it will take 2 weeks to install the anchors. It is again assumed that 4 workers will be present per machine. This leads to 640 work hours in this phase.

This phase will start in week 26. The excavators are not fully finished with their phase, but they will be at one end of the pit, while the anchoring can start at the other end. When this phase finishes in week 27, the excavators will already be started with the next phase. They will start in week 27 at the location where the first anchors were installed.

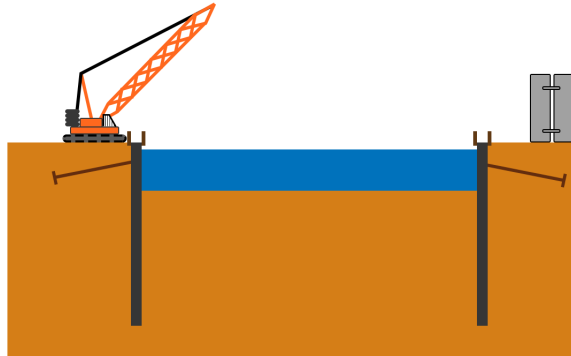


Figure AH.8: Phase 4, installing first wall anchor row

### Phase 5

In this phase, the excavating continues digging to a depth of 2 m below the next anchor row. This depth is at T.P. -17 m. This results that 12 m has to be excavated. This will take 8 weeks and 1920 work hours. This work will be done between the week 27 and week 34.

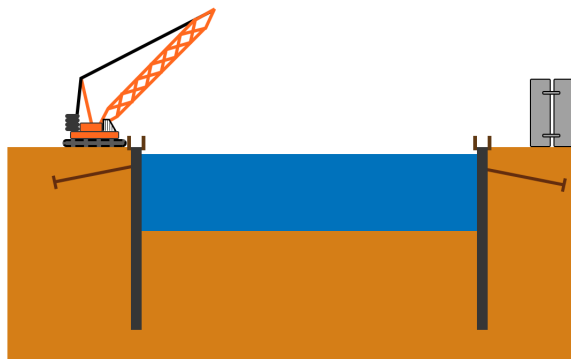


Figure AH.9: Phase 5, excavating the pit

### Phase 6

In order to excavate further in phase 7, the second anchor row will be installed in this phase. Just like with the first row, this will take 2 weeks and 640 work hours, executed in week 34 and 35.

### Phase 7

Phase 7 marks the last excavation stage, in which excavation will continue till the bottom level of the pit: at T.P. -28 m. 11 m has to be excavated to reach this level. This will take 7 weeks and 1680 work hours. Work will run from week 35 to week 41.

### Phase 8

In order to excavate further in phase 9, the third anchor row will be installed in this phase. Just like with the first row, this will take 2 weeks and 640 work hours, executed in week 41 and 42.

### Phase 9

Before the UWC floor can be installed, tension piles have to be installed. The UWC floor and tension pile plan have not been designed, but assuming those piles are placed every 3 m in both directions, 726 piles are required. Those will be installed from the pontoons as well. Using 2 machines with each 4 workers. It has been assumed it takes half an hour to install a single tension pile. As a result, it takes 5 weeks to install all the piles. This results in 1600 work hours, executed in week 43 to 47.



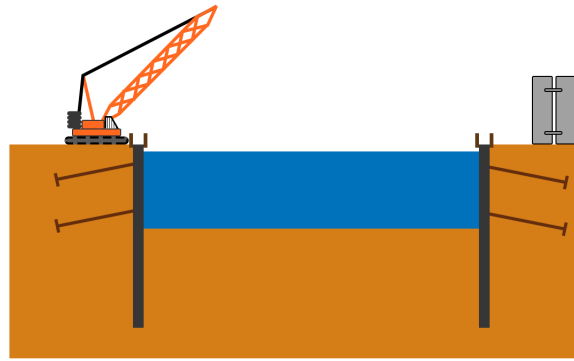


Figure AH.10: Phase 6, installing second wall anchor row

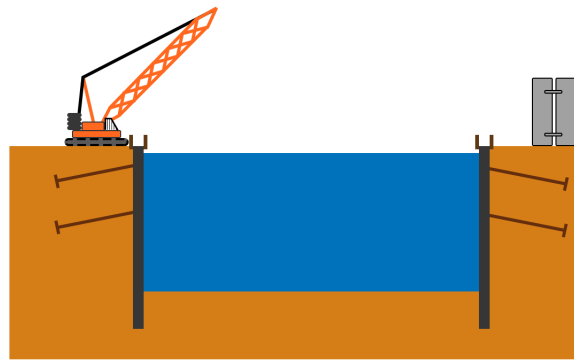


Figure AH.11: Phase 7, excavating the pit

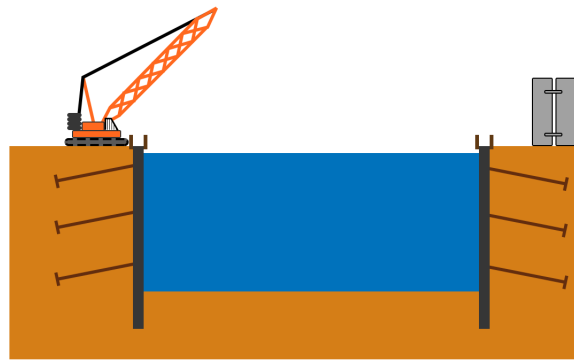


Figure AH.12: Phase 8, installing third wall anchor row

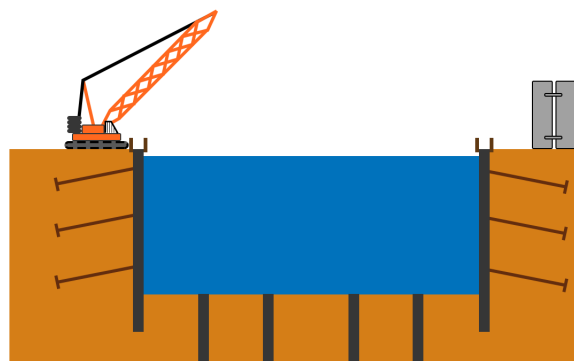


Figure AH.13: Phase 9, installing tension piles

### Phase 10

In phase 10, the UWC floor will be installed. This has to be done without a pause, so the work will go on 24 hours a day. It has been assumed that the work is completed within 5 days. The required crew consists of about 20 workers. This leads to 2400 work hours. The work will be done in week 47.

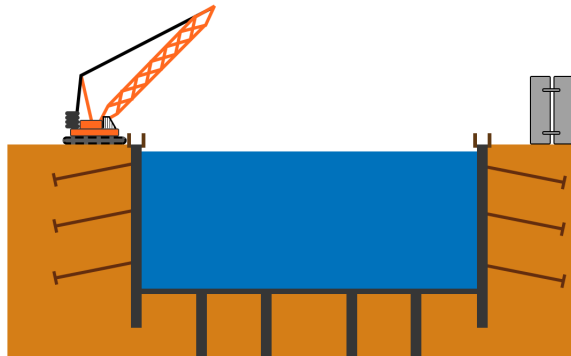


Figure AH.14: Phase 10, installing UWC

### Phase 11

The last phase will be used to pump the pit dry. This phase will be executed in week 48. This phase will not require many work hours. Week 49 will be used to let the UWC dry and finish the starting and reception shaft. From week 50 on, the shaft can be used by the TBM.

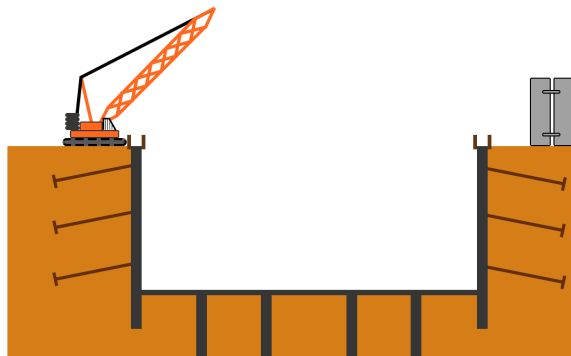


Figure AH.15: Phase 11, anchoring the walls

To sum up, it takes 49 weeks and 14,080 working hours to construct the building pit. It is assumed that during the whole process 10 extra workers are present to support the construction. This gives that the total working hours comes to 33,680 hours. The construction of the pit at the outlet will not start at the same time. When certain equipment is not required anymore at the first pit, it will be moved to the second one and run the same phase there again. A week in between is given for transport. This gives that the equipment for the diaphragm walls is needed for 29 weeks and the excavation machinery 75 weeks. The equipment for the tension piles and the UWC will be rented for two periods, one periods per pit. At each pit, a crane will need to be present. The costs of these cranes are not included in this section, but are included in a general section which will be discussed later.

## AH.2.2. Planning

The planning for the construction of the building pits has been presented in the following tables:

Phase	Start week	Weeks
Site preparation & installing equipment	14	4
Construct diaphragm walls	18	14
Excavate pit & install anchors	32	24
Driving tension piles	56	5
Cast underwater concrete floor	61	1
Pumping dry pit & curing UWC floor	62	2

Table AH.2: Construction phases excavation pit inlet

Phase	Start week	Weeks
Site preparation & installing equipment	32	4
Construct diaphragm walls	36	14
Excavate pit & install anchors	50	24
Driving tension piles	74	5
Cast underwater concrete floor	79	1
Pumping dry pit & curing UWC floor	80	2

Table AH.3: Construction phases excavation pit outlet

### AH.2.3. Costs

The costs has been calculated for both the pits together. First, the costs of equipment are given. For cost explanations, see appendix AI. After that, the material costs are defined per pit. The prices are based on a fact sheet on soil and water retaining structures [90]. In tables AH.4 and AH.5, the prices can be found. The equipment costs €2,400,000, the materials for 1 pit costs €10,500,000. With 33,680 man-hours estimated, the cost is increased by €1,347,200, assuming a rate of €40 / hour. This brings the total costs to €24,747,200.

Equipment	Weeks used for both pits	Costs	Total costs
2 Excavators	74	€ 7,500/week/piece	€ 1,100,000
2 Anchor drivers	12	€ 20,000/week/piece	€ 480,000
6 pontoons	32 (average)	€ 1,500/week/piece	€ 288,000
2 piledrivers	8	€ 20,000/week/piece	€ 320,000
UWC installing equipment	2	€ 100,000/week	€ 200,000
		Total	€ 2,388,000

Table AH.4: Total equipment costs

Material	Quantity	Price	Total costs
Diaphragm wall	34680 $m^3$	€ 350/ $m^3$	€ 12,138,000
Excavation of soil at diaphragm wall	22,600 $m^3$	€ 20/ $m^3$	€ 452,000
Anchors	996	€ 600/Anchor	€ 597,600
Excavation of the soil, wet	448,800	€ 8/ $m^3$	€ 3,590,400
UWC	13,200 $m^2$	€ 250/ $m^2$	€ 3,300,000
Tension piles	1,452	€ 600/Pile	€ 871,200
		Total	€ 10,474,600

Table AH.5: Total material costs

### AH.3. Bored tunnel

The costs and the planning of the bored part of the tunnel have been determined in this section. To determine those two, reference information has been used. Unfortunately, very detailed information on the costs and planning of bored tunnels are unavailable. The number of tunnels bored yearly is small. Companies do not publish exact numbers, only total project costs and planning. A reference project with a public planning has been used. Although the provided planning has not much detail, it provides a well defined initial estimate. This project consists of boring a tunnel in The Hague, the Netherlands. The planning is roughly based on this boring process [91]. The costs are based on data from the course 'CIE5305 Bored and immersed tunnelling' given at the TU Delft, September 2017 [13].

#### AH.3.1. Construction process

The construction process of a bored tunnel has been described in appendix AB.

#### AH.3.2. Planning

An overview of the planning of the bored tunnel is presented in table AH.6.

Phase	Start week	Weeks
Supplying TBM parts	58	1
TBM assembly	59	8
Boring tunnel #1	67	15
Transport TBM back to start	82	4
Boring tunnel #2	86	15
TBM disassembly	101	6

Table AH.6: Construction phases tunnel boring

Once the starting shaft is complete and the reception shaft is near completion, the boring process can start. Before the boring can start, a lot has to be done. First of all, the TBM has to be delivered to the building site. Then, on a part of the site, it has to be partly assembled out of sub-parts before going into the shaft for the final line-up of the TBM. The construction of the bore shield will be done in sub-parts and be assembled on site. Assembling all sub-parts will take approximately 4 weeks. The assembling of different parts can take place at the same time. The time between the first arrival of the first sub-parts and start of the assembling takes approximately 1 week. When the first parts arrive on site, it will take 5 weeks until the first parts will enter the starting shaft. Once down in the shaft, it will take another 4 weeks to assemble all the parts together to form the TBM. Once the TBM is assembled, it is ready to start boring.

When the bore has removed the first meters and is on full speed, it can excavate between 10 and 20 metres a day. To reach this number, the bore has to be operational 24 hours a day, 7 days a week. The distance between the shafts is 1000 m. This gives that it requires the TBM approximately 75 days to reach the end. The start and end of the bore process requires some more time. This has two reasons. Firstly, the required precision around the shafts is much higher than halfway the tunnel. Secondly, the soil around the shaft is grouted to prevent soil instability (see appendix AB). This has as a result that it is harder to bore through the soil. It has been estimated that it takes about two weeks extra to get into the soil and out of it each, so 4 weeks extra in total. In the end, it takes 103 days to get from one shaft to the other, which is rounded up to 15 weeks.

Once the TBM has arrived in the reception shaft, it has to be disassembled, transported back to the start shaft, and assembled again for the boring process of the second tunnel. Because the first tunnel is already bored, the TBM can be transported through this tunnel. The bore shield, including the steel shell, has to be disassembled again because this does not fit within the tunnel lining, but the other parts can be returned immediately and placed again in the starting shaft. Once disassembled, the shield is disassembled, transported, and assembled in the starting shaft again. This whole process is expected to take 4 weeks. Again, it will take another 15 weeks to get the TBM in the reception shaft. Once arrived in the shaft, the TBM is separated into multiple parts again, taken out of the shaft, separated further into sub-parts, and removed from the building site. In total, it will take 6 weeks to remove the total TBM from the building site.

Diameter	6	8	10	13	18 (2500 m)	18 (1000 m)
<b>TBM</b>						
Purchase	8180	11930	17720	27270	45000	45000
Mobilisation	850	1120	1430	2040	2700	2700
Turn around TBM	610	750	880	1150	1600	1600
Demobilisation	270	340	440	640	1300	1300
Rest value	-1020	-1360	-1700	-2380	-3300	-3300
<b>Other installations</b>						
Purchase	810	1360	2110	3400	6600	6600
Mobilisation	510	680	1020	1700	3000	3000
Turn around TBM	230	300	400	680	1000	1000
Rest value	-400	-680	-1050	-1700	-2500	-2500
<b>General</b>						
Removal soil	2410	4280	6690	11300	20000	7200
Lining	24710	38760	62140	90340	250000	90000
Groutinjection	1200	1600	2000	2600	3800	1368
Cables	4090	5110	6470	8520	12000	4320
Bentonite	1060	1880	2940	4970	9000	3240
Energie	2380	2880	3560	4220	5500	1980
Maintenance	2410	4280	6770	11300	22000	7920
Saleries	15110	17180	20440	24980	31000	11160
Subtotal	63410	90410	132260	191030	408700	182588
Extra's	20%	20%	20%	20%	20%	20%
Total	76092	108492	158712	229236	490440	219105,6
Total per m	15,2	21,7	31,7	45,8	98,1	121,7

Table AH.7: Tunneling costs of several TBM diameters. Costs in €, x1000

### AH.3.3. Costs

The costs are, as mentioned above, based on very indicative but detailed standard costs. An overview is given in table AH.7. Costs are specified for tunnels bored with a TBM with a diameter of 6 m, 8 m, 10 m and 13 m. The costs are based on two tubes, each with a length of 2500 m. To get to the costs of a TBM with a diameter of 18 m, the costs are estimated based on the other diameters. This is done for two tubes with a length of 2500 m. Now, the costs are translated to a length of 1000 m. In table AH.7 it has been found found that 2 tunnels of 900 m costs approximately 183 million euros. This has been rounded up to €185,000,000.

### AH.3.4. Additional safety measurements

The bore technique of tunnels has proven itself to be a reliable and safe technique. However, when management is not done well it can become a dangerous technique. The main risks occur at the bore shield. As shown in appendix AB, the shield pressure has a certain range to be in to guarantee safety. The pressure has to be monitored continuously to adjust it when it becomes too high or too low. The soil data in a final design is based on tests made on several locations. Data of each part of the trajectory is unlikely to be obtained, as it requires excessive soil probing. Therefore, uncertainties in the soil data will be present. This may result in a bore shield pressure that can be too low or too high, although it is within its calculated range. When this occurs, settlements can occur at ground surface. To prevent unfavourable effects on surface, the surface should be monitored along the tunnel route. When monitoring gives that settlements are developing in an unexpected way, the shield pressure can be adapted to prevent too large settlements. Monitoring of the ground surface can be done by conventional monitoring.

### AH.4. In- and outlet tubes

This section concerns the construction, planning and cost estimate of the S-shaped transition tubes at both ends of the tunnel. These can be seen in figure AH.16.

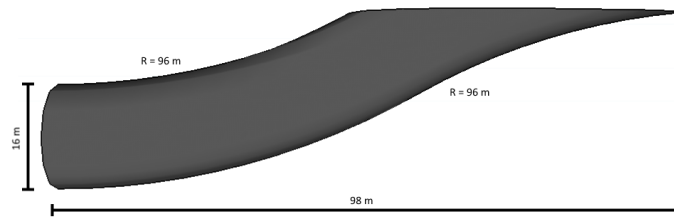


Figure AH.16: Transition tube surface to tunnel

#### AH.4.1. Construction process

After the TBM has been disassembled, construction of the inlet and outlet tubes can start. A general overview of the construction process is given in figures AH.17 and AH.18.

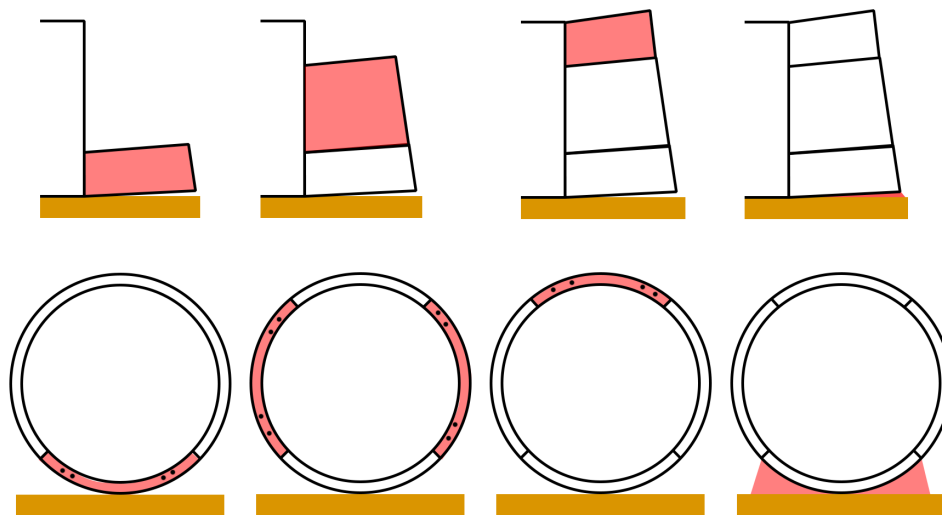


Figure AH.17: Construction process transition tube. Red parts indicate construction steps.

The construction process of the tubes consists of the following actions, in chronological order:

1. Constructing concrete tubes
2. Backfilling excavation pit
3. Compacting soil
4. Scabbling / removing upper part tubes
5. Applying epoxy layer

The constructing of the concrete tube and the backfilling are carried out simultaneously. The scabbling of the top is to happen after the concrete funnel on the surface has been constructed.

#### Constructing concrete tubes

Lowering of the concrete segments has been illustrated in the following figure:

Elements can be attached to the crane using the bolt holes already present, the ones required for connecting the segments. Special bolts can be bolted into the segment to allow for it to be hooked to the crane. This can be seen in figure AH.20.

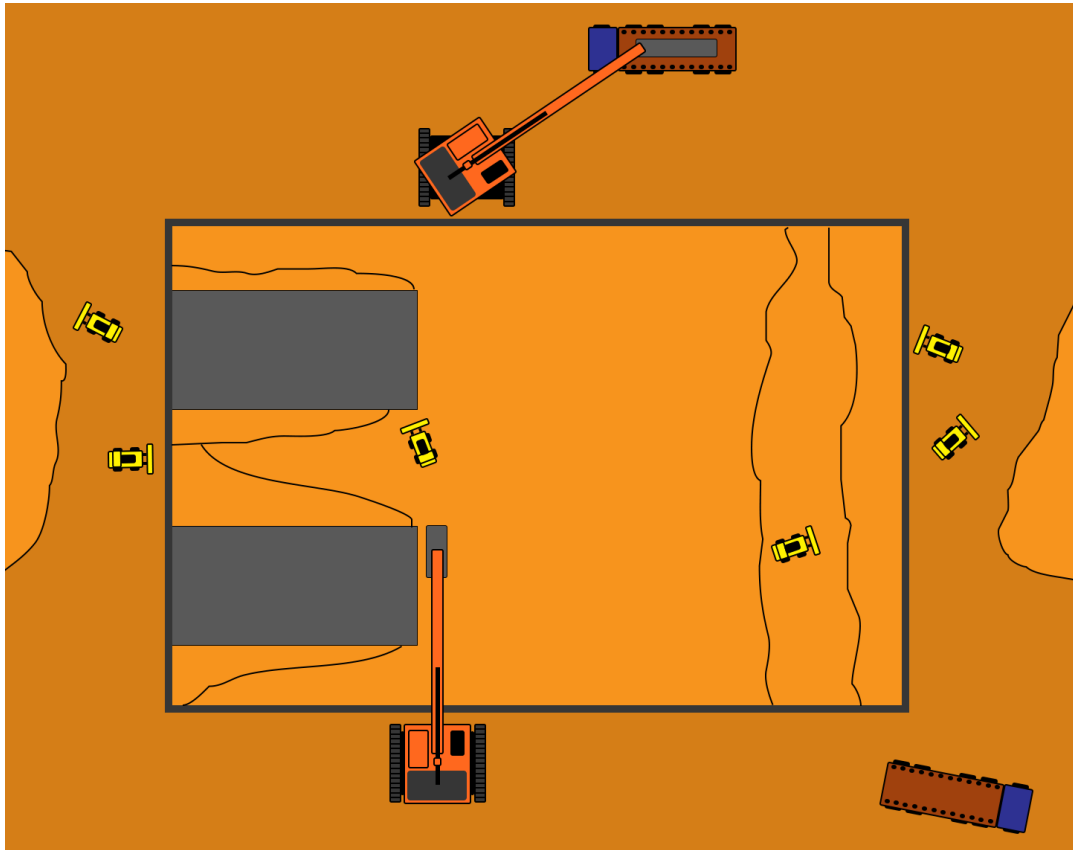


Figure AH.18: Top view construction site

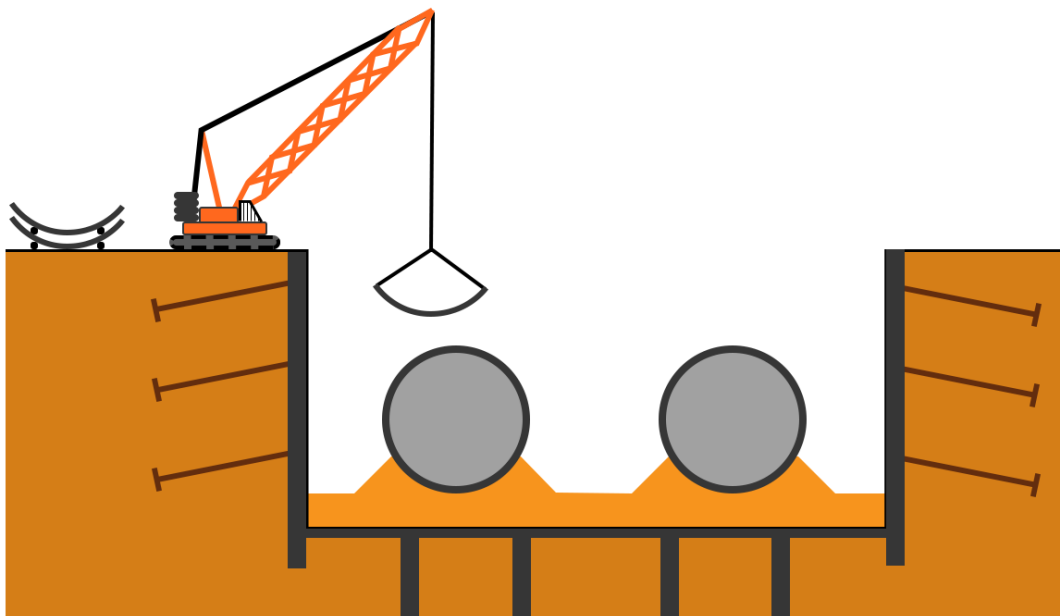


Figure AH.19: Lowering of concrete segments tube

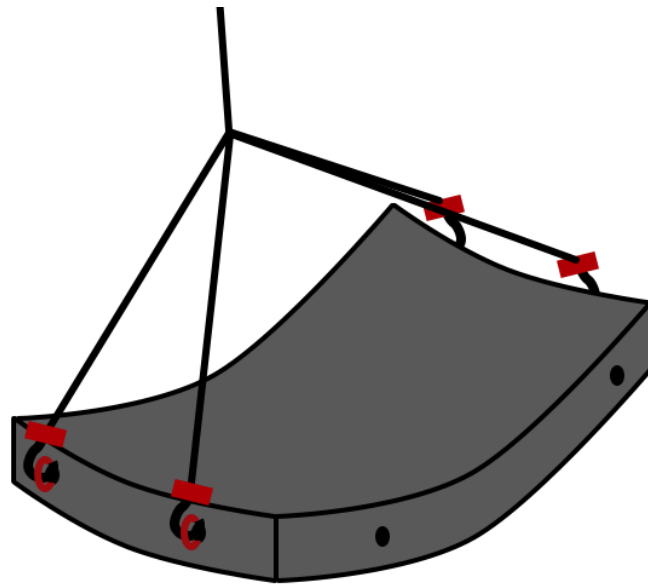


Figure AH.20: Connection segment to crane

When still attached to the crane, the segment is attached to the existing part of the tunnel using bolts. When the segment is attached to the tunnel, the crane is disconnected after which it can go and pick up the next segment. Meanwhile, the connection bolts are removed from the segments, these can be taken up by the crane next time it goes to collect a new segment. Crew on the surface can take these bolts and already attach them to new segments prior to the crane picking them up. The same cranes are to be used as for the diaphragm walls and assembling and supplying the TBM.

Two tubes are to be constructed at both the inlet and the outlet, as there are two tunnels. Construction of the tubes is to start at the outlet side. Cranes are already present, as they have just disassembled the TBM. Both tubes will be worked on at the same time. After both tubes have been completed at the outlet, construction will start on the ones at the inlet. In a later phase, the top part of the tube is to be removed, until it is level with the surface. Hence, it is not required to make full circles at the top.

#### Backfilling excavation pit

The other main action during the construction phase of the tubes is the backfilling of the excavation pit. This will happen gradually during the construction of the tubes. The sand will be propped up underneath the tube to act as a support. The process is illustrated in figures AH.21 and AH.22.



Figure AH.21: Backfilling process



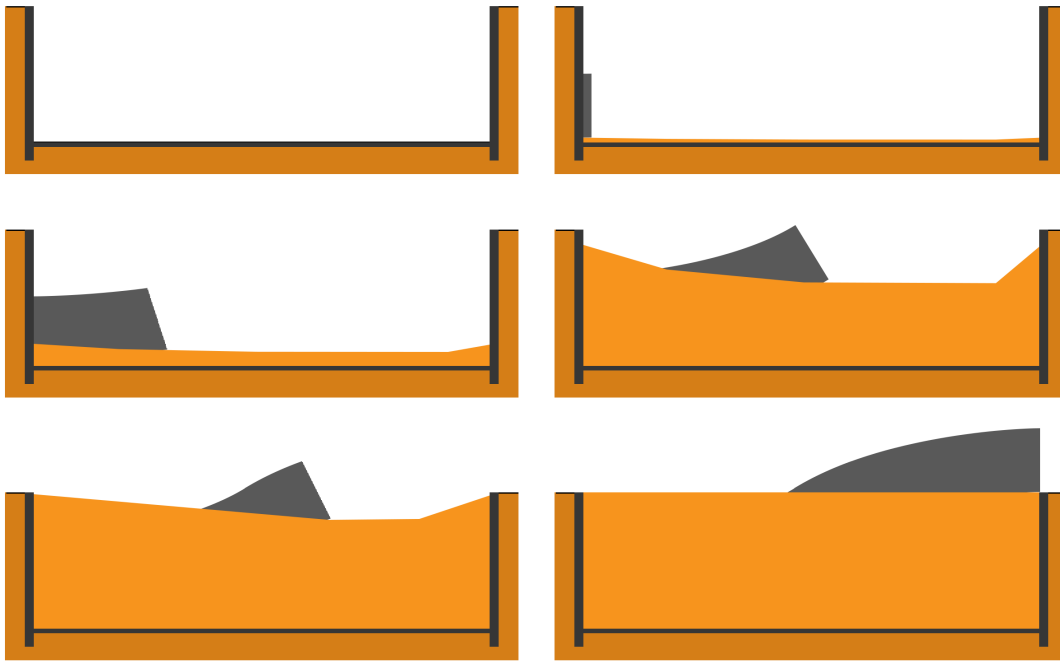


Figure AH.22: Backfilling process

When a ring is completed, loaders will move sand underneath the tube to act as a support. Sand will be supplied by bulldozers dumping sand over the edge. Gradually, the excavation pit will be filled up with the sand, with its level going up with the tube. The loaders can be lowered into the building pit using the cranes.

**Compacting soil**

After the excavation pit has been backfilled, the soil is to be compacted. By doing so, the tube will remain on the desired level. When the tube were to settle too much relative to the concrete funnel on the surface, leakage might occur, causing scour. The compaction is to be done using vibrating rollers.

**Scabbling / removing upper part tubes**

The scabbling of the top part of the tubes is to happen after the floor of the funnel has been cured, marked in red in figure AH.23. The top part of the tunnel is to be removed to improve the flow of the water. If the whole tube were to remain, it would introduce too much energy losses in the flow, reducing the efficiency of the tunnel. The tube is therefore to be levelled to the top of the concrete floor. The rubble is later to be removed from the tube by the loaders.

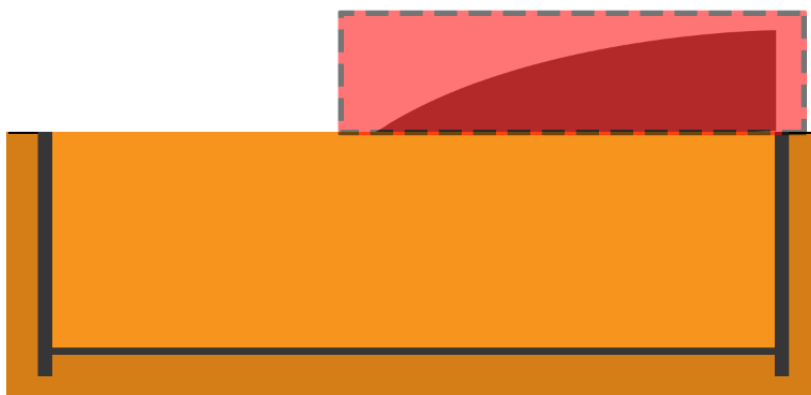


Figure AH.23: Part tube to be removed indicated in red

### Applying epoxy layer

In order to achieve the required discharge capacity, the tunnels are to be lined using an epoxy coating. By doing so, the smoothness of the tunnel increases, allowing for more discharge. The epoxy is to be applied over the whole surface on the inside of the tube. Similar operations have been carried out [92, 93], where tunnels have been coated with epoxy membranes. To achieve this, spray equipment as seen in figure AH.24 is to be used.



Figure AH.24: Epoxy spray equipment [92]

The epoxy is applied by using a robot that can either be controlled or set to automatic. By using a spray on a telescopic arm as presented here, the problem of how to coat the ceiling has been solved.

### AH.4.2. Planning

An overview of the planning for the connections tubes is given in the following tables.

Phase	Start week	Weeks
Construction transition tubes	107	4
Backfilling & compacting soil pit	111	2
Scabbling tubes	113	1
Applying epoxy, starting at outlet	114	7

Table AH.8: Construction planning outlet tube

Phase	Start week	Weeks
Construction transition tubes	121	4
Backfilling & compacting soil pit	125	2
Scabbling tubes	127	1
Applying epoxy, starting at outlet	128	3

Table AH.9: Construction planning inlet tube

Construction is to start at the outer tubes after the TBM has been disassembled. It has been estimated one ring segment can be installed every 20 minutes. With a tube being 103 m long and one ring 1 m, and a ring consisting of 4 segments, it has been calculated that the tube construction takes an expected 4 weeks, when rounded up. The filling of the excavation pit happens parallel to construction of the tubes. When the tubes have been completed, 1 week has been reserved for filling up the remainder of the pit, and another one for compacting the soil. For the scabbling of the top parts of the tube another week has been taken into account. At this point, the cranes are moved to the inlet to start construction of the tubes there.

After the top part of the outlet tubes has been removed, the epoxy lining can be applied. According to [92], the epoxy can be applied at a rate of 150 m<sup>2</sup>/h, or 1200 m<sup>2</sup>/day. Spraying is to start at the outlet side of the tunnels. The combined length of one tunnel and the tubes are 900 + 2 \* 103 = 1106 m. The total to be treated surface area = 1106 \*  $\pi$  \* 16 = 55,594 m<sup>2</sup> per tunnel, giving a combined 111,187 m<sup>2</sup> for the whole system. Rounded up, this results in a required 10 weeks to apply all epoxy. However, a 4 week pause takes place after 6 weeks, as the inlet tube starts to be constructed. This pause has been introduced to not expose work crew outside of the tube to the toxic fumes of the epoxy.

### AH.4.3. Costs

The costs specifically related to this construction phase are presented in table AH.10. It has been estimated that an average of 30 workers are present during these phases.

	Cost / unit	Quantity	Man-hours	Cost
Tube lining	€ 60,000 / m	412 m	134,400	€ 24,720,000
Backfilling excavation pit	€ 4 / m <sup>3</sup>	272,007 m <sup>3</sup>		€ 1,088,027
Epoxy spray equipment rent, 2 units	€ 50,000 / week / piece	14 weeks		€ 1,400,000
Epoxy	€ 150 / m <sup>2</sup>	111,187 m <sup>2</sup>		€ 16,678,084
Man-hours	€ 40 / hour	134,400		€ 5,376,000
<b>Total</b>				<b>€ 49,262,110</b>

Table AH.10: Costs of tube construction and finishing tunnel. For sources of cost rates, see appendix AI.

### AH.4.4. Additional safety measurements

#### Construction concrete tubes

During construction of the concrete tubes, heavy lifting is carried constantly. Therefore, good safety measurements are to be taken concerning lifting. Examples of these include the following:

- An overseer is to be present during lifting to guide the crane controller, one both on surface level as well on ground level
- Lifting is not to take place during bad weather conditions
- During lowering of segments, people are to stay clear of the area until the element has reached the tube

#### Backfilling excavation pit

During the backfilling of the pit, large quantities of sand are being dumped into the pit and moved around by heavy equipment. The following safety measurements should be taken:

- A designated sand dumping area in the pit should be indicated. In this area, it is safe to drop sand from the top of the pit
- Loaders will be driving around the pit. Both the loaders as the area they will be driving around must be clearly marked
- It is advised to assign an overseer to each work crew to track the vehicles moving around

#### Scabbling / removing upper part tubes

During the scabbling of the tubes, concrete rubble can fall into the tunnel. The following safety measurements should be practised during scabbling of the tubes:

- No one is allowed within 150 m of the tunnel entrance, in the tunnel itself
- No one is to enter the tunnel alone
- Before scabbling starts, it should be checked if the tunnel is clear

#### Applying epoxy layer

Fumes that escape during the application of epoxy are toxic. They can cause irritation of the nose, throat and lungs. Too much exposure can cause respiratory problems. This goes for fumes, liquids and dust particles. Therefore, the following safety measurements are to be taken:

- Sufficient air ventilation is to be installed
- Protective suits must be worn when applying epoxy
- Warning signs are to be placed indicating epoxy spraying is in progress

## AH.5. Sill and funnel

### AH.5.1. Construction process

After construction of the tunnel, a funnel and a sill connect the structure to the river. This construction process can be ordered in the following steps:

1. Preparing location
2. Constructing funnel
3. Constructing connection between funnel and river
4. Constructing sill
5. Placing recreational area

#### Preparing location

The area is excavated to the bed level of the river (TP +1.2 m). This will be done by making use of excavators. The soil material is stored partly for backfilling and flattening of the area. First, the area around the tunnels should be flattened to create the funnel.

#### Constructing funnel

A concrete floor will be cast in-situ around the tunnel entrances. First, formwork will be placed in the correct shape. The casting is done by concrete pump trucks. After the floor is installed, prefab L-shaped retaining walls for the funnel are placed with cranes. The foot of the wall is placed at the outside. After placement of the walls, soil is placed back at the outside of the structure using excavators. This will ensure the concrete walls to be stable.

#### Constructing connection between funnel and river

The area between the funnel and the river will also have walls around it. These will be placed in the same way as the walls for the funnel. The ground in the inlet area will be covered after the sill is constructed.

#### Constructing sill

Before constructing the sill, the current dike should be made smaller. Sheet piles at the river side will be used to prevent water from flowing in the area. Then, prefab concrete elements will be placed on top of the soil using cranes. At the tunnel side of the inlet, bed protection will be made by extending the use of this concrete elements. At the outlet, bed protection will be placed on the river side. Faggots will be located to the right position and submerged using the rocks. Cranes can be used to place the faggots while hydraulic excavators place the rocks onto the faggots.

#### Placing recreational area

After making sure that the construction is functional, placing of recreational area can be started. After levelling the floor, it is advised to start marking sections for the tennis- and baseball fields. Multiple groups of workers can focus on placing the grass-, baseball-, and tennis mats. Concrete pavement can also be placed during this phase. Small fences need to be placed surrounding the sport fields when placement of the mats is finished. Before delivery of the recreational area, a net needs to be placed before the entrance of the tunnels in order to avoid trespassing. The net is attached to the bottom and upper corners. At the bottom the net should be attached to multiple places to avoid people crawling under it. If a flood is approaching, the upper corners should be made loose in order to let the flow pass without too much extra resistance.

### AH.5.2. Planning

The planning of the construction will be executed as described above, using the timetable as presented in the following tables:

### AH.5.3. Costs

The costs of this phase are summarised in table AH.13. Besides these costs, profits can be expected because of the sand than can be sold.

### AH.5.4. Additional safety measurements

Since the complete workspace will be on a location which will flood in the future, flood control should be taken seriously. An efficient way to evacuate all workers and equipment might be necessary if a large flood is coming. Especially the construction of the sill is very close to the waterfront. Therefore, it is advised to keep a close eye on the flood predictions of the area.

Phase	Start week	Weeks
Excavating & levelling funnel area	114	2
Applying formwork, casting & curing floor	116	3
Applying formwork, casting & curing funnel	119	2
Placing L-shaped walls side & backfilling	119	1
Excavate dike to sill level	119	1
Place concrete block protection sill	120	1
Place bed protection	120	1
Clean up site & install sports facilities	121	3

Table AH.11: Construction phases sill and funnel, outlet side

Phase	Start week	Weeks
Excavating & levelling funnel area	124	2
Applying formwork, casting & curing floor	130	3
Applying formwork, casting & curing funnel	133	2
Placing L-shaped walls side & backfilling	133	1
Excavate dike to sill level	133	1
Place concrete block protection sill	134	1
Place bed protection	134	1
Clean up site & install sports facilities	135	3

Table AH.12: Construction phases sill and funnel, inlet side

	Cost / unit	Quantity	Man-hours	Cost
Soil excavation	€ 4 / m <sup>3</sup>	100,000 m <sup>3</sup>	-	€ 400,000
Concrete for funnel	€ 120 / m <sup>3</sup>	8500 m <sup>3</sup>	1700	€ 1,010,400
Plywood formwork	€ 20 m <sup>2</sup>	1000 m <sup>2</sup>	100	€ 20,000
Concrete L-shaped walls	€ 200 / m <sup>2</sup> (wall surface)	2500 m <sup>2</sup>	500	€ 500,000
Concrete blocks sill	€ 250 / m <sup>2</sup>	4500 m <sup>2</sup>	-	€ 1,125,000
Riprap	€ 250 / m <sup>2</sup>	4500 m <sup>2</sup>	-	€ 1,125,000
Faggots	€ 200 / m <sup>2</sup>	4500 m <sup>2</sup>	-	€ 900,000
Grass	€ 4 / m <sup>2</sup>	5000 m <sup>2</sup>	-	€ 20,000
Baseball field mat	€ 30 / m <sup>2</sup>	4000 m <sup>2</sup>	500	€ 120,000
Tennis court	€ 25,000 / field	4 fields	300	€ 100,000
Man-hours	€ 40 / hour	3100 hours	-	€ 124,000
<b>Total</b>				<b>€ 5,444,000</b>

Table AH.13: Costs of sill and funnel. For sources of cost rates, see appendix AI.



## Unit costs

This appendix lists all unit costs used for approximating the total one of the project. Unit costs without a source have been estimated.

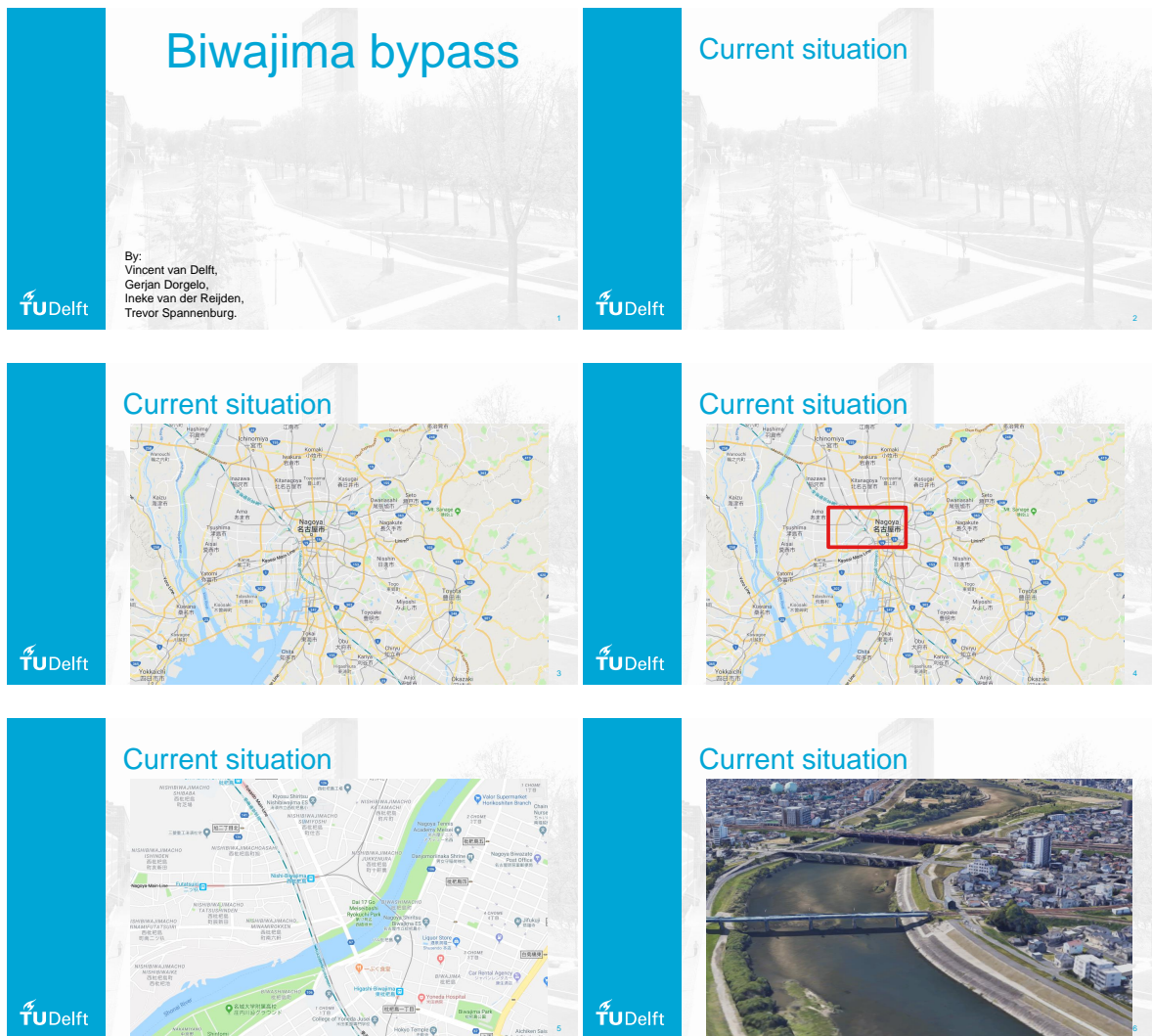
	<b>Cost</b>	<b>Unit</b>	<b>Source</b>
Property purchase	€ 3,000	m <sup>2</sup>	Living statistics Nagoya [89]
Property sale	€ 1,000	m <sup>2</sup>	
Dike	€ 40	m <sup>3</sup>	Cost estimation for fluvial defences [94]
Excavator rent	€ 7,500	week	
Anchor driver rent	€ 20,000	week	
Pontoon rent	€1,500	week	Estimation based on rental companies
Piledriver rent	€20,000	week	
UWC installation equipment	€100,000	week	
Diaphragm wall	€ 350	m <sup>3</sup>	Fact sheet soil retaining structures [90]
Anchor	€ 600	piece	Fact sheet soil retaining structures [90]
Tension pile	€ 600	piece	Fact sheet soil retaining structures [90]
Soil excavation	€ 4	m <sup>3</sup>	TU Delft course CIE4170 Construction Technology of Civil Engineering Structures [95]
Soil excavation, wet	€ 8	m <sup>3</sup>	
Underwater concrete	€ 250	m <sup>2</sup>	Fact sheet soil retaining structures [90]
Man-hour	€ 40	hour	TU Delft course CIE4170 Construction Technology of Civil Engineering Structures [95]
Bored tunnel	€ 121,700	m	TU Delft course CIE5305 Bored and Immersed Tunneling [13]
Tube lining	€ 60,000	m	TU Delft course CIE5305 Bored and Immersed Tunneling [13] cost adjusted for shape
Backfilling excavation pit	€ 4	m <sup>3</sup>	TU Delft course CIE4170 Construction Technology of Civil Engineering Structures [95]
Epoxy spray equipment rent	€ 50,000	week	
Epoxy	€ 150	m <sup>2</sup>	Costhelper.com [96]
Cast concrete	€ 120	m <sup>3</sup>	TU Delft course CIE4170 Construction Technology of Civil Engineering Structures [95]
Plywood formwork	€ 20	m <sup>2</sup>	TU Delft course CIE4170 Construction Technology of Civil Engineering Structures [95]
Concrete L-shaped walls	€ 200	m <sup>2</sup>	
Concrete blocks sill	€ 250	m <sup>2</sup>	
Riprap	€ 250	m <sup>2</sup>	British Environment Agency [97]
Faggots	€ 200	m <sup>2</sup>	British Environment Agency [97]
Grass	€ 4	m <sup>2</sup>	Grass supplier [98]
Baseball field mat	€ 30	m <sup>2</sup>	Rubber flooring supplier [99]
Tennis court	€ 25,000	court	Mat supplier [100]
Site overhead (General equipment, fuel etc.)	€ 30,000	week	TU Delft course CIE4170 Construction Technology of Civil Engineering Structures [95]
Crane rent	€ 50,000	week	

Table AI.1: Cost per unit

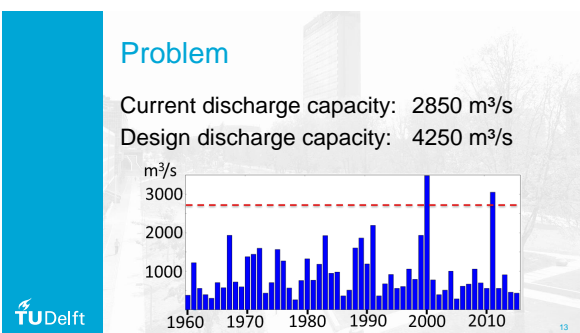
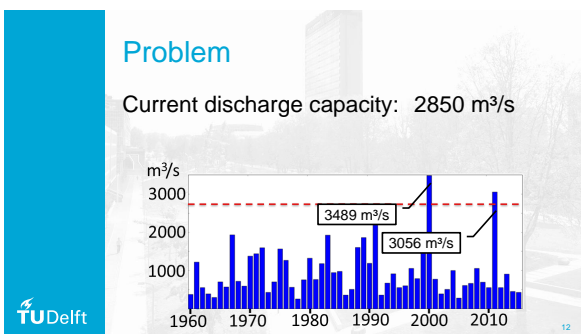
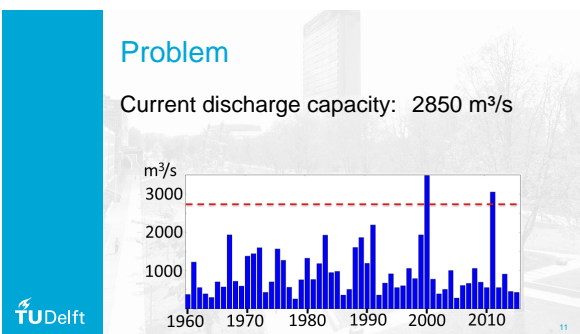
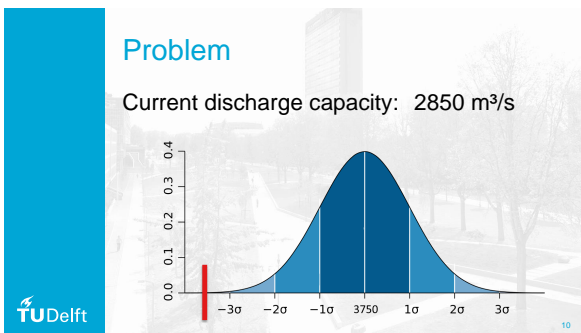
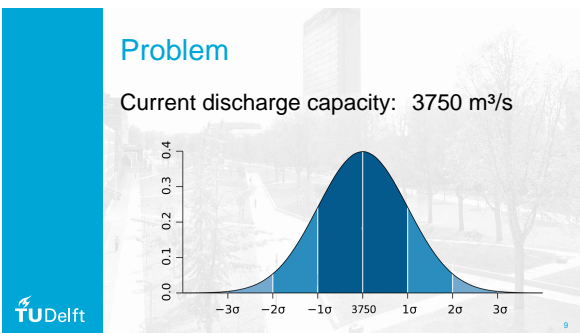
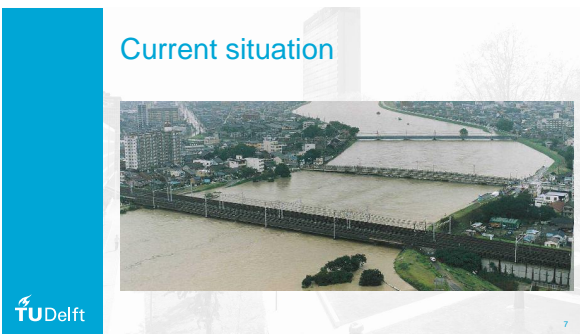
# AJ

## Slides of given presentation

A presentation has been given to Chubu Regional Development Office. The slides of this presentation are shown below. Slide 21 shows an animation which can be found here: <https://youtu.be/ehvN-xorwxQ>.







### Problem

Current discharge capacity: 2850 m<sup>3</sup>/s  
Design discharge capacity: 4250 m<sup>3</sup>/s -  
Redundant capacity: - 1400 m<sup>3</sup>/s

TU Delft



### Target


- How can the discharge capacity of the Shonai River near Biwajima be improved to modern standards?

TU Delft

### Target

- How can the discharge capacity of the Shonai River near Biwajima be improved to modern standards?

Probability of failure: 1 / 200 year



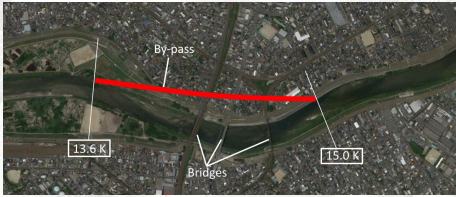
17

### Solution




18

### Solution



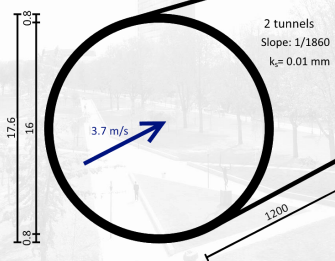

19

### Solution




20


### Solution



2 tunnels  
Slope: 1/1860  
 $k_s = 0.01 \text{ mm}$

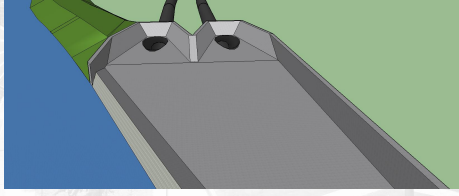

3.7 m/s

1200

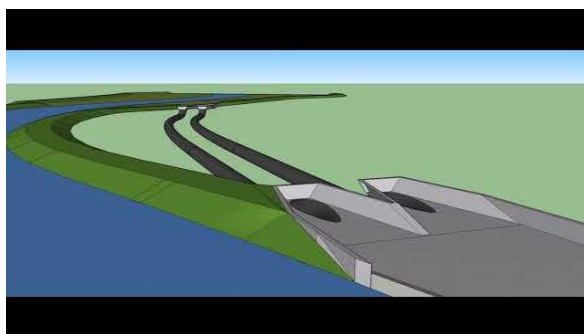



21

### Solution

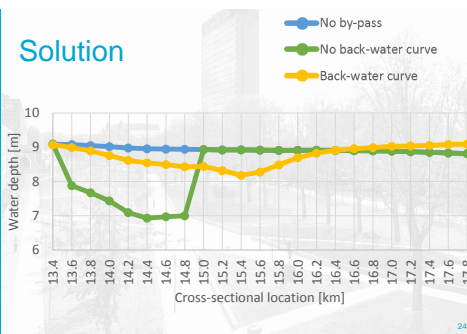



22

23

### Solution




Water depth [m]

10  
9  
8  
7  
6

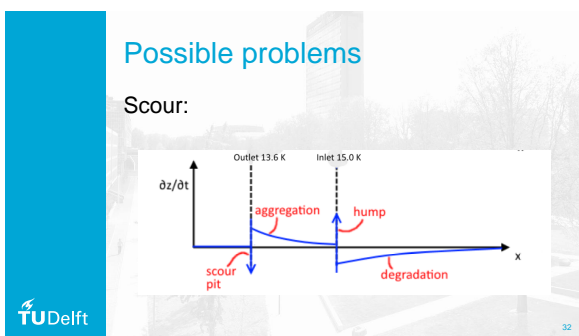
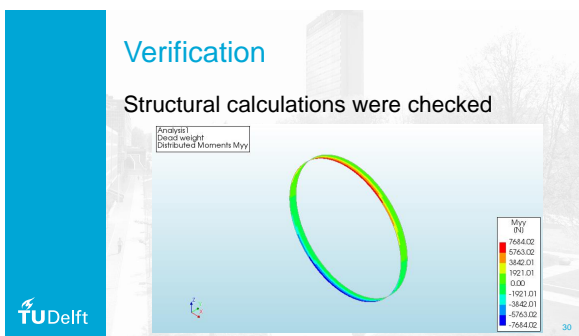
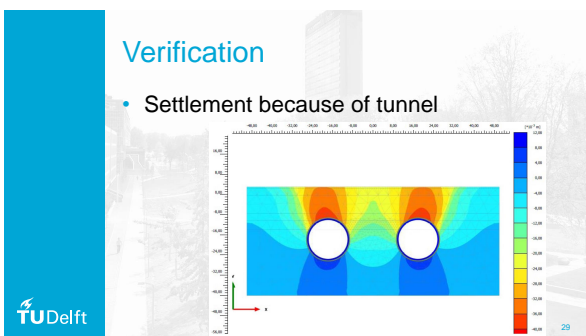
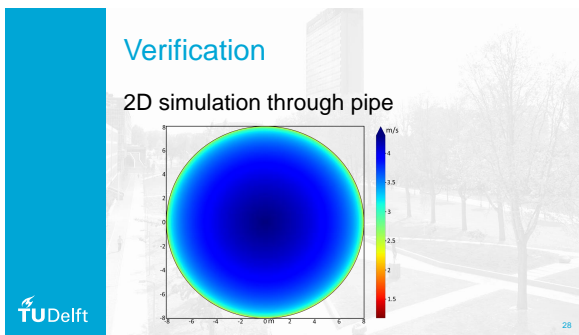
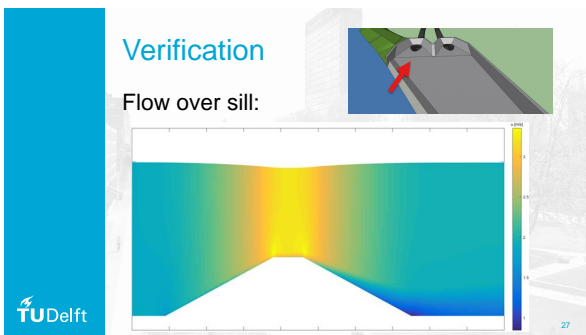
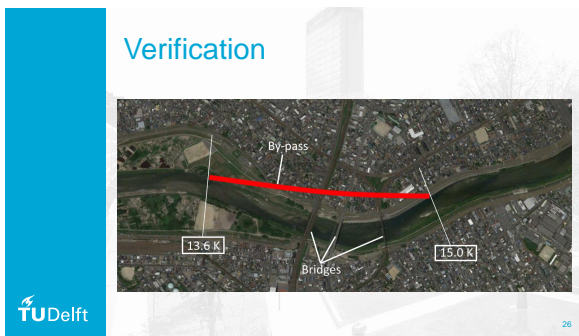
13.4 13.6 13.8 14.0 14.2 14.4 14.6 14.8 15.0 15.2 15.4 15.6 15.8 16.0 16.2 16.4 16.6 16.8 17.0 17.2 17.4 17.6 17.8

Cross-sectional location [km]

- No by-pass
- No back-water curve
- Back-water curve



24



### Costs

- Alternative: ¥ 68,400,000,000 (684 億円)




35

### Costs

- Alternative: ¥ 68,400,000,000 (684 億円)
- Our estimate: ¥ 60,000,000,000 (600 億円)




36

### Costs

- Alternative: ¥ 68,400,000,000 (684 億円)
- Our estimate: ¥ 60,000,000,000 (600 億円)
  - TBM: ¥ 24,000,000,000 (240 億円)
  - Property: ¥ 15,000,000,000 (150 億円)




37

### Recommendations

Combinations with super levee





38

### Conclusion